Banana-shaped Liquid Crystals

Promotoren

Prof. dr. E. J. R. Sudhölter, hoogleraar in de organische chemie, Wageningen Universiteit

Prof. dr. ing. D. J. Broer, hoogleraar in de polymeerchemie, Scheikundige Technologie, Technische Universiteit Eindhoven

Co-promotor

Dr. A. T. M. Marcelis, universitair hoofddocent, Laboratorium voor Organische Chemie, Wageningen Universiteit

Promotiecommissie

Prof. dr. H. van Amerongen	Wageningen Universiteit
Prof. dr. S. J. Picken	Technische Universiteit Delft
Dr. H. Fischer	TNO Science and Technology
Dr. J. Lub	Philips Research B.V.

Remko Achten

Banana-shaped Liquid Crystals

Proefschrift
ter verkrijging van de graad van doctor
op gezag van de rector magnificus
van Wageningen Universiteit,
Prof. dr. M. J. Kropff,
in het openbaar te verdedigen
op woensdag 11 januari 2006
des namiddags te vier uur in de Aula.

Contents

1

Introduction: Liquid crystals and banana-shaped liquid crystals

1.1 Liquid Crystals, an introduction

The three most common states of matter are solids, liquids, and gases. Water, for example, is a solid below 0ºC, a liquid between 0ºC and 100ºC, and a gas above 100ºC. A transition between the different states of matter (or phases) is generally induced by a change in temperature. The transition from solid to liquid is accompanied by a strong decrease in mutual ordering of the molecules and a large increase in mobility. In 1888, an intermediate state of matter between the liquid and solid state was discovered by the Austrian botanist Friedrich Reinitzer [1]. He observed two melting points while heating cholesteryl benzoate. The cloudy liquid he observed between the two melting points was the first recorded observation of a liquid crystalline phase. Liquid crystals are a class of molecules that show phases that are intermediate between the crystalline solid and the isotropic liquid. This is why these phases are also called mesophases. Molecules that exhibit mesophases are usually highly anisotropic in shape, like rods or disks. The molecules in liquid crystalline phases exhibit long-range orientational ordering and sometimes partial positional ordering. The parallel orientation of the long molecular axes is common to all mesophases of rod-like liquid crystals. Figure 1 depicts the relationship between the mobility and the order of some condensed (i.e. non-gaseous) phases. Besides the mesophase, which combines the mobility of liquids with the order of crystals, there is the glassy phase, in which the molecules are immobile and behave like a frozen liquid, or a frozen liquid crystal in case of a mesoglass.
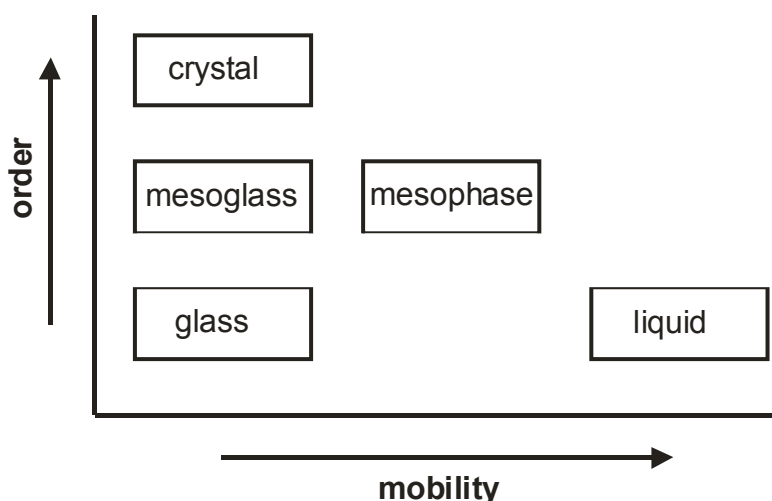

Figure 1. Phase behavior as a function of order and mobility.

The presence of domains of ordered anisotropic molecules in liquid crystalline materials means that these domains also have anisotropic physical properties, which depend on the direction of measurement. Refractive index, dielectric constant,

diamagnetic susceptibility and viscosity are examples of physical properties that can be anisotropic (non-isotropic). The diamagnetic anisotropy for instance makes that the molecules can be aligned by an external magnetic field.

Other important properties of liquid crystals are that their orientation can easily be influenced by an electric field and by surfaces. These properties have led to their application in display devices such as LCDs. A frequently used class of liquid crystals are chiral and non-chiral cyanobiphenyls [2]. Because of their chemical stability and suitable temperature range in which the liquid crystalline phase is present, they were for a long time used in LCDs. Nowadays in the current displays they have been replaced by halogenated aromatic and cycloaliphatic compounds because of their higher purity, lower viscosity and more balanced optical and dielectric properties.

Compounds that form mesophases as a function of temperature are thermotropic liquid crystals. If the liquid crystalline mesophase is induced (in a certain temperature interval) by the concentration in a solvent they are called lyotropic liquid crystals [3,4]. This thesis only deals with thermotropic liquid crystals.

1.2   Shapes of molecules and their LC phases

Molecules that show liquid crystalline behavior usually have an anisotropic shape; their liquid crystalline properties depend on non-covalent interactions. Several different types of shapes and their corresponding phases can be distinguished. Typically, certain types of molecules exhibit distinct mesophases. It is however not always possible to predict the type of mesophase based on just a molecular shape. Some general tendencies can be seen however.

1.2.1   Rod-shaped mesogens

Rod-shaped (or calamitic) molecules form most of the traditional liquid crystalline phases: nematic (1.2.1.1), cholesteric (1.2.1.2) and smectic phases (1.2.1.3). These calamitic mesogens usually are composed of two or more central ring systems (a rigid core), and one or two flexible alkyl tails [5]. The classical phase behavior of rod-shaped molecules will be discussed in the following paragraphs.

1.2.1.1   Nematic phase

The nematic mesophase has long-range orientational order and no long-range positional order (figure 2a). The molecules are oriented parallel in a certain domain of a sample (the preferred direction can vary from point to point in a medium). The

nematic phase is optically uniaxial (N_u) and is therefore frequently used in display device technology. The biaxial nematic phase (N_b), in which there is an additional correlation of the molecules perpendicular to the director, is a recently recognized sub-class of the nematic phase [6-8].
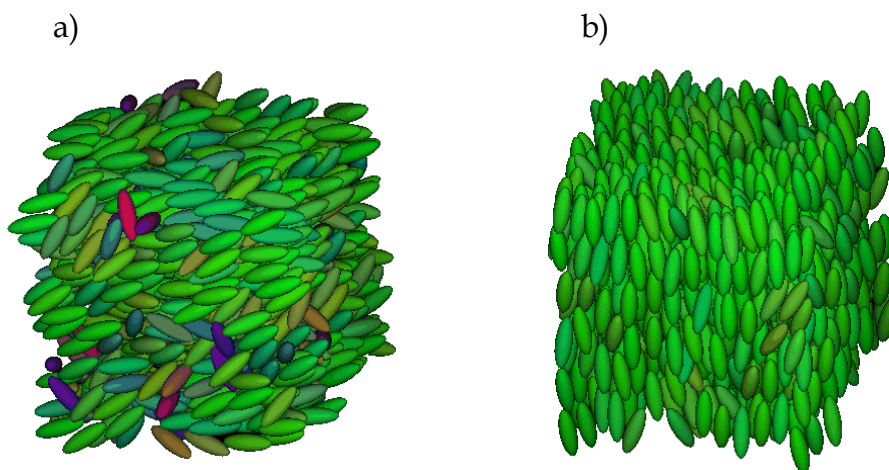
a)   b)

Figure 2. Representation of a) nematic phase, b) smectic (A) phase.

1.2.1.2   Cholesteric phase

The cholesteric phase is a nematic phase composed of chiral molecules, or induced by the presence of chiral molecules (figure 3a). As a consequence, the system acquires a helical ordering perpendicular to the long axis of the molecules. The helix may be right- or left-handed depending on the molecular chirality. The pitch is the distance after which the molecules have the same average orientation. A special property of this phase is that light of a wavelength equal to the pitch is selectively reflected and circularly polarized.

1.2.1.3   Smectic phases

Molecules in smectic phases are ordered in layers. The translation of molecules from one layer to another is limited. Within these layered systems, a variety of molecular arrangements is possible. In the most simple case, the smectic A (SmA) phase (figure 2b), there is no positional order within each layer and the long axes of the molecules are on average positioned perpendicular to the layers. Despite this partial ordering of the molecular positions, the substance still flows, and is therefore a liquid. In the smectic C (SmC) phase the molecules are tilted with respect to the layer normal.

The chiral smectic C phase (SmC*) exhibits a helical structure. In contrast to the cholesteric phase, the subsequent layers with the tilted molecules are slightly rotated with respect to each other (figure 3b). In a typical SmC* material the director rotates on the tilt cone about 1° from one layer to the next (figure 3c). In these materials, the orientation of the tilt can be influenced by an electric field, and therefore this phase can be used in displays that in theory can be switched much faster than conventional

nematic displays. When compared to a SmC phase which has C_{2h} symmetry, the symmetry of the SmC* phase is further reduced to C_2 and the phase is therefore necessarily polar.

Several higher ordered smectic phases exist in which there is an additional hexagonal or cubic ordering of the mesogens in the layers and/or additional rotational ordering [9,10].
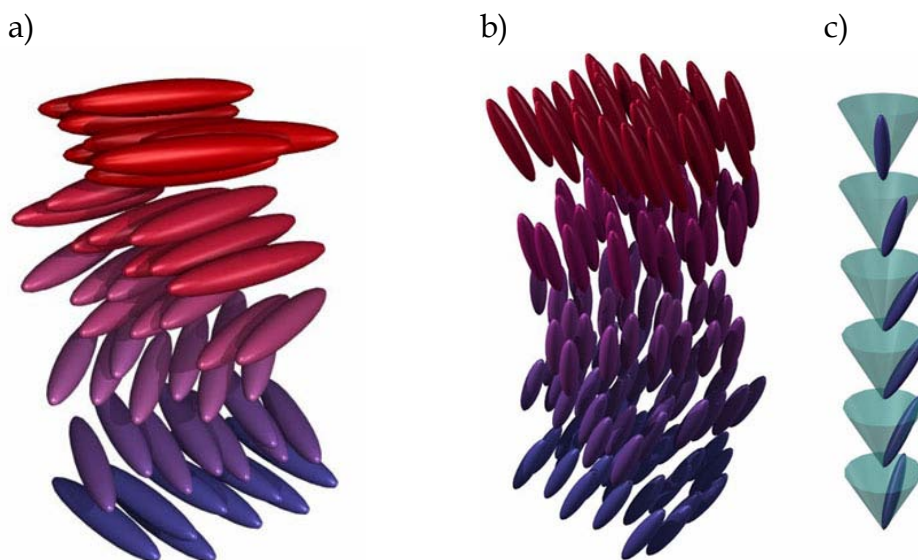

Figure 3. Representation of a) cholesteric phase, b) chiral smectic C phase (SmC), c) the change in director in subsequent layers.*

1.2.2 Disk-shaped mesogens

Disk-shaped liquid crystals usually consist of an aromatic core with pendant flexible chains. In general discotic liquid crystalline phases are derived from this class of molecules [11]. In the columnar phase stacks of disk-like molecules are present [11]. The molecules in these columns can be arranged in a number of different ways, leading to different columnar mesophases. The columns can be tilted or non-tilted and can be arranged in a hexagonal or rectangular manner. Disk-like molecules can also form lower ordered nematic phases of which several variants are known [12,13].

1.2.3 Dimeric mesogens

By covalently connecting two mesogenic units, dimeric liquid crystals are formed that show interesting properties not found in molecules composed of a single mesogenic unit. These dimeric liquid crystals [14], with two mesogenic groups connected by a flexible spacer, are also very interesting because of their ability to act as model compounds for main-chain liquid crystalline polymers.

For many dimers, composed of monomers that form smectic phases, it was found that the smectic phase behavior was suppressed [15]. This phenomenon has been

attributed to an increase in the overall molecular flexibility. On the other hand, it is known that dimers with long terminal tails promote smectic behavior [16]. Some series of compounds even exhibit a rich polymorphism of smectic phases [9].

A simple relationship between the occurrence of smectic behavior and the molecular structure of symmetric dimers was deduced from studies on the α,ω-bis(4-*n*-alkyl-anilinebenzylidene-4′-oxy)alkane series. To obtain smectic properties the length of the terminal tails must be greater than half the length of the spacer [9], in the other cases nematic behavior was observed. In this case a simple monolayer structure was present which is thought to be stabilized by the microphase segregation into three regions (figure 4a).
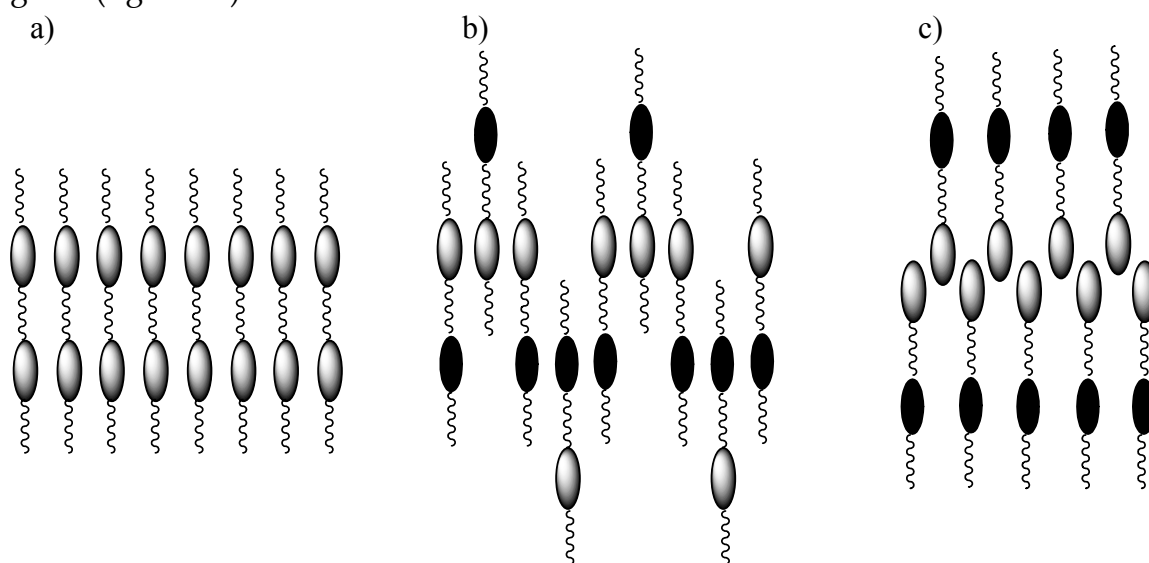
a)   b)   c)

Figure 4*. Schematic representation of SmA arrangements of dimer liquid crystals. a) monolayer b) intercalated and c) interdigitated.*

Non-symmetric dimers, in which two different mesogenic groups are linked through a flexible spacer, have also been described extensively in literature [10,17]. These compounds tend to arrange in intercalated (figure 4b) or interdigitated (figure 4c) smectic organizations [18]. The intercalated arrangement is stabilized by the increase in entropy gained from the homogeneously mixed mesogenic units (non-specific interactions). Another possible stabilizing factor is the electrostatic quadrupolar interaction between the different mesogens having quadrupole moments of opposite sign [19]. In some cases however also symmetric dimers are known to exhibit intercalated mesophases [20].

Due to the parity of the spacer usually strong odd-even effects are found in dimeric liquid crystals [20]. The odd-even effect can be understood as resulting from a conformational constraint whereby the molecules with an odd spacer tend to assume a conformation with the two mesogens tilted with respect to each other. In the even-spaced compounds the mesogenic groups are more likely to lie parallel to each other

[21] (figure 5). That is why odd-numbered spacers have a stronger tendency to form SmC-like phases while even-numbered analogues form SmA phases [20,22]. In 1999, some more striking properties of dimers with a flexible alkylene spacer were discovered [23,24]. Some compounds with an odd number of flexible units between the two mesogens adopt a bent conformation resulting in a liquid crystalline phase with electro-optical switching properties. Surprisingly, switching behavior was also observed in compounds with an even number of flexible units in the central spacer [25,26], but no reasonable rationale for this was given.

Figure 5*. Schematic representation of dimeric molecules with an odd and an even number of flexible units between the two mesogens.*

1.2.4   Non-conventionally-shaped mesogens

Non-conventionally-shaped liquid crystals are molecules with an anisotropic shape that deviates from the classical disk- and rod-shaped molecules [27]. Some of these molecules exhibit quite unusual mesophase morphologies, which sometimes combine lamellar and columnar organizations [28]. Due to their extraordinary properties some of these mesogens, like banana-shaped compounds, even have become a new sub-field in the liquid crystal area. These banana-shaped liquid crystals are also known as bent-core mesogens. Usually, these compounds are composed of a bent central aromatic part (for example a 1,3-disubstituted benzene), and two flexible tails. The symmetry of liquid crystalline phases of these compounds is sometimes broken as a result of simultaneous director tilt and polar order perpendicular to the director [29]. Hence astonishing liquid crystalline phases can exist and (anti)ferroelectricity is sometimes observed [30], a property previously only found for chiral compounds. A more extensive description of bent-core mesogens and their liquid crystalline phases is given in the following paragraph 1.3.

V-shaped mesogens have structures that are closely related to banana-shaped compounds. In contrast to banana-shaped mesogens, these compounds are often composed of a benzene ring, substituted with two mesogenic units at the 1,2-positions [31]. Despite the large bending angle of ~70° they exhibit mesophases similar to those shown by classical calamitic liquid crystals [32].

Figure 6 shows two homologous series of compounds that only differ in the position in which the two arms are attached to the central phenyl group; 1,2-substitution results in V-shaped compounds and 1,3-substitution gives banana-shaped compounds. Although these two series are structural isomers their mesophase

behavior is completely different. Upon increasing the length of the terminal chains of the V-shaped molecules [32] nematic (n ≤ 6) and SmA phases (n ≥ 3) are observed. These are typical calamitic phases that could also be expected for linearly (1,4; *para*) substituted compounds. The banana-shaped compounds [33] on the other hand show the phase sequence B6-B1-B2 upon increasing tail length and the compounds with the longer chains (B2) exhibit antiferroelectric switching properties.
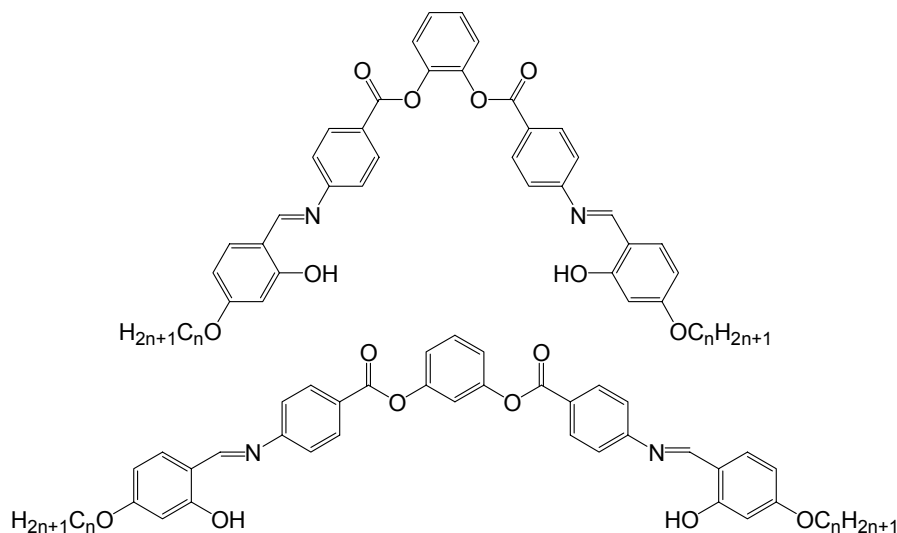

Figure 6. *Structures of V-shaped [32] and banana-shaped [33] series of compounds.*

Beside the B-phases that can be formed by banana-shaped liquid crystals, sometimes also biaxial SmA phases are formed by this type of molecules [34]. In this phase, the molecules are ordered along the layer normal, like in the SmA phase, but have an additional director in the plane of the layers.

1.3   Bananas

1.3.1   History

Although the special properties of banana-shaped liquid crystals were discovered in 1996 [35], several mesogens with a bent shape had already been synthesized in the early 20th century [36,37]. By that time, however, their peculiar properties were not recognized. Recently, one of the early synthesized banana-shaped mesogens with two short terminal tails was reinvestigated and indeed showed a B6 phase [38].

Before banana-mania was initiated in the mid-90s, ferroelectricity [39] and antiferroelectricity [40] were discovered in chiral compounds exhibiting tilted smectic phases. The possibility of smectic phases with triclinic symmetry (SmCG) was predicted by de Gennes [41] and experimentally proven for smectic liquid crystals by

Jákli *et al.* [42]. Switching behavior in materials consisting of achiral compounds was predicted by Prost *et al.* [43], provided that molecules could order in polar layers. The first evidence of ferroelectricity in a non-chiral tilted smectic phase was reported in 1992 [44] in polyphilic compounds. In 1996, Niori *et al.* [35] were the first to report on smectic phases of achiral molecules with a bent core which had ferroelectric switching properties. Later it was proven that this compound actually possessed antiferroelectric switching properties [29].

From 1996 to early 2005 about 200 scientific papers about banana-shaped liquid crystals have been published. More than a few times the phase assignment of compounds in the past proved to be incorrect due to renewed insights or improved experimental techniques.

1.3.2   Banana phases

Most banana phases that have been characterized until now do not show many similarities with the liquid crystalline mesophases formed by conventional calamitic molecules. That is why in December 1997 at the "Workshop on Banana-shaped Liquid Crystals" in Berlin, it was decided to label these new mesophases B_n. The subscript n corresponds to the sequence of discovery of the different phases. This nomenclature seems to be inadequate however since several new phases [45] and sub-phases have been discovered in the recent past. Therefore, a process to formalize the nomenclature of bent core mesogens was initiated at a Boulder Workshop in 2002 (Banana Liquid Crystals – Chirality & Polarity). This process still needs to be formalized however, and that is why we give here an overview of the different phases using the "old" nomenclature (a preliminary formalization is given in [46]).

B_1 phase

The B_1 phase can be regarded as a rectangular columnar (Col_r) mesophase. It is usually observed in compounds with relatively short terminal (alkyl) tails. Typically the number of molecules per unit cell is 6-10, which results in 3-5 molecules per building block. Just after its discovery this rectangular columnar phase was also designated as SmA'_b [47,48], and more recently the designation Col_r is frequently used [49] (figure 7). The polar direction can be parallel or perpendicular to the 2D lattice (or the columns).

Upon cooling from the isotropic phase, polarization optical microscopy (POM) of the B_1 phase shows the formation of small batonnets, which coalesce into a mosaic-like texture. A characteristic XRD pattern of a B_1 compound shows two reflections in the small angle, (11) and (20), and a broad peak in the wide angle region. On these

grounds Watanabe *et al.* [48] proposed a two-dimensional rectangular columnar (Col$_r$) structure.
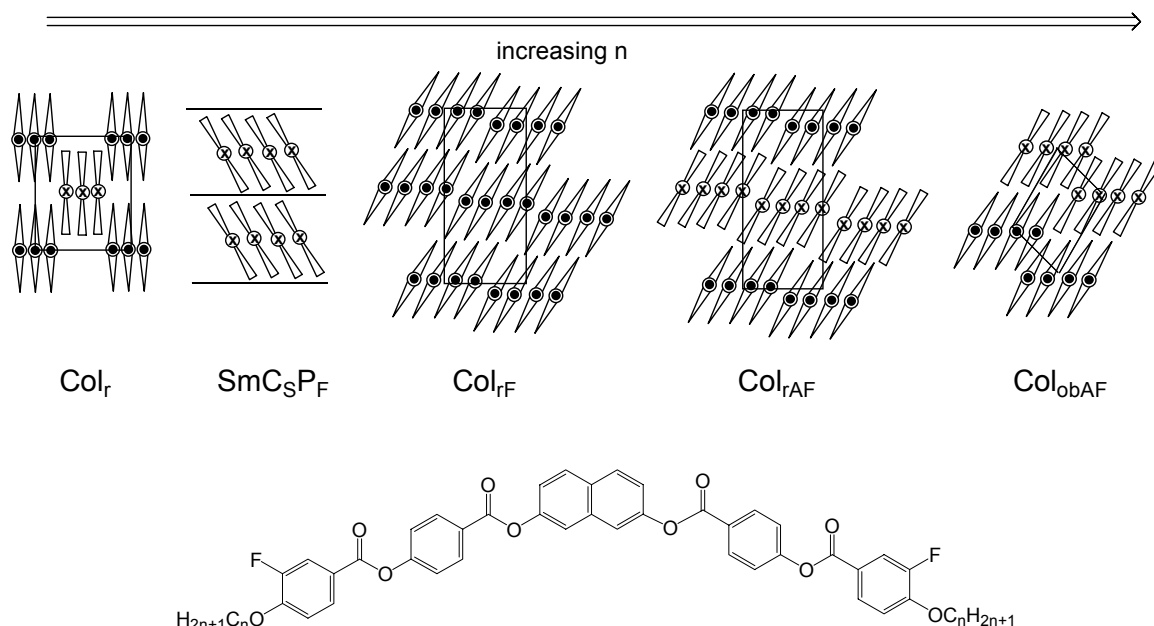

Figure 7. Phase sequence proposed for fluorinated series of compounds depicted below [50].

Recently, it was shown that the B$_1$ phase can exhibit several sub-phases wich sometimes show switching properties [51], a 3-D modulated phase structure [51] or a tilted structure [52]. Amaranatha Reddy *et al.* showed that fluorinated compounds (figure 7) with long terminal chains can also form columnar B$_1$-like phases, and additionally they proposed a new phase sequence with several columnar phases formed by bent-core mesogens (figure 7) [50]. It should be noted that in the corresponding series without the fluorine substituents a more "traditional" N-B$_1$-B$_2$ phase sequence was observed with increasing tail length.

B$_2$ phase

The B$_2$ phase is a tilted smectic mesophase with polar order. Its structure was fully elucidated in 1997 by Link *et al.* [29]. The polar and chiral layer structures arise from two symmetry-breaking events; 1) all molecular bows point in the same direction in one layer, and 2) the molecular long-axis is tilted from the layer normal (SmC-like) [53]. It is important here to realize that the chirality in the B$_2$ phase does not arise from a superhelical organization like in the SmC* phase, although the symmetry in both cases is C$_2$. On the other hand, it was suggested that some bent-core molecules may exist in chiral conformational states and are chiral only on average [54].

Figure 8 depicts the six possible isomeric structures in the SmCP phase. There are two macroscopic racemic layer structures (SmC$_S$P$_A$ and SmC$_A$P$_F$) and two

macroscopic chiral (conglomerates) layer structures (SmC_AP_A and SmC_SP_F), each showing two enantiomeric structures [53]. In the latter case the layer chirality is identical in adjacent layers.
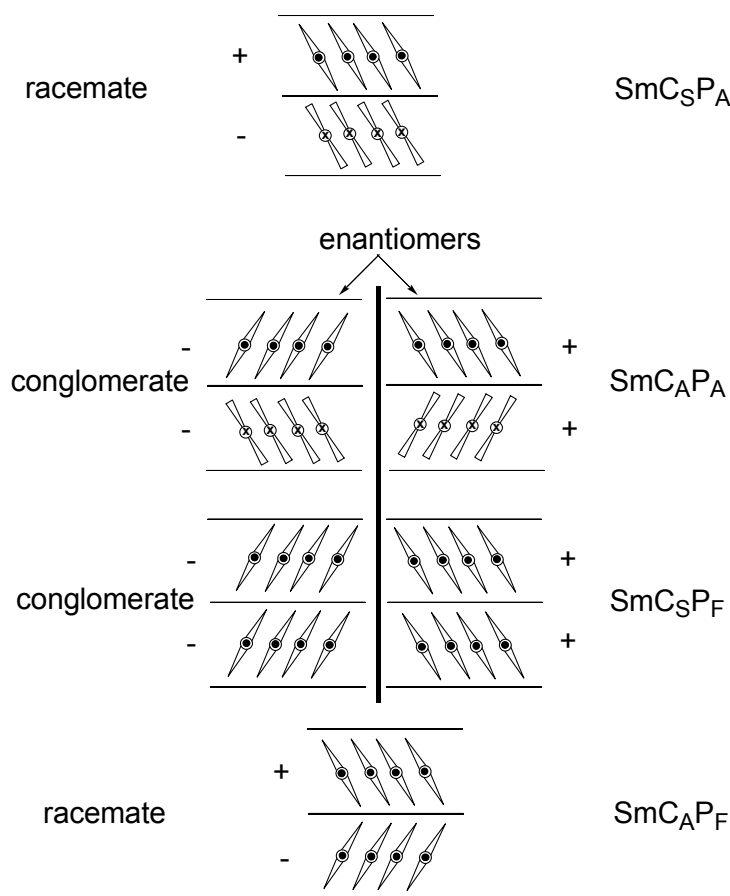

Figure 8*. Schematic representation of six isomers for the SmCP phase.*

B_3 phase

The B_3 phase is a tilted lamellar crystalline phase that does not exhibit switching behavior. Previously, it was also called SmX_2 [55] or $HexB_b$ [47]. This phase should possess SHG activity [56], also in the absence of an applied field, indicating spontaneous polar ordering. A dielectric characterization of a B_3 compound was made by Salfetnikova *et al.* [57]. Because of the crystalline character of the B_3 phase this nomenclature should not be considered as the final classification for bent-core mesogens and maybe this phase should not even be considered as a real mesophase.

B_4 phase

Just like the B_3 phase, the B_4 phase is a crystalline phase and should therefore not be considered as a real mesophase. The molecules in the B_4 phase have a helical arrangement and the most characteristic feature is its intense blue color [58]. The

nomenclature SmBlue used for the B_4 phase should not be confused with the traditional smectic blue phases formed by chiral calamitic molecules. Domains of opposite chirality, caused by the helical domains with opposite optical rotations [59], are formed with equal probability. The helical axis of the non-tilted molecules [60] is parallel to the smectic layers just like in the twist grain boundary phase [47,61]. Usually, the B_4 phase is formed as a low temperature phase in B_2 compounds [62,63] although B_4-B_7 transitions also have been observed [64].

B_5 phase

The B_5 phase is observed upon cooling from the B_2 phase and shows many similarities with this phase. The electro-optical response, POM texture and symmetry are almost the same for instance. A B_2-B_5 transition is accompanied by a sharpening of the X-ray pattern in the wide angle region and increasing viscosity [30,65-67]. Since the B_5 phase is relatively rare it has not been studied in much detail.

B_6 phase

The B_6 phase [68,69] is typically exhibited by banana-shaped compounds with very short terminal chains. It is a tilted intercalated smectic phase (SmC_c, Sm_{int} or Sm_c) with layer spacings smaller than half the length of the molecules. The B_1 and B_6 phase both result from the collapse of the polar smectic layers in the B_2 phase [70]. That is why the phase sequence B_6-B_1-B_2 is frequently observed in homologous series upon increasing the terminal chain length [33,71-76].

B_7 phase

Undoubtedly, the B_7 phase is the mesophase with the most fascinating POM textures: (double) helical filaments [77-79], checkerboard textures [80,81] or banana-leaf shaped domains [80,82] have been observed. It was only very recently that Coleman *et al.* [82] combined several techniques to conclude that the B_7 mesophase is a fluid polar smectic liquid crystal. In this phase local splay prevails in the form of periodic supermolecular-scale polarization modulation stripes coupled to layer undulation waves [82].

It has to be noted that in the past some B_7 phases have been recognized as $SmCP_A$ phases due to their AF switching properties. The underlying structure is actually SmC_SP_F and the AF nature is that of the polarization modulation [82].

Very recently a perfect overview on the recent developments in the field of banana-shaped liquid crystals and its phases was given by Amaranatha Reddy *et al.* [46].

1.3.3 Structures

Ever since the beginning of the extensive research on banana-shaped liquid crystals and their special properties in 1996 [35] about 1000 new bent-core mesogens have been synthesized. Of course, long before 1996 several molecules with bent shapes had been synthesized [36,83,84], but the observed mesophases were at that time not recognized as being extraordinary. In systematic studies a fixed aromatic central bent core is taken while the terminal (alkyl) tail lengths are varied. Most banana-shaped compounds that exhibit B-phases have five aromatic rings. Four [21,23-25,33,85,86], six [30,34,49,50,59,76,87-102] and seven [64,72,75,103-112] aromatic rings in banana-shaped mesogens are also known and the mesophase range seems to increase upon increasing the number of rings [113]. In some cases six-ring compounds form conventional smectic phases in addition to banana-phases [114].

The influence of lateral substituents on the mesophase behavior of bananas has also been studied intensively. Chlorine [72,77,94,111-113,115-129], nitro [51,77,81,113,122,128-133], fluorine [66,67,72,74-76,80,89,97-99,102,104,110-113,115,121,123-125,129,132-144], bromine [77,116,120,129,143,145], methyl [66,72,75,94,111,113,118,122,125,128,129,139,141,143,146], hydroxyl [33,107], cyano [94,104,110,113,129,130,133,147-149], methoxy [77,108,111,125], ethyl [30,75], ethoxy [125], acetyl [30], dodecyloxy [77], pentyl [77], hexyl [30,77], COOC$_8$H$_{17}$ [77] and CF$_3$ [113] groups have been used as lateral substituents to one or more of the rings, but small polar groups like fluorine seem to be most effective in retaining the desired B-phases. The position of the substituents plays a highly important role in determining the liquid crystalline properties of a bent-core mesogen [74]. In several cases the liquid crystalline properties completely disappear upon introduction of lateral substituents. In general, melting points are lowered upon introduction of lateral substituents. Bulky substituents can suppress the liquid crystalline properties completely and sometimes interesting changes in switching behavior can be observed upon introduction of small polar substituents [74].

Despite their achiral molecular structure, bananas can form chiral mesophase domains due to two symmetry-breaking events. However, bananas *with* chiral carbon atoms in the terminal tails have also been studied. In most cases the chirality is caused by methyl-branched terminal tails [150-157], but propyl-branched tails were also reported [78]. In these cases transition temperatures are lowered [150,153] and ferroelectricity is induced [78,151,154-156].

Some more exotic banana-shaped liquid crystals have also been studied; polycatenar bent-shaped mesogens [158], molecules with a combination of rod-like and banana mesogenic groups [103], hydrogen-bonded banana mesogens [91] and bananas incorporated in dendritic systems [159]. Light-emitting bent-shape liquid crystals were also designed, but B-phases were not observed for these compounds [160].

1.4   (Anti)ferroelectricity and switching

A mesophase with a permanent polarization in the absence of an electric field is called a ferroelectric mesophase. In order to have a bulk polarization, molecules have to exhibit spontaneous polarization (P_S). Hindered rotation around the molecular long axis plays an essential role in the emergence of P_S. The director of a molecular assembly with spontaneous polarization can be changed by the application of an appropriate electric field. In most ordinary liquid crystalline phases (N, SmA, SmC), the symmetry is so high that rotation around the long molecular axis prevents the occurrence of ferroelectricity. To find ferroelectricity the symmetry has to be lowered further, for example in chiral tilted smectics (SmC*).

Ferroelectricity was discovered in the beginning of the 20th century in crystals by Valasek and later also in liquid crystals for a SmC* phase by Meyer *et al.* [39]. Since the director of a SmC* phase rotates from layer to layer, a helical arrangement is present and therefore the system escapes from macroscopic polarization. The SmC* phase can be driven towards the ferroelectric state by applying an external electric field. In that case the helix unwinds and the molecules in all layers orient in the same direction. By applying an electric field of opposite sign the polarized phase (ferroelectric) will switch to the other ferroelectric state (figure 9). This behavior is often referred to as bistable switching.
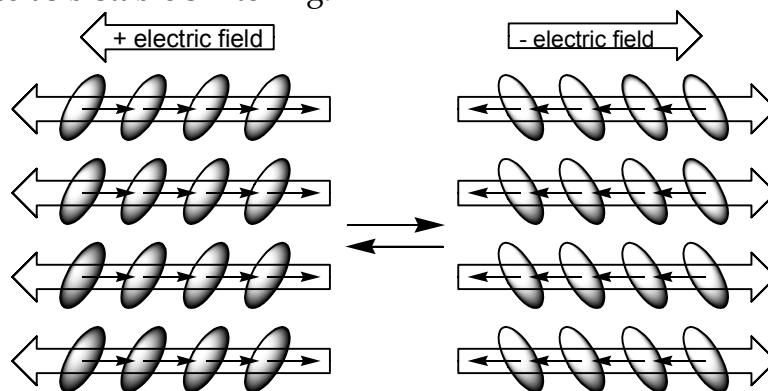

Figure 9. Bistable switching under influence of an electric field.

The main advantage of these smectic materials, compared to conventional nematics is their relatively fast switching properties [58]. The reorientation of the molecules does not require much energy when compared to nematics. This is mainly caused by the fact that the molecules rotate collectively around a cone.

Apart from the ferroelectric layer organization, in which the direction of polarization (and also tilt) is the same in all layers, there is also the antiferroelectric (tristable) structure in which the tilt alternates from layer to layer when no field is applied. In the intermediate ferri-electric phases the tilts randomly alternate (with preference for

one direction). Thus, as we move from the ferroelectric to the antiferroelectric phase, this usually occurs via the ferri-electric state.

Apart from symmetry breaking through a combination of chirality and tilt, the symmetry of the phases can also be broken by a combination of tilt, and a polar component perpendicular to the director of the molecules. This is for example found in columns of bowl-shaped molecules [161]. These columnar phases are stabilized by the one-directional stacking of molecules in the column [162]. This can generate a ferroelectric or antiferroelectric packing of the columns. This is also found for liquid crystalline phases of banana, bent-core or bow-shaped molecules. Just like the classical SmC* compounds, banana-shaped compounds can order into ferroelectric and antiferroelectric arrangements, as shown in figure 10.
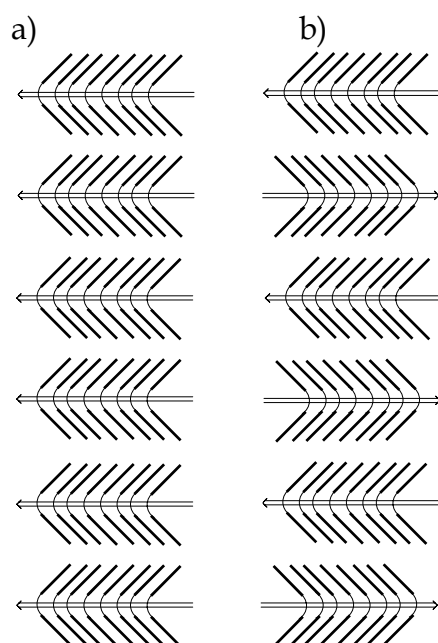
Figure 10. Two types of layer organization for bent-core molecules: a) ferroelectric, b) antiferroelectric.

The switching process in banana-shaped compounds under the influence of an electric field has always been thought to be linked with the strong π-π stacking of the aromatic cores that results in a restricted molecular rotation around the long axes. Therefore, the field-induced reorientation should take place via rotation of the molecules around the tilt cone and the chirality in the layer remains the same (tilt and polar direction reversed). Recently however, field-induced switching of chirality was also detected [50,100,127,163]. In this case the polar switching is not caused by rotation of the director around the tilt cone, but by a collective rotation of the molecules around their long axes, figure 11.

The ground state of a liquid crystalline phase can sometimes be changed from antiferroelectric to ferroelectric upon introduction of fluorine substituents in the outer rings (*ortho* to the terminal tails) [74,67,80,164], or by branching of the terminal tails [78,154-156]. The reason for this behavior might be related to dipolar interactions [74], or intermolecular interactions at the interlayer interfaces [29].
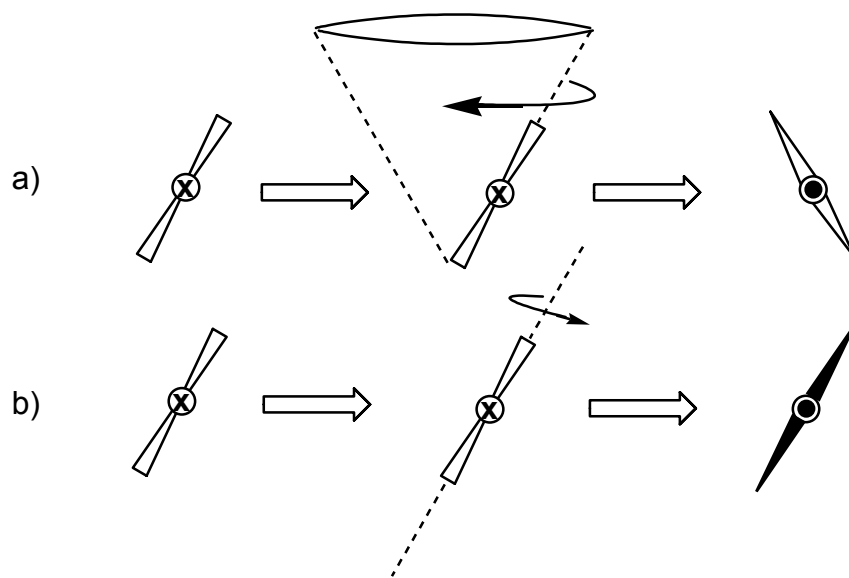

Figure 11. *Two types of polar switching; a) around a cone, b) around the molecular long axis. Open and filled molecule symbols represent layers of opposite chirality* [127].

Occasionally, a change in switching behavior was found depending on the length [163] or the parity [165] of the terminal alkyl tails. The short-tailed compounds in reference [163] showed an antiferroelectric ground state and the compounds with the longer tails a ferroelectric. According to the authors, this can be explained in terms of interlayer interactions: they could be strong for the analogues with short chains, which would clearly favor the formation of an antiferroelectric polar structure. In reference [165] alternating ferroelectric behavior for even and antiferroelectric behavior for odd terminal chain lengths was found. Also in this case interlayer steric interactions play a mayor role in the odd-even effect described for these compounds.

1.5   Polyphilic molecules

A polyphilic molecule is composed of rigid (calamitic) segments connected to at least two other chemically distinct groups (*e.g.* aliphatic chains, oligosiloxane units, ethylene oxide chains, perfluoroalkyl chains). The tendency for these groups to give microphase segregation, and different space filling requirements of these segments, can lead to columnar [166], bilayer [167] or cylindrical [168] phases. Smectic phases of these

liquid crystals can consist of a layer structure composed of three different sublayers. One special group of polyphilic molecules, the liquid crystalline siloxanes, has been studied in detail and has been found in some cases to show complicated aggregate structures [169]. Also less complicated structures, often containing chiral centers, are very interesting from a fundamental point of view [170,171].

In recent years, it was shown that attachment of siloxane [100,172,173] or silane [174,175] units to banana-shaped mesogens, or bananas with fluorinated end groups, can lead to polyphilic materials with properties that differ considerably from "ordinary" bent-core mesogens.

Most low molecular weight banana-shaped compounds without siloxane units show AF switching behavior. The driving force for this antiferroelectric layer organization is thought to originate from the escape from macroscopic polar order and by the synclinic nature of the interlayer interfaces. This synclinicity easily allows interlayer fluctuations and is therefore entropically favored as shown in figure 12. In the ferroelectric ground state the similar bending direction of the molecules in adjacent layers leads to anticlinic interlayer interfaces, which is entropically unfavorable.
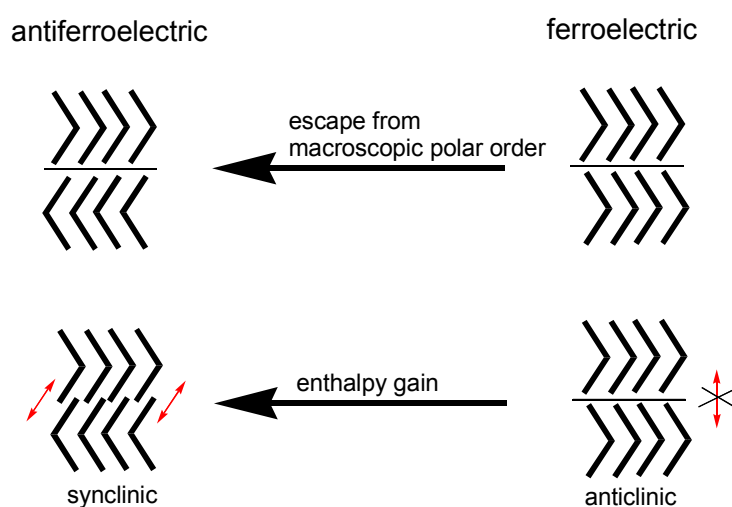
Figure 12. Two types of polar order, originating from two different types of layer clinicities [173].

Polyphilic bananas with siloxane units sometimes exhibit ferroelectric behavior, which is due to the microsegregated triple-layered systems as shown in figure 13. For these compounds the entropically favorable interlayer fluctuations are suppressed (figure 12). The phase separation of the siloxane units from the rest of the molecules (aliphatic tails and aromatic part) was confirmed by X-ray studies that indicate a layered system with two diffuse wide angle reflections [172]. These two

reflections correspond to the mean distance between the alkyl chains on the one hand and the mean distance between the siloxane units on the other hand.

Figure 13. Triple layer organization for bent-core mesogens with one terminal bulky siloxane unit [172].

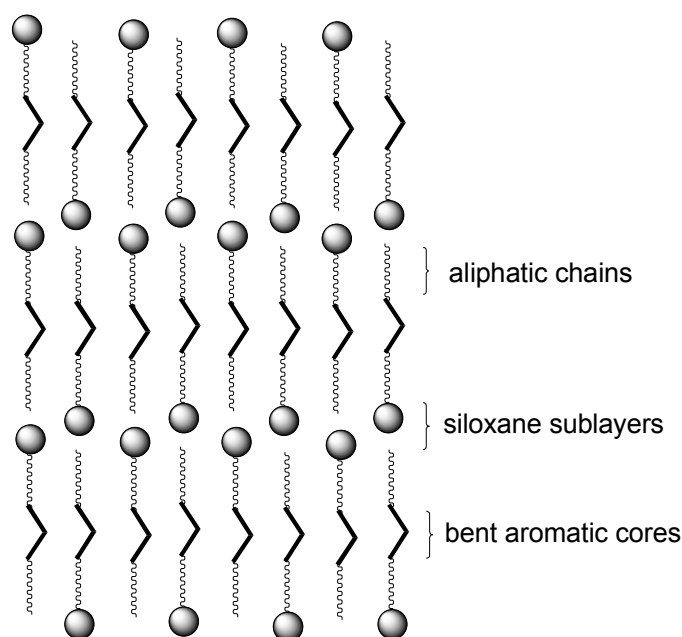Typically, these polyphilic siloxane bananas form grainy unspecific POM textures with domains of opposite handedness. Probably, the molecules are ordered in a helical arrangement, with the two helix-senses causing the different domains [70]. The mesophase is usually stabilized by the introduction of siloxane groups. Threshold voltages for the ferroelectric bistable switching are typically lower than for the antiferroelectric tristable switching process. Surprisingly, the type of applied external field (DC or AC) determines the interlayer clinicity. Hence, the type of applied external field also determines whether the antiferroelectric conglomerate (SmC$_A$P$_A$) or the ferroelectric conglomerate (SmC$_S$P$_F$) is formed after removal of the field [70].

Figure 14 shows some typical compounds, as derived from literature, that show microphase segregation. While in most cases these polyphilic compounds tend to exhibit a ferroelectric phase, compound d) has two antiferroelectric mesophases. This is probably related to the fact that the cross-sectional areas of the branched siloxane units is much larger than of the aliphatic part. This gives rise to a modulation of the layers, a large tilt and a reduced packing density of the aromatic parts [100].
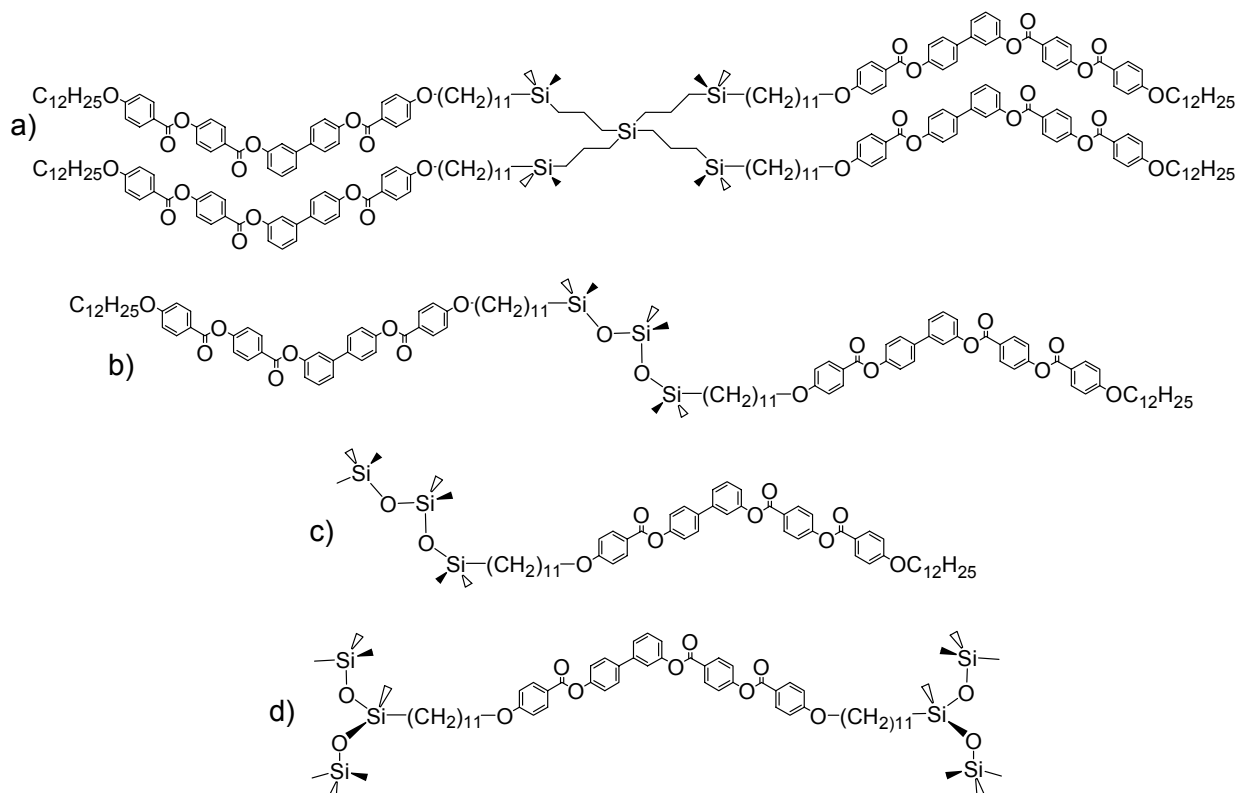
***Figure 14**. Polyphilic banana compounds; a) Carbosilane dendrimer [175], b) siloxane dimer [173], c) banana with one [172] or d) two [100] bulky siloxane groups.*

1.6   Outline of this thesis

The aim of the research described in this thesis is to synthesize and characterize new molecules with a bent or banana shape. Preferentially, the unstable imine bond, frequently used as connecting group between the aromatic rings [23], should be avoided. Investigation of structure – property relations will contribute to a better understanding of this very fascinating state of matter and the factors that determine their potential application in switchable cells. Although these molecules are not chiral, it is expected they can form chiral liquid crystalline phases. In view of any future applications, *e.g.* in electro-optical switches for display or communication applications, the banana-shaped molecules should possess liquid crystalline behavior at temperatures as close to room temperature as possible. Another objective is to obtain materials that can be attached to polymer backbones or hydrogen-terminated silicon surfaces.

In *chapter 2*, we describe the liquid crystalline properties of three series of dimers, in which the two mesogenic moieties are connected via a flexible alkyl spacer. The influence of the directions of the ester groups between the two aromatic rings and

the parity of the spacer is studied. Since several of the compounds described in this chapter have an odd number of flexible units between the mesogenic groups, these compounds might adopt a bent conformation and show B-phases. Comparable compounds described in literature were reported to have switchable B-phases.

In *chapter 3*, we describe four series of liquid crystalline dimers, all bearing a salicylaldimine group in both mesogens. Although an imine group is present, it is stabilized through intramolecular hydrogen bonds via a hydroxyl group. Comparing the four different connecting groups (phenylene; pentylene; 2,2-dimethylpentylene and 3,3-dimethylpentylene) between the two mesogens may provide more insight in the necessity of a central aromatic group for obtaining B-phases. Additionally, the influence of dimethyl substituents, and the position of these substituents on the liquid crystalline phase behavior, is studied.

In *chapters 4, 5* and *6*, several series of five-ring banana-shaped molecules with a central 1,3-substituted phenyl group, and only esters as linking groups between the rings, are investigated, to determine the effect of relatively small structure modifications on the liquid crystalline properties. In *chapter 4*, compounds with two terminal alkoxy tails of different length are prepared to introduce more non-symmetry in the molecules and thereby lower the melting points while retaining the liquid crystalline behavior. In *chapter 5*, the liquid crystalline properties of compounds with one terminal vinyl group are studied and compared with their saturated analogues from *chapter 4*. These compounds can also be used as precursors in hydrosilylation reactions (*chapter 7* and *8*). The effect of small fluorine substituents on the liquid crystalline properties and switching behavior is studied in *chapter 6*.

In *chapter 7*, the vinyl-terminated bananas (*chapter 5*) are polymerized with a relatively short and a relatively long trimethylsilyl-terminated polysiloxane backbone. The liquid crystalline properties of the long and short polymers are compared with their olefinic precursors. Retaining the switching behavior in a polymeric system would make bananas more suitable for possible future applications.

In *chapter 8*, the covalent attachment of (fluorinated) vinyl terminated bananas (*chapter 5* and *6*) to a silicon surface is described. The presence and quality of the monolayers are investigated and the thickness of the monolayers is compared with the corresponding *d*-spacings in bulk.

1.7   References

1.   Reinitzer F. *Monatsch Chem.* **1888**, *9*, 421-425.
2.   Gray G. W., Harrison K. J. and Nash J. A. *Electronics Lett.* **1973**, *9*, 130-131.

3.   Winsor P. A. *Mol. Cryst. Liq. Cryst.* **1971**, *12*, 141-178.

4.   Jákli A., Cao W., Huang Y., Lee C. K. and Chien L.-C. *Liq. Cryst.* **2001**, *28*, 1279-1283.

5.   Gray G. W. *The Molecular Physics of Liquid Crystals* **1979**, *chapter 1*.

6.   Madsen L. A., Dingemans T. J., Nakata M. and Samulski E. T. *Phys. Rev. Let.* **2004**, *92*, 145505.

7.   Chandrasekhar S., Sadashiva B. K., Ratna B. R. and Raja V. N. *Pramana* **1988**, *30*, L491-L494.

8.   Brand H. R., Cladis P. E. and Pleiner H. *Int. J. Eng. Sci.* **2000**, *38*, 1099-1122.

9.   Date R. W., Imrie C. T., Luckhurst G. R. and Seddon J. M. *Liq. Cryst.* **1992**, *12*, 203-238.

10.   Attard G. S., Date R. W., Imrie C. T., Luckhurst G. R., Roskilly S. J., Seddon J. M. and Taylor L. *Liq. Cryst.* **1994**, *16*, 529-581.

11.   Bushby R. J. and Lozman O. R. *Curr. Op. Coll. Interf. Sc.* **2002**, *7*, 343-354.

12.   Tinh N. H., Destrade C. and Gasparoux H. *Phys. Lett.* **1979**, *72A*, 25.

13.   Praefcke K., Singer D., Kohne B., Ebert M., Liebmann A. and Wendorff J. H. *Liq. Cryst.* **1991**, *10*, 147-159.

14.   Imrie C. T. and Henderson P. A. *Curr. Opin. Colloid Interface Sci.* **2002**, *7*, 298-311.

15.   Griffin A. C. and Britt T. R. *J. Am. Chem. Soc.* **1981**, *103*, 4957-4959.

16.   Gray G. W. *The molecular Physics of Liquid Crysyals* **1979**, *chapter 12*.

17.   Blatch A. E. and Luckhurst G. R. *Liq. Cryst.* **2000**, *27*, 775-787.

18.   Marcelis A. T. M., Koudijs A., Karzcmarzyk Z. and Sudhölter E. J. R. *Liq. Cryst.* **2003**, *18*, 1357-1364.

19.   Blatch A. E., Fletcher I. D. and Luckhurst G. R. *Liq. Cryst.* **1995**, *18*, 801-809.

20.   Watanabe J., Komura H. and Niori T. *Liq. Cryst.* **1993**, *13*, 455-465.

21.   Watanabe J., Izumi T., Niori T., Zennyoji M., Takanishi Y. and Takezoe H. *Mol. Cryst. Liq. Cryst.* **2000**, *346*, 77-86.

22.   Niori T., Adachi S. and Watanabe J. *Liq. Cryst.* **1995**, *19*, 139-148.

23.   Watanabe J., Niori T., Choi S.-W., Takanishi Y. and Takezoe H. *Jpn. J. appl. Phys.* **1998**, *37*, L401-L403.

24.   Choi S.-W., Zennyoji M., Takanishi Y., Takezoe H., Niori T. and Watanabe J. *Mol. Cryst. Liq. Cryst.* **1999**, *328*, 185-192.

25.   Prasad V., Shankar Rao D. S. and Krishna Prasad S. *Liq. Cryst.* **2001**, *28*, 761-767.

26.   Prasad V., Shankar Rao D. S. and Krishna Prasad S. *Liq. Cryst.* **2000**, *27*, 585-590.

27.   Tschierske C. *J. Mater. Chem.* **1998**, *8*, 1485-1508.

28.   Tschierske C. *J. Mater. Chem.* **2001**, *11*, 2647-2671.

29.   Link D. R., Natale G., Shao R., Maclennan J. E., Clark N. A., Körblova E. and Walba D. M. *Science* **1997**, *278*, 1924-1927.

30.   Pelzl G., Diele S. and Weissflog W. *Adv. Mater.* **1999**, *11*, 707-724.

31.   Attard G. S. and Douglass A. G. *Liq. Cryst.* **1997**, *22*, 349-358.

32.   Yelamaggad C. V., Shashikala I., Shankar Rao D. S. and Krishna Prasad S. *Liq. Cryst.* **2004**, *31*, 1027-1036.

33.   Achten R., Koudijs A., Karzcmarzyk Z., Marcelis A. T. M. and Sudhölter E. J. R. *Liq. Cryst.* **2004**, *31*, 215-227.

34.   Amaranatha Reddy R. and Sadashiva B. K. *J. Mater. Chem.* **2004**, *14*, 310-319.

35.   Niori T., Sekine F., Watanabe J., Furukawa T. and Takezoe H. *J. Mater. Chem.* **1996**, *6*, 1231-1233.

36.   Vorländer D. and Apel A. *Ber. Dtsch. Chem. Ges.* **1932**, *65*, 1101-1109.

37.   Vorländer D. *Ber. Dtsch. Chem. Ges.* **1929**, *62*, 2831-2838.

38.   Pelzl G., Wirth I. and Weissflog W. *Liq. Cryst.* **2001**, *28*, 969-972.

39.   Meyer R. B., Liebert L., Strelecki I. and Keller P. *J. Phys. Fr. Lett.* **1975**, *36*, L69.

40.   Chandani A. D. L., Ouchi Y., Takezoe H., Fukuda A., Terashima K., Furukawa K. and Kishi A. *Jpn. J. Appl. Phys.* **1989**, *28*, L1261.

41.   de Gennes P. G. *The Physics of Liquid Crystals* **1975**, (Clarendon Press, Oxford).
42.   Jákli A., Krüerke D., Sawade H. and Heppke G. *Phys. Rev. Let.* **2001**, *86*, 5715-5718.
43.   Prost J. and Barois P. *J. chim. Phys.* **1983**, *80*, 65-80.
44.   Tournilhac F., Blinov L. M., Simon J. and Yablonski S. V. *Nature* **1992**, *359*, 621-623.
45.   Bedel J. P., Rouillon J. C., Marcerou J. P., Laguerre M., Nguyen H. T. and Achard M. F. *Liq. Cryst.* **2001**, *28*, 1285-1292.
46.   Amaranatha Reddy R. and Tschierske C. *J. Mater. Chem.* **2005**, *15*, DOI: 10.1039/b504400f.
47.   Sekine T., Niori T., Sone M., Watanabe J., Choi S. W., Takanishi Y. and Takezoe H. *Jpn. J. Appl. Phys.* **1997**, *36*, 6455-6463.
48.   Watanabe J., Niori T., Sekine T. and Takezoe H. *Jpn. J. Appl. Phys.* **1998**, *37*, L139.
49.   Shen D., Pegenau A., Diele S., Wirth I. and Tschierske C. *J. Am. Chem. Soc.* **2000**, *122*, 1593-1601.
50.   Amaranatha Reddy R., Raghunathan V. A. and Sadashiva B. K. *Chem. Mater.* **2005**, *17*, 274-283.
51.   Szydlowska J., Mieczkowski J., Matraszek J., Bruce D. W., Gorecka E., Pociecha D. and Guillon D. *Phys. Rev. E* **2003**, *67*, 031702.
52.   Pelz K., Weissflog W., Baumeister U. and Diele S. *Liq. Cryst.* **2003**, *30*, 1151-1158.
53.   Walba D. M., Korblova E., Shao R., Maclennan J. E., Link D. R., Glaser M. A. and Clark N. A. *J. Phys. Org. Chem.* **2000**, *13*, 830-836.
54.   Earl D. J., Osipov M. A., Takezoe H., Takanishi Y. and Wilson M. R. *Phys. Rev. E* **2005**, 021706.
55.   Sekine T., Niori T., Watanabe J., Furukawa T., Choi S. W. and Takezoe H. *J. Mater. Chem.* **1997**, *7*, 1307-1309.
56.   Choi S.-W., Kinoshita Y., Park B., Takezoe H., Niori T. and Watanabe J. *Jpn. J. Appl. Phys.* **1998**, *37*, 3408-3411.
57.   Salfetnikova J., Schmalfuss H., Nadasi H., Weissflog W. and Kresse H. *Liq. Cryst.* **2000**, *27*, 1663-1667.
58.   Heppke G. and Moro D. *Science* **1998**, *279*, 1872-1873.
59.   Thisayukta J., Nakayama Y., Kawauchi S., Takezoe H. and Watanabe J. *J. Am. Chem. Soc.* **2000**, *122*, 7441-7448.
60.   Shiromo K., Sahade D. A., Oda T., Nihira T., Takanishi Y., Ishikawa K. and Takezoe H. *Angew. Chem. Int. Ed.* **2005**, *44*, 1948-1951.
61.   Thisayukta J., Takezoe H. and Watanabe J. *Jpn. J. Appl. Phys.* **2001**, *40*, 3277-3287.
62.   Niwano H., Nakata M., Thisayukta J., Link D. R., Takezoe H. and Watanabe J. *J. Phys. Chem. B* **2004**, *108*, 14889-14896.
63.   Nadasi H., Lischka C., Weissflog W., Wirth I., Diele S., Pelzl G. and Kresse H. *Mol. Cryst. Liq. Cryst.* **2003**, *399*, 69-84.
64.   Prasad V. *Liq. Cryst.* **2001**, *28*, 1115-1120.
65.   Diele S., Grande S., Kruth H., Liscka C., Pelzl G., Weissflog W. and Wirth I. *Ferroelectrics* **1998**, *212*, 169-177.
66.   Eremin A., Wirth I., Diele S., Pelzl G., Schmalfuss H., Kresse H., Nadasi H., Fodor-Csorba K., Gacs-Baitz E. and Weissflog W. *Liq. Cryst.* **2002**, *29*, 775-782.
67.   Nadasi H., Weissflog W., Eremin A., Pelzl G., Diele S., Das B. and Grande S. *J. Mater. Chem.* **2002**, *12*, 1316-1324.
68.   Diele S., Pelzl G. and Weissflog W. *Liq. Cryst. Today* **1999**, *9*, 8-9.
69.   Kresse H., Schmalfuss H. and Weissflog W. *Liq. Cryst.* **2001**, *28*, 799-801.
70.   Tschierske C. and Dantlgraber G. *Pramana* **2003**, *61*, 455-481.
71.   Rouillon J. C., Marcerou J. P., Laguerre M., Nguyen H. T. and Achard M. F. *J. Mater. Chem.* **2001**, *11*, 2946-2950.
72.   Sadashiva B. K., Raghunathan V. A. and Pratibha R. *Ferroelectrics* **2000**, *243*, 249-260.

22

73. Weissflog W., Wirth I., Diele S., Pelzl G., Schmalfuss H., Schoss T. and Wurflinger A. *Liq. Cryst.* **2001**, *28*, 1603-1609.
74. Amaranatha Reddy R. and Sadashiva B. K. *Liq. Cryst.* **2003**, *30*, 1031-1050.
75. Shreenivasa Murthy H. N. and Sadashiva B. K. *Liq. Cryst.* **2002**, *29*, 1223-1234.
76. Amaranatha Reddy R. and Sadashiva B. K. *J. Mater. Chem.* **2004**, *14*, 1936-1947.
77. Mieczkowski J., Szydlowska J., Matraszek J., Pociecha D., Gorecka E., Donnio B. and Guillon D. *J. Mater. Chem.* **2002**, *12*, 3392-3399.
78. Walba D. M., Korblova E., Shao R., Maclennan J. E., Link D. R., Glaser M. A. and Clark N. A. *Science* **2000**, *288*, 2181-2184.
79. Nastishin Y. A., Achard M. F., Nguyen H. T. and Kleman M. *Eur. Phys. J. E.* **2003**, *12*, 581-591.
80. Bedel J. P., Rouillon J. C., Marcerou J. P., Laguerre M., Nguyen H. T. and Achard M. F. *Liq. Cryst.* **2000**, *27*, 1411-1421.
81. Pelzl G., Diele S., Jakli A., Liscka C., Wirth I. and Weissflog W. *Liq. Cryst.* **1999**, *26*, 135-139.
82. Coleman D. A., Fernsler J., Chattham N., Nakata M., Takanishi Y., Korblova E., Link D. R., Shao R.-F., Jang W. G., Maclennan J. E., Mondainn-Monval O., Boyer C., Weissflog W., Pelzl G., Chien L.-C., Zasadzinski J., Watanabe J., Walba D. M., Takezoe H. and Clark N. A. *Science* **2003**, *301*, 1204-1211.
83. Jin J. J., Kong C. S. and Kung B. Y. *Bull. Korean. Chem. Soc.* **1990**, *11*, 245-249.
84. Akutagawa T., Matsunaga Y. and Yasuhara K. *Liq. Cryst.* **1994**, *17*, 659-666.
85. Takanishi Y., Izumi T., Watanabe J., Ishikawa K., Takezoe H. and Iida A. *J. Mater. Chem.* **1999**, *9*, 2771-2774.
86. Yelamaggad C. V., Anitha Nagamani S., Hiremath U. S., Shankar Rao D. S. and Krishna Prasad S. *Liq. Cryst.* **2002**, *29*, 1401-1408.
87. Prasad V., Shankar Rao D. S. and Prasad S. K. *Liq. Cryst.* **2001**, *28*, 643-646.
88. Shen D., Diele S., Wirth I. and Tschierske C. *Chem. Commun.* **1998**, 2573-2574.
89. Amaranatha Reddy R., Sadashiva B. K. and Dhara S. *Chem. Commun.* **2001**, 1972-1973.
90. Thisayukta J., Niwano H., Takezoe H. and Watanabe J. *J. Am. Chem. Soc.* **2002**, *124*, 3354-3358.
91. Gimeno N., Ros M. B., Serrano J. L. and Rosario de la Fuente M. *Angew. Chem. Int. Ed.* **2004**, *43*, 5235-5238.
92. Schmalfuss H., Shen D., Tschierske C. and Kresse H. *Liq. Cryst.* **1999**, *26*, 1767-1770.
93. Rauch S., Bault P., Sawade H., Heppke G., Nair G. G. and Jakli A. *Phys. Rev. E* **2002**, *66*, 021706.
94. Svoboda J., Novotna V., Kozmik V., Glogarova M., Weissflog W., Diele S. and Pelzl G. *J. Mater. Chem.* **2003**, *13*, 2104-2110.
95. Ortega J., de la Fuente M. R., Etxebarria J., Folcia C. L., Diez S., Gallastegui J. A., Gimeno N., Ros M. B. and Perez-Jubindo M. A. *Phys. Rev. E* **2004**, *69*, 011703.
96. Ortega J., Folcia C. L., Etxebarria J., Gimeno N. and Ros M. B. *Phys. Rev. E* **2003**, *68*, 011707.
97. Dantlgraber G., Shen D., Diele S. and Tschierske C. *Chem. Mater.* **2002**, *14*, 1149-1158.
98. Amaranatha Reddy R. and Sadashiva B. K. *Liq. Cryst.* **2000**, *27*, 1613-1623.
99. Mahajan R., Nandedkar H., Vora A. and Raina K. K. *Liq. Cryst.* **2004**, *31*, 161-167.
100. Keith C., Amaranatha Reddy R., Baumeister U. and Tschierske C. *J. Am. Chem. Soc.* **2004**, *126*, 14312-14313.
101. Achten R., Cuypers R., Giesbers M., Koudijs A., Marcelis A. T. M. and Sudhölter E. J. R. *Liq. Cryst.* **2004**, *31*, 1167-1174.
102. Amaranatha Reddy R., Sadashiva B. K. and Raghunathan V. A. *Chem. Mater.* **2004**, *16*, 4050-4062.

103. Yelamaggad C. V., Krishna Prasad S., Nair G. G., Shashikala I. S., Shankar Rao D. S., Lobo C. V. and Chandrasekhar S. *Angew. Chem. Int. Ed.* **2004**, *43*, 3429-3432.
104. Amaranatha Reddy R. and Sadashiva B. K. *Liq. Cryst.* **2004**, *31*, 1069-1081.
105. Shen D., Diele S., Pelzl G., Wirth I. and Tschierske C. *J. Mater. Chem.* **1999**, *9*, 661-672.
106. Sadashiva B. K. *Pramana* **1999**, *53*, 213-222.
107. Ortega J., Gallastegui J. A., Folcia C. L., Etxebarria J., Gimeno N. and Ros M. B. *Liq. Cryst.* **2004**, *31*, 579-584.
108. Kašpar M., Hamplová V., Novotná V., Glogarová M. and Vanek P. *J. Mater. Chem.* **2002**, *12*, 2221-2224.
109. Amaranatha Reddy R. and Sadashiva B. K. *Liq. Cryst.* **2002**, *29*, 1365-1367.
110. Amaranatha Reddy R. and Sadashiva B. K. *Liq. Cryst.* **2003**, *30,* 273-283.
111. Sadashiva B. K., Murthy H. N. S. and Dhara S. *Liq. Cryst.* **2001**, *28*, 483-487.
112. Umadevi S. and Sadashiva B. K. *Liq. Cryst.* **2005**, *32*, 287-297.
113. Weissflog W., Nadasi H., Dunemann U., Pelzl G., Diele S., Eremin A. and Kresse H. *J. Mater. Chem.* **2001**, *11*, 2748-2758.
114. Dunemann U., Schröder M. W., Pelzl G., Diele S. and Weissflog W. *Liq. Cryst.* **2005**, *32*, 151-161.
115. Shin S.-T., Choi H., Lee C.-K., Kwon S.-S., Kim T.-S., Choi E. J., Kim S.-Y., Zin W.-C., Kim D.-C. and Chien L.-C. *Liq. Cryst.* **2004**, *31*, 935-940.
116. Weissflog W., Sokolowski S., Dehne H., Das B., Grande S., Schröder M. W., Eremin A., Diele S., Pelzl G. and Kresse H. *Liq. Cryst.* **2004**, *31*, 923-933.
117. Pelzl G., Diele S., Grande S., Jakli A., Lischka C., Kresse H., Schmalfuss H., Wirth I. and Weissflog W. *Liq. Cryst.* **1999**, *26*, 401-413.
118. Fodor-Csorba K., Vajda A., Galli G., Jákli A., Demus D., Holly S. and Gács-Baitz E. *Macromol. Chem. Phys.* **2002**, *203*, 1556-1563.
119. Pelzl G., Eremin A., Diele S., Kresse H. and Weissflog W. *J. Mater. Chem.* **2002**, *12*, 2591-2593.
120. Kang S., Thisayukta J., Takezoe H., Watanabe J., Ogino K., Doi T. and Takahashi T. *Liq. Cryst.* **2004**, *31*, 1323-1336.
121. Eremin A., Nadasi H., Pelzl G., Diele S., Kresse H., Weissflog W. and Grande S. *Phys. Chem. Chem. Phys.* **2004**, *6*, 1290-1298.
122. Fodor-Csorba K., Vajda A., Jákli A., Slugovc C., Trimmel G., Demus D., Gács-Baitz E., Holly S. and Galli G. *J. Mater. Chem.* **2004**, *14*, 2499-2506.
123. Pelzl G., Schröder M. W., Dunemann U., Diele S., Weissflog W., Jones C., Coleman D. A., Clark N. A., Stannarius R., Li J., Das B. and Grande S. *J. Mater. Chem.* **2004**, *14*, 2492-2498.
124. Kwon S.-S., Kim T.-S., Lee C.-K., Shin S.-T., Oh L.-T., Choi E.-J., Kim S.-Y. and Chien L.-C. *Bull. Korean Chem. Soc.* **2003**, *24*, 274-278.
125. Lee C.-K., Kwon S.-S., Chien L.-C. and Choi E.-J. *Bull. Korean Chem. Soc.* **2000**, *21*, 1155-1158.
126. Kresse H., Schlacken H., Dunemann U., Schröder M. W., Pelzl G. and Weissflog W. *Liq. Cryst.* **2002**, *29*, 1509-1512.
127. Weissflog W., Dunemann U., Schröder M. W., Diele S., Pelzl G., Kresse H. and Grande S. *J. Mater. Chem.* **2005**, *15*, 939-946.
128. Fodor-Csorba K., Jákli A. and Galli G. *Macromol. Symp.* **2004**, *218*, 81-88.
129. Dunemann U., Schröder M. W., Amaranatha Reddy R., Pelzl G., Diele S. and Weissflog W. *J. Mater. Chem.* **2005**, *15*, 4051-4061.
130. Shreenivasa Murthy H. N. and Sadashiva B. K. *J. Mater. Chem.* **2003**, *13*, 2863-2869.
131. Jakli A., Lischka C., Weissflog W., Pelzl G. and Saupe A. *Liq. Cryst.* **2000**, *27*, 1405-1409.

132. Salfetnikova J., Nadasi H., Weissflog W., Hauser A. and Kresse H. *Liq. Cryst.* **2002**, *29*, 115-119.
133. Shreenivasa Murthy H. N. and Sadashiva B. K. *Liq. Cryst.* **2004**, *31*, 567-578.
134. Heppke G., Parghi D. D. and H., S. *Ferroelectrics* **2000**, *243*, 269-276.
135. Lee C.-K., Kim J.-H., Choi E. J., Zin W.-C. and Chien L.-C. *Liq. Cryst.* **2001**, *28*, 1749-1754.
136. Hird M., Goodby J. W., Gough N. and Toyne K. J. *J. Mater. Chem.* **2001**, *11*, 2732-2742.
137. Shreenivasa Murthy H. N. and Sadashiva B. K. *Liq. Cryst.* **2004**, *31*, 1337-1346.
138. Shreenivasa Murthy H. N. and Sadashiva B. K. *Liq. Cryst.* **2004**, *31*, 1347-1356.
139. Pyc P., Mieczkowski J., Pociecha D., Gorecka E., Donnio B. and Guillon D. *J. Mater. Chem.* **2004**, *14*, 2374-2379.
140. Shreenivasa Murthy H. N. and Sadashiva B. K. *J. Mater. Chem.* **2004**, *14*, 2813-2821.
141. Shubashree S., Sadashiva B. K. and Dhara S. *Liq. Cryst.* **2002**, *29*, 789-797.
142. Bedel J. P., Rouillon J. C., Marcerou J. P., Laguerre M., Nguyen H. T. and Achard M. F. *J. Mater. Chem.* **2002**, *12*, 2214-2220.
143. Nguyen H. T., Bedel J. P., Rouillon J. C., Marcerou J. P. and Achard M. F. *Pramana* **2003**, *61*, 395-404.
144. Wang K., Jakli A., Li H., Yang Y. and Wen J. *Liq. Cryst.* **2001**, *28*, 1705-1708.
145. Dehne H., Pötter M., Sokolowski S., Weissflog W., Diele S., Pelzl G., Wirth I., Kresse H., Schmalfuss H. and Grande S. *Liq. Cryst.* **2001**, *28*, 1269-1277.
146. Matyus E. and Fodor-Csorba K. *Liq. Cryst.* **2003**, *30*, 445-450.
147. Shreenivasa Murthy H. N. and Sadashiva B. K. *Liq. Cryst.* **2003**, *30*, 1051-1055.
148. Wirth I., Diele S., Eremin A., Pelzl G., Grande S., Kovalenko L., Pancenko N. and Weissflog W. *J. Mater. Chem.* **2001**, *11*, 1642-1650.
149. Kovalenko L., Schröder M. W., Amaranatha Reddy R., Diele S., Pelzl G. and Weissflog W. *Liq. Cryst.* **2005**, *32*, 857-865.
150. Lee C.-K., Kwon S.-S., Kim T.-S., Choi E.-J., Shin S.-T., Zin W.-C., Kim D.-C., Kim J.-H. and Chien L.-C. *Liq. Cryst.* **2003**, *30*, 1401-1406.
151. Gorecka E., Pociecha D., Araoka F., Link D. R., Nakata M., Thisayukta J., Takanishi Y., Ishikawa K., Watanabe J. and Takezoe H. *Phys. Rev. E* **2000**, *62*, R4524-R4527.
152. Maclennan J. E., Clark N. A. and Walba D. M. *Phys. Rev. E* **2001**, *64*, 031706.
153. Rauch S., Selbmann C., Bault P., Sawade H., Heppke G., Morales-Saavedra O., Huang M. Y. M. and Jákli A. *Phys. Rev. E* **2004**, *69*, 021707.
154. Nakata M., Link D. R., Araoka F., Thisayukta J., Takanishi Y., Ishikawa K., Watanabe J. and Takezoe H. *Liq. Cryst.* **2001**, *28*, 1301-1308.
155. Nakata M., Link D. R., Thisayukta J., Takanishi Y., Ishikawa K., Watanabe J. and Takezoe H. *J. Mater. Chem.* **2001**, *11*, 2694-2699.
156. Kumazawa K., Nakata M., Araoka F., Takanishi Y., Ishikawa K., Watanabe J. and Takezoe H. *J. Mater. Chem.* **2004**, *14*, 157-164.
157. Amaranatha Reddy R., Sadashiva B. K. and Baumeister U. *J. Mater. Chem.* **2005**, *15*, 3303-3316.
158. Gorecka E., Pociecha D., Mieczkowski J., Matraszek J., Guillon D. and Donnio B. *J. Am. Chem. Soc.* **2004**, *126*, 15946-15947.
159. Kardas D., Prehm M., Baumeister U., Pociecha D., Amaranatha Reddy R., Mehl G. H. and Tschierske C. *J. Mater. Chem.* **2005**, *15*, 1722-1733.
160. Cristiano R., Ely F. and Gallardo H. *Liq. Cryst.* **2005**, *32*, 15-25.
161. Budig H., Diele S., Göring P., Paschke R., Sauer C. and Tschierske C. *Chem. Commun.* **1994**, 2359-2360.
162. Kishikawa K., Nakahara S., Nishikawa Y., Kohmoto S. and Yamamoto M. *J. Am. Chem. Soc.* **2005**, *127*, 2565-2571.

163. Amaranatha Reddy R., Schröder M. W., Bodyagin M., Kresse H., Diele S., Pelzl G. and Weissflog W. *Angew. Chem. Int. Ed.* **2005**, *44*, 774-778.
164. Amaranatha Reddy R. and Sadashiva B. K. *J. Mater. Chem.* **2002**, *12*, 2627-2632.
165. Lee S. K., Heo S., Lee J. G., Kang K.-T., Kumazawa K., Nishida K., Shimbo Y., Takanishi Y., Watanabe J., Doi T., Takahashi T. and Takezoe H. *J. Am. Chem. Soc.* **2005**, *127*, 11085-11091.
166. Tschierske C. *Curr. Opin. Colloid Interface. Sc.* **2002**, *7*, 69-80.
167. Lose D., Diele S., Pelzl G., Dietzmann E. and Weissflog W. *Liq. Cryst.* **1998**, *24*, 707-717.
168. Chen B., Zeng X., Baumeister U., Ungar G. and Tschierske C. *Science* **2005**, *307*, 96-99.
169. Goodby J. W., Mehl G. H., Saez I. M., Tuffin R. P., Mackenzie G., Auzély-Velty R., Benvegnu T. and Plusquellec D. *Chem. Commun.* **1998**, 2057-2070.
170. Guillon D., Osipov M. A., Mery S., Siffert M., Nicoud J.-F., Bourgogne C. and Sebastiao P. *J. Mater. Chem.* **2001**, *11*, 2700-2708.
171. Sha Y.-A., Hsiue G.-H., Chiu C.-H., Jeng R.-J. and Tai H.-C. *Liq. Cryst.* **2003**, *30*, 71-80.
172. Dantlgraber G., Eremin A., Diele S., Hauser A., Kresse H., Pelzl G. and Tschierske C. *Angew. Chem. Int. Ed.* **2002**, *41*, 2408-2412.
173. Dantlgraber G., Diele S. and Tschierske C. *Chem. Commun.* **2002**, 2768-2769.
174. Keith C., Amaranatha Reddy R., Hahn H., Lang H. and Tschierske C. *Chem. Commun.* **2004**, 1898-1899.
175. Dantlgraber G., Baumeister U., Diele S., Kresse H., Luhmann B., Lang H. and Tschierske C. *J. Am. Chem. Soc.* **2002**, *124*, 14852-14853.

2

Symmetrical dimer liquid crystals
with tilted smectic phases

Three series of symmetrical dimer liquid crystals, i.e. bis(dodecyloxy-benzoyloxybenzoyloxy)-alkanes (BC12) and bis(dodecyloxy- and hexadecyloxybenzoyloxy-phenyl)alkane-dicarboxylates (QC12 and QC16) with a spacer ranging from two to eight methylene units, have been synthesized and their thermotropic properties were determined. The isotropization temperatures show a pronounced odd – even effect as a function of the parity of the spacers. Most compounds exhibit a SmC mesophase. The QC12 and QC16 compounds, with an octylene spacer, possess an additional low temperature tilted hexatic mesophase. Changing the orientation of the ester group as in the BC12 series results in a dramatic change of the thermotropic behavior.

2.1   Introduction

Dimeric liquid crystals containing two rigid monomeric units connected via a flexible alkylene spacer, have been investigated intensively in the last two decades [1-5]. One of the most important reasons why these compounds gain so much interest is because their properties are quite different from monomeric liquid crystals. Furthermore, their ability to act as model compounds for semi-flexible main-chain liquid crystalline polymers is very important.

We can distinguish two classes of liquid crystalline dimers: non-symmetric [5,6] and symmetric compounds. The vast majority of dimeric liquid crystals reported in literature may be termed symmetric because the mesogenic groups are identical. The phase behavior of such compounds is significantly influenced by the structure and length of the spacer as well as by the nature and position of the linking groups [7]. The alternations in isotropization temperatures and associated enthalpy changes found for these dimers is attributed to the different number of conformations with parallel (or non-parallel) orientations of the mesogenic units for *odd* and *even* dimers. Though very important, the spacer parity is not the only part of a dimeric liquid crystal that determines the thermotropic properties and liquid crystalline ordering. The mesogenic parts and (alkyl) tails play a very important role as well.

Recently, Choi *et al.* [8] have reported that dimeric compounds with a flexible pentyl spacer, α,ω-bis{4-[(4-n-dodecylphenyl)iminomethyl]benzoyloxy}pentane, gave phases possessing antiferroelectric switching behavior similar to banana-shaped liquid crystals having a 1,3-phenylene core.
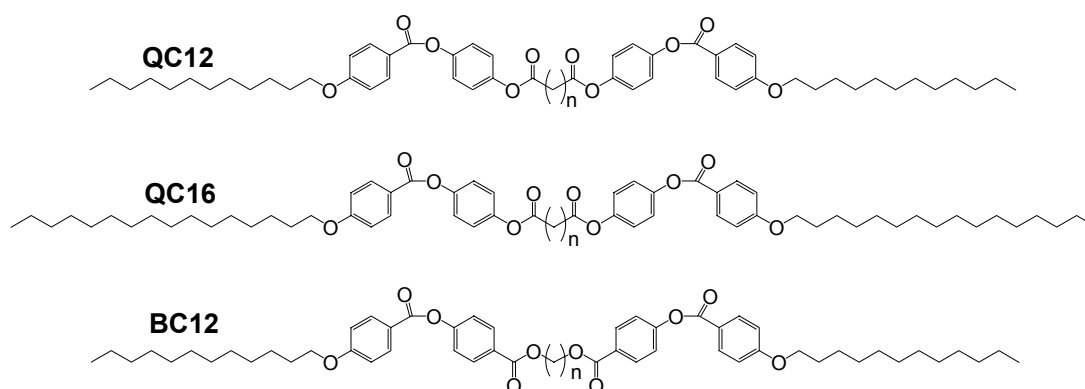

Figure 1. *Three series of dimer liquid crystals that were studied.*

We have synthesized three series of dimeric compounds with varying spacer length and studied their liquid crystalline properties (figure 1). All series contain ester groups as connecting units between the aromatic rings. In this way, the hydrolysis

sensitive imine bonds present in the compounds reported by Choi *et al.* [8] were avoided.

2.2   Experimental

The series of compounds that we have investigated are depicted in figure 1. The **QC12** and **QC16** series (n = 2-8), which differ in their terminal alkyl chain length (12 vs 16 carbon atoms), were synthesized according to scheme 1.
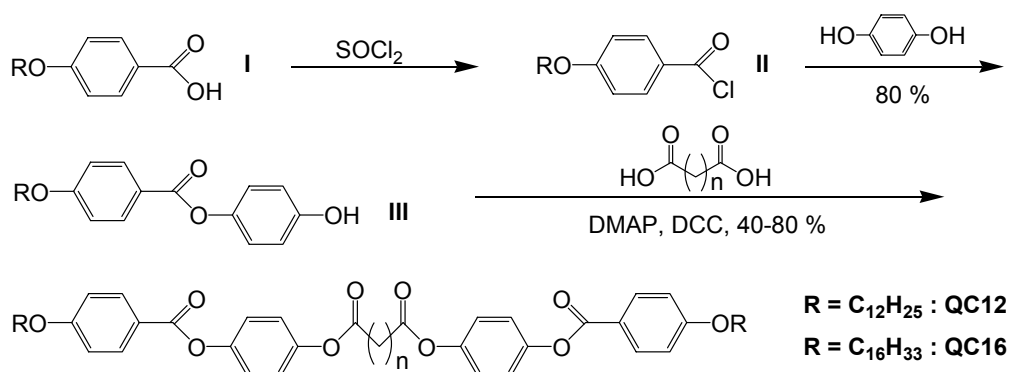
Scheme 1. *Synthesis of series QC12 and QC16.*

Carboxylic acid **I** was transformed into the acid chloride **II** with thionyl chloride and subsequently coupled to an excess of hydroquinone to yield the phenolic compound **III** in 80% yield. The end products were prepared by direct esterification of the appropriate diacids with the monomeric phenols using N,N'-dicyclohexylcarbodiimide and 4-dimethylaminopyridine as a catalyst.
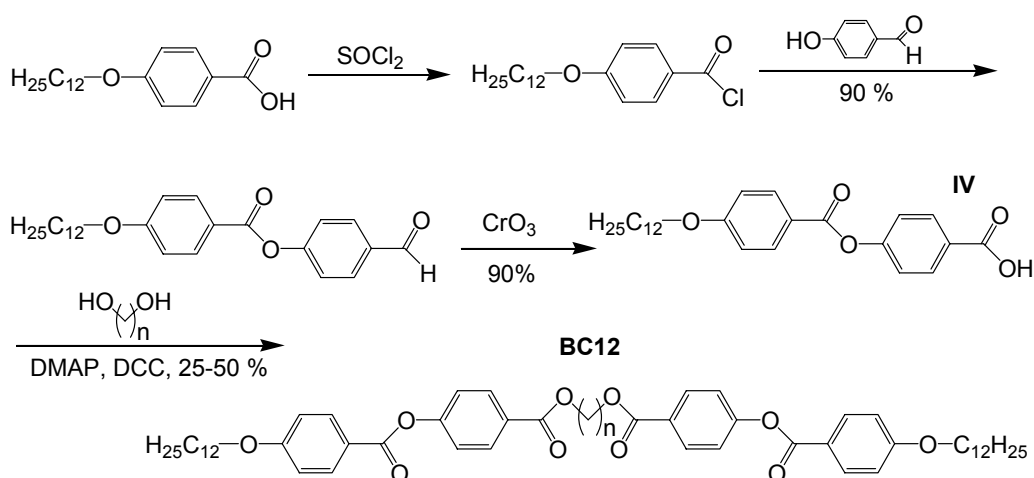
Scheme 2. *Synthesis of series BC12.*

The **BC12** series (*n* = 2-8) was synthesized according to scheme 2. 4-Dodecyloxy-benzoic acid was first reacted with thionyl chloride to its acid chloride and subsequently coupled to 4-hydroxybenzaldehyde to yield the corresponding aldehyde in 90%. Oxidation of this aldehyde with CrO_3 gave the carboxylic acid **IV** in 90% yield. Finally, the dimers **BC12** were prepared by direct esterification of the appropriate diols with the carboxylic acids **IV**, using N,N'-dicyclohexylcarbodiimide and 4-dimethylaminopyridine as a catalyst.

2.3   Results and discussion

The transition temperatures together with the associated transition enthalpies for the series **QC12** and **QC16** are given in table 1. All compounds exhibit liquid crystalline phases, their mesophases were characterized by polarizing optical microscopy and differential scanning calorimetry (DSC) as well as by X-ray diffraction measurements.

Table 1. *Transition temperatures (ºC) and transition enthalpies (kJ mol^{-1}; between square brackets) for series **QC12** and **QC16**.*

	Cr	SmF	SmC	N	I
QC12					
n=2	• 143 [31]		• 195 [13]		•
n=3	• 141 [49]		• 150 [14]		•
n=4	• 123 [29]		• 182 [18]		•
n=5	• 130 [50]		• 135 [6]	• 137 [3]	•
n=6	• 141 [38]		• 165 [19]		•
n=7	• 130 [41]		(• 127 [7])	• 132 [3]	•
n=8	• 131 [28]	• 132 [8]	• 149 [20]		•
QC16					
n=2	• 137 [32]		• 195 [17]		•
n=3	• 134 [56]		• 154 [17]		•
n=4	• 116 [38]		• 180 [18]		•
n=5	• 124 [58]		• 142 [16]		•
n=6	• 128 [28]		• 167 [21]		•
n=7	• 124 [48]		• 136 [18]		•
n=8	• 121 [35]	• 129 [8]	• 151 [24]		•

The dependence of the transition temperatures on the length of the spacer of series **QC12** is shown in Figure 2. The clearing temperatures show a marked alternation in which the even members have the higher values. The melting points show no alternating trend. All compounds (*n* = 2-8) show *Schlieren* textures (figure 3a) indicating a tilted smectic mesophase (SmC). Two brush singularities could not be observed in the *Schlieren* texture, indicating a synclinic ordering of the molecules [9]. The *n* = 5 and *n* = 7 compounds possess an additional nematic mesophase (N) in a narrow temperature interval. This could be caused by the fact that dimers with odd spacers are less ordered in their liquid crystalline phases than those with even spacers. Compounds from the same series with other lengths of the terminal tails also showed nematic and smectic C phases [10]. Most striking in series **QC12**, is the additional low temperature tilted smectic mesophase observed for the *n* = 8 compound. This transition is indicated by a partial disappearance of the *Schlieren texture*, and appearance of a *Mosaic-Schlieren* texture (figure 3), which points to a low temperature SmF phase [9].
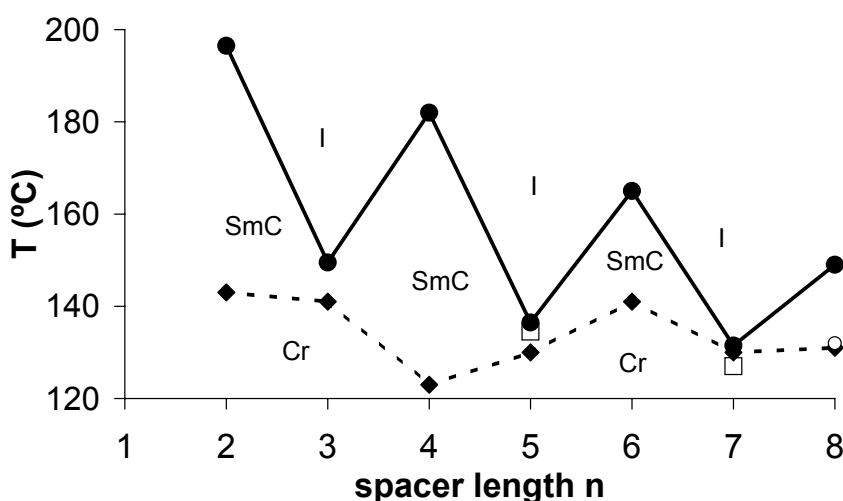

Figure 2. *Dependence of the melting points (- -♦- -), SmC-N transitions (□), SmF-SmC transition (o) and isotropization temperatures (—●—) on the number of methylene groups in the spacer of series **QC12**.*

From the Bragg reflections in the small angle region, the layer spacing *d* from the smectic layers in series **QC12** was determined (Figure 4). It was found that the layer spacing for the smectic phases do not change markedly with temperature. Figure 4 shows that the *n* = 8 compound exhibits two smectic modifications. The layer spacing increases discontinuously at the smectic-smectic transition.

From the broad wide angle diffraction band a liquid-like order in the high temperature SmC mesophase is confirmed. The low temperature smectic mesophase

for $n = 8$ shows one sharp peak in the wide angle region at 4.5 Å. This corresponds to the side-to-side separation of the molecules, and confirms the presence of a tilted hexatic SmF mesophase.
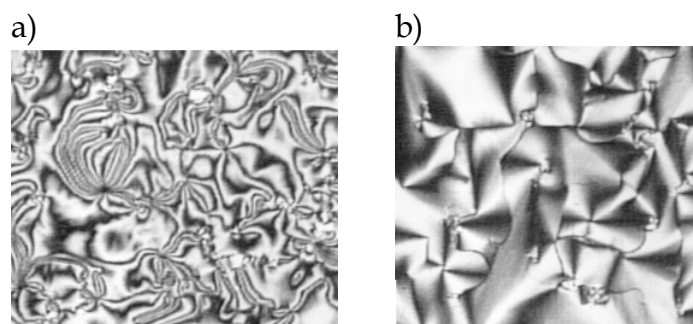

Figure 3. *Optical texture change from a) SmC (145ºC) to b) SmF (130ºC) for **QC12** n = 8.*
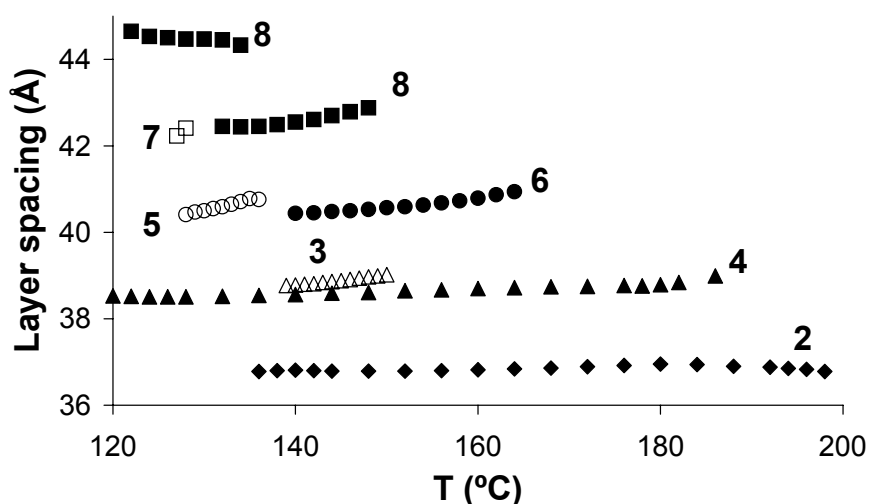

Figure 4. *Temperature dependence of the layer spacing of series **QC12** (n = 2-8).*

The thermotropic properties of series **QC16** are also given in table 1. Their properties are very similar to those of the **QC12** series, except that the nematic phases are absent in this series. As in the **QC12** series, the compound with $n = 8$ shows two smectic phases.

The thermotropic behavior of series **BC12** in which the ester bond between the mesogenic units and the spacer is reversed is given in table 2. The small change in chemical structure (**QC12** vs **BC12**) changes the liquid crystalline properties of these compounds dramatically. The liquid crystalline range becomes significantly smaller and three different mesophases are present in this series. The $n = 6$ and $n = 8$ compounds have only a nematic phase, the $n = 3$ and $n = 5$ compounds are only SmA and the $n = 2$ and $n = 7$ compounds only show a tilted smectic phase (SmC). The $n = 4$ compound has a SmC-N transition. Apparently, in this series the tilted smectic phases quickly become unfavorable for the even members and for the higher

members only nematic phases are observed, while the ordering of the odd members increases from SmA for $n = 3$ and 5 to a tilted smectic for $n = 7$.

*Table 2. Transition temperatures (^{o}C) and transition enthalpies (kJ mol^{-1}; between square brackets) for series **BC12**.*

BC12	Cr			SmC			SmA		N			I
n=2	•	131	[55]	•	137	[23]						•
n=3	•	107	[68]				(• 101 [10])					•
n=4	•	125	[75]	(•	113	[3])			•	126	[10]	•
n=5	•	86	[41]				•	98 [10]				•
n=6	•	104	[44]						•	111	[11]	•
n=7	•	72	[57]	•	88	[15]						•
n=8	•	111	[102]						(• 105 [13])			•

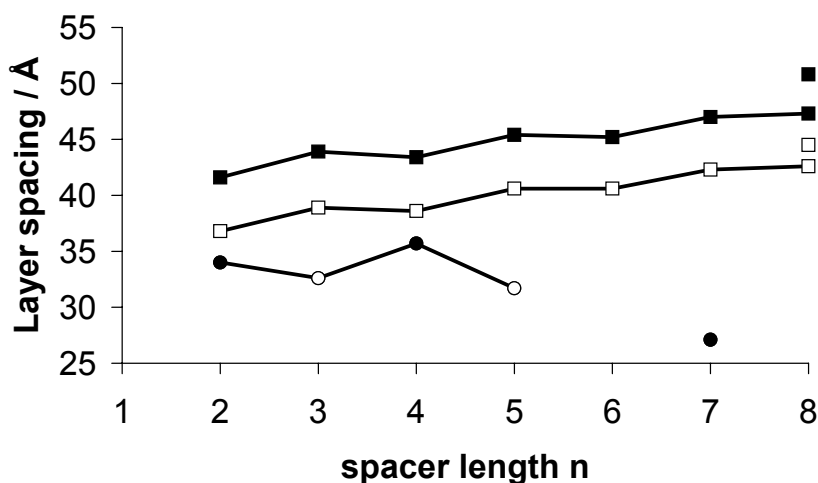*Figure 5. Dependence of the average layer spacings of the **QC12** series (——□——), the **QC16** series (——■——) and the **BC12** series (SmA (——o——) and SmC (——●——)) on the number of methylene groups in the spacer.*

The layer spacings for the three series of compounds are depicted in figure 5. The layer spacings for the **QC12** and **QC16** series increase with increasing spacer length as one would expect. The layer thickness of the **QC16** compounds is on average 4.8 Å larger than that of the corresponding **QC12** compounds. The increase in layer spacings with spacer length is not linear; this is probably caused by different conformations or tilt angles of the "odd" molecules in comparison with the "even" molecules. At the transition from the SmC to the higher ordered tilted SmF phase for the $n = 8$ compounds, the layer spacings increases ~2 Å (**QC12**) and ~3 Å (**QC16**). These changes in layer spacings are probably caused by the formation of the hexatic

mesophase accompanied by a decrease in tilt angle of the molecules. SmC-SmF transitions have in the past shown to be accompanied by a sudden jump of the tilt angle [11].

The layer spacings for the **BC12** series show an unexpected behavior since they seem to decrease with increasing spacer length. For the SmC compounds (n = 2, 4 and 7), there is a transition from a strongly tilted SmC phase (n = 2 and 4) to an intercalated layer structure for the n = 7 compound. For n = 7, the estimated all-*trans* molecular length of this compound is about twice the layer thickness. The SmA compounds (n = 3 and 5) both have d-spacings, which are roughly half the molecular length, pointing to an intercalated SmA phase. The larger layer spacing for the n = 3, if compared to n = 5, is still unclear. A comparable phenomenon was observed in a similar series of compounds with shorter terminal chains [12], but no explanation was given. The absence of a smectic phase for n = 6 could indicate a spacer-dependent change in smectic organization upon going from short to long spacers.

2.4   Conclusions

All the compounds of the three series of dimers exhibit liquid crystalline phases. The compounds of the **QC12** and **QC16** series show a tilted smectic mesophase (SmC) and a strong odd-even effect in the isotropization temperatures. The increase in terminal alkyl tail suppresses the nematic mesophase. Both n = 8 compounds show an additional low temperature tilted hexatic mesophase, probably SmF. This low temperature mesophase has an increased layer spacing probably caused by a decrease in tilt angle.

A small change in chemical structure (**QC12** vs **BC12**) results in a dramatic change in liquid crystalline properties of the **BC12** series. Besides tilted smectic and nematic phases these compounds also form intercalated SmA phases. The layer spacings of the smectic phases of this **BC12** series show an unexpected trend since there is a slight decrease in layer spacings for the compounds with the longest spacers. This could be related to a change from monolayer or partially interdigitated smectic structure for small n (2 and 4) to an interdigitated or intercalated smectic structure for longer n. The odd and even members of this series seem to show a different trend with increasing spacer length.

2.5   References

1.   Weissflog W., Lischka C., Diele S., Wirth I. and Pelzl G. *Liq. Cryst.* **2000**, *27*, 43-50.

2.   Prasad V., Shankar Rao D. S. and Krishna Prasad S. *Liq. Cryst.* **2001**, *28*, 761-767.
3.   Date R. W., Imrie C. T., Luckhurst G. R. and Seddon J. M. *Liq. Cryst.* **1992**, *12*, 203-238.
4.   Watanabe J., Izumi T., Niori T., Zennyoji M., Takanishi Y. and Takezoe H. *Mol. Cryst. Liq. Cryst.* **2000**, *346*, 77-86.
5.   Attard G. S., Date R. W., Imrie C. T., Luckhurst G. R., Roskilly S. J., Seddon J. M. and Taylor L. *Liq. Cryst.* **1994**, *16*, 529-581.
6.   Marcelis A. T. M., Koudijs A. and Sudhölter E. J. R. *Liq. Cryst.* **1995**, *18*, 843-850.
7.   Imrie C. T. and Luckhurst G. R. *Handbook of liquid crystals* **1998**, *2B*, 801.
8.   Choi S.-W., Zennyoji M., Takanishi Y., Takezoe H., Niori T. and Watanabe J. *Mol. Cryst. Liq. Cryst.* **1999**, *328*, 185-192.
9.   Nishiyama I., Yamamoto J., Goodby J. W. and Yokoyama H. *J. Mater. Chem.* **2003**, *13*, 2429-2435.
10.   Mori A., Takemoto M. and Ujiie S. *Mol. Cryst. Liq. Cryst.* **2004**, *411*, 163-167.
11.   Guillon D., Skoulios A. and Benattar J. J. *J. de Physique* **1986**, *47*, 133-138.
12.   Aguilera C. *Polymer Bulletin* **1998**, *41*, 267-274.

Liquid crystalline properties of salicylaldimine-based dimers

The synthesis and thermotropic properties of four homologous series of salicylaldimine-based dimer liquid crystals are reported. Two 4-(4-alkoxy-2-hydroxybenzylideneamino)benzoyloxy groups are connected to a central part consisting of a 1,3-phenylene, 1,5-pentylene, 2,2-dimethyl-1,5-pentylene or 3,3-dimethyl-1,5-pentylene unit. All compounds of the series with the central phenyl part exhibit enantiotropic B-phases, and the sequence B_6-B_1-B_2 on increasing terminal chain length was observed. Replacement of the central phenyl with a pentyl spacer partly suppresses formation of B-phases. The longer homologues of this series show the B_1 phase, while the shorter exhibit an intercalated SmC_c mesophase. The introduction of methyl substituents to the pentyl spacer causes the melting points to fall dramatically and formation of B-phases is totally suppressed.

3.1   Introduction

Before 1996 (anti)ferroelectricity in liquid crystals was restricted to phases consisting of molecules with a chiral molecular structure. Niori *et al.* [1] were the first to report this striking phenomenon in phases composed of non-chiral molecules with a bent or banana shape. In recent years, a variety of banana-shaped molecules have been synthesized and studied. Banana-shaped compounds can form new smectic and two-dimensional ordered phases, which are different from those obtained from normal calamitic molecules. According to recommendations of the workshop on Banana-shaped Liquid Crystals: Chirality by Achiral Molecules, held in Berlin in 1997, these phases are simply designated B_1 to B_7. Since this nomenclature does not take the structure and symmetry of the mesophase into account, it can be considered as a preliminary nomenclature. At this moment it is still difficult to establish a direct relationship between observed optical microscopy textures and phase assignment.

From the seven B-phases known to date now the B_3 and B_4 phase [2] are "solid-like"; the B_4 phase is also designated as the "blue phase" [3]. The B_1 (Col_r) phase is a two-dimensional periodic phase [4,5] and the B_6 phase can be compared to an intercalated SmC phase, but is generated by bent molecules [2].

At least three of the B-phases possess electro-optical switching properties. The B_2 (SmCP) phase, first described by Niori *et al*. [1] is the most frequently investigated banana mesophase, which is associated with antiferroelectric characteristics. The B_5 mesophase has an additional short range order within the layer, but shows the same electro-optic response as the B_2 phase [6]. The B_7 phase corresponds to different phases all exhibiting the characteristic textures seen in the original B_7 phase of nitro compounds [7]. Recently, high resolution experiments have proven that the B_7 phase is a modulated smectic phase with splay polarization [8]. "New" banana phases are already reported [9] and it is very likely that additional new mesophases will be reported in the future.

To understand the relationship between molecular structure and mesomorphic properties, banana-shaped compounds can be designed in numerous different ways. Most molecules that exhibit banana-phases (containing five, six or seven phenyl rings) are composed of symmetrical resorcinol derivatives substituted at the 1 and 3 position [9-14]. Also, the 3,4'-disubstituted biphenyl central fragment has proven to be a suitable building block for obtaining banana-shaped molecules [5,15,16]. Another way to design molecules with a bent shape is by the introduction of a central alkylene chain with an odd number of flexible units between two mesogenic units [17-20]. These compounds however are not so often studied as their aromatic counterparts. Compounds with an even number of flexible units between the two mesogenic

groups have also been reported to show switching properties [21]. The introduction of substituents to the central spacer seems to promote the formation of intercalated layer structures [22,23]. The linking groups between the wings of the aromatic fragments of the bent-shaped molecule can also be varied, and the most common are the imine and ester linking groups. The introduction of lateral substituents (fluorine [24], chlorine [25,26], methyl [27], methoxy [28], cyano [29,30], nitro [31], bromine [32] or a combination of different substituents [33,31]) in the wings or in the central part of a banana-shaped compound is also used to modify the thermotropic properties of bent-shaped molecules. The length of the terminal alkyl(oxy) chain or fluorination of the terminal chain can also have a pronounced effect on the mesomorphic properties of bent-shaped molecules.
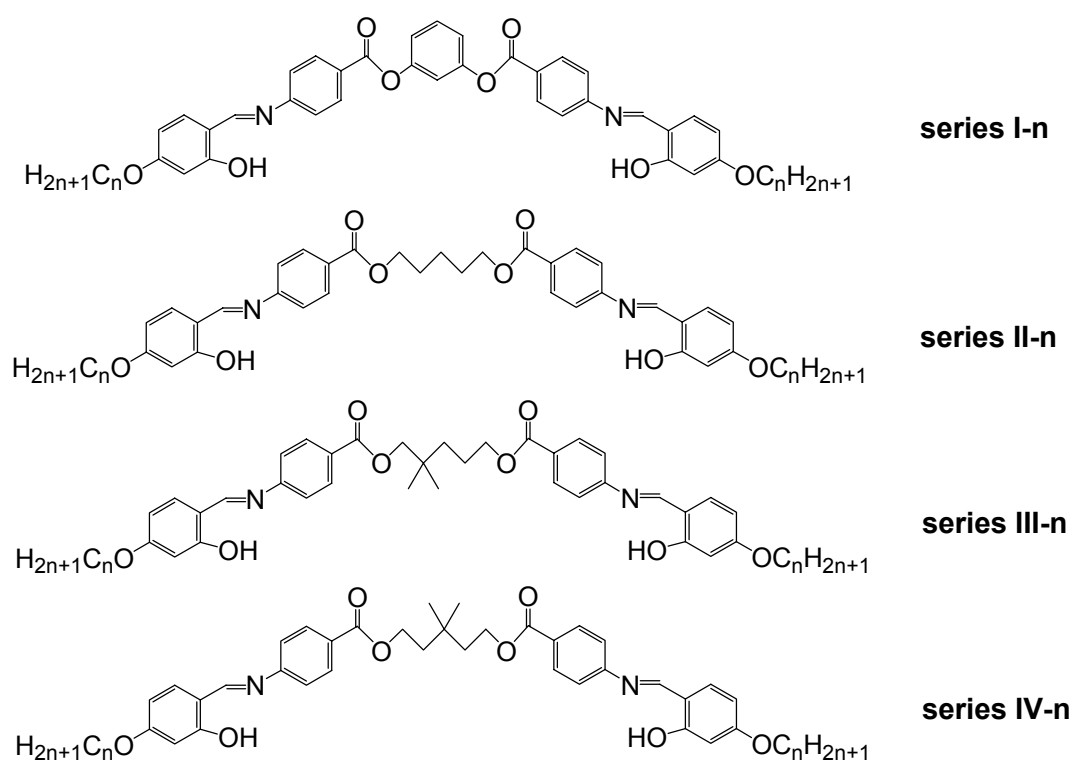

Figure 1. *Structures of the series **I-n**, **II-n**, **III-n** and **IV-n**.*

In recent years, several homologous series of banana-shaped compounds have been synthesized and studied. In most cases, only a limited number of homologues were prepared; in particular, compounds with short terminal chains are often missing. Instead of the unstable, light and moisture-sensitive imine bond, which is often used in banana-shaped compounds, we have prepared four series of more stable salicylaldimine-based dimers with terminal chains ranging from 4 to 16 carbon atoms in length. To study the influence of the central part of the molecule on the liquid crystalline properties we prepared four series of compounds so that the nature

of the connecting group between the two salicylaldimine wings was varied; phenyl (series **I-*n***), pentyl (series **II-*n***), 2,2-dimethylpentyl (series **III-*n***) and 3,3-dimethylpentyl (**IV-*n***) (figure 1). Three compounds of the **I-*n*** series (*n* = 9, 10 and 16) have been extensively studied by other groups [34-36], and the **II-*n*** series was partly studied by Yelamaggad *et al.* [37]. In the present study, we describe all compounds of the **I-*n*** and **II-*n*** series (*n* = 4-12, 14 and 16). In addition, we have prepared and studied two series in which the central pentyl spacer was symmetrically substituted (**IV-*n***) and non-symmetrically substituted (**III-*n***) with two methyl groups.

3.2   Experimental

3.2.1   Synthesis

The four series of compounds were prepared according to scheme 1. For the series with the methyl-substituted pentyl spacers (series **III-*n*** and **IV-*n***), the diols were prepared by reduction of the appropriate substituted glutaric acids with LiAlH$_4$ in THF according to the method used by Eilbracht *et al.* [38]. For the **I-*n*** and **II-*n*** series, the central diols (resorcinol and 1,5-pentanediol) were obtained from Aldrich. The synthesis of the aldehydes **3-*n*** was performed according to literature procedures [37].

The bis(4-nitrobenzoate) compounds **1a-d** were prepared by treating 4-nitrobenzoyl chloride with the appropriate diol in the presence of pyridine. Subsequently, the dinitro compounds **1a-d** were reduced by catalytic hydrogenation (H$_2$/Pd-C) to yield the diamines **2a-d**. The alkoxybenzaldehydes **3-*n*** were prepared by heating 2,4-dihydroxybenzaldehyde with 1-*n*-bromoalkanes in the presence of KHCO$_3$ and a catalytic amount of KI in MEK. Finally, the desired compounds were obtained by condensing 2-hydroxy-4-*n*-alkoxybenzaldehyde **3-*n*** with the diamino compounds **2a-d.**

All dimers gave NMR spectra in agreement with the proposed structure, and showed correct elemental analysis.

Since the preparation of the bis(4-nitrobenzoate) compounds **1a** and **1b** and the diamines **2a** and **2b** have been described elsewhere [37,35], we will only describe the synthesis of compounds **1c**, **1d**, **2c** and **2d**. From the final list of liquid crystal compounds, we will describe the synthesis of one short-tailed (*n* = 7) and one long-tailed (*n* = 14) compound of each series.

*1,5-Bis(4-nitrobenzoyloxy)-2,2-dimethylpentane (**1c**).*
In a 250 ml round-bottomed flask equipped with a nitrogen inlet and a septum 1.32 g (10.0 mmol, 1 equiv.) of 2,2-dimethyl-1,5-pentanediol was dissolved in 20 ml of dry

pyridine and 20 ml of dry benzene. The solution was then cooled in an ice-bath and a solution of 4-nitrobenzoyl chloride (4.65 g, 25 mmol, 2.5 equiv.) in 20 ml of dry benzene was added dropwise. The reaction mixture was stirred for 24h at room temperature; it was then acidified with 3 M HCl and extracted twice with CH_2Cl_2. The combined organic layers were washed successively with 1M NaOH (twice) and brine. The organic layer was dried over Na_2SO_4 and filtered; the filtrate was concentrated and the residue recrystallized from $CHCl_3$/MeOH. Yield 84%, Mp 114°C. ^{1}H NMR (200 MHz, $CDCl_3$): δ 8.30-8.15 (m, 8H, Ar), 4.37 (t, 2H, OCH_2), 4.13 (s, 2H, OCH_2C), 1.80 (m, 2H, CH_2), 1.54 (m, 2H, CCH_2), 1.07 (s, 6H, 2 x CH_3). Elemental analysis for $C_{21}H_{22}N_2O_8$ (M = 430.41): calc. C 58.60, H 5.15, N 6.51; found C 58.21, H 5.07, N 6.36%.
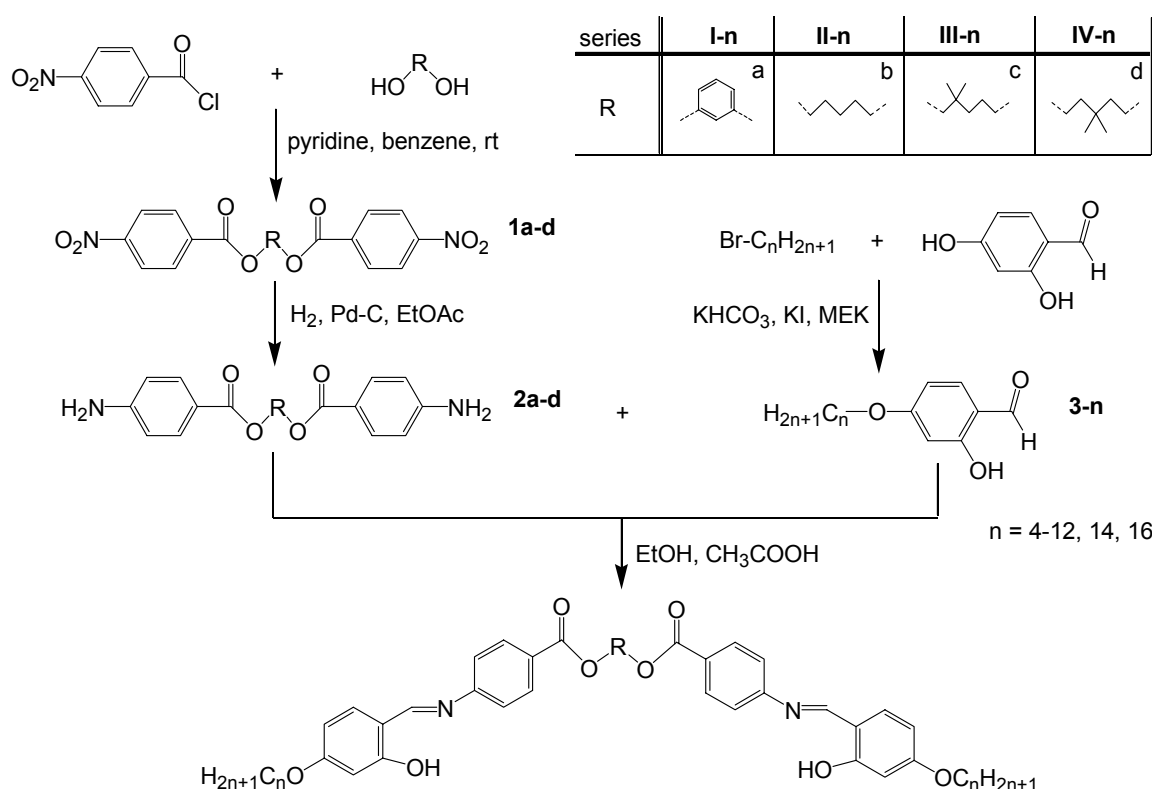
Scheme 1. *Synthetic pathways for the series **I-n**, **II-n**, **III-n** and **IV-n**.*

*1,5-Bis(4-nitrobenzoyloxy)-3,3-dimethylpentane (**1d**).*
This compound was prepared similarly to **1c**, from 3,3-dimethyl-1,5-pentanediol and 4-nitrobenzoyl chloride. Yield 91%, Mp 98-99°C. ^{1}H NMR (200 MHz, $CDCl_3$): δ 8.27 (d, 4H, Ar), 8.17 (d, 4H, Ar), 4.48 (t, 4H, 2 x OCH_2), 1.84 (t, 4H, 2 x CH_2), 1.10 (s, 6H, 2 x CH_3). Elemental analysis for $C_{21}H_{22}N_2O_8$ (M = 430.41): calc. C 58.60, H 5.15, N 6.51; found C 58.27, H 4.96, N 6.45%.

*1,5-Bis(4-aminobenzoyloxy)-2,2-dimethylpentane (**2c**).*

A mixture of 3.60 g (8.4 mmol) of compound **1c**, 70 ml dry ethyl acetate and 200 mg Pd-C (10%) was hydrogenated in a Parr apparatus at 4 bar for 3 h. The reaction mixture was then filtered to remove the catalyst and the solvent evaporated, yielding the pure product in quantitative yield as an oil. ^{1}H NMR (200 MHz, CDCl$_3$): δ 7.82 (m, 4H, Ar), 6.61 (m, 4H, Ar), 4.24 (t, 2H, OCH$_2$), 4.00 (s, 2H, OCH$_2$C), 1.72 (m, 2H, CH$_2$), 1.52 (m, 2H, CCH$_2$), 1.01 (s, 6H, 2 x CH$_3$).

*1,5-Bis(4-aminobenzoyloxy)-3,3-dimethylpentane (**2d**).*

This compound was prepared similarly to **2c**, from compound **1d**, in quantitative yield, Mp 105-106 ˚C. ^{1}H NMR (200 MHz, CDCl$_3$): δ 7.81 (d, 4H, Ar), 6.59 (d, 4H, Ar), 4.35 (t, 4H, OCH$_2$), 1.76 (t, 4H, CH$_2$), 1.04 (s, 6H, 2 x CH$_3$). Elemental analysis for C$_{21}$H$_{26}$N$_2$O$_4$ (M = 370.44): calc. C 68.09, H 7.07, N 7.56; found C 67.70, H 7.08, N 7.15%.

*General procedure for preparing the liquid crystals (**I-n**, **II-n**, **III-n** and **IV-n**).*

A mixture of the bis(4-aminobenzoate) **2a-d** (0.5 mmol, 1 equiv.), 2-hydroxy-4-alkoxybenzaldehyde **3-n** (1.0 mmol, 2.0 equiv.), absolute ethanol (15 ml) and a few drops of acetic acid was heated under reflux for 2h. After cooling, the yellow precipitate was collected by filtration and washed with hot absolute ethanol. The yellow crystals were finally recrystallized from methanol/chloroform. Yield 50-75%.

*1,3-Bis-[4-(2-hydroxy-4-heptyloxybenzylideneamino)-benzoyloxy]benzene (**I-7**).*

^{1}H NMR (200 MHz, CDCl$_3$): δ 13.38 (s, 2H, 2 x –OH), 8.57 (s, 2H, 2 x CH=N), 8.24 (d, 4H, Ar), 7.49 (t, 1H, Ar), 7.36-7.16 (m, 9H, Ar), 6.51 (m, 4H, Ar), 4.01 (t, 4H, 2 x OCH$_2$), 1.80-1.32 (m, 20H, 10 x CH$_2$), 0.89 (t, 6H, 2 x CH$_3$). Elemental analysis for C$_{48}$H$_{52}$N$_2$O$_8$ (M = 784.94): calc. C 73.45, H 6.68, N 3.57; found C 73.28, H 6.66, N 3.50%.

*1,3-Bis-[4-(2-hydroxy-4-tetradecyloxybenzylideneamino)-benzoyloxy]benzene (**I-14**).*

^{1}H NMR (200 MHz, CDCl$_3$): δ 13.38 (s, 2H, 2 x –OH), 8.57 (s, 2H, 2 x CH=N), 8.24 (d, 4H, Ar), 7.50 (t, 1H, Ar), 7.37-7.21 (m, 9H, Ar), 6.51 (m, 4H, Ar), 4.01 (t, 4H, 2 x OCH$_2$), 1.82-1.26 (m, 48H, 24 x CH$_2$), 0.88 (t, 6H, 2 x CH$_3$). Elemental analysis for C$_{62}$H$_{80}$N$_2$O$_8$ (M = 981.31): calc. C 75.89, H 8.22, N 2.86; found C 75.71, H 8.23, N 2.82%.

*1,5-Bis-[4-(2-hydroxy-4-heptyloxybenzylideneamino)-benzoyloxy]pentane (**II-7**).*
^{1}H NMR (200 MHz, CDCl$_3$): δ 13.42 (s, 2H, 2 x –OH), 8.51 (s, 2H, 2 x CH=N), 8.06 (d, 4H, Ar), 7.25 (m, 6H, Ar), 6.48 (m, 4H, Ar), 4.37 (t, 4H, OCOCH$_2$), 3.99 (t, 4H, 2 x OCH$_2$), 1.92-1.31 (m, 26H, 13 x CH$_2$), 0,90 (t, 6H, 2 x CH$_3$). Elemental analysis for C$_{47}$H$_{58}$N$_2$O$_8$ (*M* = 778.97): calc. C 72.47, H 7.50, N 3.60; found C 72.55, H 7.57, N 3.58%.

*1,5-Bis-[4-(2-hydroxy-4-tetradecyloxybenzylideneamino)-benzoyloxy]pentane (**II-14**).*
^{1}H NMR (200 MHz, CDCl$_3$): δ 13.41 (s, 2H, 2 x –OH), 8.51 (s, 2H, 2 x CH=N), 8.06 (d, 4H, Ar), 7.25 (m, 6H, Ar), 6.47 (m, 4H, Ar), 4.37 (t, 4H, OCOCH$_2$), 3.99 (t, 4H, 2 x OCH$_2$), 1.91-1.26 (m, 54H, 27 x CH$_2$), 0,87 (t, 6H, 2 x CH$_3$). Elemental analysis for C$_{61}$H$_{86}$N$_2$O$_8$ (*M* = 975.34): calc. C 75.12, H 8.89, N 2.87; found C 74.84, H 8.86, N 2.81%.

*1,5-Bis-[4-(2-hydroxy-4-heptyloxybenzylideneamino)-benzoyloxy]-2,2-dimethylpentane (**III-7**).*
^{1}H NMR (200 MHz, CDCl$_3$): δ 13.41 (s, 2H, 2 x –OH), 8.50 (s, 2H, 2 x CH=N), 8.04 (m, 4H, Ar), 7.21 (m, 6H, Ar), 6.45 (m, 4H, Ar), 4.33 (t, 2H, OCOCH$_2$), 4.09 (s, 2H, OCOCH$_2$), 3.98 (t, 4H, 2 x OCH$_2$), 1.86-1.30 (m, 24H, 12 x CH$_2$), 1.06 (s, 6H, CH$_3$CCH$_3$), 0,89 (t, 6H, 2 x CH$_3$). Elemental analysis for C$_{49}$H$_{62}$N$_2$O$_8$ (*M* = 807.03): calc. C 72.93, H 7.74, N 3.47; found C 72.93, H 7.79, N 3.42%.

*1,5-Bis-[4-(2-hydroxy-4-tetradecyloxybenzylideneamino)-benzoyloxy]-2,2-dimethylpentane (**III-14**).*
^{1}H NMR (200 MHz, CDCl$_3$): δ 13.42 (s, 2H, 2 x –OH), 8.50 (s, 2H, 2 x CH=N), 8.05 (m, 4H, Ar), 7.22 (m, 6H, Ar), 6.45 (m, 4H, Ar), 4.33 (t, 2H, OCOCH$_2$), 4.09 (s, 2H, OCOCH$_2$), 3.98 (t, 4H, 2 x OCH$_2$), 1.86-1.26 (m, 52H, 26 x CH$_2$), 1.06 (s, 6H, CH$_3$CCH$_3$), 0,87 (t, 6H, 2 x CH$_3$). Elemental analysis for C$_{63}$H$_{90}$N$_2$O$_8$ (*M* = 1003.40): calc. C 75.41, H 9.04, N 2.79; found C 75.46, H 9.14, N 2.73%.

*1,5-Bis-[4-(2-hydroxy-4-heptyloxybenzylideneamino)-benzoyloxy]-3,3-dimethylpentane (**IV-7**).*
^{1}H NMR (200 MHz, CDCl$_3$): δ 13.41 (s, 2H, 2 x –OH), 8.45 (s, 2H, 2 x CH=N), 8.03 (d, 4H, Ar), 7.22 (m, 6H, Ar), 6.46 (m, 4H, Ar), 4.44 (t, 4H, OCOCH$_2$), 3.98 (t, 4H, 2 x OCH$_2$), 1.87-1.31 (m, 24H, 12 x CH$_2$), 1.10 (s, 6H, CH$_3$CCH$_3$), 0,90 (t, 6H, 2 x CH$_3$). Elemental analysis for C$_{49}$H$_{62}$N$_2$O$_8$ (*M* = 807.03): calc. C 72.93, H 7.74, N 3.47; found C 72.53, H 7.65, N 3.41%.

*1,5-Bis-[4-(2-hydroxy-4-tetradecyloxybenzylideneamino)-benzoyloxy]-3,3-dimethylpentane (**IV-14**).*
^{1}H NMR (200 MHz, CDCl$_3$): δ 13.41 (s, 2H, 2 x –OH), 8.45 (s, 2H, 2 x CH=N), 8.03 (d, 4H, Ar), 7.22 (m, 6H, Ar), 6.45 (m, 4H, Ar), 4.44 (t, 4H, OCOCH$_2$), 3.97 (t, 4H, 2 x OCH$_2$), 1.89-1.26 (m, 52H, 26 x CH$_2$), 1.10 (s, 6H, CH$_3$CCH$_3$), 0,87 (t, 6H, 2 x CH$_3$). Elemental analysis for C$_{63}$H$_{90}$N$_2$O$_8$ (*M* = 1003.40): calc. C 75.41, H 9.04, N 2.79; found C 75.23, H 9.12, N 2.74%.

3.2.2 Measurements

Melting points, thermal phase transition temperatures and optical studies of the liquid crystalline phases were determined on samples between ordinary glass slides using an Olympus BH-2 polarized light microscope equipped with a Mettler FP82HT hot stage, which was controlled by a Mettler FP80HT central processor. Differential scanning calorimetry (DSC) thermograms were obtained on a Perkin Elmer DSC-7 system using 2-5 mg samples in 30 μL sample pans and a scan rate of 5°Cmin^{-1}. ΔH is expressed in kJmol^{-1}. Temperature dependent X-ray diffraction curves of the liquid crystals were measured on a Panalytical X'pert Pro diffractometer equipped with an Anton Paar camera for temperature control. For the measurements in the small angle region, the sample was spread in the isotropic or the liquid crystalline phase on a thin glass slide (about 15 μm thick), which was placed on a temperature-regulated flat copper sample stage. This sample preparation sometimes caused very high intensities of X-ray reflections (> 500 kc/s) because of partial or complete orientation of the molecules in the liquid crystalline state. For measurements in the wide-angle region, glass capillaries (diameter 0.5 mm, glass thickness 0.01 mm) were used.

3.3   Results and discussion

*The **I-n** series*
The thermotropic properties of the **I-n** series containing a central phenyl group are given in table 1. The optical textures are shown in figure 2. All compounds in this series exhibit one enantiotropic liquid crystalline B-phase, its type depending on the length *n* of the terminal alkyl tail. The melting and isotropization temperatures are shown in figure 3. Compound **I-16** has been described previously, and like Shankar Rao *et al*. [36], we observe the growth of thread-like and spiral nuclei upon cooling from the isotropic liquid. Characteristic optical textures are shown in figure 2a).

Table 1. *Transition temperatures (ºC), transition enthalpies (kJ mol⁻¹; between square brackets) and layer spacings d (Å) of the **I-n** series.*

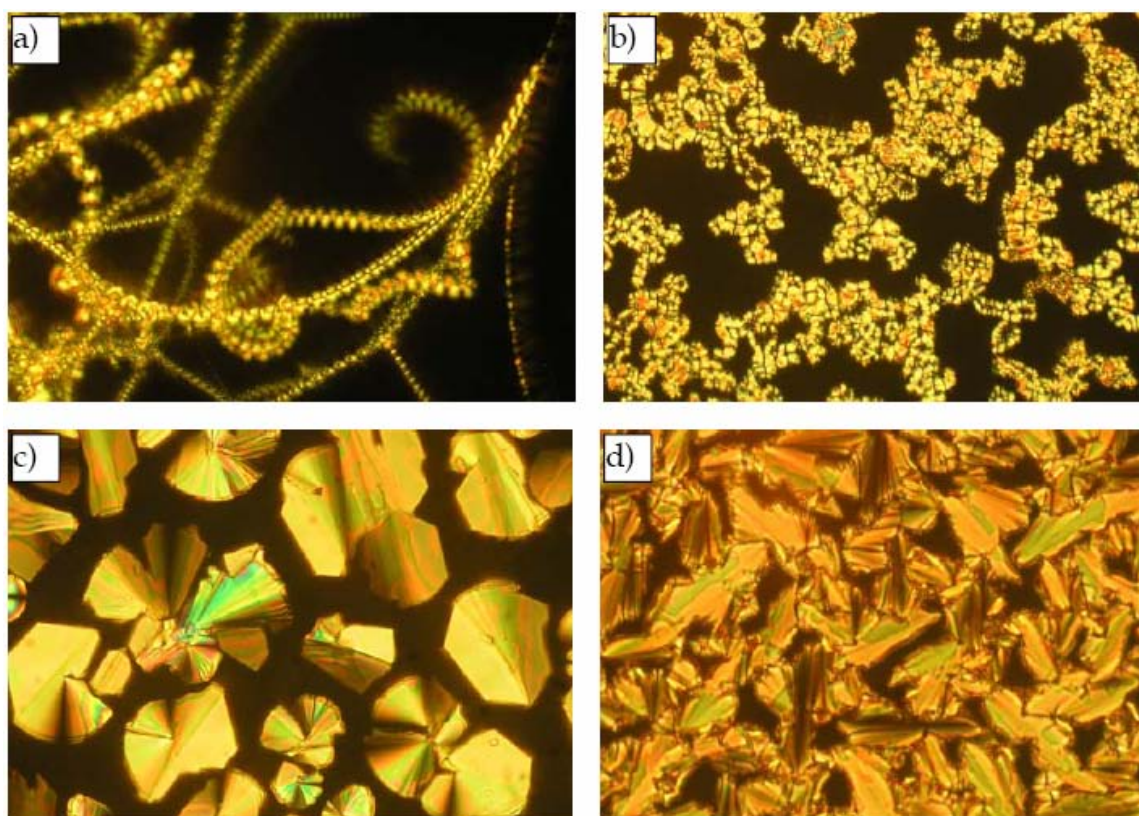| *n*	Cr	B_6	B_1	B_2		I	*d*
4	● 188 [36]	● 196 [13]				●	17.8
5	● 160 [32]		● 179 [16]			●	37.2
6	● 143 [11]		● 174 [17]			●	38.6
7	● 128 [20]			● 173.5 [17]		●	36.4
8	● 126 [20]			● 174.5 [18]		●	37.9
9	● 119 [19]			● 176.5 [19]		●	39.7
10	● 117 [20]			● 178.5 [21]		●	41.1
11	● 114 [20]			● 177 [20]		●	42.2
12	● 114 [21]			● 178 [22]		●	43.8
14	● 112 [21]			● 175 [23]		●	46.6
16	● 113 [76]			● 172 [23]		●	49.2

Figure 2. *Optical photomicrographs of the textures observed on cooling from the isotropic state for series **I-n**. a: **I-16**, B₂; b: **I-12**, B₂; c: **I-6**, B₁; d: **I-4**, B₆.*

The X-ray pattern we observed was also similar to the results Shankar Rao *et al*. obtained (figure 4). Based on these observations, this phase was assigned as B_7. However, because growth of spirals is not unique for the B_7 phase [39,40], and because

the X-ray pattern does not resemble the pattern of the original B_7 compound [7], we have some doubts about this assignment. The X-ray pattern of **I-16**, which is similar to the patterns of **I-14** and **I-12**, indicates a lamellar structure with a *d*-spacing of 49.2 Å and weak higher order reflections. Since this layer spacing fits perfectly in the trend observed for compounds **I-7** to **I-14** and because antiferroelectric switching behavior was observed for **I-16**, we assume that this phase is B_2 although a B_7 phase cannot be completely excluded.
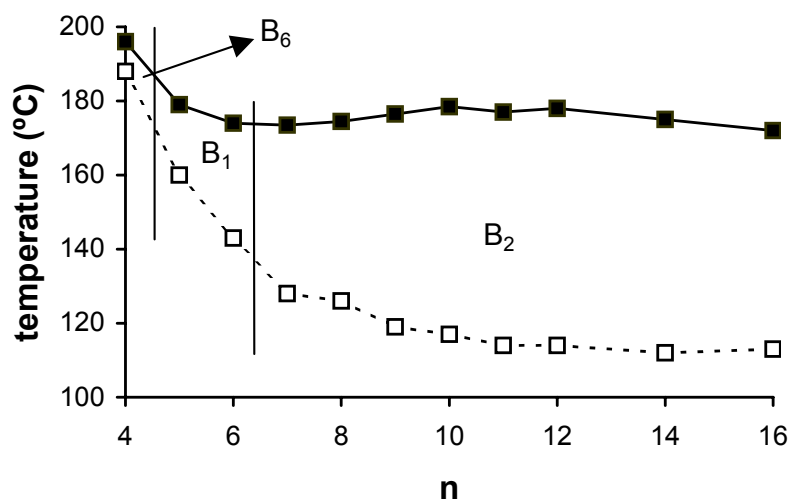

Figure 3. *Dependence of the melting points (---□---) and isotropization temperatures (——■——) of the compounds of series **I-n** on the number of carbon atoms n in the terminal chains.*

Compounds **I-9** and **I-10** have been described previously in the literature [34,35]. As for several other series, the longer homologues of the **I-n** series exhibit the B_2 mesophase. An example of the textures observed for these compounds is given in figure 2b) for compound **I-12**; it shows similarities with those found for other B_2 phases [2]. Upon cooling from the isotropic liquid a smectic focal-conic texture develops. X-ray diffraction patterns of the compounds that exhibit the liquid crystalline B_2 phase (**I-7** to **I-14**) all show a significant similarity to those observed for B_2 phases of other bent-shaped molecules [11] (figure 4). Together with the optical texture, the X-ray patterns of oriented samples indicate a tilted smectic in which the layer spacing increases linearly from 36.4 Å for **I-7** to 46.6 Å for **I-14** (table 1). A broad peak in the wide-angle region proves the liquid-like order within the layers (not shown).

For the short-tailed members (**I-5** and **I-6**) of the **I-n** series, the B_1 phase was observed on cooling from the isotropic state by formation of small batonnets, which coalesce into a mosaic-like texture, figure 2c).
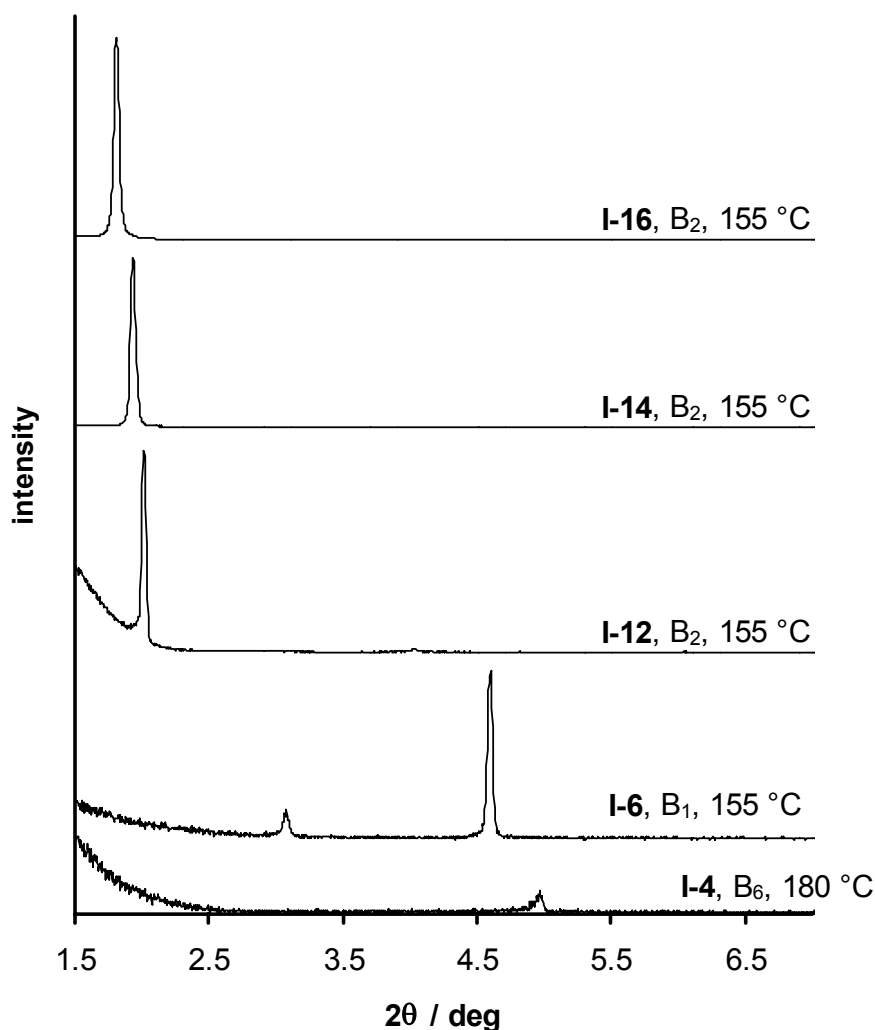
Figure 4. X-ray intensity profiles of five compounds of series I-n.

For the B_1 phase, a rectangular columnar structure was proposed by Watanabe *et al.*[4]. The X-ray diffractogram of compound **I-6** (figure 4) exhibits two reflections in the small-angle region, pointing to a two-dimensional rectangular cell. These two reflections in the small angle region of the B_1 phase have been evaluated on the basis of a rectangular cell by analogy to the B_1 phase of other compounds [11,29]. The periodicities d_1 and d_2 for **I-6** in the small angle region are 28.8 Å and 19.3 Å, respectively. The corresponding lattice parameters for a modulated phase with a rectangular lattice, assuming the reflection indexing (0 0 2) and (1 0 1), are a = 43.3 Å for the in-plane parameter and c = 38.6 Å for the layer thickness (table 1). Assuming a molecular length of 44.4 Å, the calculated molecular tilt is 30°. For **I-5** the periodicities d_1 and d_2 in the small angle region are 25.0 Å and 18.6 Å. The corresponding lattice parameters are a = 33.7 Å and c = 37.2 Å. Assuming a molecular length of 41.9 Å, the calculated molecular tilt is 27°. Tilt angles of 25-30° for the B_1 phase have been reported previously in the literature [11,13].

Compound **I-4** shows only one reflection in the small angle region (figure 4). The corresponding period is smaller than half the molecular length. In consideration with the observed fan-shaped optical texture, figure 2d), this mesophase was assigned as the intercalated B_6 phase.

In conclusion, the **I-n** series shows the phase sequence B_6-B_1-B_2 with increasing terminal chain length. This sequence has been reported previously [13,41]; in these reported series, however, there were always one or more compounds exhibiting two mesophases.

*The **II-n** series*

Six compounds (*n* = 6, 8, 10, 11, 12 and 16) of the **II-n** series with the pentyl spacer have been described by Yelamaggad *et al.* [37]. We have synthesized additional intermediate and short-tailed homologues. The thermotropic properties of series **II-n** are given in table 2 and the values of those described before are very similar to the reported values. The melting points and isotropization temperatures are shown in figure 5. All compounds in the **II-n** series show liquid crystalline properties.

*Table 2. Transition temperatures (^{o}C), transition enthalpies (kJ mol^{-1}; between square brackets) and layer spacings d (Å) of the **II-n** series.*

n	Cr	SmC$_c$	B$_1$	I	*d*
4	• 134 [33]	• 160 [12]		•	19.4
5	• 142 [41]	• 151 [12]		•	20.2
6	• 142 [41]	• 147 [13]		•	21.0
7	• 143 [57]	(• 141 [13])		•	21.8
8	• 141 [56]		(• 139 [a])	•	a
9	• 140 [57]		(• 138 [14])	•	a
10	• 139 [59]		(• 137 [16])	•	a
11	• 138 [61]		(• 136 [a])	•	a
12	• 138 [42]		• 138 [17]	•	a
14	• 133 [42]		• 136 [17]	•	51.3
16	• 131 [41]		• 135 [16]	•	53.9

[a] Could not be determined

Only the long- and short-tailed compounds exhibit enantiotropic mesophases. The longer (*n* = 14 and 16) homologues show the two-dimensional B_1 phase. On cooling from the isotropic phase, the B_1 phase appears as a mosaic texture with spherulitic domains, figure 6(a). X-ray measurements for **II-14** and **II-16** show patterns similar to those described in the literature [37]. The compounds with intermediate tail lengths

(n = 8-11) show a similar B_1 mesophase according to polarizing optical microscopy observations, figure 6(c). It was impossible, however, to make X-ray measurements on these monotropic compounds, since crystallization occurred very soon after the formation of the liquid crystalline mesophase during cooling from the isotropic state. Compound **II-12** showed a different optical texture as shown in figure 6b.
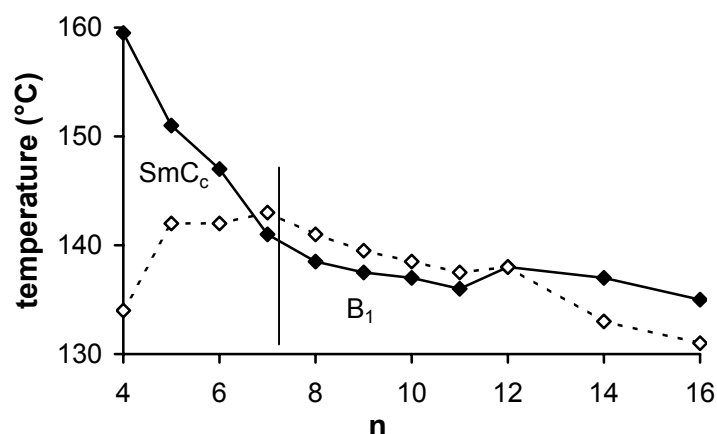

Figure 5. *Dependence of the melting points (---◊---) and isotropization temperatures (—♦—) of series II-n on the number of carbon atoms n in the terminal chains.*
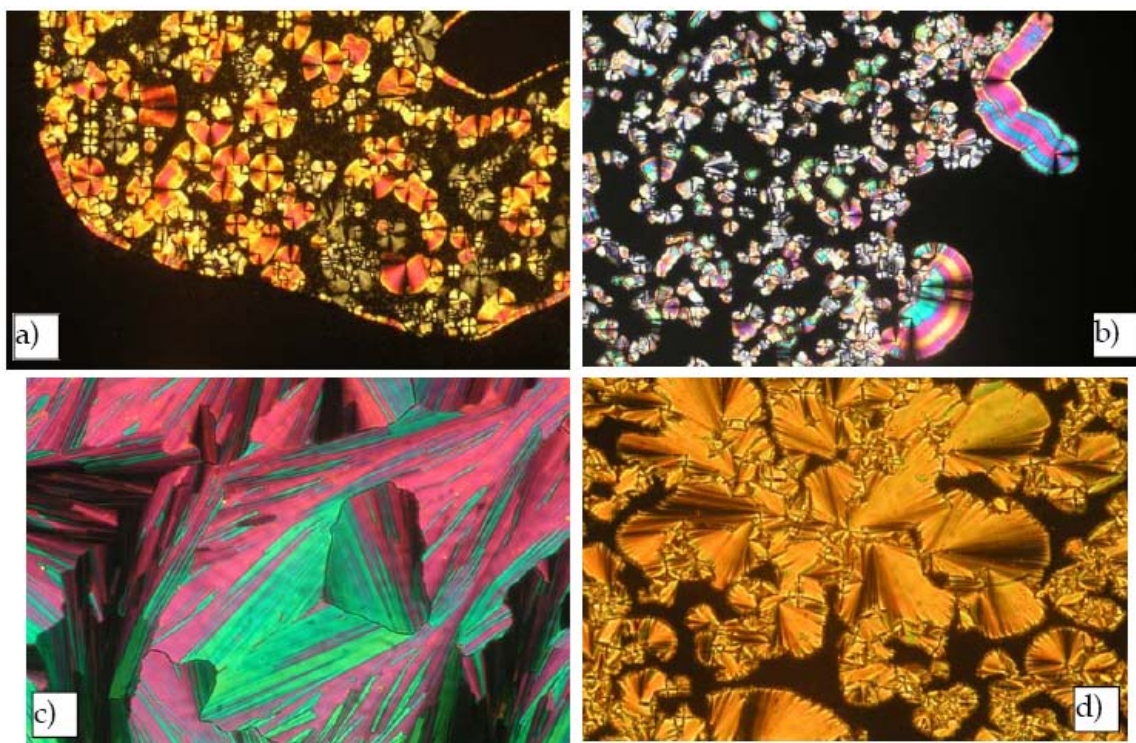

Figure 6. *Optical photomicrographs of the textures observed on cooling from the isotropic state for series II-n. a: II-16, B_1; b: II-12, B_1; c: II-8, B_1; d: II-6, SmC$_c$.*

The liquid crystalline phases of the shorter homologues of the **II-*n*** series (*n* = 4-7) were identified as intercalated SmC mesophases (SmC$_c$). Upon cooling from the isotropic phase a focal-conic texture appeared, figure 6(d). Simultaneously, the Schlieren optical texture was also observed. The sharp first order reflection in the low angle region of the XRD pattern points to a layer spacing less than half the length of the molecule in the most extended conformation (table 2). In the wide angle region a broad peak is present, characteristic of a liquid-like arrangement of the molecules within the layers. Based on these observations, we conclude that this phase is the intercalated SmC$_c$ mesophase.

*The **III-*n*** series*

Table 3 lists the thermotropic properties of the non-symmetric **III-*n*** series. The dependence of the transition temperatures on the length of the terminal alkyl chains is shown in figure 7. Compared to the **II-*n*** series, the liquid crystalline range is larger, mainly as a result of the lower melting points. On cooling from the isotropic phase, the longer members (*n* = 9-16) of the **III-*n*** series form focal conic fans, which implies a smectic layered structure. Upon shearing the glass slides, dark areas were observed containing no Schlieren textures, indicating an orthogonal arrangement of the director with respect to the layer planes. XRD patterns show broad peaks in the wide-angle region. In the small-angle region, the first order Bragg peak is observed corresponding to the (0 0 1) planes. For the compounds **III-9** to **III-16**, the layer spacing is approximately half the estimated molecular lengths, resulting in a *d/l* ratio of ~0.5 (table 3). Consequently, this mesophase is assigned as an intercalated SmA phase (SmA$_c$).

Table 3. *Transition temperatures (°C), transition enthalpies (kJ mol⁻¹; between square brackets) and layer spacings d (Å) of the **III-*n*** series.*

n	Cr		SmC$_c$		SmA$_c$		I	*d*
4	● 97.5	[27]	● 139.5	[10]			●	20.8
5	● 99	[23]	● 135	[12]			●	21.8
6	● 97	[24]	● 135	[12]			●	22.6
7	● 95	[37]	● 133	[12]			●	23.9
8	● 97.5	[38]	● 132	[12]			●	25.2
9	● 97	[39]			● 132	[12]	●	27.8
10	● 102	[47]			● 133	[12]	●	29.6
11	● 96	[37]			● 133	[12]	●	30.9
12	● 101	[44]			● 134	[13]	●	32.3
14	● 109	[56]			● 135	[13]	●	34.8
16	● 112	[78]			● 135	[14]	●	37.5

For the compounds of the **III-*n*** series with the short tails (*n* = 4-8), spherulitic domains and focal-conics are seen, figure 8(a). On cooling from the isotropic melt, fan-shaped textures were also observed in a dendritic-like texture, figure 8(b). Schlieren textures were observed in the homeotropic regions of the sample indicating a tilted phase. X-ray measurements show broad peaks in the wide-angle region, and given the small *d*-spacing this mesophase is assigned as an intercalated SmC$_c$ phase. Table 3 lists the layer spacings of the phases seen for the **III-*n*** compounds.
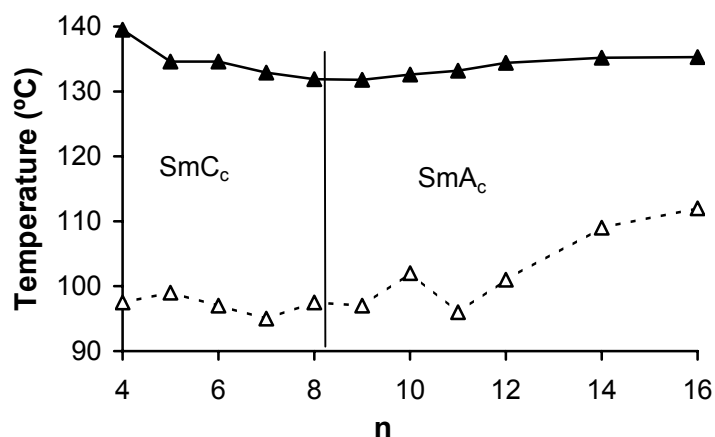

Figure 7. *Dependence of the melting points (---Δ---) and isotropization temperatures (-▲-) of series **III-n** on the number of carbon atoms n in the terminal chains.*

In the **III-*n*** series, the intercalated SmC$_c$ phase is present for the short homologues, as seen also for the non-substituted **II-*n*** series. The longer homologues of the **II-*n*** series show the B$_1$ phase, which is replaced by the intercalated SmA$_c$ phase in the substituted **III-*n*** series. Substitution of the central spacer seems to suppress formation of the B$_1$ mesophase because of steric reasons. The densely packed core of columns in the B$_1$ phase cannot be formed because of the dimethyl substituents. Replacement of the B$_1$ phase with the intercalated SmA$_c$ phase is unexpected, however, since the terminal alkyl chains are much longer than half the spacer length. In general, the formation of intercalated layer structures in dimeric compounds is promoted if the terminal chains lengths are shorter than half the spacer length. A smectic monolayer is in general observed if the terminal chains are longer than half the length of the spacer [42]. In the latter case a microphase separation occurs leading to three regions; mesogenic groups, spacers and terminal chains. On the other hand, the presence of substituents on the central spacer has been shown to promote formation of intercalated smectic phases [22,23].

The presence of an intercalated layer structure has previously been explained in terms of either an increase in entropy gained from the homogeneous mixing of the

mesogenic moieties, an electrostatic quadrupolar interaction, or by an excluded volume or space filling constraint [43]. From the study performed by Blatch and Luckhurst [44], it was suggested that some specific (dipolar) interaction is required between different mesogenic groups to stabilize the intercalated structure.
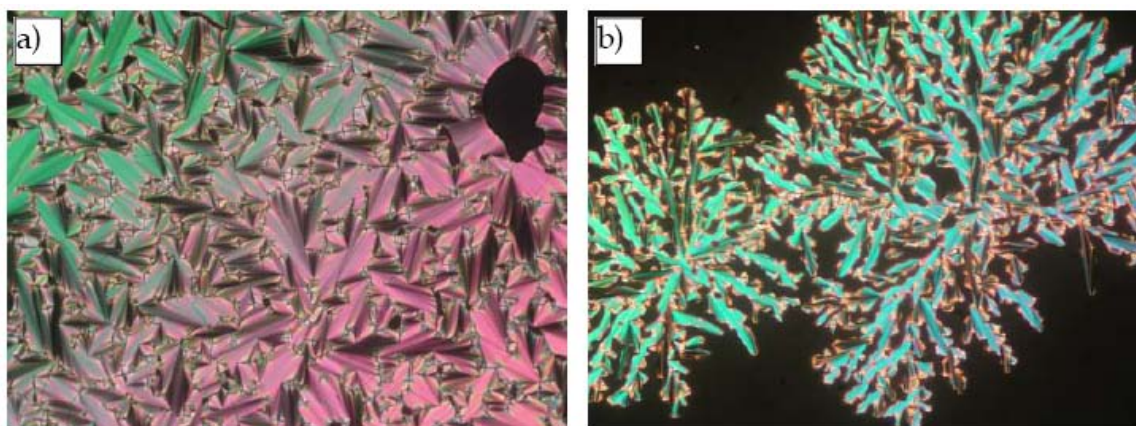

Figure 8. *Optical photomicrographs of the textures observed on cooling from the isotropic state for series* **III-n**. *a:* **III-7**, *SmC$_c$; b:* **III-5**, *SmC$_c$.*

A transition from the intercalated SmA$_c$ to the intercalated SmC$_c$ phase upon decreasing the terminal chain length such as seen for the **III-n** series, has to our knowledge only once been reported in literature [45]. In a series studied by Weissflog *et al.*, three-ring mesogenic units connected via a bis(carbonyloxy)propylene spacer exhibit thermotropic properties comparable to the **III-n** series. The most important difference in properties between the two series is the absence of intermediate compounds in the **III-n** series that possess both smectic modifications in one compound. In particular, the occurrence of the intercalated SmA$_c$ mesophase despite the odd-numbered spacer (which favors, in general, a bent molecular structure [43,46]) is an unexpected phenomenon. Two possible reasons were suggested for this phenomenon [45]. First, the stabilization of the SmA$_c$ phase on increasing the chain length could be related to a stretching of the spacer, favored because of space filling conditions. Second, the strong lateral cohesion of the mesogenic moieties could be enhanced by the antiparallel aligned dipoles of the mesogenic units.

*The **IV-n** series*

In the **IV-n** series, the pentyl spacer is substituted with two methyl groups at the central carbon atom. The thermotropic properties and layer spacings *d* of this series are given in table 4 and the melting points and isotropization temperatures shown in figure 9.

***Table 4**. Transition temperatures (°C), transition enthalpies (kJ mol^{-1}; between square brackets) and layer spacings d (Å) of the **IV-n** series.*

n	Cr	SmA$_c$	SmC$_c$	SmA$_c$	I	d
4	• 102 [43]	• 121 [0.7]	• 157 [11]		•	22.8 / 21.5
5	• 118 [36]		• 153 [12]		•	22.9
6	• 112 [33]		• 151 [12]		•	24.0
7	• 113 [39]		• 149 [13]		•	25.3
8	• 109 [40]			• 148 [13]	•	27.1
9	• 102 [56]			• 147 [13]	•	28.8
10	• 100 [59]			• 147 [14]	•	30.1
11	• 99 [55]			• 148 [15]	•	31.4
12	• 99 [65]			• 149 [15]	•	32.7
14	• 101 [105]			• 149 [15]	•	35.3
16	• 104 [125]			• 148 [17]	•	37.9

The compounds of this series show broader liquid crystalline ranges than those of series **II-n** series, also mainly as a result of lower melting points. The thermotropic behavior of this series is very similar to that of the **III-n** series. As in the non-symmetrical **III-n** series, the compounds with the long alkyl tails exhibit the intercalated SmA$_c$ phase. For the short homologues the intercalated SmC$_c$ phase is observed.
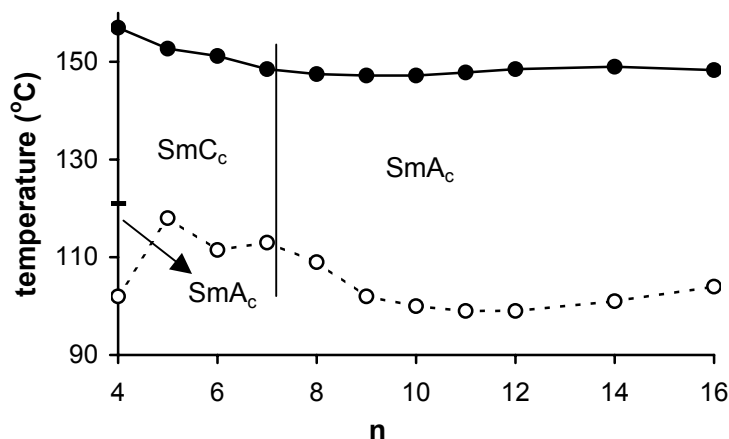

***Figure 9**. Dependence of the melting points (---o---) and isotropization temperatures (—•—) of series **IV-n** on the number of carbon atoms n in the terminal chains. The vertical line denotes the SmA$_c$ to SmC$_c$ transition.*

Compound **IV-4** exhibits an additional low temperature phase, which is absent in the **III-n** series. Upon cooling the SmC$_c$ phase of **IV-4** a texture appears in which homeotropic regions with no birefringence are observed. These optical textures are

typical of a SmA phase. The XRD pattern for the **IV-4** compound shows no changes in the wide-angle region at this transition, so a more highly ordered mesophase, such as the SmB phase can be excluded. The layer thickness increases slightly from 21.5 to 22.8 Å at the transition; this corresponds to half the molecular length. Therefore, we conclude that this low temperature mesophase is probably a SmA$_c$ phase.

The inverse phase sequence SmA → SmC with increasing temperature is unusual but not completely unknown [45]. It is assumed that such a transition is connected with a change of the molecular conformation from a rod-like molecule in SmA, to a more bent molecule in the SmC phase. The stretching of the spacer is promoted by the decreasing temperature. Thus, on cooling the SmC$_c$ phase of **IV-4** the spacer stretches and a transition from SmC$_c$ to SmA$_c$ occurs. The enthalpy change associated with this transition is only 0.7 kJ mol^{-1}. The strong lateral interaction between the dipoles of adjacent mesogenic units might also play a role in this striking phenomenon.

*Comparison between series **I-n**, **II-n**, **III-n** and **IV-n***

In figure 10, the isotropization temperatures of all four series of compounds are compared. This figure clearly shows that the compounds of the series with the central aromatic part (**I-**n) have the highest clearing temperatures. Non-symmetrical introduction of methyl substituents on the central pentyl spacer in the **III-**n series results in a decrease in isotropization temperatures as compared with the unsubstituted **II-**n series. Introduction of the substituents at the central carbon atom (series **IV-**n), on the other hand, results in an increase of the isotropization temperatures, especially for the longer members of the series.
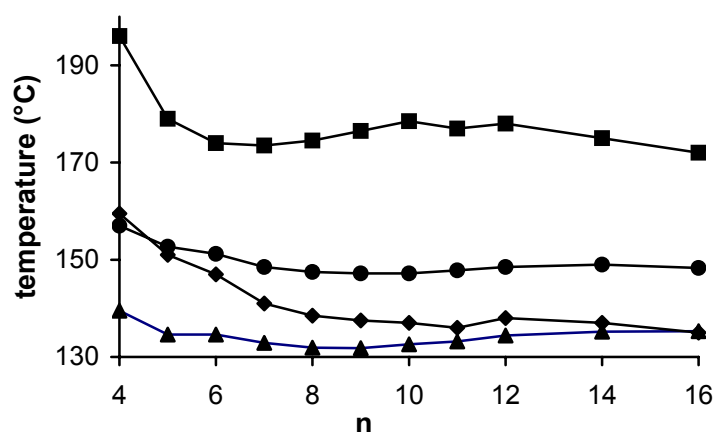

Figure 10. *Dependence of the isotropization temperatures of the compounds of series **I-n** (-■-), **II-n** (-♦-), **III-n** (-▲-) and **IV-n** (-●-) on the number of carbon atoms n in the terminal chains.*

Comparison of the melting points of all four series (tables 1-4) shows that the influence of both symmetrical and non-symmetrical substitution is pronounced. The introduction of these substituents causes the melting points to drop by as much as 40°C as compared with those of the **II-*n*** series.

The **I-*n*** series differs in a number of ways from the other three series. The melting points, isotropization temperatures and phase behavior are significantly different. The main reason for this different behavior is probably related to the fact that the molecules of the **I-*n*** series can be regarded as liquid crystals with one mesogenic unit and two alkyl tails. As a result, smectic monolayer behavior (*n* = 7-16) is found, and because the mesogenic units have a bent shape they form banana-phases. The series with the flexible alkyl spacers (**II-*n***, **III-*n*** and **IV-*n***) can be regarded as liquid crystal dimers with significantly different mesomorphic properties.

The layer spacings of the **III-*n*** and **IV-*n*** series are shown in figure 11. The transition from the intercalated SmA_c to the intercalated SmC_c phase, as deduced from polarizing optical microscopy, is also clear from the deviation of a linear decrease of the layer spacing with decreasing *n*. The slightly larger layer spacings for the symmetrical **IV-*n*** compounds was anticipated. Thus the bulky dimethyl substituents give rise to steric hindrance, which forces the molecules in the symmetrical **IV-*n*** series to adopt an irregular structure. For the non-symmetrical **III-*n*** series, the molecules can be positioned in an alternating manner in which the steric hindrance is reduced.
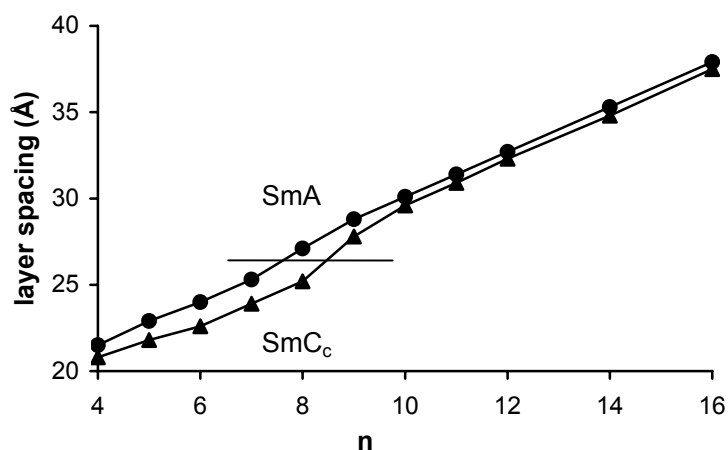

***Figure 11**. Layer spacings for the compounds of series **III-n** (—▲—) and **IV-n** (—•—) as a function of the number of carbon atoms n in the terminal chains.*

The short homologues of all the series with flexible spacers (**II-*n***, **III-*n*** and **IV-*n***) exhibit the intercalated SmC_c phase, probably because of their relatively short terminal alkyl chains and the odd-numbered spacer. Intercalation for the longer homologues of series **III-*n*** and **IV-*n*** is caused by the substituents, which suppress

the B_1 phase found in **II-*n***. In a B_1 phase there is local microphase separation in which the central aromatic parts, including the spacers of a number of molecules are located in columns surrounded by the alkyl tails. By introduction of dimethyl substituents, the spacer-spacer interaction in the B_1 phase becomes unfavorable. The unfavorable spacer-spacer interaction is reduced in the SmA_c phase. The fact that intercalated structures are found for all dimeric compounds (series **II-*n***, **III-*n*** and **IV-*n***) is probably caused by the possibility of the dipoles of the mesogenic groups to align antiparallel in the intercalated structures.

With long terminal groups the interaction between the antiparallel dipoles of the mesogenic groups will be relatively weak. With decreasing terminal chain lengths these interactions will become stronger, which could result in the transition to the SmC_c phase. Because the layer thickness of the **IV-*n*** compounds is larger than for the **III-*n*** series, it is possible that this is the reason why the transition to SmC_c occurs for a shorter terminal tail in the **IV-*n*** series.

3.4   Conclusions

All 44 salicylaldimine-based compounds that have been synthesized exhibit liquid crystalline mesophases. The nature of the central part and length of the terminal alkyl chains has a remarkable influence on the mesomorphic properties.

As in most banana-shaped liquid crystals, a phenyl or biphenyl central part promotes formation of B-phases. For the **I-*n*** series three different B-phases were observed, and these show the phase sequence B_6-B_1-B_2 on increasing the terminal chain length. Replacement of the phenyl spacer (**I-*n***) with a pentyl spacer (**II-*n***) results in the partial disappearance of B-phases and formation of the intercalated SmC_c phase for the shorter homologues. The longer homologues (n = 8 to n = 16) of the **II-*n*** series exhibit the two-dimensional B_1 phase.

The introduction of two methyl substituents to the central pentyl spacer (series **III-*n*** and **IV-*n***) dramatically decreases the melting temperatures, and also the formation of B-phases is suppressed, probably because of steric hindrance. Both substituted series exhibit the intercalated SmA_c phase for the longest homologues in spite of their odd-numbered spacers, whereas the short homologues exhibit the intercalated SmC_c phase. Thus the random mixing of the central part and terminal chain occurs for both phases. The occurrence of the unusual phase sequence $SmC_c \rightarrow SmA_c$ for **IV-4** on decreasing the temperature might be related to the stretching of the spacer which is promoted by decreasing temperature.

Although some dimeric compounds with an odd number of flexible units between the two mesogenic parts exhibit switchable B-phases, these phases are not so common as in the compounds with a central phenyl or biphenyl segment. In the series described in this paper, replacement of the central phenyl group with a pentyl or substituted pentyl group results in the disappearance of the switchable B_2 phase.

3.5   References

1.   Niori T., Sekine F., Watanabe J., Furukawa T. and Takezoe H. *J. Mater. Chem.* **1996**, *6*, 1231-1233.
2.   Pelzl G., Diele S. and Weissflog W. *Adv. Mater.* **1999**, *11*, 707-724.
3.   Salfetnikova J., Schmalfuss H., Nadasi H., Weissflog W. and Kresse H. *Liq. Cryst.* **2000**, *27*, 1663-1667.
4.   Watanabe J., Niori T., Sekine T. and Takezoe H. *Jpn. J. Appl. Phys.* **1998**, *37*, L139-L142.
5.   Shen D., Pegenau A., Diele S., Wirth I. and Tschierske C. *J. Am. Chem. Soc.* **2000**, *122*, 1593-1601.
6.   Diele S., Grande S., Kruth H., Liscka C., Pelzl G., Weissflog W. and Wirth I. *Ferroelectrics* **1998**, *212*, 169-177.
7.   Pelzl G., Diele S., Jakli A., Liscka C., Wirth I. and Weissflog W. *Liq. Cryst.* **1999**, *26*, 135-139.
8.   Coleman D. A., Fernsler J., Chattham N., Nakata M., Takanishi Y., Korblova E., Link D. R., Shao R.-F., Jang W. G., Maclennan J. E., Mondainn-Monval O., Boyer C., Weissflog W., Pelzl G., Chien L.-C., Zasadzinski J., Watanabe J., Walba D. M., Takezoe H. and Clark N. A. *Science* **2003**, *301*, 1204-1211.
9.   Bedel J. P., Rouillon J. C., Marcerou J. P., Laguerre M., Nguyen H. T. and Achard M. F. *Liq. Cryst.* **2001**, *28*, 1285-1292.
10.   Rouillon J. C., Marcerou J. P., Laguerre M., Nguyen H. T. and Achard M. F. *J. Mater. Chem.* **2001**, *11*, 2946-2950.
11.   Bedel J. P., Rouillon J. C., Marcerou J. P., Laguerre M., Achard M. F. and Nguyen H. T. *Liq. Cryst.* **2000**, *27*, 103-113.
12.   Heppke G., Parghi D. D. and Sawade H. *Liq. Cryst.* **2000**, *27*, 313-320.
13.   Weissflog W., Wirth I., Diele S., Pelzl G., Schmalfuss H., Schoss T. and Wurflinger A. *Liq. Cryst.* **2001**, *28*, 1603-1609.
14.   Prasad V. *Liq. Cryst.* **2001**, *28*, 1115-1120.
15.   Rauch S., Bault P., Sawade H., Heppke G., Nair G. G. and Jakli A. *Phys. Rev. E* **2002**, *66*, 021706.
16.   Shen D., Diele S., Wirth I. and Tschierske C. *Chem. Commun.* **1998**, 2573-2574.
17.   Watanabe J., Izumi T., Niori T., Zennyoji M., Takanishi Y. and Takezoe H. *Mol. Cryst. Liq. Cryst.* **2000**, *346*, 77-86.
18.   Watanabe J., Niori T., Choi S.-W., Takanishi Y. and Takezoe H. *Jpn. J. appl. Phys.* **1998**, *37*, L401-L403.
19.   Choi S.-W., Zennyoji M., Takanishi Y., Takezoe H., Niori T. and Watanabe J. *Mol. Cryst. Liq. Cryst.* **1999**, *328*, 185-192.
20.   Prasad V., Shankar Rao D. S. and Krishna Prasad S. *Liq. Cryst.* **2001**, *28*, 761-767.
21.   Prasad V., Shankar Rao D. S. and Krishna Prasad S. *Liq. Cryst.* **2000**, *27*, 585-590.
22.   Prasad V., Lee K.-H., Park Y. S., Lee J.-W., Oh D.-K., Han D. Y. and Jin J.-I. *Liq. Cryst.* **2002**, *29*, 1113-1119.

23. Pociecha D., Kardas D., Gorecka E., Szydlowska J., Mieczkowski J. and Guillon D. *J. Mater. Chem.* **2003**, *13*, 34-37.
24. Amaranatha Reddy R. and Sadashiva B. K. *J. Mater. Chem.* **2002**, *12*, 2627-2632.
25. Pelzl G., Eremin A., Diele S., Kresse H. and Weissflog W. *J. Mater. Chem.* **2002**, *12*, 2591-2593.
26. Pelzl G., Diele S., Grande S., Jakli A., Lischka C., Kresse H., Schmalfuss H., Wirth I. and Weissflog W. *Liq. Cryst.* **1999**, *26*, 401-413.
27. Fodor-Csorba K., Vajda A., Galli G., Jákli A., Demus D., Holly S. and Gács-Baitz E. *Macromol. Chem. Phys.* **2002**, *203*, 1556-1563.
28. Kašpar M., Hamplová V., Novotná V., Glogarová M. and Vanek P. *J. Mater. Chem.* **2002**, *12*, 2221-2224.
29. Weissflog W., Kovalenko L., Wirth I., Diele S., Pelzl G., Schmalfuss H. and Kresse H. *Liq. Cryst.* **2000**, *27*, 677-681.
30. Wirth I., Diele S., Eremin A., Pelzl G., Grande S., Kovalenko L., Pancenko N. and Weissflog W. *J. Mater. Chem.* **2001**, *11*, 1642-1650.
31. Weissflog W., Nadasi H., Dunemann U., Pelzl G., Diele S., Eremin A. and Kresse H. *J. Mater. Chem.* **2001**, *11*, 2748-2758.
32. Dehne H., Pötter M., Sokolowski S., Weissflog W., Diele S., Pelzl G., Wirth I., Kresse H., Schmalfuss H. and Grande S. *Liq. Cryst.* **2001**, *28*, 1269-1277.
33. Shubashree S., Sadashiva B. K. and Dhara S. *Liq. Cryst.* **2002**, *29*, 789-797.
34. Walba D. M., Korblova E., Shao R. and Clark N. A. *J. Mater. Chem.* **2001**, *11*, 2743-2747.
35. Yelamaggad C. V., Hiremath U. S., Anitha Nagamani S., Shankar Rao D. S. and Krishna Prasad S. *J. Mater. Chem.* **2001**, *11*, 1818-1822.
36. Shankar Rao D. S., Nair G. G., Krishna Prasad S., Anitha Nagamani S. and Yelamaggad C. V. *Liq. Cryst.* **2001**, *28*, 1239-1243.
37. Yelamaggad C. V., Anitha Nagamani S., Hiremath U. S., Shankar Rao D. S. and Krishna Prasad S. *Liq. Cryst.* **2002**, *29*, 1401-1408.
38. Eilbracht P., Acker M. and Totzauer W. *Chem. Ber.* **1983**, *116*, 238-242.
39. Amaranatha Reddy R. and Sadashiva B. K. *Liq. Cryst.* **2002**, *29*, 1365-1367.
40. Amaranatha Reddy R. and Sadashiva B. K. *Liq. Cryst.* **2003**, *30*, 273-283.
41. Shreenivasa Murthy H. N. and Sadashiva B. K. *Liq. Cryst.* **2002**, *29*, 1223-1234.
42. Date R. W., Imrie C. T., Luckhurst G. R. and Seddon J. M. *Liq. Cryst.* **1992**, *12*, 203-238.
43. Imrie C. T. and Henderson P. A. *Curr. Opin. Colloid Interface Sci.* **2002**, *7*, 298-311.
44. Blatch A. E. and Luckhurst G. R. *Liq. Cryst.* **2000**, *27*, 775-787.
45. Weissflog W., Lischka C., Diele S., Wirth I. and Pelzl G. *Liq. Cryst.* **2000**, *27*, 43-50.
46. Watanabe J., Komura H. and Niori T. *Liq. Cryst.* **1993**, *13*, 455-465.

Asymmetric banana-shaped liquid crystals with two different terminal alkoxy chains

Two series of asymmetric banana-shaped compounds have been synthesized and studied. In the 1,3-phenylene bis[4-(4'-alkoxybenzoyloxy)]benzoate series the lack of symmetry was derived solely from the difference in length of the two terminal alkoxy chains. In the 3,4'-biphenylene bis[4-(4'-alkoxybenzoyloxy)]benzoate series the asymmetric nature originates from the 3,4'-substitution of the central biphenyl group and from the difference in length of the two terminal chains. All the melting points of the asymmetric compounds in the series with the central phenyl unit are lower than those of the symmetrical compounds. In the series with the central biphenyl unit, the compounds with the shortest chain attached to the para-position of the central biphenyl unit have the lowest melting points. The observed switching behavior of both the symmetric and asymmetric compounds with a B_2 phase was antiferroelectric in both series.

4.1   Introduction

In 1996, Niori *et al.* [1] discovered that some non-chiral molecules with a bent or banana shape possess unusual and interesting physical properties. These banana-shaped compounds can form new smectic and two-dimensional ordered phases, which are unlike those obtained from normal calamitic molecules [2]. These new phases are designated B_1-B_7 in order of their discovery. In recent years, the number of new banana and sub-banana phases has risen dramatically. One of the most interesting banana mesophases is the B_2 phase in which the molecules are packed in layers and tilted with respect to the layer normal. The dipole moment arising from the bent shape of the molecules does not coincide with the layer normal or the tilt direction, thus giving rise to chiral domains. Current response measurements of the compounds which exhibit the B_2 phase gave evidence that the ground state is in most cases antiferroelectric (SmCP$_A$) [3].

The fact that these non-chiral bent-core molecules exhibit antiferroelectric switching properties makes them very interesting for potential use in optical devices. Over the last 10 years numerous series of banana-shaped compounds have been synthesized and investigated. In general four parts of the banana-shaped molecules have been varied to study the influence of structure variations on mesomorphic properties and transitions temperatures. 1) The central part of the molecule: most of these compounds are composed of resorcinol derivatives substituted at the 1- and 3-positions. Also the 3,4'-disubstituted biphenyl central unit has proved to be a suitable building block for obtaining banana-shaped molecules [4]. Several attempts to introduce new central units in banana-shaped compounds have been made previously but few of these compounds exhibit the desired B-phases [5]; recently, naphthalene-2,7-diol was introduced as a new type of central unit [6,7]. Another way to obtain molecules with a bent shape is by introduction of a central alkylene chain with an odd number of flexible units between two mesogenic units [8,9], although compounds with these structures do not give banana phases as often as compounds with a central aromatic part. 2) The nature, position and direction of the linking groups between the rings. Ester [10] and a combination of ester and imine groups [11] are the most commonly used linking groups; by introducing different linking groups in each wing of the molecule, asymmetric banana-shaped compounds may be obtained [12]. 3) The length [13] and nature [4] of the terminal alkyl(oxy) chains. 4) Lateral substituents, introduced to one of the aromatic rings of the banana-shaped compound [14-16].

One reason for synthesizing different series of bent-core mesogens is to investigate whether changes in the structure might lower the melting points while retaining the

desired liquid crystalline B-phase. In this chapter we investigate two asymmetric series of banana-shaped compounds in which the lack of symmetry derives from differences in the terminal alkoxy chain lengths; in particular we study the effects of the asymmetry on the phase behavior and phase transition temperatures. In the series *m*-**P**-*n*, the central part of the molecule is a 1,3-disubstituted benzene; in the series *k*-**BP**-*l*, the central part of the molecules is a 3,4′-disubstituted biphenyl. The asymmetric nature of the central part of the compounds in the *k*-**BP**-*l* series results in two different molecules for two given terminal chains. The shorter tail can be attached to either the *para*(4′)- or the *meta*(3) position of the biphenyl group.

4.2 Experimental

4.2.1 Synthesis
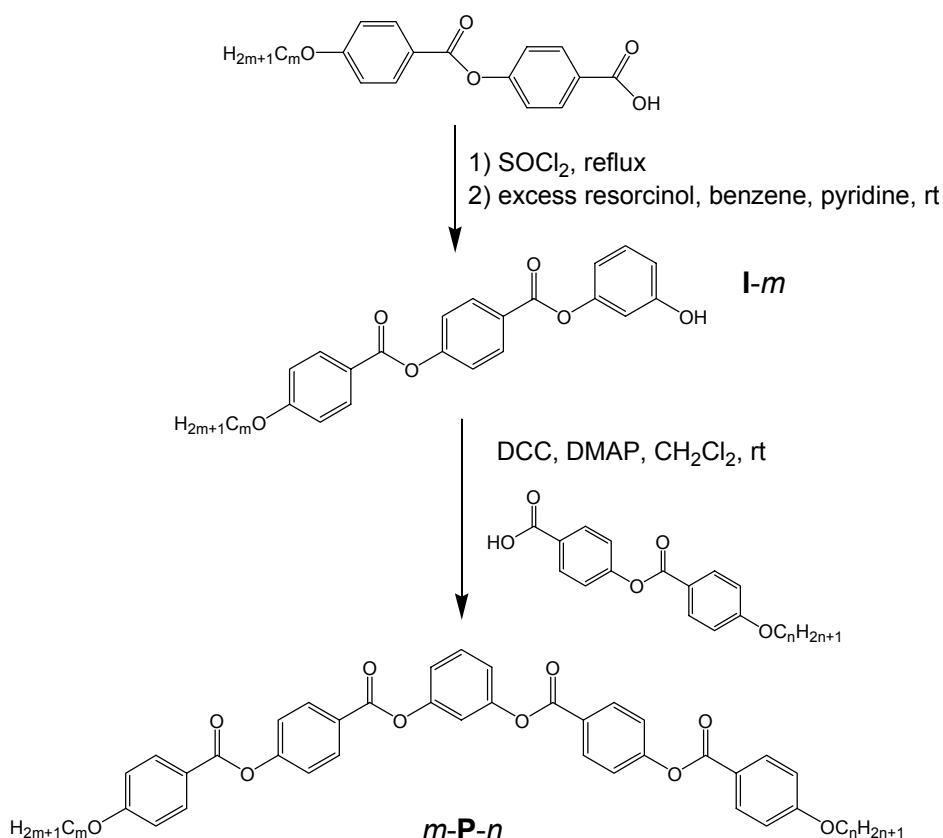
Scheme 1. *Synthetic pathway used for the preparation of compounds m-P-n.*

The compounds of series *m*-**P**-*n* were prepared according to scheme 1. The 4-(4-alkyloxybenzoyloxy)benzoic acids were obtained by esterification of 4-alkyloxybenzoyl chlorides with 4-hydroxybenzaldehyde [17] followed by NaClO$_2$

oxidation [18]. After conversion to the acid chloride with thionyl chloride, the first wing was attached to the central unit by reaction with excess resorcinol yielding compounds **I**-*m*. The second wing was attached via carbodiimide esterification [19] to yield the final compounds *m*-**P**-*n*. The symmetric compounds of the *m*-**P**-*n* series (*m* = *n*) were synthesized according to literature procedures [4].

The synthesis of the asymmetric compounds of the *k*-**BP**-*l* series is shown in scheme 2. The monosubstituted biphenol compounds (with one wing attached) were synthesized according to literature procedures [20]. The second wing was attached via the carbodiimide method [19] to yield the final compound. The symmetrically substituted compounds of the *k*-**BP**-*l* series (*k* = *l*) were synthesized according to literature procedures [4].
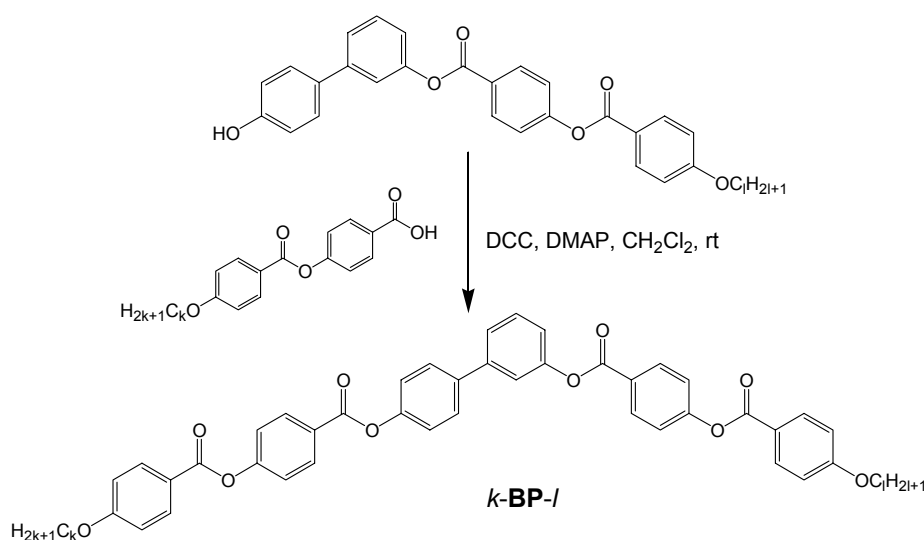
Scheme 2. Synthetic pathway used for the preparation of compounds k-BP-l.

*3-[4-(4-Dodecyloxybenzoyloxy)benzoyloxy]-phenol (**I-12**).*
4-(4-Dodecyloxybenzoyloxy)benzoic acid (0.90 g, 2.1 mmol) was heated under reflux in thionyl chloride (10 ml) for 2h. The excess of thionyl chloride was removed by distillation under reduced pressure. The resulting acid chloride was dissolved in 10 ml dry benzene and added to a solution of 1.16 g (10.5 mmol) resorcinol in anhydrous pyridine (10 ml). The reaction mixture was stirred for 24h at room temperature; it was then acidified with a 2 M HCl solution and extracted twice with CH_2Cl_2. The combined organic layers were washed with brine, then dried with Na_2SO_4 and filtered. The filtrate was concentrated and the residue was purified by column chromotography (eluant: 1% MeOH in CH_2Cl_2). Yield 55%, Mp 125°C. ^1H NMR (200 MHz, $CDCl_3$) δ (ppm): 8.26 (d, 2H, Ar), 8.15 (d, 2H, Ar), 7.35 (d, 2H, Ar), 7.25 (m, 1H, Ar), 6.98 (d, 2H, Ar), 6.72 (m, 3H, Ar), 4.05 (t, 2H, OCH_2), 1.83 (m, 2H,

OCCH$_2$), 1.60-1.27 (m, 18H, 9 x CH$_2$), 0.88 (t, 3H, CH$_3$). ^{13}C NMR (200 MHz, CDCl$_3$) δ (ppm): 164.7, 164.5, 163.9, 156.7, 155.4, 151.7, 132.5, 131.9, 130.2, 126.8, 122.2, 120.8, 114.4, 113.8, 113.3, 109.4, 68.4, 31.9, 29.7, 29.6, 29.4, 29.1, 26.0, 22.7, 14.2. Elemental analysis for C$_{32}$H$_{38}$O$_6$ (M = 518.64): calc. C 74.11, H 7.38; found C 74.25, H 7.40.

*1-[4-(4-Dodecyloxybenzoyloxy)benzoyloxy]-3-[4-(4-hexadecyloxybenzoyloxy)benzoyloxy]-benzene (12-**P**-16).*

To a mixture of 0.30 g (0.58 mmol) **I**-12, 0.28 g (0.58 mmol) 4-(4-hexadecyloxy-benzoyloxy)benzoic acid and a catalytic amount of 4-(*N,N*-dimethylamino)pyridine (DMAP) in 15 ml CH$_2$Cl$_2$ was added 0.18 g (0.87 mmol) *N,N*-dicyclohexylcarbodiimide (DCC) in 5 ml of CH$_2$Cl$_2$. This mixture was stirred for 24h at room temperature under N$_2$. The precipitate was filtered off and washed with CH$_2$Cl$_2$. The filtrate was concentrated and the residue was purified by column chromotography (eluant: 10% petroleum ether 40-60 in CH$_2$Cl$_2$). Finally, recrystallization from a mixture of petroleum ether 40-60 and CH$_2$Cl$_2$ gave colorless crystals; yield 68 %. ^{1}H NMR (200 MHz, CDCl$_3$) δ (ppm): 8.28 (d, 4H, Ar), 8.15 (d, 4H, Ar), 7.48 (t, 1H, Ar), 7.39 (d, 4H, Ar), 7.20 (s+d, 3H, Ar), 6.98 (d, 4H, Ar), 4.05 (t, 4H, OCH$_2$), 1.84 (m, 4H, OCCH$_2$), 1.60-1.20 (m, 44H, 22 x CH$_2$), 0.91 (t, 6H, CH$_3$). ^{13}C NMR (200 MHz, CDCl$_3$) δ (ppm): 164.1, 163.8, 155.5, 151.4, 132.5, 131.9, 129.9, 126.6, 122.2, 120.9, 119.3, 115.8, 114.4, 68.4, 31.9, 29.7, 29.6, 29.4, 29.1, 26.0, 22.7, 14.2. Elemental analysis for C$_{62}$H$_{78}$O$_{10}$ (M = 983.28): calc. C 75.73, H 8.00; found C 76.01, H 8.16.

*3-[4-(4-Hexadecyloxybenzoyloxy)benzoyloxy]-4′-[4-(4-dodecyloxybenzoyloxy)benzoyloxy]-biphenyl (12-**BP**-16).*

To a mixture of 0.20 g (0.31 mmol) 3-[4-(4-hexadecyloxybenzoyloxy)benzoyloxy]-4′-hydroxybiphenyl, 0.13 g (0.31 mmol) 4-(4-dodecyloxybenzoyloxy)benzoic acid and a catalytic amount of DMAP in 15 ml CH$_2$Cl$_2$, 0.10 g (0.49 mmol) DCC in 5 ml of CH$_2$Cl$_2$ was added. This mixture was stirred for 24h at room temperature under N$_2$. The precipitate was filtered off and washed with CH$_2$Cl$_2$. The filtrate was concentrated and the residue was purified by column chromotography (eluant: 10% petroleum ether 40-60 in CH$_2$Cl$_2$). Finally, recrystallization from a mixture of petroleum ether 40-60 and CH$_2$Cl$_2$ gave colorless crystals; yield 65 %. ^{1}H NMR (200 MHz, CDCl$_3$) δ (ppm): 8.30 (dd, 4H, Ar), 8.15 (d, 4H, Ar), 7.70-7.20 (m, 12H, Ar), 6.98 (d, 4H, Ar), 4.05 (t, 4H, OCH$_2$), 1.82 (m, 4H, OCCH$_2$), 1.45-1.10 (m, 44H, 22 x CH$_2$), 0.88 (t, 6H, CH$_3$). ^{13}C NMR (200 MHz, CDCl$_3$) δ (ppm): 164.4, 163.8, 155.4, 151.3, 150.6, 142.1, 138.0, 132.5, 131.9, 129.9, 128.4, 126.8, 124.7, 122.2, 120.9, 120.5, 114.4,

68.4, 31.9, 29.7, 29.6, 29.4, 29.1, 26.0, 22.7, 14.2. HRMS calcd for $C_{68}H_{82}O_{10}$ 1058.5908; found 1058.5908.

4.2.2 Measurements

Melting points, phase transition temperatures and optical inspection of the liquid crystalline phases were determined on samples between ordinary glass slides using an Olympus BH-2 polarization microscope equipped with a Mettler FP82HT hot stage, which was controlled by a Mettler FP80HT central processor. Differential scanning calorimetry (DSC) thermograms were obtained on a Perkin Elmer DSC-7 system using 2-5 mg samples in 50 µl sample pans and a scan rate of 5°C/min. Temperature dependent X-ray diffraction curves of the liquid crystals were measured on a Panalytical X'pert Pro diffractometer equipped with an Anton Paar camera for temperature control. For the measurements in the small angle region, the sample was spread in the isotropic or the liquid crystalline phase on a thin glass slide (about 15 µm thick), which was placed on a temperature-regulated flat copper sample stage. This sample preparation sometimes caused a preferential planar orientation of the molecules in the liquid crystalline state. Current response measurements were performed on polyimide-coated ITO cells with 6 µm spacing and a measuring area of 0.36 cm² by applying a triangular voltage.

4.3   Results and discussion

*1,3-Phenylene compounds m-**P**-n*

The transition temperatures and corresponding enthalpies of the compounds of series *m*-**P**-*n* are summarized in table 1. The transition temperatures of three symmetrical compounds of the *m*-**P**-*n* series (*m* = *n*) are also presented in this table. The transition temperatures of these symmetrical compounds (8-**P**-8, 12-**P**-12 and 16-**P**-16) agree reasonably well with some recently published values [10,21]. All members of the *m*-**P**-*n* series show liquid crystalline properties and all are enantiotropic, with a single mesophase between the melting point and the transition to the isotropic phase. Compound 8-**P**-12 forms an exception, exhibiting a monotropic mesophase observed during supercooling of the sample. In figure 1, the mesomorphic properties of the *m*-**P**-*n* series are represented schematically.

On increasing the terminal chain lengths, the three symmetrical compounds show the trend anticipated for banana-shaped compounds. The short homologue 8-**P**-8 exhibits the columnar banana phase (B_1). This phase can be detected on cooling from the isotropic state by the formation of a mosaic-like texture. For this phase a

rectangular columnar structure has been proposed [22]. The XRD pattern for this compound shows a broad peak in the wide-angle region and two reflections in the small angle region. From these reflections, the lattice parameters $a = 30.3$ Å and $c = 41.6$ Å were calculated. This indicates the presence of ~5 molecules per unit cell or 2.5 (two or three) molecules per building block. As found in several other homologous series of banana-shaped compounds, the longer homologues of the *m*-**P**-*n* series (12-**P**-12 and 16-**P**-16) exhibit the SmCP$_A$ (B$_2$) mesophase. The textures which were observed for these compounds on cooling from the isotropic phase showed similarities with the textures found for other compounds with B$_2$ phases [2]. The XRD patterns for these compounds show first and second order layer reflections, which point to a smectic phase. The broad peak in the wide angle region proves the liquid-like order of the molecules within the layers. The layer periodicities are given in table 1. According to Shen *et al.* [4] the B$_1$ phase is stable only if a partial overlap of the aromatic cores is possible. The B$_2$ phase can be obtained only if sufficiently long and flexible chains are present, which can suppress the formation of the frustrated B$_1$ structure. The critical terminal chain length for obtaining the B$_2$ phase increases with the size of the rigid aromatic core of the molecules.

Table 1. *Transition temperatures (°C), transition enthalpies (kJ mol⁻¹; between square brackets) and layer spacings d (Å) of the m-**P**-n series.*

Compound	Cr	B$_1$	B$_2$	I	d
*8-**P**-8*	● 121 [57]	● 121 [a]		●	
*12-**P**-12*	● 104 [42]		● 115 [22]	●	36.1
*16-**P**-16*	● 108 [57]		● 120 [25]	●	40.7
*8-**P**-11*	● 104 [42]	● 107 [a]		●	
*8-**P**-12*	● 103 [37]	(● 102.5) [a]		●	
*11-**P**-12*	● 99 [37]		● 113 [21]	●	35.5
*8-**P**-16*	● 91 [33]		● 107 [19]	●	36.3
*11-**P**-16*	● 90 [38]		● 115 [22]	●	38.1
*12-**P**-16*	● 92 [41]		● 115 [23]	●	38.5

[a] Could not be determined

In the *m*-**P**-*n* series, six compounds with two different terminal chain lengths were studied. For compounds 8-**P**-11 and 8-**P**-12 a mosaic-like texture was observed on cooling from the isotropic state, which is characteristic for the columnar B$_1$ phase. Both compounds have a lower melting point than the symmetrical compound which also exhibits the B$_1$ phase (8-**P**-8).
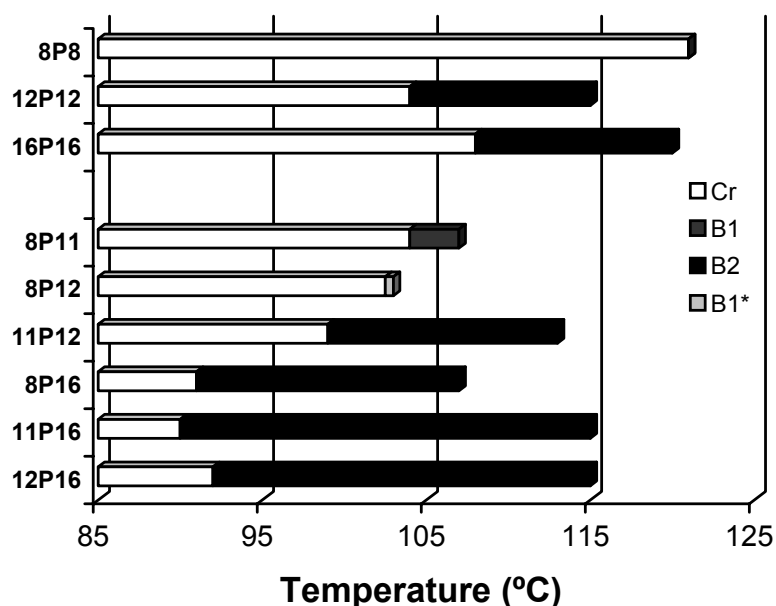
Figure 1. *Graphical representation of the phase transition temperatures of compounds m-**P**-n (*monotropic B₁ phase).*

The asymmetric compound 8-**P**-12 has a monotropic liquid crystal phase. The total number of carbon atoms in the terminal tails of 8-**P**-12 is 20. To determine the influence of asymmetry, we have compared this compound with symmetric compound 10-**P**-10 [10,21] which also has 20 C-atoms in its terminal chains. Although both compounds have 20 carbon atoms in their terminal chains, their liquid crystalline properties are completely different. Symmetric compound 10-**P**-10 exhibits the B_2 mesophase while the asymmetric compound 8-**P**-12 exhibits the B_1 phase. It must be noted, however, that according to Schröder *et al*. [21] compound 10-**P**-10 shows coexisting B_1 and B_2 phases over a small temperature range. Apparently, the thermotropic properties of this series of compounds is not determined solely by the total number of C-atoms in the terminal chains. As proposed by Shen *et al*. [4], the long terminal chains in 10-**P**-10 prevent partial overlap between the aromatic bent cores of the antiparallel arranged molecules and hence the B_1 phase is suppressed. For compound 8-**P**-12, formation of the B_1 phase is still favored over the formation of a layered structure such as the B_2 phase. Apparently asymmetry in banana-shaped compounds, by introducing two different terminal tail lengths, destabilizes the B_2 phase or makes partial overlap of the aromatic cores possible.

The compounds with the longer terminal chains 11-**P**-12, 8-**P**-16, 11-**P**-16 and 12-**P**-16 all exhibit the B_2 mesophase. On cooling, the optical textures of these compounds show small colored domains with some fans, but also Schlieren textures were observed. This is typical for B_2 textures as was also observed in several other B_2 compounds [2]. Figure 2 shows the electric response of compound 12-**P**-16 under a

triangular wave voltage. Two peaks were recorded during a half period indicating antiferroelectric switching behavior. The spontaneous polarization determined by integration of the switching current peaks was 870 nC / cm².
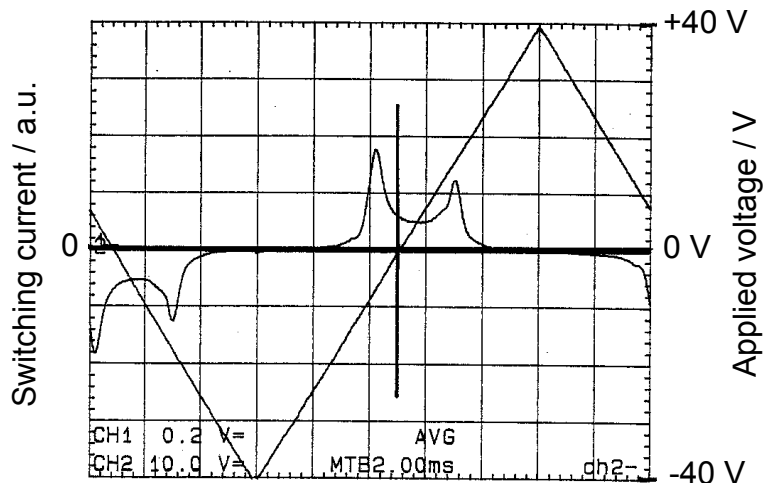

Figure 2. *Switching current response (a.u.) obtained in the B₂ phase of compound 12-**P**-16 at 106°C by applying a triangular voltage (50 Hz).*

Asymmetric materials usually have a broader mesophase range than their symmetric analogues [23,24]. From table 1 and figure 1, it can indeed be seen that the compounds with two different terminal alkoxy tails have the broadest mesophase ranges. This is caused by a lowering of the melting points. For this series of compounds a difference in length of the terminal chains of five or six carbon atoms is probably required to make the lowering of the melting points as large as possible.
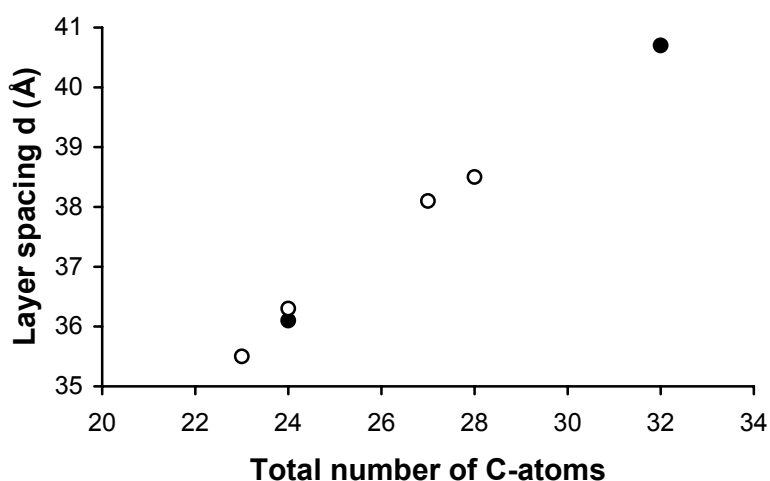

Figure 3. *Dependence of the layer spacings d of the symmetric and asymmetric compounds of the m-**P**-n series on the total number of C-atoms in the terminal chains (m = n, ●; m ≠ n, ○).*

The X-ray patterns of planar oriented samples exhibiting the B_2 phase all indicate a tilted smectic phase in which the layer spacing d steadily increases with the total number of C-atoms (table 1). Figure 3 shows the relationship between the total number of C-atoms in the terminal alkyl chains of these compounds and the layer spacing. The linear relationship shows that in all cases the layer organization (tilt angle) for the symmetric and asymmetric compounds are very similar. For all compounds in the m-**P**-n series that exhibit the B_2 mesophase, a tilt angle of approximately 45° was calculated from the molecular lengths (assuming a bending angle of 120°) and the layer spacings d. This was also observed in other series [4,25].

*3,4′-Biphenyl compounds k-**BP**-l*

To investigate further the influence of two different terminal chains, we synthesized a second series of compounds in which the central phenyl group of the m-**P**-n series is replaced by a biphenyl group. The bent shape of the molecules in the k-**BP**-l series is caused by the 3,4′-disubstitution of the central biphenyl unit. The thermotropic properties of the symmetrically substituted compounds with terminal chains ranging from 8 to 14 have been described by Shen *et al.* [4]. We have synthesized and studied three symmetrically substituted compounds ($k = l = 8$, 12 and 16), and seven asymmetrically substituted compounds with different combinations of terminal chain lengths. The transition temperatures together with the associated transition enthalpies of the compounds of series k-**BP**-l are given in table 2. All melting points are determined on the first heating. It must be noted that in some cases melting points are significantly lower on second and third heating.

Table 2. *Transition temperatures (°C), transition enthalpies (kJ mol⁻¹; between square brackets) and layer spacings d (Å) of the k-**BP**-l series.*

Compound	Cr	B_1	B_2	I	*d*
*8-**BP**-8*	● 132 [25]	● 176 [20]		●	
*12-**BP**-12*	● 109 [38]		● 157 [23]	●	38.9
*16-**BP**-16*	● 91 [52]		● 160 [27]	●	43.8
*8-**BP**-12*	● 105 [29]	● 164 [20]		●	
*12-**BP**-8*	● 113 [56]	● 157 [19]		●	
*8-**BP**-16*	● 112 [a]		● 149 [21]	●	39.4
*16-**BP**-8*	● 116 [62]		● 149 [20]	●	39.7
*12-**BP**-16*	● 99 [a]		● 158 [25]	●	41.6
*16-**BP**-12*	● 109 [42]		● 157 [24]	●	41.6
*11-**BP**-12*	● 105 [35]		● 156 [24]	●	38.4

[a] Could not be determined

The mesomorphic properties of the compounds of series *k*-**BP**-*l* (and also of the parent compounds 8-**BP**-8, 12-**BP**-12 and 16-**BP**-16*)* are represented schematically in figure 4. Exchanging the 1,3-disubstituted resorcinol unit in the *m*-**P**-*n* series for the 3,4′-disubstituted biphenyl in the *k*-**BP**-*l* series results, for the symmetrically substituted compounds, in an increase of the liquid crystalline range. All three parent compounds retain their liquid crystalline mesophase on increasing the size of the rigid core of the molecule. As predicted by Shen *et al*. [4], the transition from the columnar B_1 phase to the switchable B_2 phase occurs in the **P**-series at 9-**P**-9 to 10-**P**-10 [10] and in the **BP**-series at 11-**BP**-11 to 12-**BP**-12 due to the increase in size of the rigid core.
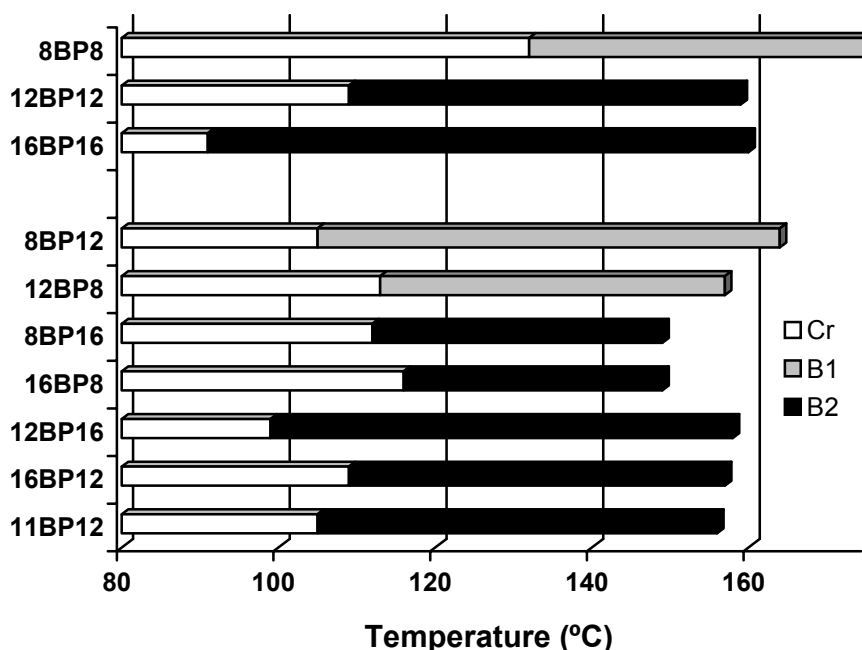

Figure 4. *Graphical representation of the phase transition temperatures of k-BP-l.*

We have studied three pairs of non-symmetrically substituted compounds in the *k*-**BP**-*l* series. The pair with the shortest chains (8-**BP**-12 and 12-**BP**-8) exhibits the B_1 phase while the other pairs show the B_2 phase. Figure 5 shows an optical photomicrograph of the B_1 texture obtained of compound 12-**BP**-8 and the Schlieren pattern obtained for the B_2 mesophase of compound 12-**BP**-16. For all three asymmetric pairs with the same total number of carbon atoms in the tails the compounds with the shortest tail attached to the *para*-position of the biphenyl group have the lowest melting points. A lowering of the melting point could however not be achieved by asymmetric substitution of the **BP**-compounds when compared with those of the symmetrically substituted **BP**-compounds.
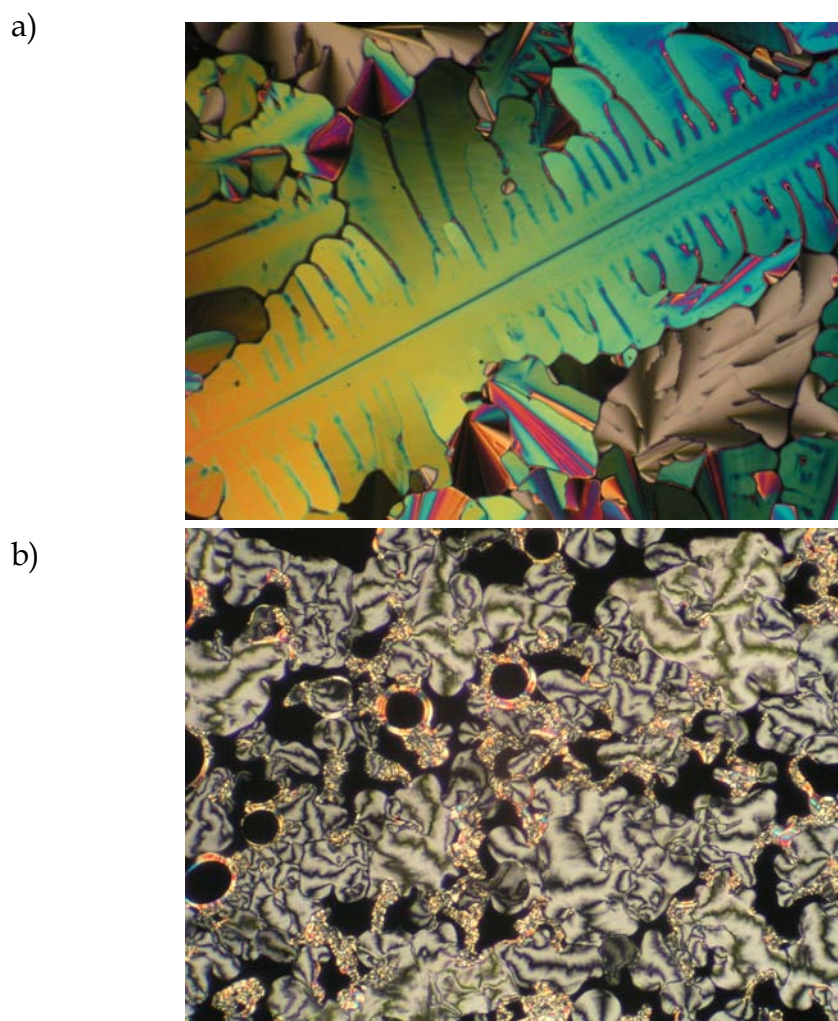
*Figure 5. Optical photomicrographs of the textures observed on cooling from the isotropic state at 155ºC for a) B₁ phase of compound 12-**BP**-8 and b) B₂ phase of compound 12-**BP**-16.*

Asymmetric molecules usually have a broader mesophase range than their symmetric analogues mainly due to a lowering of the melting points. According to Mieczkowski *et al*. [24], this also has a strong influence on the polar structure of the mesophase; asymmetric compounds have a tendency to form ferroelectric phases instead of antiferroelectric phases. As was the case for the **P**-series, the switching behavior of the **BP**-series was antiferroelectric. This corresponds to observations for the symmetrically substituted compounds [10].

In the **BP**-series, we have studied mainly compounds which differ by four or eight C-atoms in their terminal tails. To investigate whether a smaller difference in length of terminal chains will result in a lower melting point, we have also synthesized compound 11-**BP**-12 (B₂ phase). When compared with 12-**BP**-12 the melting point has decreased by 4°C to 105°C, which suggests that for the compounds in the *k*-**BP**-*l* series, only a small difference in number of C-atoms in the terminal chains is effective in lowering the melting point.
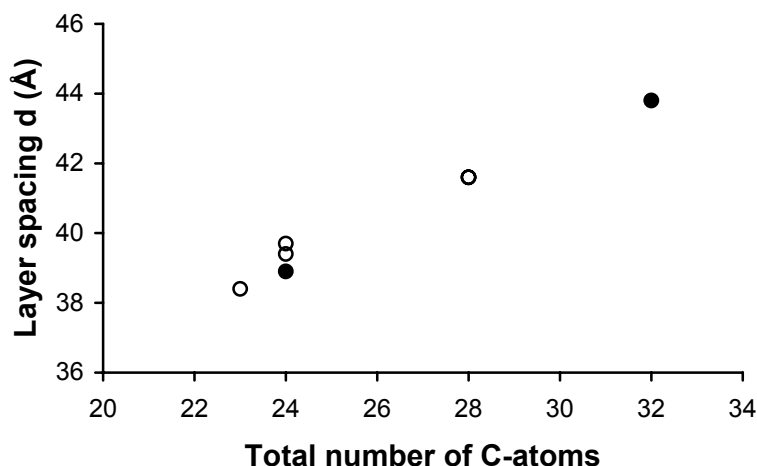
Figure 6*. Dependence of the layer spacings d of the symmetrically substituted compounds and non-symmetric compounds of the k-**BP**-l series on the total number of C-atoms in the terminal chains (k = l, ● ; k ≠ l, ○).*

The X-ray patterns of all compounds of the *k*-**BP**-*l* series show a diffuse wide angle peak. The compounds which exhibit the B_1 phase all show two reflections in the small angle region pointing to the presence of a two-dimensional rectangular cell. From the cell dimensions the number of molecules per building block can be calculated [26]. It was found to increase from ~2.5 for 8-**BP**-8 to ~3 for 8-**BP**-12 and 12-**BP**-8. The layer spacings *d* of the compounds with a B_2 phase are listed in table 2 and shown in figure 6. Again it seems that there is barely any change in layer organization due to the introduction of two different terminal alkyl chains. For all compounds there is a linear relationship between the total number of C-atoms in the terminal chains, and the layer spacing *d*. In all cases the tilt angle of the molecules in the smectic layers is ~45° (assuming a bending angle of 120°). It has to be noted, however, that the layer spacings for the compounds with the largest asymmetric component (8-**BP**-16 and 16-**BP**-8) are slightly larger than the expected layer spacing for symmetrically substituted compounds.

4.4 Conclusions

Two series of asymmetrical ester-like banana-shaped compounds with different terminal chain lengths have been synthesized and studied. Going from the symmetrical *m*-**P**-*n* series with a central phenyl group to the symmetrically substituted *k*-**BP**-*l* series with a central biphenyl group, the liquid crystalline range increases dramatically with retention of the liquid crystalline B-phases. For the asymmetrical compounds of the **P**-series the melting points are lower when

compared with those of the parent compounds. To most efficiently lower the melting points for this series of compounds a difference in terminal chain length of ~5 C-atoms (11-**P**-16) is required.

For the compounds of the **BP**-series, it seems more difficult to lower the melting points. Since all compounds (also compounds with *k* = *l*) of the **BP**-series have an asymmetric central part it is difficult to introduce even more asymmetry to lower the melting points. A small difference in terminal chain length however (11-**BP**-12) can result in a small reduction of the melting point. Surprisingly, the asymmetrically substituted compounds in the *k*-**BP**-*l* series with k < l (shortest terminal chain attached to the *para*-position of the central biphenyl group) give the lowest melting points.

This study has shown that the *m*-**P**-*n* series shows antiferroelectric switching behavior. Introduction of two different terminal alkyl chains can lower the melting points of banana-shaped compounds that exhibit the switchable B_2 phase, thus expanding on the temperature range where they can be operated in potential devices.

4.5   References

1. Niori T., Sekine F., Watanabe J., Furukawa T. and Takezoe H. *J. Mater. Chem.* **1996**, *6*, 1231-1233.
2. Pelzl G., Diele S. and Weissflog W. *Adv. Mater.* **1999**, *11*, 707-724.
3. Link D. R., Natale G., Shao R., Maclennan J. E., Clark N. A., Körblova E. and Walba D. M. *Science* **1997**, *278*, 1924-1927.
4. Shen D., Pegenau A., Diele S., Wirth I. and Tschierske C. *J. Am. Chem. Soc.* **2000**, *122*, 1593-1601.
5. Shen D., Diele S., Pelzl G., Wirth I. and Tschierske C. *J. Mater. Chem.* **1999**, *9*, 661-672.
6. Svoboda J., Novotna V., Kozmik V., Glogarova M., Weissflog W., Diele S. and Pelzl G. *J. Mater. Chem.* **2003**, *13*, 2104-2110.
7. Thisayukta J., Nakayama Y., Kawauchi S., Takezoe H. and Watanabe J. *J. Am. Chem. Soc.* **2000**, *122*, 7441-7448.
8. Watanabe J., Izumi T., Niori T., Zennyoji M., Takanishi Y. and Takezoe H. *Mol. Cryst. Liq. Cryst.* **2000**, *346*, 77-86.
9. Prasad V., Shankar Rao D. S. and Krishna Prasad S. *Liq. Cryst.* **2001**, *28*, 761-767.
10. Amaranatha Reddy R. and Sadashiva B. K. *Liq. Cryst.* **2003**, *30*, 1031-1050.
11. Bedel J. P., Rouillon J. C., Marcerou J. P., Laguerre M., Nguyen H. T. and Achard M. F. *Liq. Cryst.* **2000**, *27*, 1411-1421.
12. Prasad V., Kang S.-W. and Kumar S. *J. Mater. Chem.* **2003**, *13*, 1259-1264.
13. Achten R., Koudijs A., Karzcmarzyk Z., Marcelis A. T. M. and Sudhölter E. J. R. *Liq. Cryst.* **2004**, *31*, 215-227.
14. Weissflog W., Nadasi H., Dunemann U., Pelzl G., Diele S., Eremin A. and Kresse H. *J. Mater. Chem.* **2001**, *11*, 2748-2758.

15. Bedel J. P., Rouillon J. C., Marcerou J. P., Laguerre M., Nguyen H. T. and Achard M. F. *J. Mater. Chem.* **2002**, *12*, 2214-2220.
16. Sadashiva B. K., Murthy H. N. S. and Dhara S. *Liq. Cryst.* **2001**, *28*, 483-487.
17. Tschierske C. and Zaschke H. *J. Prakt. Chem.* **1988**, *330*, 1-14.
18. Lee G. S., Lee Y-J., Choi S. Y., Park Y. S. and Yoon K. B. *J. Am. Chem. Soc.* **2000**, *122*, 12151-12157.
19. Tschierske C. and Zaschke H. *J. Prakt. Chem.* **1989**, *331*, 365-366.
20. Dantlgraber G., Eremin A., Diele S., Hauser A., Kresse H., Pelzl G. and Tschierske C. *Angew. Chem. Int. Ed.* **2002**, *41*, 2408-2412.
21. Schröder M. W., Diele S., Pelzl G. and Weissflog W. *Chem. Phys. Chem.* **2004**, *5*, 99-103.
22. Watanabe J., Niori T., Sekine T. and Takezoe H. *Jpn. J. Appl. Phys.* **1998**, *37*, L139.
23. Blatch A. E. and Luckhurst G. R. *Liq. Cryst.* **2000**, *27*, 775-787.
24. Mieczkowski J., Gomola K., Koseska J., Pociecha D., Szydlowska J. and Gorecka E. *J. Mater. Chem.* **2003**, *13*, 2132-2137.
25. Fodor-Csorba K., Vajda A., Galli G., Jákli A., Demus D., Holly S. and Gács-Baitz E. *Macromol. Chem. Phys.* **2002**, *203*, 1556-1563.
26. Pelz K., Weissflog W., Baumeister U. and Diele S. *Liq. Cryst.* **2003**, *30*, 1151-1158.

5

# Non-symmetric bent-core mesogens with one terminal vinyl group

Two series of non-symmetric banana-shaped compounds, both with one alkyl and one alkenyl terminal tail, have been synthesized and studied. Both series were compared with the corresponding series with two saturated terminal alkyl tails. All the compounds have a bent central 1,3-phenylene bis(4-benzoyloxy)benzoate core; their mesophases were characterized by polarizing optical microscopy, differential scanning calorimetry, X-ray diffraction and switching current response experiments. The short-tailed compounds show monotropic or enantiotropic B_1 phases and the long-tailed compounds the B_2 phase. The introduction of one terminal vinyl group slightly lowers the transition temperatures. The introduction of a second terminal vinyl group further suppresses the liquid crystalline properties. All compounds with B_2 phases have layer spacings that suggest a tilt of ~45° of the bent molecules in the layers, and their switching behavior is antiferroelectric.

5.1 Introduction

Ferroelectricity [1] and antiferroelectricity [2] were first discovered in chiral tilted smectic phases. In 1996, Niori *et al.* [3] were the first to report smectic phases of achiral molecules with a bent core which had ferroelectric switching properties. Ever since, these so-called banana-shaped liquid crystals have attracted great interest [4,5]. Among the eight B-phases (B_1 – B_8) known to date [4,6] the B_2 phase is the most interesting. In this B_2 phase the molecules are ordered in a layered arrangement (Sm) in which the bent molecules are tilted (C) and the dipoles point along a common direction within the layer (P); therefore this phase is also designated as a SmCP phase. The ground state is mainly regarded as antiferroelectric [7], although ferroelectric ground states have also been reported [8].

In the past eight years several hundred banana-shaped compounds have been synthesized and studied [4,9-12]. It is, however, still very difficult to establish structure-property relationships for these kinds of compounds. Most bent-core molecules studied so far in the literature are symmetric. Some compounds, however, lack an internal mirror plane and are therefore referred to as asymmetric or non-symmetric. When using the term "asymmetry" this should not be confused with "chirality". Non-symmetry for banana-shaped compounds can and has been achieved in a number of ways: (1) by a non-symmetrically substituted central group [9,13-17]; (2) by two different terminal end groups or chains [18-28]; (3) by different linking groups in each wing of the molecule [19,23,28]; (4) by different (polar) substituents in each wing of the molecule [20-22,26]. In most of these cases, however, the non-symmetric nature of the investigated compounds arises from a combination of two of these possibilities.
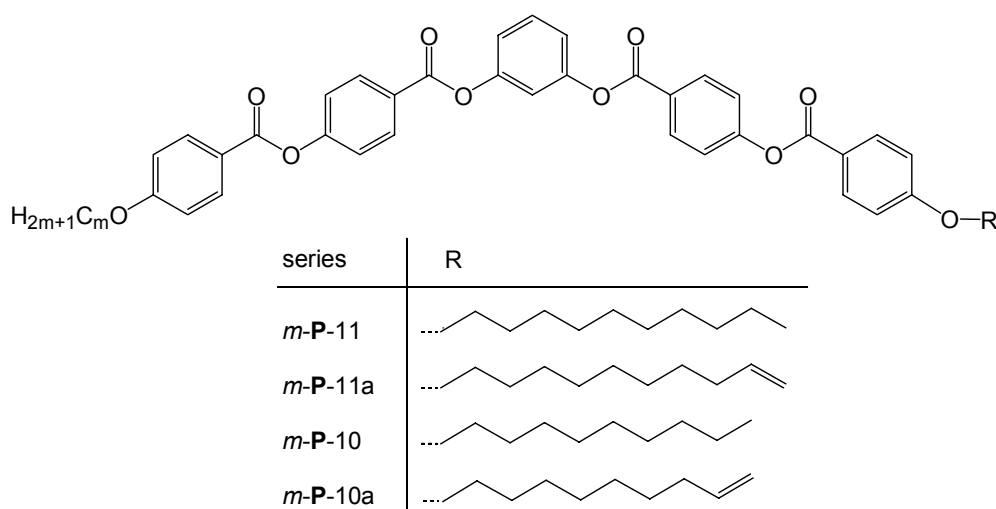
Scheme 1. General structures of the four homologous series.

In a previous study [27] we investigated the influence of non-symmetry in a series of banana-shaped compounds with two terminal alkoxy tails of different length. In the present study, we have extended the number of compounds in this *m*-**P**-*n* series, but have also synthesized and studied compounds with one or two terminal alkene groups. These compounds are of interest for preparing oligomeric or polymeric siloxanes by a hydrosilylation reaction. Four homologous series, each consisting of six compounds have been studied (scheme 1). In the *m*-**P**-11 and *m*-**P**-10 series, the lack of symmetry is derived solely from the difference in length of the two terminal alkoxy tails. In series *m*-**P**-11a and *m*-**P**-10a, the lack of symmetry is derived from the difference in length of the two terminal tails and the presence of one terminal vinyl group.

5.2 Experimental

5.2.1 Synthesis

The compounds of series *m*-**P**-*n* (with no terminal double bonds present) were prepared according to literature procedures [27]. The compounds of series *m*-**P**-*n*(a) were prepared according to scheme 2. Monosubstituted resorcinol derivatives **P**-*m* were obtained by first converting the 4-(4-alkyloxybenzoyloxy)benzoic acid (*m*) with thionyl chloride to the acid chlorides, and subsequent reaction with excess resorcinol. Compounds **I**-*n*(a) were obtained by etherification of the corresponding bromoalkene (*n* = 10 and 11) with methyl 4-hydroxybenzoate with K_2CO_3 as base, followed by hydrolysis with KOH. Compounds *n*(a) were obtained by esterification of the acid chlorides of **I**-*n*(a) with 4-hydroxybenzaldehyde, to give **II**-*n*(a), followed by $NaClO_2$ oxidation [29]. End products *m*-**P**-*n*(a) were obtained via carbodiimide esterification of **P**-*m* and *n*(a) [30].

4-[4-(9-Decenyloxy)benzoyloxy]benzaldehyde (II-10a).
Compound **I**-10a (4.50 g, 16.3 mmol) was heated under reflux conditions in thionyl chloride (30 ml) for 2h. Excess thionyl chloride was removed by distillation under reduced pressure. The resulting acid chloride was dissolved in 15 ml dry toluene and added to a solution of 2.07 g (17.0 mmol) 4-hydroxybenzaldehyde in a mixture of 20 ml pyridine and 15 ml toluene. The reaction mixture was stirred for 24h at room temperature; it was then acidified with a 2M HCl solution and extracted twice with CH_2Cl_2. The combined organic layers were washed with brine, then dried with Na_2SO_4 and filtered. The filtrate was concentrated and the residue purified by column chromatography (eluant: CH_2Cl_2); yield 95%, Cr 64 (N 51) I (ºC). ^{1}H NMR

(200 MHz, CDCl$_3$) δ (ppm): 10.02 (s, 1H, CHO), 8.14 (d, 2H, Ar), 7.96 (d, 2H, Ar), 7.39 (d, 2H, Ar), 6.98 (d, 2H, Ar), 5.81 (m, 1H, =CH), 4.98 (m, 2H, =CH$_2$), 4.04 (t, 2H, OCH$_2$), 2.02 (m, 2H, =CCH$_2$), 1.82 (m, 2H, OCCH$_2$) 1.60-1.33 (m, 10H, 5 x CH$_2$). ^{13}C NMR (CDCl$_3$) δ (ppm): 191.1, 164.3, 163.9, 155.9, 139.2, 133.9, 132.5, 131.3, 122.6, 120.8, 114.4, 114.2, 68.4, 33.8, 29.4, 29.3, 29.1, 28.9, 26.0.
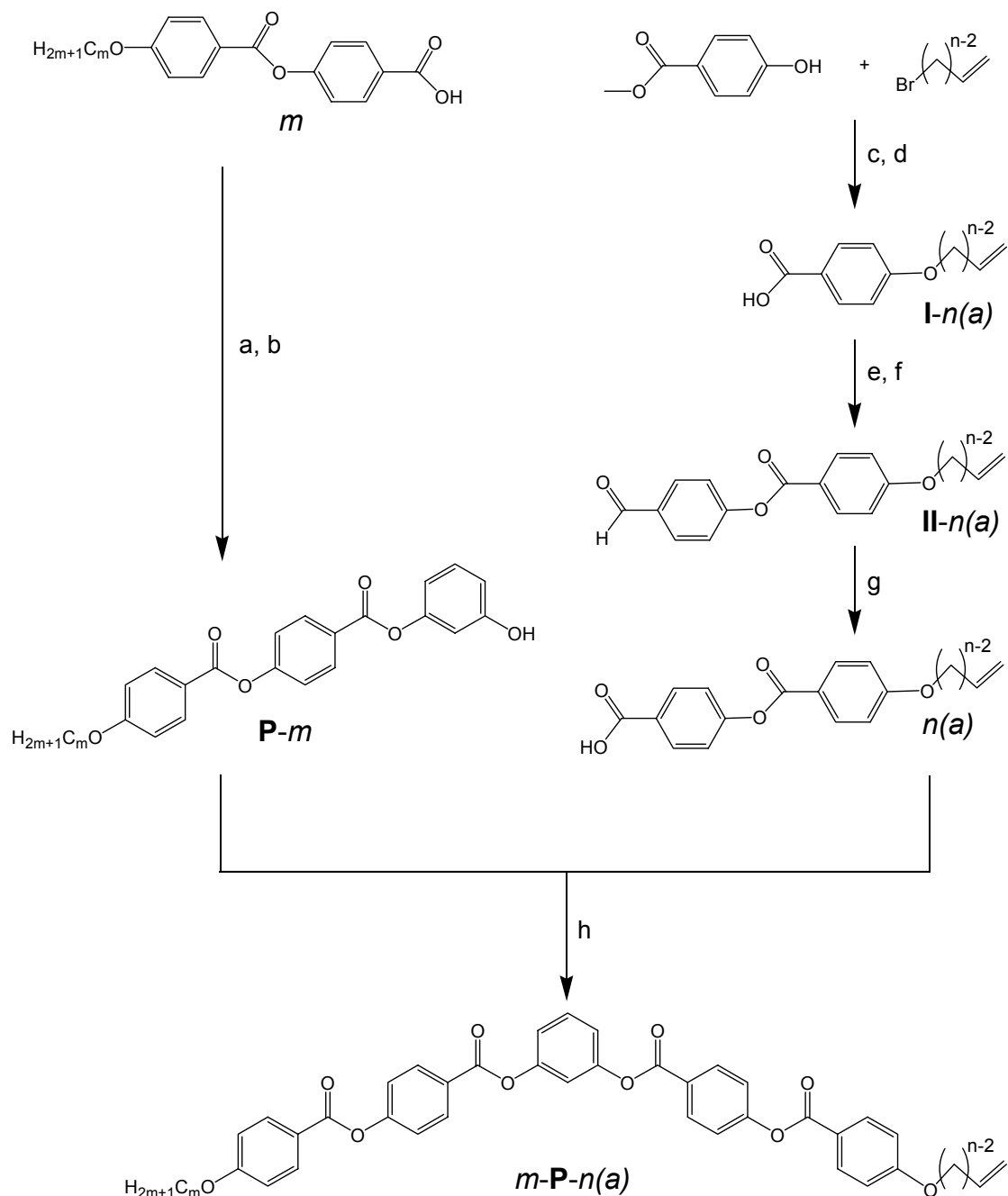
Scheme 2. *Synthesis of compounds m-**P**-n(a): a) SOCl$_2$, reflux; b) excess resorcinol, toluene, pyridine, rt; c) K$_2$CO$_3$, butanone, reflux; d) KOH, EtOH, reflux; e) SOCl$_2$, reflux; f) 4-hydroxybenzaldehyde, toluene, pyridine, rt; g) NaClO$_2$, resorcinol, NaH$_2$PO$_4$, t-BuOH, H$_2$O, rt [29]; h) DCC, DMAP, CH$_2$Cl$_2$, rt.*

4-[4-(9-Decenyloxy)benzoyloxy]benzoic acid (10a)

Compound **II**-10a (5.90 g, 15.5 mmol) and resorcinol (2.20 g) were dissolved in *tert*-butyl alcohol (300 ml). To this solution was added dropwise, over 10 min, a solution of sodium chlorite (80%, Aldrich) (8.10 g, 89.6 mmol) and sodium dihydrogenphosphate monohydrate (6.42 g, 46.5 mmol) in 85 ml water. The resulting pale yellow reaction mixture was then stirred at room temperature overnight. Volatile components were removed *in vacuo* and the residue was dissolved in 250 ml water. The aqueous solution was acidified to pH 3 by adding 1M HCl. The white precipitate was filtered, washed successively with water and hexane, and dried in the air; yield 87%, Cr 114 SmC 180 N 220 I (°C). ^{1}H NMR (200 MHz, CDCl$_3$) δ (ppm): 8.17 (dd, 4H, Ar), 7.33 (d, 2H, Ar), 6.98 (d, 2H, Ar), 5.82 (m, 1H, =CH), 4.98 (m, 2H, =CH$_2$), 4.04 (t, 2H, OCH$_2$), 2.02 (m, 2H, =CCH$_2$), 1.82 (m, 2H, OCCH$_2$) 1.60-1.34 (m, 10H, 5 x CH$_2$). ^{13}C NMR (CDCl$_3$) δ (ppm): 171.5, 164.4, 163.8, 155.6, 139.2, 132.4, 131.9, 126.7, 122.0, 120.9, 114.4, 114.2, 68.4, 33.8, 29.4, 29.3, 29.1, 28.9, 26.0.

*1-{4-[4-(10-Undecenyloxy)benzoyloxy]benzoyloxy}-3-[4-(4-octyloxybenzoyloxy)benzoyloxy]-benzene (8-**P**-11a).*

To a mixture of 0.46 g (1.0 mmol) 3-[4-(4-octyloxybenzoyloxy)benzoyloxy]phenol (**P**-8) 0.41 g (1.0 mmol) 4-[4-(10-undecenyloxy)benzoyloxy]benzoic acid, and a catalytic amount of 4-(*N,N*-dimethylamino)pyridine (DMAP) in 25 ml CH$_2$Cl$_2$ was added 0.31 g (1.5 mmol) *N,N'*-dicyclohexylcarbodiimide (DCC) in 10 ml of CH$_2$Cl$_2$. This mixture was stirred for 24h at room temperature under N$_2$ atmosphere. The precipitate was filtered off and washed with CH$_2$Cl$_2$. The filtrate was concentrated and the residue purified by column chromatography (eluant CH$_2$Cl$_2$). Finally, recrystallization from a mixture of petroleum ether 40-60 and CH$_2$Cl$_2$ gave colorless crystals; yield 64 %. ^{1}H NMR (200 MHz, CDCl$_3$) δ (ppm): 8.28 (d, 4H, Ar), 8.16 (d, 4H, Ar), 7.50 (t, 1H, Ar), 7.38 (d, 4H, Ar), 7.19 (s+d, 3H, Ar), 7.00 (d, 4H, Ar), 5.81 (m, 1H, =CH), 4.96 (m, 2H, =CH$_2$), 4.05 (t, 4H, OCH$_2$), 2.03 (m, 2H, C=CCH$_2$), 1.79 (m, 4H, OCCH$_2$), 1.55-1.32 (m, 22H, 11 x CH$_2$), 0.90 (t, 3H, CH$_3$). ^{13}C NMR (CDCl$_3$) δ (ppm): 164.3 164.1, 163.8, 155.5, 151.4, 139.2, 132.5, 131.9, 129.9, 126.6, 122.2, 120.9, 119.3, 115.9, 114.4, 114.2, 68.4, 33.8, 31.8, 29.5, 29.4, 29.3, 29.1, 28.9, 26.0, 22.7, 14.1. Elemental analysis for C$_{53}$H$_{58}$O$_{10}$ (*M* = 855.04): calc. C 74.45, H 6.84; found C 74.74, H 6.92%. HRMS calc. for C$_{53}$H$_{58}$O$_{10}$ 854.4030; found 854.4013.

*1-[4-(4-Undecyloxybenzoyloxy)benzoyloxy]-3-[4-(4-octyloxybenzoyloxy)benzoyloxy]benzene (8-**P**-11).*

This compound was prepared similarly to 8-**P**-11a from 4-(4-undecyloxybenzoyloxy)benzoic acid (*m* = 11) and **P**-8; yield 64 %. ^{1}H NMR (200 MHz, CDCl$_3$) δ (ppm): 8.27 (d, 4H, Ar), 8.14 (d, 4H, Ar), 7.49 (t, 1H, Ar), 7.36 (d, 4H, Ar), 7.18 (s+d, 3H, Ar), 6.98 (d, 4H, Ar), 4.05 (t, 4H, OCH$_2$), 1.78 (m, 4H, OCCH$_2$), 1.55-1.27 (m, 26H, 13 x CH$_2$), 0.87 (t, 6H, CH$_3$). ^{13}C NMR (CDCl$_3$) δ (ppm): 164.3, 164.1, 163.8, 155.5, 151.4, 132.5, 131.9, 129.9, 126.6, 122.2, 120.9, 119.3, 115.9, 114.4, 68.4, 31.9, 31.8, 29.6, 29.4, 29.2, 29.1, 26.0, 22.7, 14.2. Elemental analysis for C$_{53}$H$_{60}$O$_{10}$ (*M* = 857.05): calc. C 74.28, H 7.06; found C 74.44, H 7.10%.

*1-{4-[4-(9-Decenyloxy)benzoyloxy]benzoyloxy}-3-[4-(4-octyloxybenzoyloxy)benzoyloxy]-benzene (8-**P**-10a).*

This compound was prepared similarly to 8-**P**-11a from compounds 10a and **P**-8; yield 68 %. ^{1}H NMR (200 MHz, CDCl$_3$) δ (ppm): 8.28 (d, 4H, Ar), 8.16 (d, 4H, Ar), 7.50 (t, 1H, Ar), 7.38 (d, 4H, Ar), 7.19 (s+d, 3H, Ar), 6.99 (d, 4H, Ar), 5.81 (m, 1H, =CH), 4.97 (m, 2H, =CH$_2$), 4.05 (t, 4H, OCH$_2$), 2.04 (m, 2H, C=CCH$_2$), 1.83 (m, 4H, OCCH$_2$), 1.60-1.34 (m, 20H, 10 x CH$_2$), 0.90 (t, 3H, CH$_3$). ^{13}C NMR (200 MHz, CDCl$_3$) δ (ppm): 164.3 164.1, 163.8, 155.5, 151.4, 139.2, 132.5, 131.9, 129.9, 126.6, 122.2, 120.9, 119.3, 115.9, 114.4, 114.2, 68.4, 33.8, 31.8, 29.4, 29.3, 29.1, 28.9, 26.0, 22.7, 14.2. Elemental analysis for C$_{52}$H$_{56}$O$_{10}$ (*M* = 841.01): calc. C 74.26, H 6.71; found C 74.23, H 6.75%.

5.2.2   Measurements

Melting points, thermal phase transition temperatures and optical characters of the liquid crystalline phases were determined on samples between ordinary glass slides using an Olympus BH-2 polarization microscope equipped with a Mettler FP82HT hot stage, which was controlled by a Mettler FP80HT central processor. Differential scanning calorimetry (DSC) thermograms were obtained on a Perkin Elmer DSC-7 system using 2-4 mg samples in 50 μL sample pans and a scan rate of 5°C/min. ΔH is calculated in kJ/mol. Temperature dependent X-ray diffraction curves of the liquid crystals were measured on a Panalytical X'pert Pro diffractometer equipped with an Anton Paar camera for temperature control. For the measurements in the small angle region, the sample was spread in the isotropic or the liquid crystalline phase on a thin glass slide (about 15 μm thick) which was placed on a temperature-regulated flat copper sample stage. This sample preparation sometimes caused a preferential planar orientation of the molecules in the liquid crystalline state. Current response measurements were performed on 6 μm thick polyimide-coated ITO cells with a measuring area of 0.36 cm^2 by applying a triangular voltage.

5.3   Results and discussion

*m-**P**-11 and m-**P**-11a series*

In table 1 the phase transition temperatures and corresponding enthalpies of the compounds of series *m-**P**-11* and *m-**P**-11a* are summarized. In the compounds of the *m-**P**-11* series one of the terminal tails is $OC_{11}H_{23}$; the other is varied between OC_8H_{17} (*m* = 8) and $OC_{16}H_{33}$ (*m* = 16). In the compounds of the *m-**P**-11a* series one of the terminal tails is $O(CH_2)_9CH=CH_2$ (*11a*) and *m* is varied between 8 and 16.

Table 1. *Transition temperatures (°C), transition enthalpies (kJ mol⁻¹; between square brackets) and layer spacings d (Å) of the m-**P**-11 and m-**P**-11a series.*

Compound	Cr	B₁	B₂	I	d
*8-**P**-11* [27]	● 104 [42]	● 107 [a]		●	-
*10-**P**-11*	● 98 [34]		● 111 [20]	●	34.0
*11-**P**-11* [10]	● 104 [38]		● 113 [21]	●	34.9
*12-**P**-11* [27]	● 99 [37]		● 113 [21]	●	35.5
*14-**P**-11*	● 90 [35]		● 115 [22]	●	37.0
*16-**P**-11* [27]	● 90 [38]		● 115 [22]	●	38.1
*8-**P**-11a*	● 103 [37]	(● 100.5) [16]		●	-
*10-**P**-11a*	● 103 [a]		● 104 [19]	●	33.8
*11-**P**-11a*	● 102 [29]		● 105 [18]	●	34.8
*12-**P**-11a*	● 91 [32]		● 103.5 [19]	●	35.4
*14-**P**-11a*	● 85 [35]		● 107 [21]	●	36.5
*16-**P**-11a*	● 84 [33]		● 107 [21]	●	38.1

[a] The transition enthalpy could not be determined

The mesomorphic properties of the compounds in the *m-**P**-11* series are represented schematically in figure 1. All compounds in this series show enantiotropic liquid crystalline B-phases. Only compound 8-**P**-11 with one short OC_8H_{17} tail shows the columnar B₁ phase; all the other compounds in this series show the B₂ phase. The phase sequence B₁-B₂ with increasing terminal tail length is often observed in banana-shaped liquid crystals [9]. On increasing *m*, the isotropization temperatures of the compounds in series *m-**P**-11* gradually increase from 107 to 115°C. The symmetric series (*m-**P**-m*; *m* = 1-18) also shows a slight increase in the B₂-I transition temperatures with increasing *m* (*m* = 10; T_I = 110°C and *m* = 18; T_I = 121.5°C) [10]. The melting points of the compounds in the *m-**P**-11* series decrease considerably upon increasing *m*. This is caused by the increasing non-symmetric shape of the compounds with the largest *m*. Due to the symmetric shape of compound 11-**P**-11, a

maximum in melting point for this compound was observed. In contrast to the non-symmetric m-**P**-11 series, the symmetric series [10] shows an increase of melting point with increasing tail length.
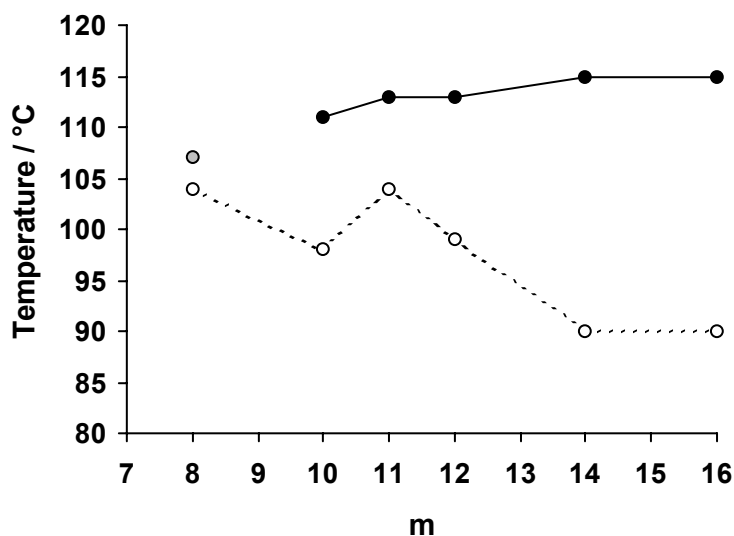

Figure 1. *Dependence of the melting points (- -o- -), B$_1$-I transition (•) and B$_2$-I transitions (— • —) on m for series m-**P**-11.*
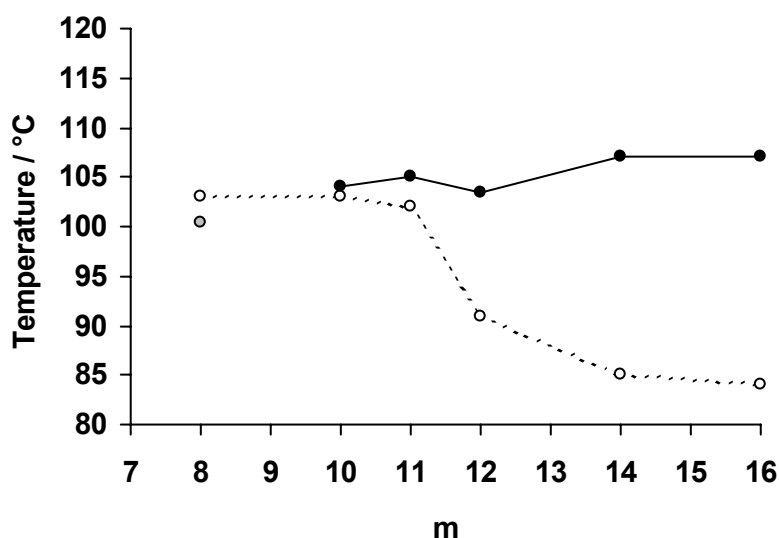
Figure 2. *Dependence of the melting points (- -o- -), B$_1$-I transition (•) and B$_2$-I transitions (— • —) on m for series m-**P**-11a.*

In table 1 and figure 2 the mesomorphic properties of the compounds in series m-**P**-11a series are given. All long-tailed compounds (m = 10-16) exhibit an enantiotropic B$_2$ mesophase. The compound with the shortest tail shows a monotropic columnar B$_1$ phase. Again the isotropization temperatures gradually increase and the melting points gradually decrease with increasing m. Hence, the B$_2$ mesophase range increases upon increasing m.

Figure 3 shows the electric response of compound 14-**P**-11a under a triangular wave voltage. Two peaks were recorded during a half period indicating antiferroelectric switching behavior.
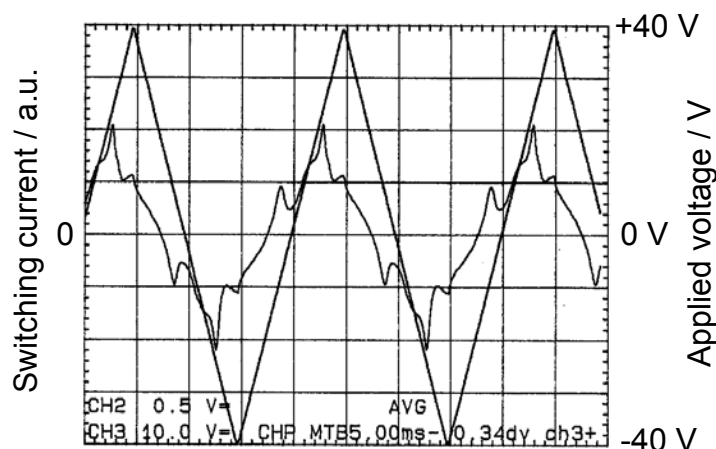

Figure 3. *Switching current response (a.u.) obtained in the B₂ phase of compound 14-**P**-11a at 100°C by applying a triangular voltage of 50 Hz.*

XRD measurements showed that all B_2 compounds in the *m*-**P**-11 and *m*-**P**-11a series have a sharp reflection in the small angle region corresponding to the layer spacing *d* (table 1). Sometimes also second and third order reflections were observed. The liquid-like order within the B_2 mesophase was demonstrated by a diffuse wide angle scattering. In all cases, a tilt angle of the molecules in the smectic layers of ~45° was calculated (assuming a bending angle of 120°). As expected, the layer spacings *d* and tilt angle of the B_2 compounds in series *m*-**P**-11a are comparable with those of compounds in the *m*-**P**-11 series. Both series show a linear relation between *d* and *m*.

*m-**P**-10 and m-**P**-10a series*

The phase transition temperatures and the associated enthalpy values for the compounds in series *m*-**P**-10 with one terminal decyloxy ($OC_{10}H_{21}$) tail are summarized in table 2. The compound with the shortest tail (8-**P**-10) shows, on cooling from the isotropic phase, a typical mosaic-like texture characteristic for the B_1 mesophase. All other compounds in this series show spherulitic domains with a fringe pattern on cooling from the isotropic phase. This can be regarded as a typical B_2 pattern [31]. The isotropization temperatures of all six compounds in this series are almost equal (figure 4). The melting points on the other hand decrease with increasing *m*. An explanation for the monotropic behavior of compound 10-**P**-10 can be found in the symmetric shape of this compound. It is known that symmetric compounds usually have a higher melting point than their non-symmetric analogues [32], as was also found in the *m*-**P**-11 series.

Table 2. *Transition temperatures (°C), transition enthalpies (kJ mol⁻¹; between square brackets) and layer spacings d (Å) of the m-**P**-10 and m-**P**-10a series.*

Compound	Cr	B₁	B₂	I	*d*
*8-**P**-10*	● 106 [19]	● 111 [18]		●	-
*10-**P**-10* [10]	● 111 [53]		(● 110) [20]	●	33.7
*11-**P**-10*	● 98 [34]		● 111 [20]	●	34.0
*12-**P**-10*	● 92 [32]		● 111 [21]	●	34.6
*14-**P**-10*	● 89 [34]		● 112 [21]	●	35.7
*16-**P**-10*	● 88 [29]		● 112 [21]	●	37.1
*8-**P**-10a*	● 106 [36]	(● 103.5) [16]		●	-
*10-**P**-10a*	● 107 [61]	(● 101.5) [18]		●	-
*11-**P**-10a*	● 102 [a]		● 102 [a]	●	33.8
*12-**P**-10a*	● 98 [15]		● 102 [16]	●	34.8
*14-**P**-10a*	● 82 [18]		● 104 [19]	●	35.7
*16-**P**-10a*	● 82 [7]		● 104 [19]	●	37.4

[a] Could not be determined

Table 2 and figure 5 show the liquid crystalline properties of the compounds in series *m*-**P**-10a, with the terminal decenyloxy tail. The mesophase behavior is similar to the compounds of series *m*-**P**-10 although the transition temperatures are lower due to the introduction of the terminal double bond. In contrast to the *m*-**P**-10 series, the transition from the B₁ to the B₂ mesophase occurs in series *m*-**P**-10a at $m = 10$ to 11 due to the introduction of a double bond. Figure 6 shows the growth of columnar B₁ domains of compound 8-**P**-10a on cooling from the isotropic phase.
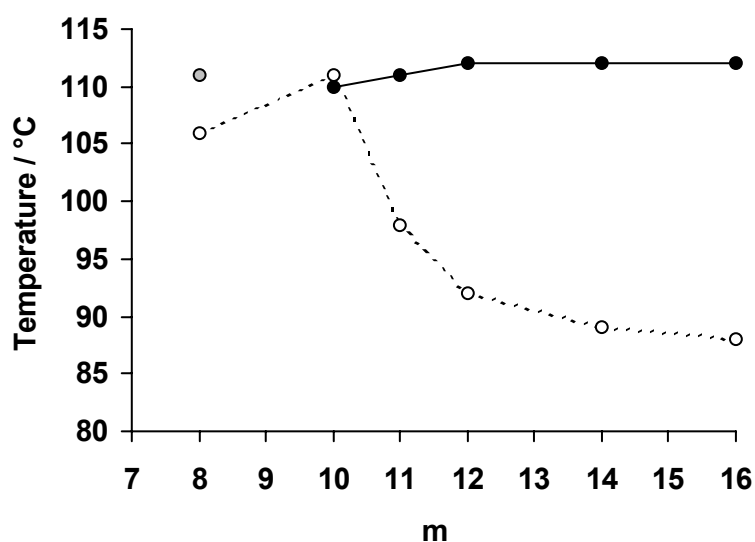

Figure 4. *Dependence of the melting points (- -o- -), B₁-I transitions (●) and B₂-I transitions (− ● −) on m for series m-**P**-10.*

The layer spacings d, determined from XRD experiments, from the smectic layer structures (B_2 phase) are listed in table 2 and are comparable with the corresponding compounds from the m-**P**-11(a) series. In both series a linear relationship between d and m was found. In all cases a tilt angle of the molecules in the layers of ~ 45° was calculated.
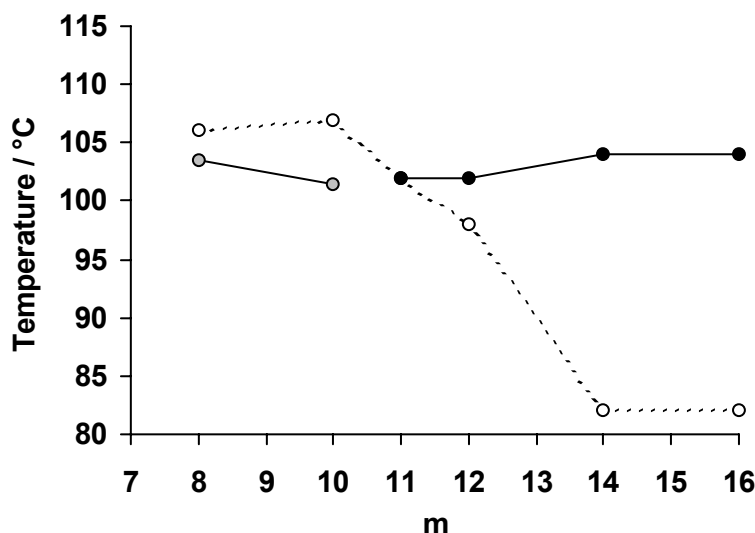

*Figure 5. Dependence of the melting points (- -o- -), B_1-I transition $(-\bullet-)$ and B_2-I transitions $(-\bullet-)$ on m for series m-**P**-10a.*

Comparison between the four series

Increasing the length of terminal tails suppresses formation of the B_1 phase due to a lack of overlap of the aromatic cores of the antiparallel arranged molecules at the ribbon interfaces [9]. Therefore, a B_1 to B_2 transition is often observed in several homologous series upon increasing the terminal tail length. In three of the four series studied the transition from the B_1 to the B_2 phase occurs at m = 8 to 10. In the m-**P**-10a series, however, this transition occurs at m = 10 to 11. When compared to compound 10-**P**-10 which exhibits the B_2 phase, compound 10-**P**-10a shows the B_1 phase. This must be related to the fact that the latter compound has a terminal vinyl group. Hence, we think that the presence of a terminal double bond slightly destabilizes the B_2 phase. It has to be noted however, that according to references [9,33] compound 10-**P**-10 shows coexisting B_1 and B_2 phases in a small temperature range.

Figure 7 shows that in all four series the isotropization temperatures increase with m. In all cases the isotropization temperature of the long-tailed series (m-**P**-11 and m-**P**-11a) are about 3°C higher than their short-tailed analogues (m-**P**-10 and m-**P**-10a). On going from the vinyl terminated series (m-**P**-10a and m-**P**-11a) to the corresponding alkyl terminated series (m-**P**-10 and m-**P**-11) an increase in isotropization temperature of about 8°C is observed. The melting points of all four series decrease

with increasing non-symmetry. The two symmetric compounds have the highest melting points in their series.
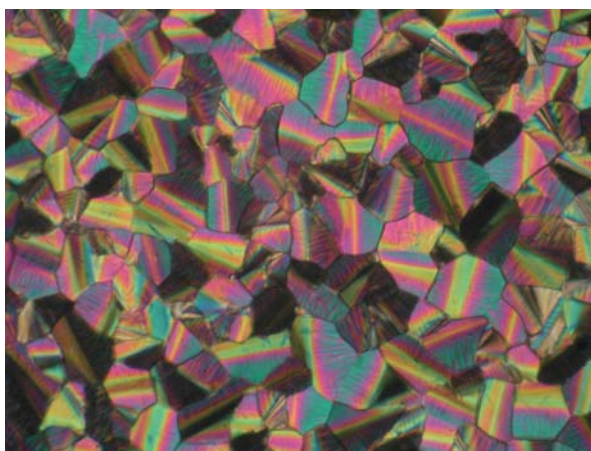

Figure 6*. Optical photomicrograph of the growth of B_1 domains of compound 8-**P**-10a on cooling from the isotropic phase.*
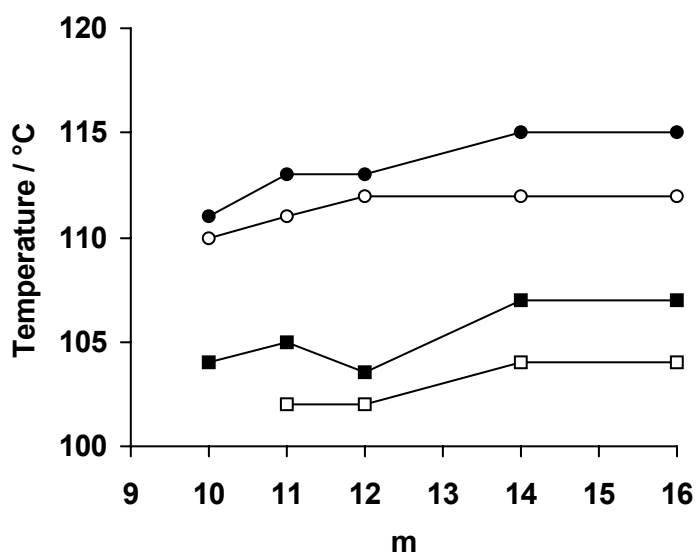

Figure 7. *Dependence of the B_2-I transition temperatures of the compounds of series m-**P**-11 $(-\bullet-)$, m-**P**-11a $(-\blacksquare-)$, m-**P**-10 $(-\circ-)$, m-**P**-10a $(-\square-)$ on m.*

Compounds with two terminal vinyl groups

In order to study the influence of double bond-terminated compounds in more detail we have also synthesized compounds 11a-**P**-11a, 10a-**P**-10a and 10a-**P**-11a (table 3). As can be seen from tables 1 and 3 both the isotropization temperatures and the melting points of the compounds in series 11(a)-**P**-11(a) decrease on increasing the number of terminal alkene bonds. The isotropization temperatures, however, decrease faster than the melting points and as a result compound 11a-**P**-11a shows only a monotropic B_2 mesophase. Remarkably, non-symmetric compound 11-**P**-11a

does not show the lowest melting point when compared to symmetric compounds 11-**P**-11 and 11a-**P**-11a. All three compounds, 11-**P**-11, 11-**P**-11a and 11a-**P**-11a, show antiferroelectric switching behavior. The introduction of two terminal alkene groups has been reported to lead in some cases to a change in switching behavior. Whereas 1,3-phenylene bis[4-(4-octyloxyphenyliminomethyl)benzoate] [34] shows an antiferroelectric B_2 phase, the analogue with two terminal alkene bonds, 1,3-phenylene bis{4-[4-(7-octenyloxy)phenyliminomethyl]benzoate} [35] has been reported to show ferroelectric switching.

*Table 3. Transition temperatures (^{o}C), transition enthalpies (kJ mol^{-1}; between square brackets) and layer spacings d (Å) of the ma-**P**-na series.*

Compound	Cr	B_1	B_2	I	d
*10a-**P**-10a* [36]	• 102 [69]			•	-
*10a-**P**-11a*	• 98 [47]	(• 91) [16]		•	-
*11a-**P**-11a* [36,37]	• 101 [51]		(• 96) [16]	•	34.3

In tables 2 and 3 the thermotropic properties of compounds 10(a)-**P**-10(a) are given. As in the 11(a)-**P**-11(a) series, a gradual decrease of the melting points is observed on increasing the number of terminal vinyl groups in the 10(a)-**P**-10(a) series. The liquid crystalline behavior changes completely upon increasing number of terminal vinyl groups; 10-**P**-10 monotropic B_2, 10-**P**-10a monotropic B_1, while 10a-**P**-10a showed no mesophase.

In table 3 the thermotropic properties of compound 10a-**P**-11a are shown. Surprisingly, this compound exhibits a monotropic B_1 phase. There are three other compounds with one C_{10} and one C_{11} terminal tail (10-**P**-11, 10a-**P**-11 and 10-**P**-11a). Only compound 10-**P**-11 with no terminal vinyl groups shows an enantiotropic B_2 phase over a reasonable temperature range. Intermediate compounds 10a-**P**-11 and 10-**P**-11a show very similar behavior; both exhibit the B_2 phase, and the compound with the double bond in the shortest tail (11-**P**-10a) has slightly lower transition temperatures.

5.4   Conclusions

The introduction of terminal double bonds in banana-shaped compounds lowers both the isotropization temperatures and melting points when compared to the corresponding alkyl-terminated compounds. The B_2 phase is slightly destabilized

upon introduction of terminal vinyl groups. The switching behavior remains antiferroelectric upon the introduction of one or two terminal double bonds. Layer spacings and tilt angles of the corresponding compounds with no, one or two terminal vinyl groups are also almost unchanged. The vinyl-terminated compounds described in this chapter might be suitable for incorporation as side chains in an oligomeric or polymeric system.

5.5   References

1.   Meyer R. B., Liebert L., Strelecki I. and Keller P. *J. Phys. Fr. Lett.* **1975**, *36*, L69.
2.   Chandani A. D. L., Ouchi Y., Takezoe H., Fukuda A., Terashima K., Furukawa K. and Kishi A. *Jpn. J. Appl. Phys.* **1989**, *28*, L1261.
3.   Niori T., Sekine F., Watanabe J., Furukawa T. and Takezoe H. *J. Mater. Chem.* **1996**, *6*, 1231-1233.
4.   Pelzl G., Diele S. and Weissflog W. *Adv. Mater.* **1999**, *11*, 707-724.
5.   Tschierske C. and Dantlgraber G. *Pramana* **2003**, *61*, 455-481.
6.   Bedel J. P., Rouillon J. C., Marcerou J. P., Laguerre M., Nguyen H. T. and Achard M. F. *Liq. Cryst.* **2001**, *28*, 1285-1292.
7.   Link D. R., Natale G., Shao R., Maclennan J. E., Clark N. A., Körblova E. and Walba D. M. *Science* **1997**, *278*, 1924-1927.
8.   Walba D. M., Korblova E., Shao R., Maclennan J. E., Link D. R., Glaser M. A. and Clark N. A. *Science* **2000**, *288*, 2181-2184.
9.   Shen D., Pegenau A., Diele S., Wirth I. and Tschierske C. *J. Am. Chem. Soc.* **2000**, *122*, 1593-1601.
10.   Amaranatha Reddy R. and Sadashiva B. K. *Liq. Cryst.* **2003**, *30*, 1031-1050.
11.   Weissflog W., Nadasi H., Dunemann U., Pelzl G., Diele S., Eremin A. and Kresse H. *J. Mater. Chem.* **2001**, *11*, 2748-2758.
12.   Bedel J. P., Rouillon J. C., Marcerou J. P., Laguerre M., Nguyen H. T. and Achard M. F. *J. Mater. Chem.* **2002**, *12*, 2214-2220.
13.   Prasad V., Shankar Rao D. S. and Krishna Prasad S. *Liq. Cryst.* **2001**, *28*, 643-646.
14.   Rauch S., Bault P., Sawade H., Heppke G., Nair G. G. and Jakli A. *Phys. Rev. E* **2002**, *66*, 021706.
15.   Pelz K., Weissflog W., Baumeister U. and Diele S. *Liq. Cryst.* **2003**, *30*, 1151-1158.
16.   Schröder M. W., Diele S., Pelzl G., Dunemann U., Kresse H. and Weissflog W. *J. Mater. Chem.* **2003**, *13*, 1877-1882.
17.   Schröder M. W., Pelzl G., Dunemann U. and Weissflog W. *Liq. Cryst.* **2004**, *31*, 633-637.
18.   Shreenivasa Murthy H. N. and Sadashiva B. K. *Liq. Cryst.* **2004**, *31*, 361.
19.   Prasad V. and Jakli A. *Liq. Cryst.* **2004**, *31*, 473-479.
20.   Sadashiva B. K., Amaranatha Reddy R., Pratibha R. and Madhusudana N. V. *Chem. Commun.* **2001**, 2140-2141.
21.   Amaranatha Reddy R. and Sadashiva B. K. *J. Mater. Chem.* **2004**, *14*, 310-319.
22.   Mieczkowski J., Gomola K., Koseska J., Pociecha D., Szydlowska J. and Gorecka E. *J. Mater. Chem.* **2003**, *13*, 2132-2137.
23.   Prasad V., Kang S.-W. and Kumar S. *J. Mater. Chem.* **2003**, *13*, 1259-1264.

24. Sadashiva B. K., Amaranatha Reddy R., Pratibha R. and Madhusudana N. V. *J. Mater. Chem.* **2002**, *12*, 943-950.
25. Dantlgraber G., Eremin A., Diele S., Hauser A., Kresse H., Pelzl G. and Tschierske C. *Angew. Chem. Int. Ed.* **2002**, *41*, 2408-2412.
26. Shreenivasa Murthy H. N. and Sadashiva B. K. *Liq. Cryst.* **2004**, *31*, 567-578.
27. Achten R., Cuypers R., Giesbers M., Koudijs A., Marcelis A. T. M. and Sudhölter E. J. R. *Liq. Cryst.* **2004**, *31*, 1167-1174.
28. Prasad V., Kang S.-W., Qi X. and Kumar S. *J. Mater. Chem.* **2004**, 1495-1502.
29. Lee G. S., Lee Y-J., Choi S. Y., Park Y. S. and Yoon K. B. *J. Am. Chem. Soc.* **2000**, *122*, 12151-12157.
30. Tschierske C. and Zaschke H. *J. Prakt. Chem.* **1989**, *331*, 365-366.
31. Sekine T., Niori T., Sone M., Watanabe J., Choi S. W., Takanishi Y. and Takezoe H. *Jpn. J. Appl. Phys.* **1997**, *36*, 6455-6463.
32. Blatch A. E. and Luckhurst G. R. *Liq. Cryst.* **2000**, *27*, 775-787.
33. Schröder M. W., Diele S., Pelzl G. and Weissflog W. *Chem. Phys. Chem.* **2004**, *5*, 99-103.
34. Diele S., Grande S., Kruth H., Liscka C., Pelzl G., Weissflog W. and Wirth I. *Ferroelectrics* **1998**, *212*, 169-177.
35. Lee C.-K., Kwon S.-S., Shin S.-T., Choi E.-J., Lee S. and Chien L.-C. *Liq. Cryst.* **2002**, *29*, 1007-1013.
36. Fodor-Csorba K., Vajda A., Galli G., Jákli A., Demus D., Holly S. and Gács-Baitz E. *Macromol. Chem. Phys.* **2002**, *203*, 1556-1563.
37. Jákli A., Huang Y.-M., Fodor-Csorba K., Vajda A., Galli G., Diele S. and Pelzl G. *Adv. Mater.* **2003**, *15*, 1606-1610.

6

Monofluorinated unsymmetrical bent-core mesogens

The synthesis and mesomorphic properties of 30 bent-core compounds with a fluorine substituent in one of the outer rings are reported. The banana-shaped compounds are all derived from resorcinol and contain esters as linking groups between the five aromatic rings. The different mesophases have been characterized by polarizing optical microscopy, differential scanning calorimetry, X-ray diffraction studies and electro-optical investigations. The compounds with the longer terminal chains exhibit an antiferroelectric SmCP phase. Upon introduction of a fluorine substituent the layer spacing increases, as compared with the corresponding unsubstituted compound. The introduction of one terminal vinyl group in the mono-substituted bent-core mesogens has no significant influence on the liquid crystalline properties and the switching remains antiferroelectric. Due to the introduction of the terminal double bond, these banana-shaped compounds are suitable for the preparation of siloxane polymers or attachment to a hydrogen terminated silicon surface.

6.1   Introduction

Before 1996 all (anti)ferroelectric smectics were composed of tilted enantiomerically enriched molecules. In 1996 however, Niori *et al.* [1] reported ferroelectricity in achiral banana-shaped molecules possessing C_{2v} symmetry. Since then a number of different, so-called B-phases have been discovered [2]. The most frequently described B-phase is the B_2 phase (SmCP), which in most cases is found for bent molecules with relatively long terminal tails [3]. Due to the synclinic and anticlinic layer organization of the molecules in a ferroelectric or antiferroelectric polar order, four types of layer organization in the SmCP phase are possible [4]. As a result of the close packing of these bent-core mesogens there is limited rotational freedom around their molecular long axis. Recently it was shown, however, that some compounds do show collective rotation around the molecular long axis under an external electric field with some special experimental conditions, which can result in field-induced switching of supramolecular chirality [5,6].

Among the more than a thousand banana-shaped molecules reported to date [2,3,7] several structural variations have been introduced to study their influence on the liquid crystalline properties. The influence of lateral substituents [8-13] and especially of fluorine substituents, has been studied extensively. The polar fluorine substituents can be introduced symmetrically at both arms of the molecules [8-12,14-21], but also non-symmetrically at only one arm of the molecule [22-24] or at the core, *e.g.* at a 3,4'-biphenyl central unit [25].

In this paper we study the influence of mono-fluorine substitution in one of the outer phenyl rings, *ortho* to the terminal tail of an ester-connected bent-core mesogen, series *m*-**P**-*Fn* (scheme 1). Part of this series has already been studied by Shreenivasa Murthy *et al.* [23]. It is known that the antiferroelectric ground state of compounds without substituents, can change to ferroelectric upon introduction of F-substituents at this special position in both arms of the molecule [19,26]. Additionally, we have synthesized a second series in which one terminal double bond is introduced into the mono-fluorinated mesogen, series 11a-**P**-*Fn* (scheme 1).
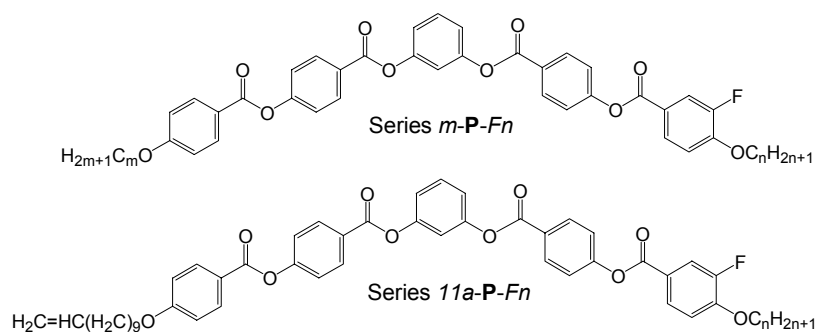
Scheme 1. *Bent-core structures of the compounds of series m-**P**-Fn and 11a-**P**-Fn.*

6.2   Experimental

6.2.1   Synthesis

The compounds of series *m*-**P**-*Fn* were prepared according to scheme 2. The monosubstituted resorcinol derivatives **P**-*m* were synthesized according to a literature procedure [27]. 4-Bromo-2-fluorophenol was obtained from Aldrich and used without further purification. The compounds from series 11a-**P**-*Fn* were prepared according to the same procedure, by using **P**-11a [27] instead of **P**-*m*.

Compounds **I**-*nF* were obtained by etherification of 4-bromo-2-fluorophenol with the corresponding bromoalkanes (*n* = 8, 10, 12, 14 and 16) and K_2CO_3 as base. **II**-*nF* was obtained by carboxylation of the Li-analogue of **I**-*nF* with carbon dioxide. Compounds **IV**-*nF* were obtained by esterification of the acid chlorides of **II**-*nF* with 4-hydroxybenzaldehyde (compound **III**-*nF*) followed by $NaClO_2$ oxidation [28]. The banana-shaped products (*m*-**P**-*Fn*) were obtained by esterification of the acid chloride of **IV**-*nF* and **P**-*m* in THF with DMAP as base.

*4-Bromo-2-fluoro-1-tetradecyloxybenzene (I-14F)*

A mixture of 9.50 g (49.7 mmol) 4-bromo-2-fluorophenol, 15.13 g (54.6 mmol) 1-bromo-tetradecane and 11.2 g K_2CO_3 in 100 ml of butanone was heated under reflux overnight. After cooling the mixture was concentrated and 100 ml CH_2Cl_2 was added. After filtration of the salts the filtrate was concentrated and the colorless oil was used in the next step without further purification. Yield: 95%.

^{1}H NMR (200 MHz, $CDCl_3$) δ (ppm): 7.18 (m, 2H, Ar), 6.81 (t, 1H, Ar), 3.98 (t, 2H, OCH_2), 1.83 (m, 2H, $OCCH_2$), 1.55-1.25 (m, 22H, 11 x CH_2), 0.87 (t, 3H, CH_3). HRMS calc. for $C_{20}H_{32}BrFO$ 386.1621; found 386.1617.

3-Fluoro-4-tetradecyloxybenzoic acid (II-14F)

To a solution of 18.37 g 4-bromo-2-fluoro-1-tetradecyloxybenzene (**I**-14F; 47.4 mmol) in 100 ml of dry THF at -60°C, was added 35.6 ml of a 1.6 M solution of butyllithium in hexane (57.0 mmol). After stirring for 0.5h at -78°C, the cold solution was poured onto crushed solid CO_2, and allowed to warm to room temperature. Thereafter, the reaction mixture was acidified to pH 2 with a 10% HCl solution. Subsequently, the mixture was partly concentrated and the precipitate was filtered off, and washed with water. Recrystallization from EtOH and washing with PE 40-60 gave white/yellow crystals. Yield: 14%. Cr 112 (N 109 I) (°C).

^{1}H NMR (200 MHz, $CDCl_3$) δ (ppm): 7.82 (m, 2H, Ar), 6.98 (t, 1H, Ar), 4.09 (t, 2H, OCH_2), 1.85 (m, 2H, $OCCH_2$), 1.45-1.25 (m, 22H, 11 x CH_2), 0.87 (t, 3H, CH_3). HRMS calc. for $C_{21}H_{33}FO_3$ 352.2414; found 352.2417.
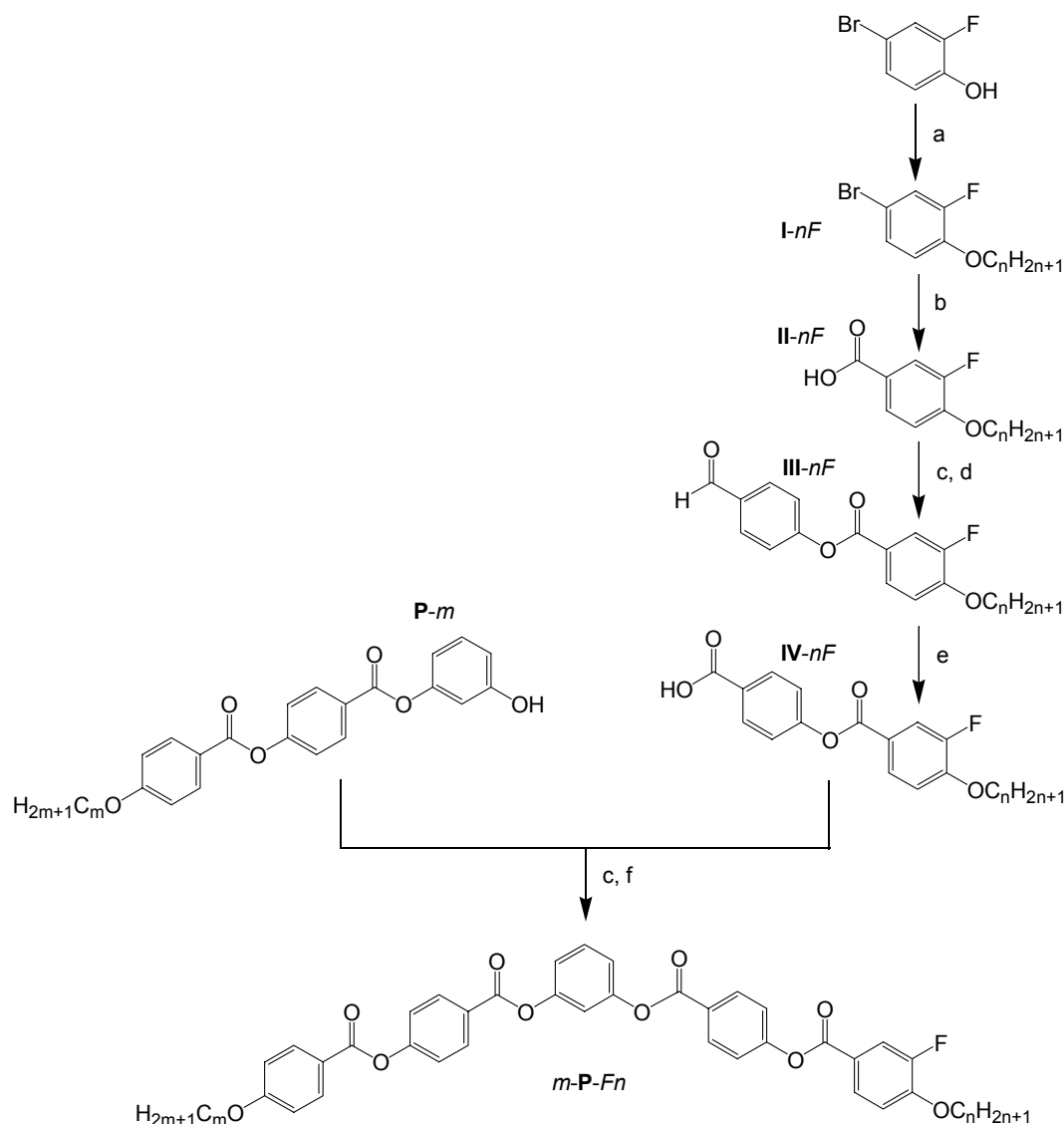
Scheme 2. *Synthesis of compounds in series m-**P**-Fn: a) H(CH₂)ₙ-Br (n = 8, 10, 12, 14, 16), K₂CO₃, butanone, reflux; b) n-BuLi, -78°C, CO₂ (s); c) SOCl₂, reflux; d) 4-hydroxybenzaldehyde, DMAP, THF, rt; e) NaClO₂, resorcinol, NaH₂PO₄, THF, H₂O, rt; f) DMAP, THF, rt.*

4-(3-Fluoro-4-n-tetradecyloxybenzoyloxy)benzaldehyde (III-14F)

Compound **II**-14F (2.28 g, 6.5 mmol) was heated under reflux in thionyl chloride (20 ml) for 2h. Excess thionyl chloride was removed by distillation under reduced pressure. The resulting acid chloride was dissolved in 20 ml dry THF, and 0.79 g (6.5 mmol) 4-hydroxybenzaldehyde was added. To this clear solution 2 equivalents (1.58 g; 12.9 mmol) of DMAP were added, and the reaction mixture was stirred for 24h at room temperature under a N₂ atmosphere. After removal of the THF, 200 ml of CH₂Cl₂ was added. The organic layer was washed with a 1M HCl solution (2x) and a

saturated NaHCO$_3$ solution and dried over Na$_2$SO$_4$. Multiple recrystallizations from EtOH yielded white crystals. Yield: 63%. Cr 86 (SmC 71 I) (°C).

^{1}H NMR (400 MHz, CDCl$_3$) δ (ppm): 10.05 (s, 1H, CHO),7.99 (d, 3H, Ar), 7.92 (d, 1H, Ar), 7.43 (d, 2H, Ar), 7.07 (t, 1H, Ar), 4.15 (t, 2H, OCH$_2$), 1.90 (m, 2H, OCCH$_2$), 1.55-1.29 (m, 22H, 11 x CH$_2$), 0.90 (t, 3H, CH$_3$). HRMS calc. for C$_{28}$H$_{37}$FO$_4$ 456.2676; found 456.2680.

*4-(3-Fluoro-4-n-tetradecyloxybenzoyloxy)benzoic acid (**IV**-14F)*

Compound **III**-14F (1.85 g, 4.1 mmol) and resorcinol (0.58 g; 5.3 mmol) were dissolved in THF (50 ml). To this solution was added dropwise, over 10 min, a solution of sodium chlorite (NaClO$_2$, 80%; Aldrich) (2.13 g, 23.6 mmol) and sodium dihydrogenphosphate monohydrate (1.70 g, 12.3 mmol) in 20 ml water. The resulting pale yellow reaction mixture was then stirred overnight at room temperature. Volatile components were removed *in vacuo* and the residue was dissolved in 100 ml water. The aqueous solution was acidified to pH 2 by adding 1M HCl. The white precipitate was filtered, washed with water, and dried in air. The white crystals were then washed with PE 40-60. Yield 95%. Cr 140 SmC 190 N 207 I (°C).

^{1}H NMR (400 MHz, CDCl$_3$) δ (ppm): 8.19 (d, 2H, Ar), 7.99 (d, 1H, Ar), 7.95 (d, 1H, Ar), 7.34 (d, 2H, Ar), 7.07 (t, 1H, Ar), 4.15 (t, 2H, OCH$_2$), 1.89 (m, 2H, OCCH$_2$), 1.67-1.29 (m, 22H, 11 x CH$_2$), 0.91 (t, 3H, CH$_3$). HRMS calc. for C$_{28}$H$_{37}$FO$_5$ 472.2625; found 472.2628.

*1-[4-(4-Decyloxybenzoyloxy)benzoyloxy]-3-[4-(3-fluoro-4-n-tetradecyloxybenzoyloxy)-benzoyloxy]benzene (10-**P**-F14)*

Compound **IV**-14F (0.15 g, 0.32 mmol) was refluxed in thionyl chloride (5 ml) for two hours. Excess thionyl chloride was then removed by distillation under reduced pressure. The resulting acid chloride was dissolved in 8 ml freshly distilled dry THF and to this stirred solution 0.16 g (0.32 mmol) of **P**-10 was added. Subsequently, 2 equivalents of DMAP (0.08 g; 0.64 mmol) were added. The reaction mixture was stirred for 24 hours at room temperature under N$_2$ atmosphere. Thereafter, the THF was removed under *vacuo* and ~50 ml CH$_2$Cl$_2$ was added. The organic layer was washed successively with 1M HCl (2 x) and a saturated NaHCO$_3$ solution and dried over anhydrous Na$_2$SO$_4$. After filtration of the salts the filtrate was concentrated and the residue was purified by column chromatography (eluant: 10% PE 40-60 in CH$_2$Cl$_2$). Finally, recrystallization from acetonitrile and washing with PE 40-60 gave colorless crystals. Yield: 53%

¹H NMR (400 MHz, CDCl₃) δ (ppm): 8.31 (d, 4H, Ar), 8.18 (d, 2H, Ar), 8,00 (d, 1H, Ar), 7.93 (d, 1H, Ar) 7.53 (t, 1H, Ar), 7.40 (d, 4H, Ar), 7.22 (s+d, 3H, Ar), 7.07 (t, 1H, Ar), 7.02 (d, 2H, Ar), 4.16 (t, 2H, OCH₂), 4.08 (t, 2H, OCH₂), 1.88 (m, 4H, 2 x OCCH₂), 1.57-1.29 (m, 36H, 18 x CH₂), 0.91 (t, 6H, CH₃).

¹³C NMR (CDCl₃) δ (ppm): 164.7, 164.5, 164.4, 164.2, 155.9, 155.6, 151.8, 132.8, 132.3, 130.5, 130.3, 128.0, 127.9, 127.2, 127.0, 122.6, 122.4, 121.3, 119.7, 118.4, 118.1, 116.2, 114.8, 113.8, 69.9, 68.8, 32.3, 30.1, 30.0, 29.9, 29.8, 29.7, 29.5, 29.4, 26.4, 26.3, 23.1, 14.5.

1-{4-[4-(10-Undecenyloxy)benzoyloxy]benzoyloxy}-3-[4-(3-fluoro-4-n-tetradecyloxybenzoyloxy)benzoyloxy]benzene (*11a*-**P**-*F14*).

This compound was prepared using the same procedure as for compound 10-**P**-F14 starting from **IV**-14F and **P**-11a.

Yield: 73%

¹H NMR (400 MHz, CDCl₃) δ (ppm): 8.21 (d, 4H, Ar), 8.08 (d, 2H, Ar), 7.90 (d, 1H, Ar), 7.83 (d, 1H, Ar) 7.42 (t, 1H, Ar), 7.30 (d, 4H, Ar), 7.11 (s+d, 3H, Ar), 6.97 (t, 1H, Ar), 6.91 (d, 2H, Ar), 5.73 (m, 1H, =CH), 4.88 (m, 2H, =CH₂), 4.05 (t, 2H, OCH₂), 3.97 (t, 2H, OCH₂), 1.97 (m, 2H, C=CCH₂), 1.77 (m, 4H, 2 x OCCH₂), 1.65-1.11 (m, 34H, 17 x CH₂), 0.81 (t, 3H, CH₃).

¹³C NMR (CDCl₃) δ (ppm): 164.7, 164.5, 164.4, 164.2, 155.9, 155.6, 151.8, 139.6, 132.8, 132.3, 130.3, 128.0, 127.2, 127.0, 122.6, 122.5, 121.3, 119.7, 116.2, 114.8, 114.6, 113.8, 69.9, 68.8, 34.2, 32.3, 30.1, 30.0, 29.9, 29.8, 29.7, 29.5, 29.3, 26.4, 26.3, 23.1, 14.6.

6.2.2   Measurements

Melting points, thermal phase transition temperatures and optical inspection of the liquid crystalline phases were performed on samples between ordinary glass slides using an Olympus BH-2 polarizing microscope equipped with a Mettler FP82HT hot stage, which was controlled by a Mettler FP80HT central processor. Differential scanning calorimetry (DSC) thermograms were obtained on a Perkin Elmer DSC-7 system using 0.5-3 mg samples in 50 μL sample pans and a scan rate of 5°C/min. ΔH was determined in the third heating scan and calculated in kJ/mol. Temperature dependent X-ray diffraction curves of the liquid crystals were measured on a Panalytical X'pert Pro diffractometer equipped with an Anton Paar camera for temperature control. For measurements in the small angle region the sample was spread in the isotropic or the liquid crystalline phase on a thin glass slide (about 15 μm thick) which was placed on a temperature-regulated flat copper sample stage. The switching behavior was determined using the triangular wave method with a 6 μm polyimide coated ITO cell and the cells were filled in the isotropic state. Electro-optical measurements were carried out using a combination of function synthesizer

(Keithley, 3910 model), amplifier (Krohn-Hite, 7500 model) and the current response traces were recorded using Oscilloscope (Hewlett Packard, 54610A model) across a 5 kΩ resistance.

6.3 Results and discussion

*m-**P**-Fn series*

Table 1. *Transition temperatures (°C), transition enthalpies (kJ mol^{-1}; between square brackets) and layer spacings d (Å) of the compounds in series m-**P**-Fn.*

Compound	Cr	B$_1$	SmCP$_A$	I	d
*8-**P**-F8*	● 121 [36.4]	(● 114) [11.3 [a]]		●	-
*10-**P**-F8*	● 100 [16.8]		● 113 [19.3]	●	34.4
*12-**P**-F8* [23]	● 100 [17.2]		● 114 [19.6]	●	36.0
*14-**P**-F8*	● 95 [12.3]		● 115 [19.5]	●	38.1
*16-**P**-F8*	● 95 [13.7]		● 114 [19.7]	●	39.6
*8-**P**-F10*	● 108 [22.4 [a]]		● 113 [18.3 [a]]	●	34.7
*10-**P**-F10*	● 112 [20.9]		● 119 [19.2]	●	36.0
*12-**P**-F10* [23]	● 102 [20.3]		● 119 [21.2]	●	37.6
*14-**P**-F10*	● 99 [19.1]		● 120 [21.6]	●	38.6
*16-**P**-F10*	● 95 [14.1]		● 120 [20.5]	●	40.0
*8-**P**-F12*	● 101 [18.0]		● 114 [19.4]	●	36.0
*10-**P**-F12*	● 105 [28.2]		● 119 [19.7]	●	37.2
*12-**P**-F12* [23]	● 108 [23.3]		● 124 [21.8]	●	38.3
*14-**P**-F12*	● 101 [22.6]		● 123 [22.9]	●	39.5
*16-**P**-F12*	● 95 [21.5]		● 122 [23.1]	●	40.7
*8-**P**-F14*	● 101 [19.1]		● 116 [20.4]	●	37.4
*10-**P**-F14*	● 99 [20.3]		● 120 [21.9]	●	38.4
*12-**P**-F14* [23]	● 102 [23.1]		● 122 [23.1]	●	39.7
*14-**P**-F14*	● 104 [25.8]		● 124 [23.6]	●	40.5
*16-**P**-F14*	● 99 [25.6]		● 124 [24.5]	●	42.0
*8-**P**-F16*	● 98 [18.6]		● 115 [16.6]	●	38.9
*10-**P**-F16*	● 98 [19.0]		● 121 [19.6]	●	40.1
*12-**P**-F16* [23]	● 97 [22.6]		● 123 [23.2]	●	41.0
*14-**P**-F16*	● 95 [31.0]		● 122 [23.8]	●	42.3
*16-**P**-F16*	● 102 [43.6]		● 124 [23.9]	●	43.1

[a] determined upon cooling

The transition temperatures and associated enthalpies of the compounds in the *m*-**P**-*Fn* series are given in table 1. Five of the 25 compounds studied in this series have already been described and characterized by Shreenivasa Murthy *et al.* [23] and we obtained similar transition temperatures. Compound 8-**P**-F8 is the only one in this series that has a monotropic columnar B_1 phase. All other compounds in the *m*-**P**-*Fn* series show enantiotropic liquid crystalline SmCP phases. The melting points and isotropization temperatures are also presented in 3D graphs (figures 1 and 2). Figure 1 shows that all compounds with *m* = *n* exhibit a maximum in melting point. In series *m*-**P**-F12, for example, the analogue with *m* = 12 has the highest melting point. This is another clear indication that the unsymmetrical compounds reduce the packing efficiency and hence lower the melting points. In this case however, none of the molecules in the *m*-**P**-*Fn* series is truly symmetric due to the fluorine atom in only one of the arms. The influence of one small polar substituent on the melting point is apparently very small. The transition temperatures, of homologues with equal *m* + *n*, are barely influenced by the presence of the F-atom in either the ring connected to the shortest (*e.g.* 16-**P**-F14) or the longest (*e.g.* 14-**P**-F16) terminal tail.
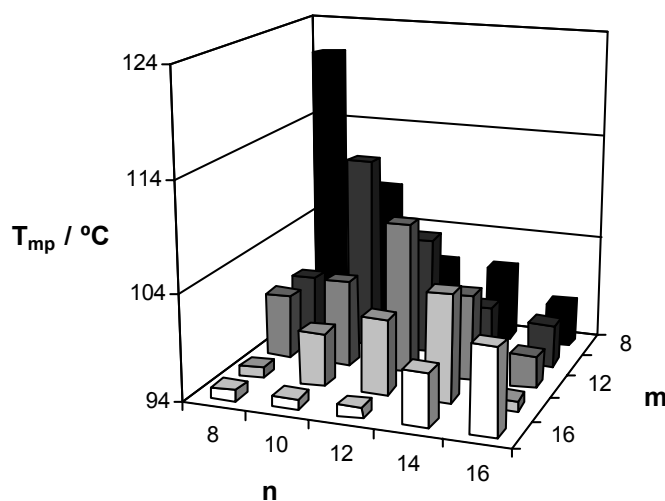
Figure 1. *3D representation of the melting points of the compounds from series m-**P**-Fn.*

In most cases the isotropization temperatures gradually increase and reach a plateau value upon increasing *m* or *n* (figure 2), as observed in several other series of banana-shaped compounds [19]. On cooling from the isotropic phase the SmCP compounds all show a grainy unspecific texture under polarizing optical microscopy. Sometimes domains of opposite handedness, but with the typical SmCP fringe pattern were observed. As anticipated, the compounds all behave quite similarly; the SmCP mesophase range varies between 5 and 27°C. Only one

compound, with the shortest terminal tails, 8-**P**-F8, showed a mosaic-like texture typical for the columnar B_1 (Col$_r$) phase. Due to partial crystallization we were unable to carry out X-ray diffraction (XRD) measurements for 8-**P**-F8 in the liquid crystalline phase.
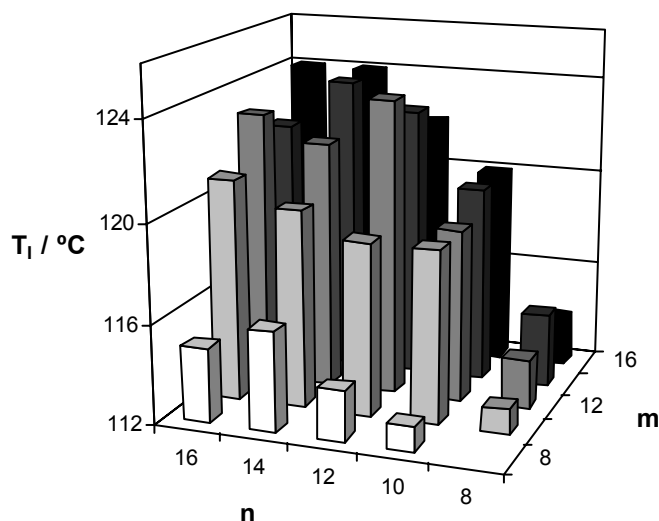

*Figure 2. 3D representation of the isotropization temperatures (only SmCP-I transitions) of the compounds in series m-**P**-Fn.*

XRD experiments were also carried out on the other 24 compounds in the *m*-**P**-*Fn* series. For these SmCP compounds usually two reflections (1 0 0 and 2 0 0) in the small angle region were observed. The corresponding *d*-spacings are summarized in table 1 and figure 3. There is an almost linear relationship between the number of carbon atoms in one of the terminal tails and the layer spacing *d*.
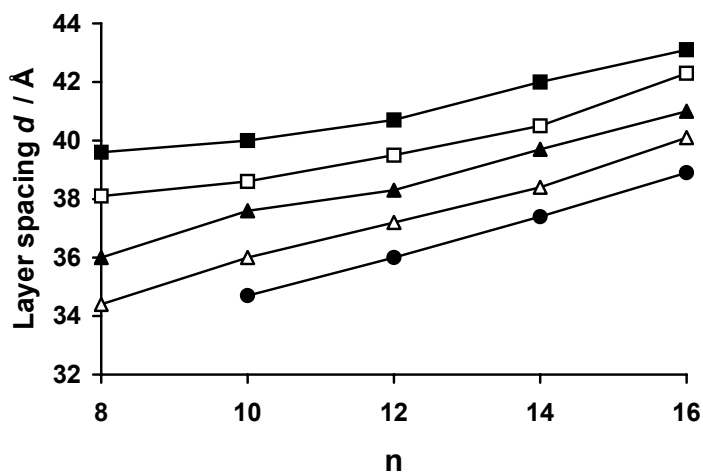
*Figure 3. Dependence of the layer spacing d, on m and n of the compounds in series m-**P**-Fn (m = 8 ●; 10 △; 12 ▲; 14 □; 16 ■).*

As discussed [23], the SmCP compounds in the *m-**P**-Fn* series show antiferroelectric switching properties upon application of a modified triangular-wave electric field.

*The m-**P**-Fn series in comparison with the m-**P**-n and mF-**P**-Fn series.*

First, we compare the mono-fluorinated molecules with two terminal tails of the same length (*m-**P**-Fn* series; $m = n$), with the corresponding compounds with no (*m-**P**-n* series; $m = n$) [19,27] or two (*mF-**P**-Fn* series; $m = n$) [19,20] fluorine substituents (figure 4).

Fluorine substitution *ortho* to the alkoxy chains stabilizes the liquid crystalline phase, since the isotropization temperatures increase upon introduction of F-substituents, figure 4. The isotropization temperatures of the compounds with one F-substituent are in between those with no or two F-substituents.
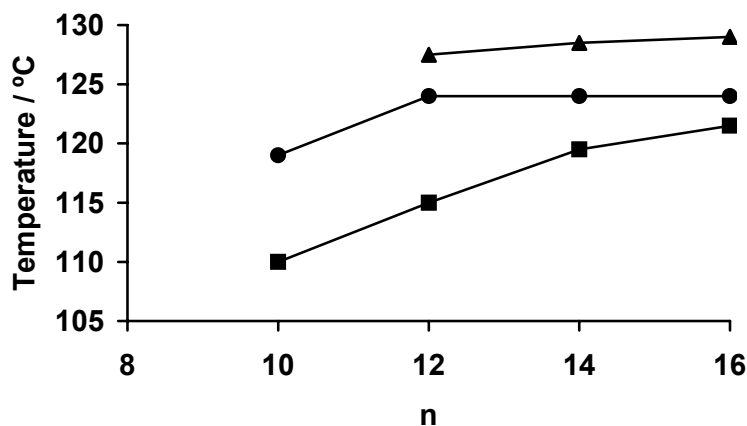
*Figure 4. Comparison of the isotropization temperatures for the compounds of series m-**P**-n [19,27] (■), m-**P**-Fn (●) and mF-**P**-Fn [19,20] (▲) (m = n).*

The mesophase range, on the other hand, is largest for the series with one F-substituent. The mesophase range of series *m-**P**-n* is relatively small with a maximum of ~12°C [19,27]. For the compounds with one F-substituent, a larger mesophase range is found (up to ~27°C). Surprisingly, the melting points of series *m-**P**-Fn* and *m-**P**-n* ($m = n$) are rather similar, and significantly lower than for series *mF-**P**-Fn* ($m = n$). Compound 10F-**P**-F10, and probably also 8F-**P**-F8, are not liquid crystalline due to their high melting points [19]. Therefore the *mF-**P**-Fn* series shows the smallest mesophase range.

On going from series *m-**P**-n* and *m-**P**-Fn* ($m = n$; with no or one F-substituent), to the difluorine substituted compounds (*mF-**P**-Fn* series; $m = n$) the switching behavior changes from antiferroelectric (AF) to ferroelectric (FE) [19,23]. Compounds 12F-**P**-F12, 14F-**P**-F14 and 16F-**P**-F16 exhibit a FE switching SmCP phase, with synclinic tilt

organization; SmC_SP_F [20]. In other series of bent-core mesogens it has also been shown that F-substitution at the *ortho* position to the terminal tails, can induce FE switching [26]. Apparently, both arms of the molecules need to be substituted by a fluorine atom to change the switching behavior from AF to FE.

In contrast to the other positions on the rings, disubstitution *ortho* to the alkoxy chains significantly increases the layer spacing *d* when compared to the non-substituted parent compounds [19]. The intermediate compounds with only one F-substituent all show intermediate layer spacing as shown in figure 5. However, at present the reason for this is not clear although may be explained in two possible ways. One explanation is that a F-substituent at this position induces a change (decrease) in tilt angle. When a second F-substituent is introduced the tilt angle decreases further resulting in a change of layer organization from AF to FE. This could however not be verified, since no X-ray patterns of oriented domains could be obtained. The second possibility could be that the fluorine substitution at *ortho* position to the alkoxy chains can change the inter-layer interactions at the inter-layer interfaces. The ferroelectric organization, for example, decreases the inter-layer interactions, which obviously increases the layer spacing.
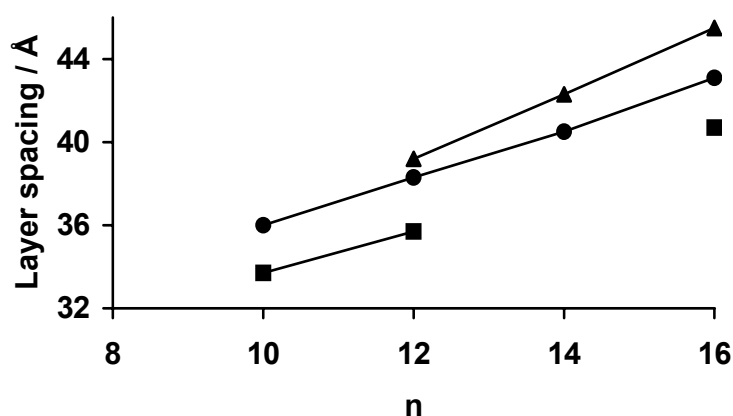

Figure 5. *Comparison of layer spacings d for the compounds of series m-**P**-n [19,27] (■), m-**P**-Fn (●) and mF-**P**-Fn [19,20] (▲) (m = n).*

The compounds with no fluorine substituents (10-**P**-*n* series) with two terminal tails of different lengths described previously [29], are compared with the mono-fluorine substituted series 10-**P**-*Fn* and *m*-**P**-F10. In all cases the isotropization temperatures of the F-substituted compounds are ~8°C higher than the corresponding non-fluorinated compounds. The layer spacings *d* are 2.3 to 3.0 Å larger for the analogous mono-fluorine compounds with the same tail lengths.

*11a-**P**-Fn series*

Table 2. *Transition temperatures (°C), transition enthalpies (kJ mol⁻¹; between square brackets) and layer spacings d (Å) of the compounds in series 11a-**P**-Fn.*

Compound	Cr	SmCP$_A$	I	*d*
*11a-**P**-F8*	● 97 [17.0 [a]]	● 102 [17.3 [a]]	●	35.1
*11a-**P**-F10*	● 101 [[b]]	● 110 [[b]]	●	36.0
*11a-**P**-F12*	● 98 [19.5]	● 110 [18.2]	●	37.4
*11a-**P**-F14*	● 93 [19.9]	● 112 [21.4]	●	38.5
*11a-**P**-F16*	● 90 [14.9]	● 112 [18.2]	●	40.9

[a] determined upon cooling; [b] could not be determined

The thermotropic properties of the double bond terminated compounds in series 11a-**P**-*Fn*, having in all 5 compounds one undecenyloxy chain with a terminal vinyl group, are summarized in table 2. All the compounds are liquid crystalline and exhibit the SmCP$_A$ phase, similar to the compounds from the *m*-**P**-*Fn* series. The mesophase range increases with *n*. Surprisingly, the isotropization temperatures (and also the melting points) of the compounds in series 11a-**P**-*Fn* show more similarities with series 11-**P**-*n* [29] than with 11a-**P**-*n* [29] as shown in figure 6.
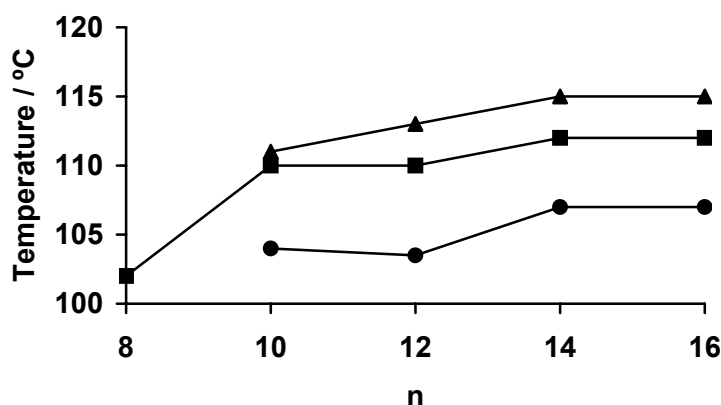
Figure 6. *Comparison of the isotropization temperatures for the compounds of series 11-**P**-n [29] (▲), 11a-**P**-Fn (■) and 11a-**P**-n [29] (●).*

This can be explained by the realizing that introducing a terminal vinyl group lowers the isotropization temperatures [29], and a fluorine substituent increases the isotropization temperature. Just as in series *m*-**P**-*Fn*, the isotropization temperatures of compounds in series 11a-**P**-*Fn* are higher (5 or 6°C) than the analogues with no fluorine substituents. In contrast to the short-tailed compounds (*n* = 8) from series

11-**P**-n and 11a-**P**-n which exhibit a B$_1$ phase, compound 11a-**P**-F8 shows the SmCP phase. Apparently the polar F-substituent stabilizes the SmCP phase.

The XRD data, figure 7, show that the d-spacings for compounds 11a-**P**-Fn are 2 or 3 Å larger than for the corresponding compounds without the F-substituent, 11a-**P**-n, and also for series 11-**P**-n [29].
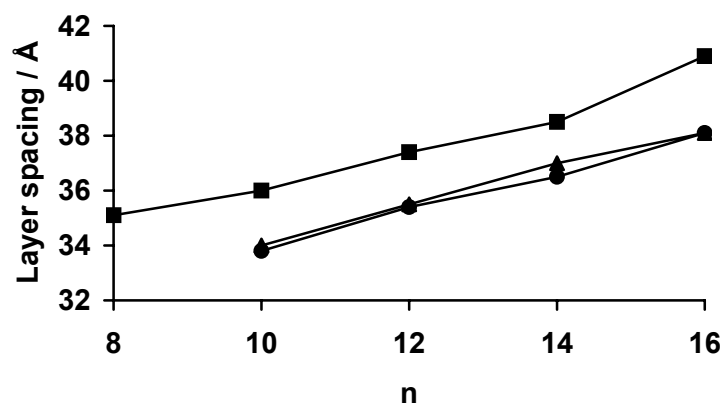

***Figure 7**. Comparison of layer spacings d for the compounds of series 11-**P**-n [29] (▲), 11a-**P**-Fn (■) and 11a-**P**-n [29] (●).*

The optical texture of the vinyl-terminated series shows a grainy texture but also chiral domains of opposite handedness, as observed for compound 11a-**P**-F14 (figure 8), upon slightly decrossing the polarizers in the microscoop. These observations show that an anticlinic antiferroelectric correlation in adjacent layers is present (SmC$_A$P$_A$).

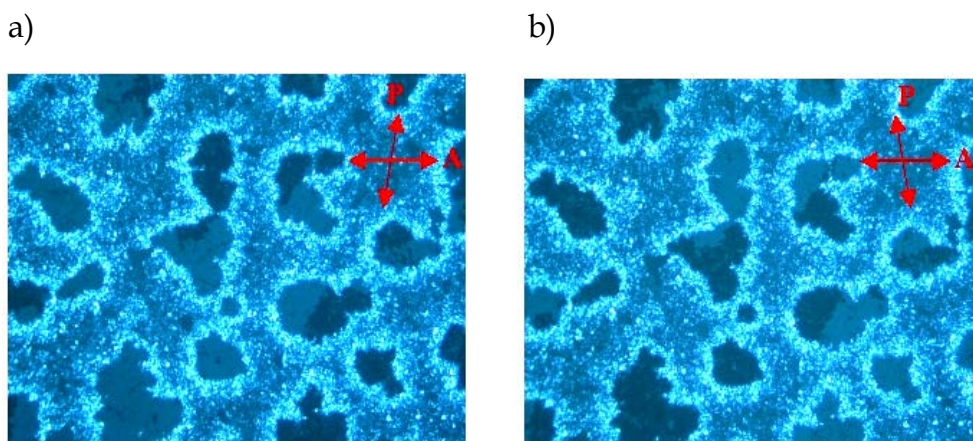a)   b)

***Figure 8**. Optical photomicrographs obtained for the mesophase of compound 11a-**P**-F14 as seen between slightly decrossed (5-10°) polarizers in either one (a) or the other (b) direction.*

The electro-optical switching properties were investigated for a short (11a-**P**-F8) and a long (11a-**P**-F14) homologue in this series. Compound 11a-**P**-F14 showed, on application of a triangular-wave voltage (threshold: 160 Vpp for a 6 μm cell at 10

Hz), two polarization current peaks for each half-period of the wave, figure 9. This indicates antiferroelectric tristable switching for the SmCP mesophase, with a spontaneous polarization of ~ 1100 nC cm^{-2} at 95°C. Under these experimental conditions, a more birefringent fan-shaped texture was obtained, stable for several hours even after removal of the applied field (surface alignment effect). The short-tailed homologue, 11a-**P**-F8, showed the same optical and switching properties (P$_S$ ~ 950 nC cm^{-2} at 95°C).
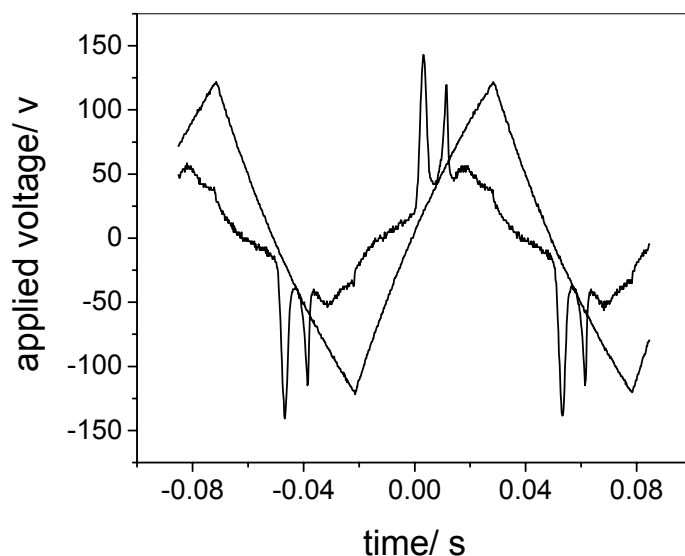
Figure 9. *Switching current response trace obtained for compound 11a-**P**-F14 on applying a triangular-wave voltage (240 Vpp for 6 μm cell thickness, at 10 Hz).*

6.4   Conclusions

The influence of a fluorine substituent, at the *ortho* position with respect to the alkoxy group in one of the outer aromatic groups, of a five-ring banana-shaped molecule has been studied. In contrast to the difluorine substituted compounds, which show ferroelectric switching, these compounds exhibit a SmCP mesophase with antiferroelectric switching properties. The layer thickness of the compounds in the SmCP phase are intermediate between the non- and difluorine substituted compounds. The SmCP phase is slightly stabilized upon introduction of one F-substituent, since compounds with relatively short terminal chains also show this mesophase. A second mono-fluorinated series, in which one of the terminal alkoxy chains is replaced by an undecenyloxy tail, exhibits similar SmCP phases. As in the previously described series, the ground state of the vinyl-terminated banana compounds is antiferroelectric. Due to the terminal vinyl groups these molecules are

suitable for attachment to hydrogen-terminated silicon species via a hydrosilylation reaction.

6.5   References

1.   Niori T., Sekine F., Watanabe J., Furukawa T. and Takezoe H. *J. Mater. Chem.* **1996**, *6*, 1231-1233.
2.   Pelzl G., Diele S. and Weissflog W. *Adv. Mater.* **1999**, *11*, 707-724.
3.   Shen D., Pegenau A., Diele S., Wirth I. and Tschierske C. *J. Am. Chem. Soc.* **2000**, *122*, 1593-1601.
4.   Link D. R., Natale G., Shao R., Maclennan J. E., Clark N. A., Körblova E. and Walba D. M. *Science* **1997**, *278*, 1924-1927.
5.   Keith C., Amaranatha Reddy R., Baumeister U. and Tschierske C. *J. Am. Chem. Soc.* **2004**, *126*, 14312-14313.
6.   Amaranatha Reddy R., Schröder M. W., Bodyagin M., Kresse H., Diele S., Pelzl G. and Weissflog W. *Angew. Chem. Int. Ed.* **2005**, *44*, 774-778.
7.   Nguyen H. T., Bedel J. P., Rouillon J. C., Marcerou J. P. and Achard M. F. *Pramana* **2003**, *61*, 395-404.
8.   Weissflog W., Nadasi H., Dunemann U., Pelzl G., Diele S., Eremin A. and Kresse H. *J. Mater. Chem.* **2001**, *11*, 2748-2758.
9.   Shreenivasa Murthy H. N. and Sadashiva B. K. *Liq. Cryst.* **2002**, *29*, 1223-1234.
10.   Amaranatha Reddy R. and Sadashiva B. K. *Liq. Cryst.* **2003**, *30*, 273-283.
11.   Sadashiva B. K., Murthy H. N. S. and Dhara S. *Liq. Cryst.* **2001**, *28*, 483-487.
12.   Shubashree S., Sadashiva B. K. and Dhara S. *Liq. Cryst.* **2002**, *29*, 789-797.
13.   Achten R., Koudijs A., Karzcmarzyk Z., Marcelis A. T. M. and Sudhölter E. J. R. *Liq. Cryst.* **2004**, *31*, 215-227.
14.   Nadasi H., Weissflog W., Eremin A., Pelzl G., Diele S., Das B. and Grande S. *J. Mater. Chem.* **2002**, *12*, 1316-1324.
15.   Amaranatha Reddy R. and Sadashiva B. K. *J. Mater. Chem.* **2004**, *14*, 1936-1947.
16.   Amaranatha Reddy R. and Sadashiva B. K. *Liq. Cryst.* **2000**, *27*, 1613-1623.
17.   Bedel J. P., Rouillon J. C., Marcerou J. P., Laguerre M., Nguyen H. T. and Achard M. F. *J. Mater. Chem.* **2002**, *12*, 2214-2220.
18.   Amaranatha Reddy R. and Sadashiva B. K. *J. Mater. Chem.* **2002**, *12*, 2627-2632.
19.   Amaranatha Reddy R. and Sadashiva B. K. *Liq. Cryst.* **2003**, *30*, 1031-1050.
20.   Amaranatha Reddy R., Raghunathan V. A. and Sadashiva B. K. *Chem. Mater.* **2005**, *17*, 274-283.
21.   Amaranatha Reddy R., Sadashiva B. K. and Raghunathan V. A. *Chem. Mater.* **2004**, *16*, 4050-4062.
22.   Shreenivasa Murthy H. N. and Sadashiva B. K. *Liq. Cryst.* **2004**, *31*, 1337-1346.
23.   Shreenivasa Murthy H. N. and Sadashiva B. K. *J. Mater. Chem.* **2004**, *14*, 2813-2821.
24.   Shreenivasa Murthy H. N. and Sadashiva B. K. *Liq. Cryst.* **2004**, *31*, 1347-1356.
25.   Dantlgraber G., Shen D., Diele S. and Tschierske C. *Chem. Mater.* **2002**, *14*, 1149-1158.
26.   Bedel J. P., Rouillon J. C., Marcerou J. P., Laguerre M., Nguyen H. T. and Achard M. F. *Liq. Cryst.* **2000**, *27*, 1411-1421.
27.   Achten R., Cuypers R., Giesbers M., Koudijs A., Marcelis A. T. M. and Sudhölter E. J. R. *Liq. Cryst.* **2004**, *31*, 1167-1174.
28.   Lee G. S., Lee Y-J., Choi S. Y., Park Y. S. and Yoon K. B. *J. Am. Chem. Soc.* **2000**, *122*, 12151-12157.

29.   Achten R., Koudijs A., Giesbers M., Marcelis A. T. M. and Sudhölter E. J. R. *Liq. Cryst.* **2005**, *32*, 277-285.

7

Banana-shaped side chain liquid crystalline siloxanes

Eight banana-shaped side chain liquid crystalline oligomers and polymers have been synthesized by hydrosilylation of vinyl-terminated bent-core mesogens with trimethylsilyl terminated siloxanes. The short-tailed olefins form a Col$_r$ mesophase, whereas those with longer chains exhibit the SmCP$_A$ mesophase. All studied oligomers and polymers show liquid crystalline properties and do not crystallize upon cooling. Most oligomers with ~4 repeating siloxane units, show a lamellar (layer) structure and antiferroelectric switching properties, the SmCP$_A$ phase. The XRD experiments show that the layer spacings are hardly influenced by the length of the terminal tails. The oligomer prepared from the smallest olefinic precursor, having the shortest alkyl tail, shows an X-ray diffraction pattern reminiscent of a columnar phase, although POM displays domains of opposite chirality and no switching behavior could be detected.

The polymers with ~35 repeating siloxane units are liquid crystalline, but due to the high viscosity a thorough characterization of the liquid crystalline phases was impossible.

7.1   Introduction

One of the most exciting developments in liquid crystal research in the past few years is the discovery of (anti)ferroelectricity in liquid crystals with a non chiral bent-core or banana-shaped molecular structure, by Niori *et al*. [1]. Of all known "banana" phases [2-8] the smectic B_2 phase, nowadays designated as SmCP phase, is the most interesting. Both ferroelectric and antiferroelectric ground states have been observed in this phase. In combination with two states of clinicity, four different types of layer organization can be distinguished. Depending on the molecular structure, all four sub-phases have been observed [3]: SmC_AP_A, SmC_AP_F, SmC_SP_A and SmC_SP_F. A related mesophase, designated as B_7 phase, is a polarization modulated layer structure which is derived from the SmC_SP_F phase [7]. The exact nature of this phase is still under discussion however [9].

Due to their relatively high transition temperatures and poor processability, low molecular weight banana-mesogens, might become more appealing if incorporated in a polymeric system. Nevertheless, only very few attempts to polymerize bent-shaped compounds have been made [10-14]. In almost all reported cases the mesogens of the banana-shaped monomers have two polymerizable groups that are cross-linked into a polymer network [12-14]. The azomethine polymers containing banana-shaped mesogens, synthesized by Choi *et al*. [10], showed B_2 properties, but due to the high viscosity the switching properties could not be investigated. Barberá *et al*. [11] were the first to prove indisputable that via in *situ* photopolymerization of banana-shaped bisacrylates SmCP networks were created. The first side-chain polymer with incorporated bent-core mesogens, was reported by Keith *et al*. [15]. To avoid highly viscous materials a polysiloxane *co*-polymer was used in which the banana-shaped mesogens were strongly diluted.

In contrast to most low molecular weight bent-core molecules, with an antiferroelectric ground state [16,17], bananas with siloxane [15,18-20] or carbosilane [21] groups attached, tend to show a ferroelectric organization due to a microsegregation of the three incompatible units [8]. The typical optically isotropic textures with domains of opposite handedness are often observed for bent-core molecules with siloxane segments. The optical isotropy seems to arise from a strongly deformed layer structure, where smectic slabs are organized randomly in space. The origin of the chiral domains is not clear yet. It seems that this is *not* due to formation of a helical superstructure, as initially proposed [20]. Presently, there are at least two models under discussion. Chirality might arise from a deracemization of molecular conformers in the confined geometry of the polar layers [8] or alternatively, it might be due to the intrinsic chirality of the layers themselves [22]. This chirality is a result of the

tilted organization of the molecules in polar layers, where layer normal, tilt direction and polar direction describe either a right handed or left handed system [3]. It was suggested that this inherent chirality becomes detectable if the mesophase itself is non-birefringent [22].

In this chapter we present new banana-shaped side-chain liquid crystal siloxane oligomers and polymers. The trimethylsilyl terminated siloxanes, contain x methylhydrosiloxane units with $x\sim4$ (oligomers) or $x\sim35$ (polymers). The compounds were synthesized by hydrosilylation of mono-unsaturated banana-shaped compounds, and their liquid crystalline properties were investigated.

7.2   Experimental

7.2.1   Synthesis

The synthesis of the olefinic precursors *ma*-**P**-*n* is described elsewhere [23]. All polymers were prepared by a hydrosilylation reaction (scheme).
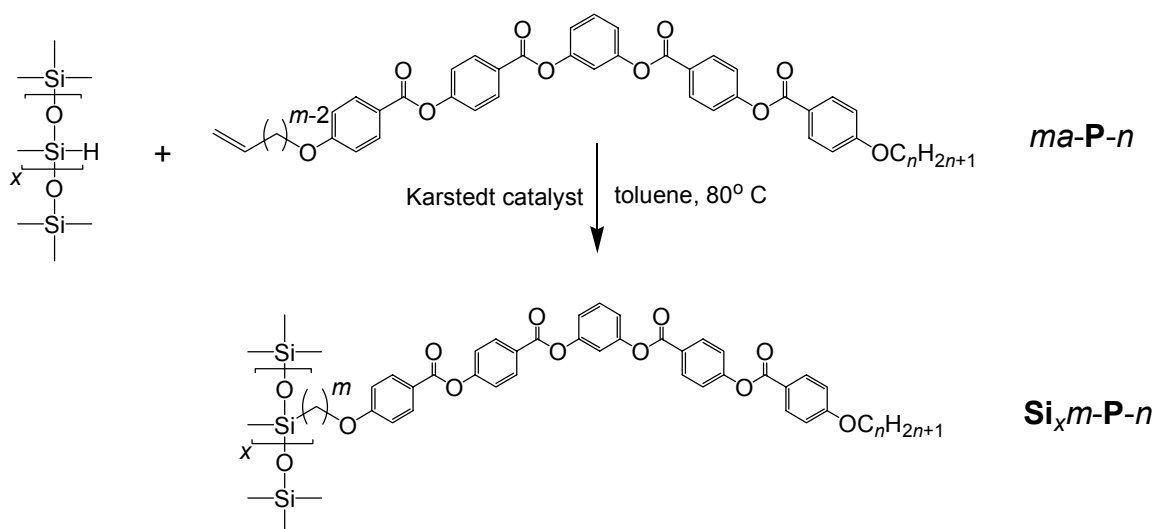
Scheme. *Synthetic pathway for the compounds in series **Si**_xm-**P**-n.*

The poly(methylhydrosiloxane) backbone and olefinic precursor *ma*-**P**-*n* (10 mol% excess with respect to the number of Si-H groups in the polymer backbone) were dissolved in dry toluene (~ 0.2 mmol *ma*-**P**-*n* per 10 ml toluene). The solution was heated to 80°C under N_2 atmosphere and platinum(0)-1,3-divinyl-1,1,3,3-tetramethyl disiloxane complex (Karstedt catalyst, ~ 2 µl per 10 ml toluene) in xylenes (0.1 M) was added. This solution was refluxed for 24h. After this reaction time, the solvent was evaporated under reduced pressure and the crude product was purified by column chromatography on silica gel (eluant: $CH_2Cl_2 \rightarrow$ 2% THF in CH_2Cl_2).

7.2.2 Measurements

Transition temperatures and optical inspection of the liquid crystalline phases were determined on samples between ordinary glass slides using an Olympus BH-2 polarization optical microscope equipped with a Mettler FP82HT hot stage, which was controlled by a Mettler FP80HT central processor. Differential scanning calorimetry (DSC) thermograms were obtained on a Perkin Elmer DSC-7 system using 2-4 mg samples in 50 µL sample pans at a scan rate of 5°C/min. ΔH is calculated in kJ/mol for the olefinic precursors and in J/g for the oligomers/polymers. Temperature dependent X-ray diffraction curves of the liquid crystals were measured on a Panalytical X'pert Pro diffractometer equipped with an Anton Paar camera for temperature control. For the measurements in the small angle region the sample was spread in the isotropic or the liquid crystalline phase on a thin glass slide (about 15 µm thick), which was placed on a temperature, regulated flat copper sample stage. The switching behavior was determined using the triangular wave method with a 6 µm polyimide coated ITO cell and the cells were filled in the isotropic state. Electro-optical measurements were carried out using a combination of function synthesizer (Keithley, 3910 model), amplifier (Krohn-Hite, 7500 model) and the current response traces were recorded using Oscilloscope (Hewlett Packard, 54610A model) across 5 kΩ resistance. The Matrix-assisted laser desorption / ionization Time of flight Mass Spectrometer (Maldi-Tof MS) mass spectrum for compound $\mathbf{Si}_{3.8}11$-$\mathbf{P}$-12 was obtained on an Ultraflex spectrometer using 2,5-dihydroxybenzoic acid (DHB; Sigma-Aldrich) as a matrix.

7.3 Results and discussion

*Olefinic precursors (ma-**P**-n)*

Five different olefinic precursors, all belonging to series *ma*-$\mathbf{P}$-*n*, were used to synthesize the oligomers/polymers; 11a-$\mathbf{P}$-8, 11a-$\mathbf{P}$-12 and 11a-$\mathbf{P}$-16 with a 10-undecenyloxy tail, and 10a-$\mathbf{P}$-8 and 10a-$\mathbf{P}$-12 with a 9-decenyloxy tail. Upon cooling from the isotropic phase the three olefins with the longest terminal tails (11a-$\mathbf{P}$-12, 11a-$\mathbf{P}$-16 and 10a-$\mathbf{P}$-12), show a smectic focal conic texture, typical for the SmCP$_A$ phase (B$_2$ phase) [23]. Schlieren textures were also observed for these compounds. For the short-tailed olefinic precursors (11a-$\mathbf{P}$-8 and 10a-$\mathbf{P}$-8), spherulitic and dendritic textures, typical for the columnar Col$_r$ phase (B$_1$ phase) [24] were observed. Upon increasing *n* in series 11a-$\mathbf{P}$-*n*, the melting points decrease and the isotropization temperatures increase (table 1). The SmCP compounds showed antiferroelectric switching properties [23] whereas the Col$_r$ phase is non-switching.

Table 1. *Transition temperatures (°C), transition enthalpies (kJ mol⁻¹; between square brackets), layer spacings d (Å), and the lattice parameters a and c (Å), of the compounds in series ma-P-n.*

Compound	Cr	Col$_r$	SmCP$_A$	I	d	a	c
11a-**P**-8	● 103 [37]	(● 100.5) [16] -		●	-	34.4	50.4
11a-**P**-12	● 91 [32]	-	● 103.5 [19]	●	35.4	-	-
11a-**P**-16	● 84 [33]	-	● 107 [21]	●	38.1	-	-
10a-**P**-8	● 106 [36]	(● 103.5) [16] -		●	-	#	#
10a-**P**-12	● 98 [15]	-	● 102 [16]	●	34.8	-	-

could not be determined due to crystallization

The liquid crystalline phases of the banana-shaped olefinic precursors were investigated by XRD studies. Compound 11a-**P**-8 showed two reflections in the small angle region at $d_1 = 28.4$ Å and $d_2 = 25.2$ Å which can be assigned to a rectangular 2D-lattice (B$_1$-type mesophase). A diffuse peak in the wide angle region indicated the liquid-like behavior of the phase. The lattice parameters calculated from the (1,1) and (0,2) reflections were $a = 34.4$ Å and $c = 50.4$ Å (table 1). A rough estimation of the number of molecules per unit cell, using the calculation described by Pelz *et al*. [25], results in ~6 molecules, or three per column (ribbon). The POM observations for monomer 10a-**P**-8, point to the Col$_r$ phase as well. This could however not be confirmed by XRD experiments due to the monotropic nature of this mesophase.

The other olefinic precursors with the longer terminal tails (11a-**P**-12, 11a-**P**-16 and 10a-**P**-12) all showed sharp first and second order reflections in the small angle region corresponding to the layer spacing. The liquid-like order within the SmCP mesophase of these compounds was proven by a diffuse wide-angle scattering. The layer thickness of 11a-**P**-12 and 11a-**P**-16 was 35.4 Å and 38.1 Å, respectively. In all cases, a tilt angle of the molecules in the smectic layers of ~45° was calculated (assuming a bending angle of 120° of the central aromatic core).

*Oligomers (**Si**$_{3.8}$m-**P**-n)*

From the ¹H-NMR spectra the ratio between the Si-CH$_3$ and OCH$_2$ (or C-CH$_3$) protons could be calculated for oligomers **Si**$_{3.8}$m-**P**-n. Combined with the Si-H peak that was sometimes observed, we conclude that in all five cases the backbone of the oligomers was not fully occupied. By changing the reaction conditions; temperature (60 - 90°C), reaction time (6 – 72h), catalyst (hydrogen hexachloroplatinate (IV) hydrate), olefinic precursor to siloxane ratio (1 - 2.5), we were not able to increase the degree of substitution.
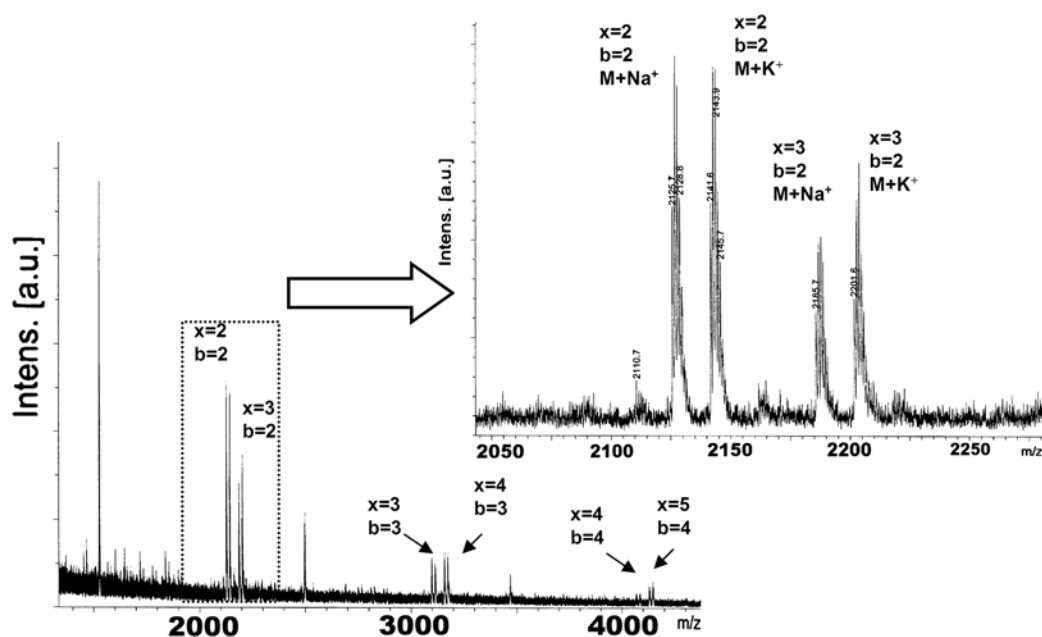
Figure 1. Maldi-Tof mass spectrum of Si₃.₈11-P-12 (b = number of olefinic precursors attached to backbone).

The polydisperse nature of the oligomers was analyzed by measuring Maldi-Tof mass spectra of **Si**$_{3.8}$11-**P**-12 (figure 1). They show the expected signals at m/z = [M + Na]$^+$ and [M + K]$^+$. For **Si**$_{3.8}$11-**P**-12 peaks corresponding with M = 2103, 3073, 4044 and 5014 were observed indicating a fully occupied backbone ($x = b$; b = number of olefinic precursors attached to backbone) with 2, 3, 4 or 5 repeating units x. Smaller peaks corresponding with M = 2163, 3133, 4104 and 5074 were observed indicating the mass of the compounds with $x = 3$ ($b = 2$), 4 ($b = 3$), 5 ($b = 4$) and 6 ($b = 5$), with one unoccupied Si-H group. Sometimes these small Si-H signals were also observed in the ¹H-NMR spectra. This incomplete reaction could be caused by steric hindrance by the large side-chain mesogenic groups (M ranging from 841 to 967).

Upon cooling from the isotropic phase the POM textures of oligomers **Si**$_{3.8}$11-**P**-n and **Si**$_{3.8}$10-**P**-n all appear to be optically isotropic. By slightly rotating the polarizer however, regions of different brightness can be distinguished. Upon rotation of the polarizer in the other direction the brightness of the domains reverses as shown in figure 2 (*i.e.* the dark domains become light-colored and the light domains become dark-colored). This phenomenon has been observed before in siloxane containing compounds [20,19], and also in conventional banana-shaped compounds [24,26-28] and as mentioned above the origin of this chirality is not yet clear.
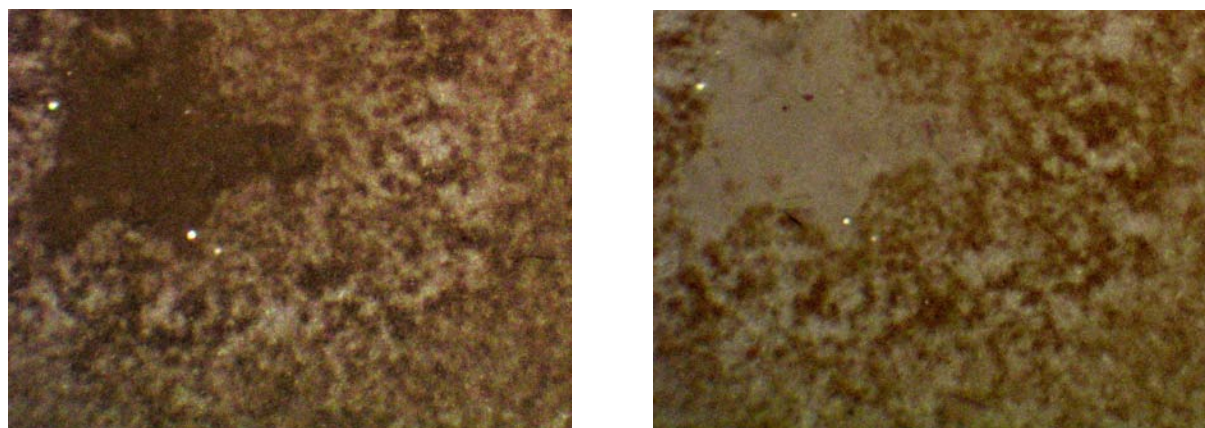
Figure 2. *Optical photomicrographs obtained for the mesophase of oligomer* $Si_{3.8}11$-P-16 *as seen between slightly decrossed (5-10°) polarizers in either one or the other direction.*

The isotropization temperatures of the oligomers are higher than those of the monomers. However, in contrast to the olifinic precursors the isotropization temperatures of the oligomers tend to decrease upon increasing n (table 2). Additionally, the oligomerization seems to stabilize the lamellar SmCP structure since the columnar mesophase of monomer 11a-P-8 is suppressed in the corresponding oligomer $Si_{3.8}11$-P-8. This might be due to the stronger incompatibility of the oligosiloxane units with the aromatic cores, which destabilizes the ribbon structure of the columnar phase with respect to flat layers. Upon cooling the mesophase, DSC thermograms show that the oligomers all have an additional phase transition at 70-90°C but no crystallization could be detected. This transition leads to slightly higher d-values in the X-ray spectra, but no additional changes in XRD or POM were observed.

Table 2. *Isotropization temperatures (°C), transition enthalpies (J g⁻¹; between square brackets), and layer spacings d (Å), of the compounds in series* $Si_{3.8}m$-P-n.

Compound	Col $_x$ (*)	SmCP$_A$(*)	I	d
$Si_{3.8}10$-P-8	● 150 [19.6]		●	
$Si_{3.8}10$-P-12		● 140 [13.8]	●	41.8
$Si_{3.8}11$-P-8		● 150 [20.6]	●	41.7
$Si_{3.8}11$-P-12		● 145 [20.6]	●	41.9
$Si_{3.8}11$-P-16		● 135 [17.6]	●	42.4

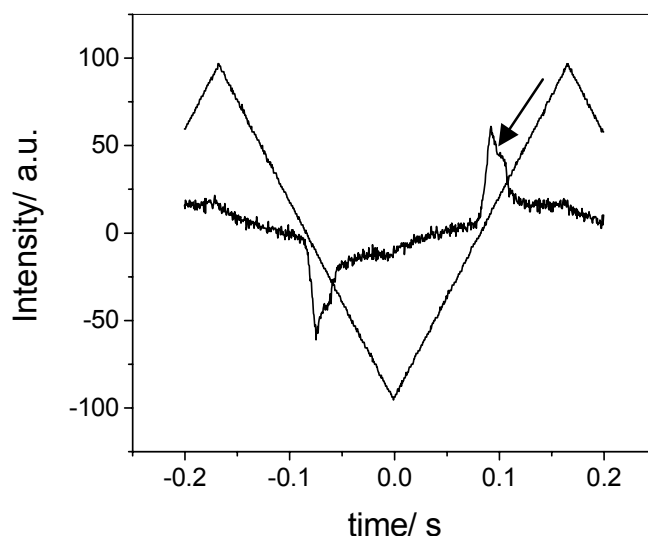(*) indicates mesophases with chiral domains formed by achiral molecules

Figure 3. *Switching current response trace obtained for oligomer **Si**$_{3.8}$11-**P**-12 on applying a triangular-wave voltage (200 Vpp for 6 μm cell thickness, at 3 Hz, Temp: 100°C).*

The switching behavior of **Si**$_{3.8}$11-**P**-12 was investigated using the triangular wave method. At low frequency, the apparent single polarization peak splits into two peaks (indicated by the arrow in figure 3) indicating antiferroelectric switching. Upon starting the switching experiments, the first threshold voltage is rather high (~200 V_{PP}); after inducing the ferroelectric state, the threshold for the switching process decreases to 100 V_{PP}. The polarization value (P_s) is temperature dependent as shown in figure 4. The maximum P_s observed is 930 nC/cm^2 at ca. 10 °C below the clearing temperature. The gradual increase of P_s upon cooling from the isotropic phase is probably related to the relative broad transition region (~35°C), which was also observed in the DSC-thermogram. The P_s-value is significantly higher than for the side-chain polymer described by Keith *et al.* [15]. This is probably related to the dilution of the mesogenic units in the *co*-polymer.
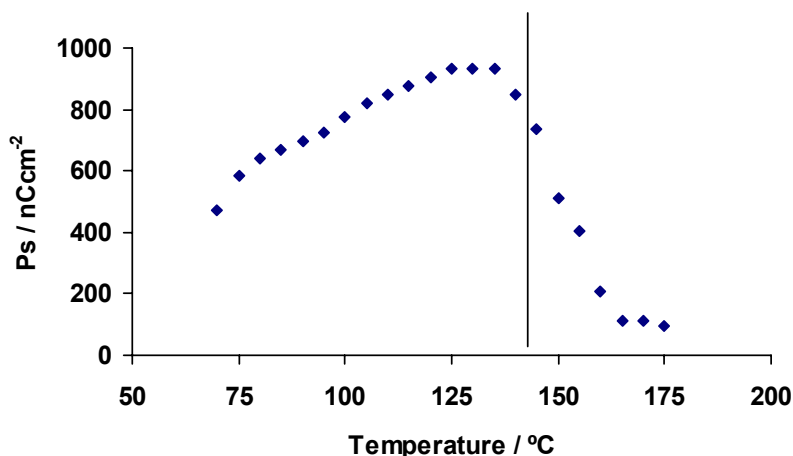

Figure 4. *Spontaneous polarization P_s as a function of temperature for oligomer **Si**$_{3.8}$11-**P**-12.*

The switching process was also investigated optically on circular domains grown by slow cooling under a d.c. electrical field. The extinction crosses of the circular domains are inclined with the polarization direction of the crossed polarizers by ca 45° (SmC$_S$P$_F$) and relax to positions parallel to analyzer and polarizer on terminating the applied field, which indicates the anticlinic organization of molecules in the antiferroelectric ground state (figure 5). We therefore conclude that this oligomer, as most other oligomers (table 2), exhibits the SmC$_A$P$_A$ mesophase as ground state structure. However, in some places in the centers of these circular domains still some small field-induced ferroelectric domains (synclinic) could be seen (see figure 5b). These field-induced FE domains are probably stabilized by surface interactions. Hence it seems that these materials are at the borderline of the transition to a ferroelectric switching behavior. Another possibility for this observation might be the fact that a small fraction of the polydisperse oligomer mixture, with FE properties, selectively segregates from the mixture during the cooling process at the centers of the circular domains.

On application of a triangular-wave electrical field up to about 350 V$_{PP}$ (5 µm cell thickness) oligomer **Si**$_{3.8}$10-**P**-8 did not show a current response. Apparently, this oligomer with the shortest terminal alkyl chain possesses a non-switchable mesophase under our experimental conditions.
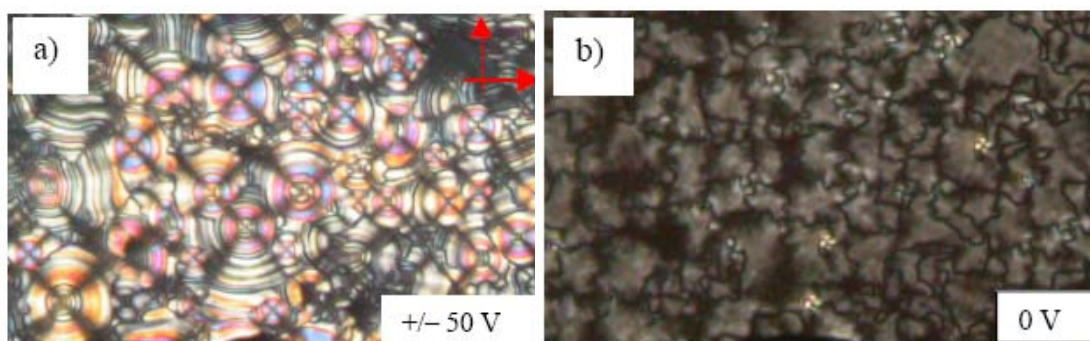

Figure 5. *Optical photomicrograph of a) circular domains obtained for oligomer Si$_{3.8}$11-**P**-12 under a d.c. field (80 V for 6µm cell thickness), b) after relaxation on terminating the applied field.*

Usually, banana-shaped compounds exhibit antiferroelectric switching because the AF ground state is stabilized by the escape from macroscopic polar order. The synclinic nature of the interlayer interfaces and the interlayer fluctuations resulting thereof, also play a role in the preference for an AF layer organization [8]. In microsegregated siloxane systems however, the above-mentioned interlayer fluctuations [19] are (partly) suppressed, therefore allowing a ferroelectric structure more easily [15,18]. Nevertheless, siloxane [19,20,29] or carbosilane [21] systems, showing antiferroelectric mesophases, have also been reported. Reasons given in the literature

for the occurrence of AF mesophases in these systems are: a small number of Si-containing segments per mesogenic group [20,21], an even number of SiO units in dimers [19], or a large cross-sectional area of branched siloxane units which gave rise to an antiferroelectric columnar $Col_{ob}P_A$ phase [29].

In the presently described oligomers, most pairs of adjacent mesogens are also present on adjacent silicon atoms of the backbone (mesogens separated by one Si-O-Si group). These dimeric moieties could be compared with the dimers described by Dantlgraber *et al.* [19]. These dimers exhibit an odd-even effect in switching behavior dependent on the parity of the number of Si-O units. The dimer with three Si-atoms between the bananas is ferroelectric, and the dimer with four is antiferroelectric. According to the Maldi-Tof mass spectrum, the major part of oligomer **Si**$_{3.8}$**11-P-12** has two Si-atoms between the bananas (**Si**$_{3.8}$**11-P-12**, with $x = 2$, $b = 2$; and part of $x = 3$, $b = 2$; and a part of **Si**$_{3.8}$**11-P-12**, with $x \geq 3$). This might explain the antiferroelectric behavior of **Si**$_{3.8}$**11-P-12**. Furthermore, the Si-O to banana ratio for **Si**$_{3.8}$**11-P-12** is relatively low, which could also promote the antiferroelectric phases [20,21].
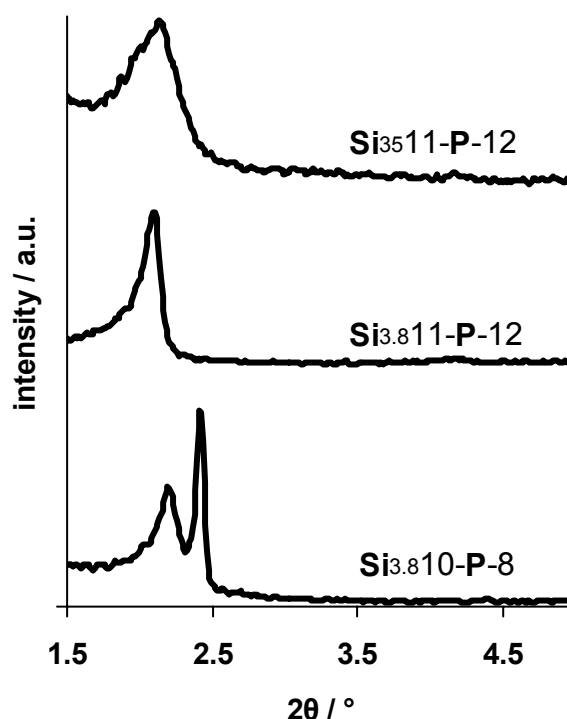

Figure 6*. XRD pattern for oligomers **Si**$_{3.8}$**10-P-8** and **Si**$_{3.8}$**11-P-12**, and polymer **Si**$_{35}$**11-P-12**, all recorded at 100 °C.*

Upon cooling from the isotropic phase, the small angle XRD patterns of oligomer **Si**$_{3.8}$**11-P-12**, shows two relatively broad reflections which are indexed as (001) and (002; very weak), as shown in figure 6. The appearance of only one reflection and its second order is unusual for bent core molecules, where usually reflections up to the

4th or 6th order can be observed. It seems that the close packing of the mesogenic units along the oligosiloxane backbone might give rise to some disorder which reduces the sharpness of the interlayer interfaces. The layer spacing was calculated to be 41.9 Å. The two other oligomers with a C_{11} spacer, **Si$_{3.8}$11-P-8** and **Si$_{3.8}$11-P-16** exhibit very similar XRD patterns. The layer thickness of all three oligomers in the **Si$_{3.8}$11-P-n** series, was hardly temperature dependent. The layer spacing d increases only slightly with increasing tail length (from 41.7 to 41.9 to 42.4 Å for n = 8, 12 and 16 respectively, table 2). The thickness of these oligomer smectic layers is significantly larger than those of the corresponding olefinic precursors. This could be expected since the siloxane backbone has a thickness of ~ 7 Å.

It seems that due to the stacking of the central aromatic part of the bananas a microsegregated system can exist which consists of a siloxane backbone part, an aliphatic spacer/tail part, and an aromatic part. To a certain extent the layer thickness d is only dependent on the spacer length m. It has to be noted however that the influence of m also seems relatively small (**Si$_{3.8}$10-P-12** versus **Si$_{3.8}$11-P-12**). Upon further cooling the SmCP phase, the transition to the low temperature phase (70-90°C) could be detected as a small increase in d-spacing.

Furthermore, the rather broad shape of the layer reflections is remarkable. This could be due to a strongly distorted structure of the smectic layers where the correlation length of the smectic slabs is significantly smaller than the wavelength of visible light (POM observations). This is in line with the proposed disordered structure of these smectic phases.
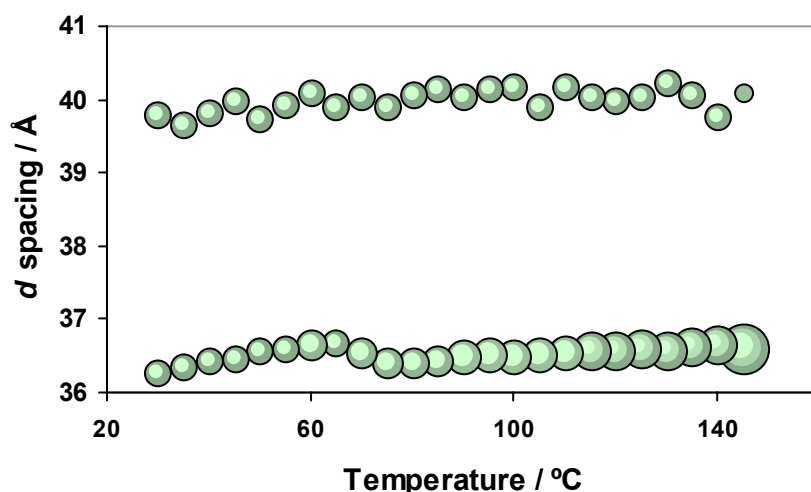

Figure 7. *Temperature dependent XRD reflections of oligomer* ***Si$_{3.8}$10-P-8*** *(intensity indicated by the circle size) upon cooling from the isotropic phase.*

Oligomer **Si**$_{3.8}$10-**P**-8 with a slightly shorter, even numbered, spacer between the aromatic core and the oligosiloxane unit shows a different XRD pattern than the other oligomers, with one broad and an additional relatively sharp reflection (figure 6). From figure 7, which shows the two reflections plotted against the temperature, the low temperature phase transition of the oligomer at ~70°C can be detected. This transition was also observed in the DSC thermogram at ~70°C upon cooling. The XRD pattern indicates the presence of a mesophase with 2D lattice (columnar mesophase). However, due to the presence of only two reflections a more precise assignment was not possible. It can be assumed that this mesophase is a modulated smectic phase, in which the modulation could be due to the different size of the siloxane and aliphatic parts of these systems or due to an escape from polar order. An undulated (sinusoidal deformed) smectic phase with an undulation period of about 114 Å could also be a possibility. The fact that no switching was observed points to a modulated smectic (*i.e.* columnar) phase driven by an escape from polar order. This would also be in line with the fact that the columnar phase is found for the homologue with the shortest alkyl chain length.

Additionally, and this is most remarkable, this columnar phase is optically isotropic and shows chiral domains while normally, columnar phases are birefringent. There is no previous report about a columnar phase with a dark conglomerate texture, but Pelzl *et al.* [9] have reported a B$_7$ phase with an oblique cell, which was formed upon cooling from a high temperature smectic phase with dark textures, explaining the dark texture in the B$_7$ phase at lower temperature (paramorphotic texture). A related situation, where a high temperature smectic phase that could induce the dark texture in the columnar mesophase below, could however not be detected in the presently investigated oligomer. It seems that this new mesophase with a 2D lattice is a modulated variant of the dark conglomerate smectic phases. In this case, the optical activity might be due to the superstructural layer chirality within the modulated layers, which becomes visible in the optically isotropic mesophase [22]. On the other hand, a deracemization of chiral (helical) conformers in the confined geometry of the smectic ribbons could lead to chirality in the ribbons which could probably also leads to a chirality induced distortion of the ribbons [8].

Although the exact structure of the mesophase of **Si**$_{3.8}$10-**P**-8 is unclear, a simple smectic structure can be excluded and therefore this unknown non-switchable columnar phase is designated as Col$_x$(*).

*Polymers(**Si**$_{35}$m-**P**-n)*

Just like the oligomers with the short backbone not all Si-H groups of the longer siloxanes (x~35) have reacted with a banana-shaped olefinic precursor. According to

the ^{1}H-NMR spectrum about 70% of all available Si-H sites have reacted. On cooling from the isotropic phase the polymers with 35 repeating units, **Si$_{35}$m-P-n**, remain optically isotropic. Even after slightly rotating the polarizer no regions of different brightness can be observed. One possibility is, that the chiral domains are too small to be observed under the polarizing microscope. However, it is also possible that the phase itself is achiral, as reported for another example [30]. The isotropization temperatures were determined from the DSC thermograms. Changing the length of the spacer or the terminal tail does not influence the transition temperatures significantly (table 3). All polymers have a low temperature phase transition, similar to the ones observed for the oligomers. These transitions are observed at lower temperatures however (45-60°C). Unfortunately, we were unable to perform switching experiments since the polymers were very viscous, and could not be introduced into the cells.

Table 3. *Transition temperatures (°C), transition enthalpies (J g^{-1}; between square brackets), and layer spacings d (Å), of the compounds in series **Si$_{35}$m-P-n**.*

Compound	SmCP	I	*d*
Si$_{35}$10-P-12	● 140 [8]	●	#
Si$_{35}$11-P-12	● 150 [11]	●	~41
Si$_{35}$11-P-16	● 155 [15]	●	~42

Could not be determined

The X-ray diffraction patterns of polymers **Si$_{35}$11-P-n** (*n* = 12 and 16) show weak, relatively broad reflection in the small angle region at ~42 Å (table 3, figure 6). The broad reflections are an indication for short correlation lengths, which might be caused by very small domains. This might also be the reason that no clear texture is revealed by POM. Due to the similar backbone structure and the similar layer thickness as found for the oligomers, the polymers also have a layered organization and this could be a SmCP organization.

Our findings show that the unique properties of banana-shaped molecules can be maintained in side chain liquid crystalline oligosiloxanes. However, because of the high viscosity these materials soon become unprocessable with increasing polymer chain length. An approach employed by Keith *et al*. [15] in which siloxanes were used with a low degree of substitution seems to be more promising.

7.4 Conclusions

Eight new banana-shaped side chain liquid crystalline oligomers/polymers have been synthesized and characterized. According to the ^{1}H-NMR and Maldi-Tof mass spectra the backbones of the oligomers/polymers are not fully occupied and some unreacted Si-H groups are still present. The olefinic precursors all show conventional Col$_r$ or SmCP$_A$ mesophases. In the pristine state all oligomers have an optically isotropic mesophase composed of domains of opposite chirality (dark conglomerate phases). Electro-optical investigations indicate antiferroelectric switching properties with a predominately anticlinic layer structure at zero voltage. They are therefore believed to have a distorted SmC$_A$P$_A$ layer organization. One of the oligomers shows a non-switchable columnar phase, also composed of domains of opposite chirality, whose structure is not exactly clear. The polymers with the longer backbones exhibit an optical isotropic mesophase without detectable chiral domains that could not be characterized by switching experiments due to the high viscosity. Comparison of the layer spacing with the shorter oligomers indicates that a lamellar ordering is likely for these materials.

7.5 References

1. Niori T., Sekine F., Watanabe J., Furukawa T. and Takezoe H. *J. Mater. Chem.* **1996**, *6*, 1231-1233.
2. Pelzl G., Diele S. and Weissflog W. *Adv. Mater.* **1999**, *11*, 707-724.
3. Link D. R., Natale G., Shao R., Maclennan J. E., Clark N. A., Körblova E. and Walba D. M. *Science* **1997**, *278*, 1924-1927.
4. Walba D. M., Korblova E., Shao R., Maclennan J. E., Link D. R., Glaser M. A. and Clark N. A. *Science* **2000**, *288*, 2181-2184.
5. Nakata M., Link D. R., Araoka F., Thisayukta J., Takanishi Y., Ishikawa K., Watanabe J. and Takezoe H. *Liq. Cryst.* **2001**, *28*, 1301-1308.
6. Bedel J. P., Rouillon J. C., Marcerou J. P., Laguerre M., Nguyen H. T. and Achard M. F. *Liq. Cryst.* **2001**, *28*, 1285-1292.
7. Coleman D. A., Fernsler J., Chattham N., Nakata M., Takanishi Y., Korblova E., Link D. R., Shao R.-F., Jang W. G., Maclennan J. E., Mondainn-Monval O., Boyer C., Weissflog W., Pelzl G., Chien L.-C., Zasadzinski J., Watanabe J., Walba D. M., Takezoe H. and Clark N. A. *Science* **2003**, *301*, 1204-1211.
8. Amaranatha Reddy R. and Tschierske C. *J. Mater. Chem.* **2005**, *15*, DOI: 10.1039/b504400f.
9. Pelzl G., Schröder M. W., Dunemann U., Diele S., Weissflog W., Jones C., Coleman D. A., Clark N. A., Stannarius R., Li J., Das B. and Grande S. *J. Mater. Chem.* **2004**, *14*, 2492-2498.
10. Choi E.-J., Ahn J.-C., Chien L.-C., Lee C.-K., Zin W.-C., Kim D.-C. and Shin S.-T. *Macromolecules* **2004**, *37*, 71-78.

11. Barberá J., Gimeno N., Monreal L., Pinol R., Ros M. B. and Serrano J. L. *J. Am. Chem. Soc.* **2004**, *126*, 7190-7191.

12. Sentman A. C. and Gin D. L. *Angew. Chem. Int. Ed.* **2003**, *42*, 1815-1819.

13. Keum C.-D., Kanazawa A. and Ikeda T. *Adv. Mater.* **2001**, *13*, 321-323.

14. Galli G., Demel S., Slugovc C., Stelzer F., Weissflog W., Diele S. and Fodor-Csorba K. *Mol. Cryst. Liq. Cryst.* **2005**, *439*, 1909-1919.

15. Keith C., Amaranatha Reddy R. and Tschierske C. *Chem. Commun.* **2005**, 871-873.

16. Shen D., Pegenau A., Diele S., Wirth I. and Tschierske C. *J. Am. Chem. Soc.* **2000**, *122*, 1593-1601.

17. Achten R., Smits E. A. W., Amaranatha Reddy R., Giesbers M., Marcelis A. T. M. and Sudhölter E. J. R. *Liq. Cryst.* **2005**, *32*, in press.

18. Dantlgraber G., Baumeister U., Diele S., Kresse H., Lühmann B., Lang H. and Tschierske C. *J. Am. Chem. Soc.* **2002**, *124*, 14852-14853.

19. Dantlgraber G., Diele S. and Tschierske C. *Chem. Commun.* **2002**, 2768-2769.

20. Dantlgraber G., Eremin A., Diele S., Hauser A., Kresse H., Pelzl G. and Tschierske C. *Angew. Chem. Int. Ed.* **2002**, *41*, 2408-2412.

21. Keith C., Amaranatha Reddy R., Hahn H., Lang H. and Tschierske C. *Chem. Commun.* **2004**, 1898-1899.

22. Hough, L. E. and Clark N. A. *Phys. Rev. Lett.* **2005**, *95*, 107802.

23. Achten R., Koudijs A., Giesbers M., Marcelis A. T. M. and Sudhölter E. J. R. *Liq. Cryst.* **2005**, *32*, 277-285.

24. Amaranatha Reddy R. and Sadashiva B. K. *Liq. Cryst.* **2003**, *30*, 1031-1050.

25. Pelz K., Weissflog W., Baumeister U. and Diele S. *Liq. Cryst.* **2003**, *30*, 1151-1158.

26. Ortega J., Folcia C. L., Etxebarria J., Gimeno N. and Ros M. B. *Phys. Rev. E* **2003**, *68*, 011707.

27. Jákli A., Huang Y.-M., Fodor-Csorba K., Vajda A., Galli G., Diele S. and Pelzl G. *Adv. Mater.* **2003**, *15*, 1606-1610.

28. Svoboda J., Novotna V., Kozmik V., Glogarova M., Weissflog W., Diele S. and Pelzl G. *J. Mater. Chem.* **2003**, *13*, 2104-2110.

29. Keith C., Amaranatha Reddy R., Baumeister U. and Tschierske C. *J. Am. Chem. Soc.* **2004**, *126*, 14312-14313.

30. Liao G., Stojadinovic S., Pelzl G., Weissflog W., Sprunt S. and Jákli A. *Elec. Liq. Cryst. Comm.* **2004**.

8

Covalent attachment of bent-core molecules to silicon surfaces

Three different vinyl-terminated banana-shaped molecules, of which two bear a fluorine substituent at a distinct position in the bent core, have been covalently attached to a hydrogen-terminated silicon surface. This was done via a mild procedure, using visible light at room temperature. The presence and quality of the monolayers was investigated using static water contact angles, infrared reflection-absorption spectroscopy, atomic force microscopy, X-ray reflectivity and angle-resolved X-ray photoelectron spectroscopy (AR-XPS). The monolayer without a fluorine substituent shows a thickness of about 34 Å by X-ray reflectivity, which is comparable to the d-spacing in bulk. This indicates a monolayer in which the attached molecules have an average tilt of about 45° with respect to the surface normal. Additional information on the orientation of the molecules in the monolayers comes from AR-XPS measurements on monolayers derived from two fluorine substituted bananas, one with the fluorine close to the alkene group, and the other one with the fluorine at a more distant position from the double bond. The AR-XPS-based relative depth profile confirms that the F-atoms are located at the expected positions with respect to the surface, indicative for a relatively well-ordered monolayer.

8.1 Introduction

Achiral banana-shaped, or bent-core compounds can form polar smectic layers with ferroelectric or antiferroelectric switching properties [1]. The dipoles of the molecules in one layer all point along a common director and the molecules are tilted with respect to the layer normal. This gives rise to chiral layer symmetry, and if the chirality is the same in adjacent layers a macroscopically chiral structure can exist [2]. The most widely studied banana-phase is the SmCP phase, which can exist in an antiferroelectric (P_A) or a ferroelectric ground state (P_F), with either synclinic (C_s) or anticlinic (C_a) layer organization. The antiferroelectric ground state is the most commonly seen ground state because of the inherent tendency of fluid systems to escape from macroscopic polar order [3].

In the last ten years over thousand banana-shaped liquid crystals have been studied and their mesomorphic behavior described [3-8]. The influence of fluorine substituents on the liquid crystalline properties of these liquid crystals has also been studied intensively. Especially F-atoms substituted in the outer phenyl rings, *ortho* to the terminal tails, have a pronounced effect on the switching behavior, changing the ground state from antiferroelectric to ferroelectric [6,9-11].

The properties of bananas have almost always been studied in bulk. Langmuir [12-15], vacuum-deposited [16,17], two-dimensional assemblies [18] or free-standing films [19] of banana (sub)monolayers, are to the best of our knowledge the only examples of characterization of these compounds in (sub)monolayers. On Highly Ordered Pyrolytic Graphite (HOPG) the bananas form a monolayer as they lie flat on the surface and form rows with an antiferroelectric relation between the rows [18]. On water the orientation of the molecules depends on the hydrophobicity of the end chains [12].

Alkene-terminated bananas [20,21] can, in principle, also be used to create covalently bound monolayers on silicon surfaces by a hydrosilylation reaction [22-24]. The covalent attachment of liquid crystals, and especially banana-shaped liquid crystals, might overcome (alignment) problems usually observed for smectic liquid crystals, and could make these materials suitable for applications [25,26] like switchable alignment layers [27,28].

Several chemically distinct groups of organic molecules have been attached (by direct or indirect methods [29]) to silicon surfaces; *e.g.* sugars [30], fullerenes [31], DNA [32], and proteins [33], but mostly simple unsaturated hydrocarbons are used [23,34]. Recently, switchable self-assembled monolayers (SAMs) were simulated [35] and reported [36]. Several different methods [34,37-40] to obtain these (functionalized) SAMs to well-defined Si(111) or Si(100) surfaces, have been used in the past.

Here we present the first monolayers of covalently attached banana-shaped liquid crystals to a silicon surface. Three bent-core mesogens, figure 1, were attached to H-terminated Si(111) via an extremely mild procedure [41], using visible light (447 nm) at room temperature. The presence and quality of the monolayers were tested using a wide variety of techniques.
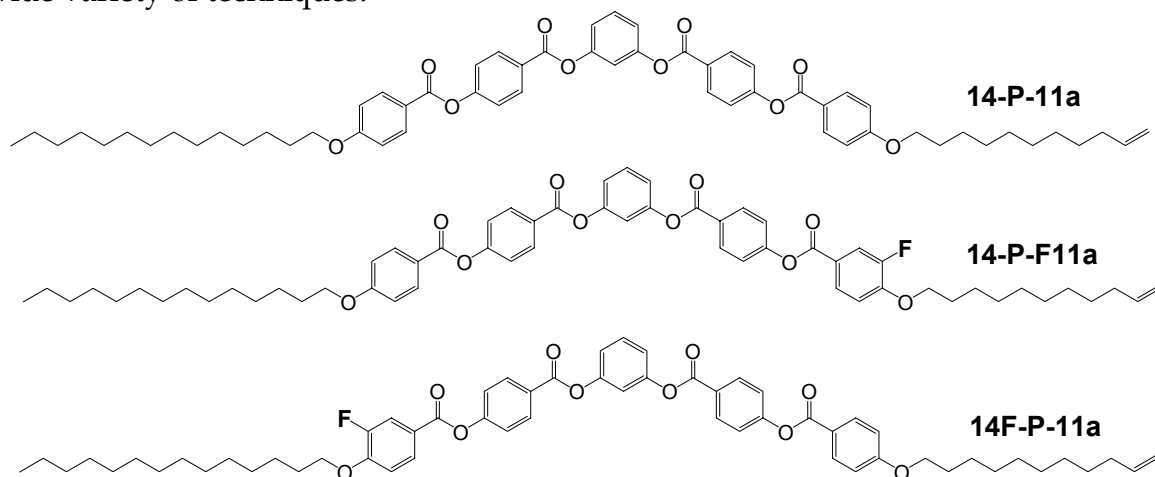

14-P-11a

14-P-F11a

14F-P-11a

Figure 1. Structures of the banana-shaped mesogens.

8.2   Experimental

8.2.1   Synthesis

The synthesis and characterization of banana-shaped compounds 14-**P**-11a [20] and 14F-**P**-11a [21] was published elsewhere. Compound 14-**P**-F11a was prepared following the synthetic pathway shown in the scheme.

Compound **P**-14 was synthesized according to a literature procedure [42]. 4-Bromo-2-fluorophenol was obtained from Aldrich and used without further purification.

Compound **I** was obtained by etherification of 4-bromo-2-fluorophenol with 11-bromo-1-undecene and K_2CO_3 as base. **II** was obtained by carboxylation of the Li-analogue of **I** with carbon dioxide. Compound **IV** was obtained by esterification of the acid chloride of **II** with 4-hydroxybenzaldehyde (giving compound **III***)* followed by $NaClO_2$ oxidation [20,21,43]. 14-**P**-F11a was obtained by esterification of the acid chloride of **IV** with **P**-14 in THF with DMAP as base.

*4-Bromo-2-fluoro-1-(10-undecenyloxy)benzene (**I**)*

A mixture of 7.30 g (38.2 mmol) 4-bromo-2-fluorophenol, 8.99 g (38.6 mmol) 11-bromo-1-undecene and 8.1 g K_2CO_3 in 100 ml of butanone was heated under reflux overnight. After cooling, the mixture was concentrated and 100 ml CH_2Cl_2 was

added. After filtration of the salts, the filtrate was concentrated and the colorless oil was used in the next step without further purification. Yield: 91%.

^{1}H NMR (300 MHz, CDCl$_3$) δ (ppm): 7.19 (m, 2H, Ar), 6.82 (t, 1H, Ar), 5.81 (m, 1H, =CH), 4.94 (t, 2H, =CH$_2$), 3.98 (t, 2H, OCH$_2$), 2.03 (m, 2H, C=CCH$_2$), 1.80 (m, 2H, OCCH$_2$), 1.53-1.30 (m, 12H, 6 x CH$_2$). ^{13}C NMR (CDCl$_3$) δ (ppm): 154.6, 151.3, 147.1, 146.9, 139.6, 127.5, 120.2, 119.9, 116.3, 114.5, 112.2, 112.1, 70.0, 34.2, 29.9, 29.8, 29.7, 29.5, 29.3, 26.2. HRMS calc. for C$_{17}$H$_{24}$BrFO 342.0995; found 342.0994.
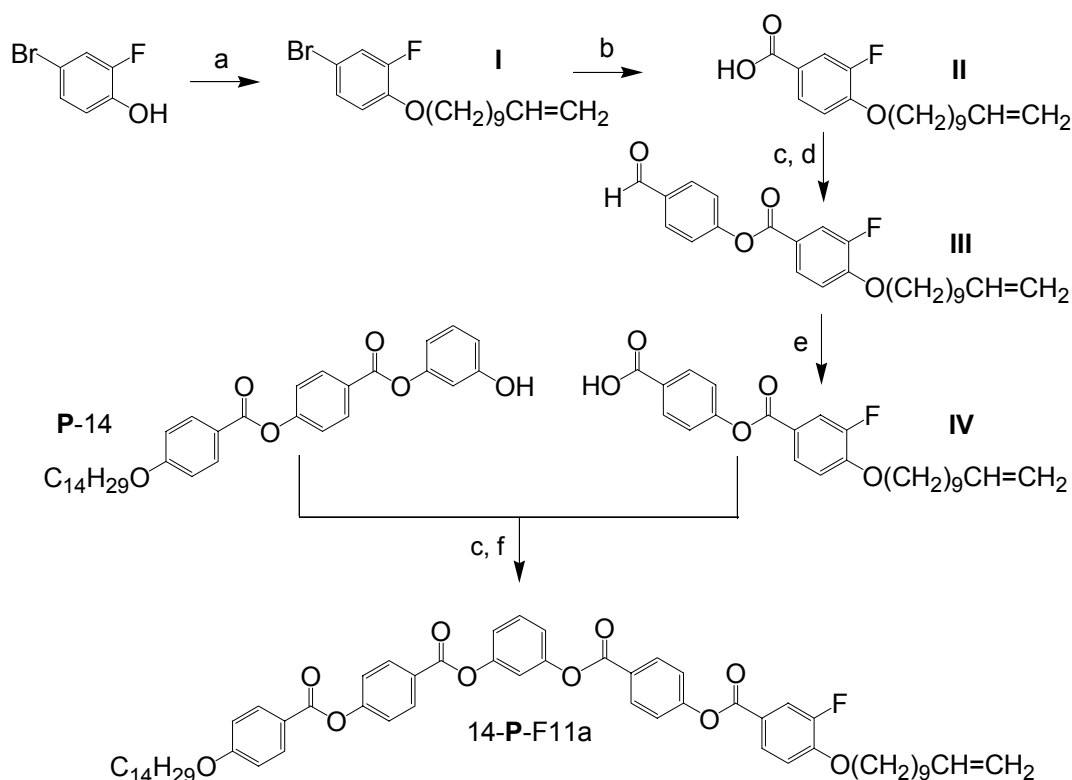
Scheme. *Synthesis of 14-**P**-F11a: a) 11-bromo-1-undecene, K$_2$CO$_3$, butanone, reflux; b) n-BuLi, -78°C, CO$_2$ (s); c) SOCl$_2$, reflux; d) 4-hydroxybenzaldehyde, DMAP, THF, rt; e) NaClO$_2$, resorcinol, NaH$_2$PO$_4$, THF, H$_2$O, rt; f) DMAP, THF, rt.*

*3-Fluoro-4-(10-undecenyloxy)benzoic acid (**II**)*

To a solution of 11.88 g (34.6 mmol) 4-bromo-2-fluoro-1-(10-undecenyloxy)benzene (**I**) in 100 ml of dry THF at -60°C, was added 26 ml of a 1.6 M solution of butyllithium in hexane (41.5 mmol). After stirring for 0.5h at -78°C, the cold solution was poured onto crushed solid CO$_2$, and allowed to warm to room temperature. Thereafter, the reaction mixture was acidified to pH 2 with a 10% HCl solution. Subsequently, the mixture was partly concentrated and the precipitate was filtered off, and washed with water. Recrystallization from EtOH and washing with PE 40-60 gave white crystals. Yield: 42%.

[^1]H NMR (400 MHz, CDCl$_3$) δ (ppm): 10.75 (bs, 1H, COOH), 7.73 (dd, 2H, Ar), 6.88 (t, 1H, Ar), 5.70 (m, 1H, =CH), 4.85 (t, 2H, =CH$_2$), 3.99 (t, 2H, OCH$_2$), 1.94 (m, 2H, C=CCH$_2$), 1.75 (m, 2H, OCCH$_2$), 1.45-1.25 (m, 12H, 6 x CH$_2$).

4-[3-Fluoro-4-(10-undecenyloxy)benzoyloxy]benzaldehyde (III)

Compound **II** (4.41 g, 14.3 mmol) was heated under reflux in thionyl chloride (30 ml) for 2h. Excess thionyl chloride was removed by distillation under reduced pressure. The resulting acid chloride was dissolved in 50 ml dry THF, and 1.75 g (14.3 mmol) 4-hydroxybenzaldehyde was added. To this clear solution 2 equivalents (3.50 g; 28.6 mmol) of DMAP were added, and the reaction mixture was stirred for 24h at room temperature under a N$_2$ atmosphere. After removal of the THF, 200 ml of CH$_2$Cl$_2$ was added. The organic layer was washed twice with a 1M HCl solution, once with a saturated NaHCO$_3$ solution and dried over Na$_2$SO$_4$. The crude product was used in the next step without further purification. Yield: 78%, Mp 49°C.

[^1]H NMR (400 MHz, CDCl$_3$) δ (ppm): 10.05 (s, 1H, CHO), 7.98 (m, 3H, Ar), 7.90 (d, 1H, Ar), 7.42 (d, 2H, Ar), 7.06 (t, 1H, Ar), 5.83 (m, 1H, =CH), 4.97 (t, 2H, =CH$_2$), 4.15 (t, 2H, OCH$_2$), 2.07 (m, 2H, C=CCH$_2$), 1.89 (m, 2H, OCCH$_2$), 1.52-1.28 (m, 12H, 6 x CH$_2$). ^{13}C NMR (CDCl$_3$) δ (ppm): 189.1, 161.6, 153.8, 151.7, 150.6, 150.4, 149.1, 137.3, 132.2, 129.4, 125.8, 125.7, 120.6, 119.3, 119.2, 116.1, 115.9, 112.3, 111.7, 67.7, 31.9, 27.6, 27.5, 27.4, 27.2, 27.1, 23.6. HRMS calc. for C$_{25}$H$_{29}$FO$_4$ 412.2050; found 412.2047.

4-[3-Fluoro-4-(10-undecenyloxy)benzoyloxy]benzoic acid (VI)

Compound **III** (4.50 g, 10.9 mmol) and resorcinol (1.56 g; 14.1 mmol) were dissolved in 140 ml THF. To this solution was added dropwise, over 10 min, a solution of sodium chlorite (NaClO$_2$, 80%; Aldrich) (5.73 g, 63.5 mmol) and sodium dihydrogenphosphate monohydrate (4.58 g, 33.1 mmol) in 50 ml water. The resulting pale yellow reaction mixture was then stirred overnight at room temperature. Volatile components were removed *in vacuo* and the residue was dissolved in 150 ml water. The aqueous solution was acidified to pH 2 by adding 1M HCl. The white precipitate was filtered, washed with water, and dried in the air. The white crystals were then washed with PE 40-60. Yield 83%. Cr 120 SmC 201 I (°C).

[^1]H NMR (400 MHz, CD$_3$OD, 50°C) δ (ppm): 8.11 (d, 2H, Ar), 7.98 (d, 1H, Ar), 7.87 (d, 1H, Ar), 7.33 (d, 2H, Ar), 7.24 (t, 1H, Ar), 5.83 (m, 1H, C=CH), 4.95 (m, 2H, C=CH$_2$), 4.20 (t, 2H, OCH$_2$), 2.06 (m, 2H, C=CCH$_2$), 1.86 (m, 2H, OCCH$_2$), 1.55-1.36 (m, 12H, 6 x CH$_2$). HRMS calc. for C$_{25}$H$_{29}$FO$_5$ 428.1999; found 428.1995.

1-[4-(4-n-Tetradecyloxybenzoyloxy)benzoyloxy]-3-{4-[3-fluoro-4-(10-
*undecenyloxy)benzoyloxy]-benzoyloxy}benzene (14-**P**-F11a)*

IV (0.71 g, 1.66 mmol) was refluxed in 10 ml thionyl chloride for two hours. The excess of thionyl chloride was removed by distillation under reduced pressure. The resulting acid chloride was dissolved in 40 ml freshly distilled dry THF and to this stirred solution 0.90 g (1.65 mmol) of **P**-14 was added. Subsequently, 2 equivalents of DMAP (0.40 g; 3.28 mmol) were added. The reaction mixture was stirred for 24h at room temperature under N_2 atmosphere. Thereafter, the THF was removed under *vacuo* and ~150 ml CH_2Cl_2 was added. The organic layer was washed successively with 1M HCl (2 x) and a saturated $NaHCO_3$ solution and dried over anhydrous Na_2SO_4. After filtration of the salts the filtrate was concentrated and the residue was purified by column chromatography (eluant: CH_2Cl_2). Finally, recrystallization from acetonitrile and washing with PE 40-60 gave colorless crystals. Yield: 37%. Cr 90 SmCP 106 I (°C).

^{1}H NMR (400 MHz, CDCl$_3$) δ (ppm): 8.30 (d, 4H, Ar), 8.17 (d, 2H, Ar), 7.96 (d, 1H, Ar), 7.92 (d, 1H, Ar) 7.52 (t, 1H, Ar), 7.39 (d, 4H, Ar), 7.22 (s+d, 3H, Ar), 7.03 (t+d, 3H, Ar), 5.82 (m, 1H, =CH), 4.98 (t, 2H, =CH$_2$), 4.15 (t, 2H, OCH$_2$), 4.07 (t, 2H, OCH$_2$), 2.06 (m, 2H, C=CCH$_2$), 1.87 (m, 4H, 2 x OCCH$_2$), 1.67-1.29 (m, 34H, 17 x CH$_2$), 0.90 (t, 3H, CH$_3$). ^{13}C NMR (CDCl$_3$) δ (ppm): 162.5, 162.3, 162.2, 162.0, 153.6, 153.4, 149.6, 149.5, 137.3, 130.6, 130.0, 128.1, 125.7, 125.0, 124.7, 120.3, 120.2, 119.1, 117.5, 114.0, 112.6, 112.3, 111.7, 67.6, 66.5, 30.1, 27.8, 27.7, 27.6, 27.5, 27.4, 27.2, 27.1, 24.1, 24.0, 20.8, 12.3.

8.2.2 Monolayer preparation

Before the hydrosilylation reaction, the Si wafers (single-polished Si(111): n-type, 475-500 µm thick, resistivity 1-5 Ωcm (low-doped) or 0.005-0.015 Ωcm (high-doped) (Addison Engineering, Inc. San Jose, CA, USA)) were cleaned. After wiping the wafers with a tissue that was saturated with acetone p.a., the samples were sonicated for at least 10 min. in acetone or rinsed excessively with acetone and dried in a stream of nitrogen. Subsequently, the wafers were placed in an oxygen plasma cleaner (Harrick PDC-32G) for at least 2 min. Then, the samples were etched in an argon-saturated 40% aqueous NH$_4$F solution for 15 min., washed thoroughly with demineralized water and dried in a stream of nitrogen.

The monolayers were prepared according to the following procedure: a 0.05 M solution of the vinyl-terminated bananas (and 1-decene) in dry mesitylene was flushed with argon for at least 30 min. Then the freshly etched hydrogen-terminated Si-wafers were added, and the solution was flushed with argon for another 30 min. Then the lamp (Jelight Co. Inc. (Irvine CA): 84-247-2 (447 ± 32 nm)), at a distance of 0.5 cm from the reaction vessel, was switched on. After illumination for the desired

time (~14 h [29]), the wafer was removed from the solution, and the surface was rinsed with subsequently PE 40-60, EtOH, and CH_2Cl_2, and finally dried in a stream of nitrogen.

8.2.3 Measurements

Melting points, thermal phase transition temperatures and optical inspection of the liquid crystalline phases were determined on samples between ordinary glass slides using an Olympus BH-2 polarization optical microscope (POM) equipped with a Mettler FP82HT hot stage, which was controlled by a Mettler FP80HT central processor. Temperature-dependent X-ray diffraction curves of the liquid crystals were measured on a Panalytical X'pert Pro diffractometer equipped with an Anton Paar camera for temperature control. For the measurements in the small angle region the sample was spread in the isotropic or the liquid crystalline phase on a thin glass slide (about 15 µm thick). The glass slide was then placed on a temperature regulated flat copper sample stage. X-ray reflectivity measurements were performed on the same machine. The layer thickness is calculated from the interference fringes.

Static water contact angles were obtained using an Erma G-1 contact angle meter. Contact angles of two or three drops were determined. The error of the contact angles is +/-1°. IRRAS spectra were recorded on a Bruker Tensor 27 instrument. All recorded spectra are a result of spectral subtraction of modified samples with a cleaned native oxide-covered silicon sample. The surface topography was imaged using a Nanoscope III atomic force microscope (AFM Digital Instruments, Santa Barbara, CA) operating in contact mode (CM-AFM) with silicon nitride cantilevers (Veeco Instruments Inc.) model NP, with a spring constant of ~ 0.58 N/m.

X-ray photoelectron spectroscopy (XPS) and angle resolved X-ray photoelectron spectroscopy (AR-XPS) analyses were performed on a Theta Probe (Thermo VG Scientific, UK) by using a monochromatic Al-K_α X-ray source with 400 µm spot runs at 100 W under UHV conditions.

Ellipsometric measurements were performed with a computer-controlled null ellipsometer (Sentech SE-400) with a He–Ne laser (λ = 632.8 nm) and an incident angle of 70°. The mode 'polarizer + retarder, aperture, strict' was used. The optical layer thickness was measured using a three-layer model in the ellipsometry software from Sentech. Values of 3.85 and 0.020 were used for the refractive index (n) and the imaginary refractive index (k) of silicon, respectively. The values obtained from these measurements were calculated by averaging the results of measurements on six different spots.

8.3   Results and discussion

The three banana-shaped compounds used for this study are shown in figure 1. All are five-ring bent mesogens with esters as connecting groups between the aromatic rings, and all have tetradecyloxy and 10-undecenyloxy terminal chains. Two of the bananas have a fluorine substituent in one of the outer phenyl rings, *ortho* to the terminal chains.

The thermotropic properties of bent-core mesogens 14-**P**-11a and 14F-**P**-11a, have already been described in earlier papers [20,21]. Both compounds show the antiferroelectric SmCP$_A$ phase over a reasonably wide temperature range. Compound 14-**P**-F11a shows the same POM textures, and comparable transition temperatures as the other two bent mesogens previously described. Additionally, the *d*-spacing is 39.2 Å, which is comparable to the layer thickness of the other F-substituted compound 14F-**P**-11a (38.5 Å). Based on our characterization and the similarities with the other two bananas, we conclude that the mesophase of compound 14-**P**-F11a is also SmCP.

*14-**P**-11a monolayers*

A frequently used method for preparing organic monolayers on silicon surfaces, *i.e.* refluxing alkene solution in mesitylene in the presence of a hydrogen terminated silicon wafer, has proven to be too harsh for bananas [44], despite the relative stability of most bananas. Therefore, a recently reported, much milder attachment method [41], using visible light at room temperature, was used to prepare the monolayers.

The presence and quality of a monolayer of non-fluorinated compound 14-**P**-11a on a Si(111) surface, were tested using static water contact angles (CA), infrared reflection-absorption spectroscopy (IRRAS), atomic force microscopy (AFM) and X-ray reflectivity.

The static water contact angle of the Si surface, modified with 14-**P**-11a was 92° ± 1, confirming the presence of a monolayer. The observed contact angle is however lower than the 110° normally observed for densely packed alkyl monolayers indicating high hydrophobicity [29]. The lower water contact angle could be due to the presence of polar functionalities (ester or ether groups) in the monolayer [41], which can be accessed by water due to a (locally) less densely modified surface. On the other hand the relatively low static water contact angle could also be an indication of a partly covered surface; *i.e.* when the attachment of a second mesogen in the vicinity of an already attached mesogen is hampered. Larger molecules are known to produce less densely packed monolayers [30].
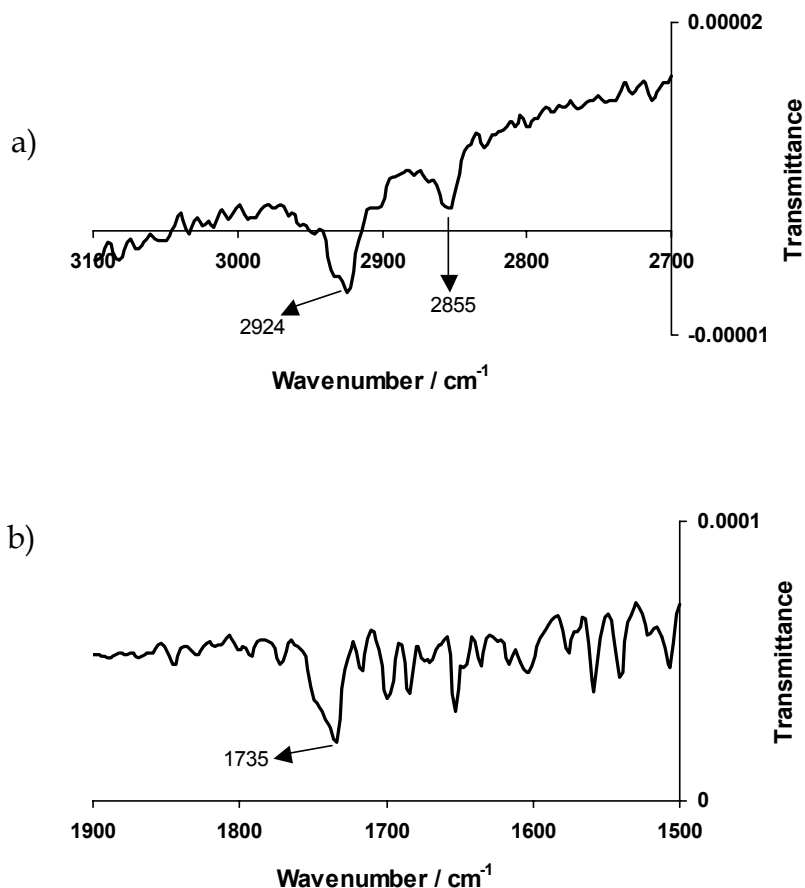
Figure 2. C-H (a) and C=O (b) stretching vibration regions of the IRRAS spectrum of 14-**P**-11a on the H-terminated Si(111) surface.

The presence of the monolayer was also confirmed by infrared reflection-absorption spectroscopy (IRRAS), which provided peaks for C-H and C=O stretching vibrations (figure 2). The antisymmetric and symmetric C-H stretching vibrations are found at 2924 and 2855 cm^{-1} as shown in figure 2a). Not only do these peaks confirm the presence of a monolayer, they also give information about their quality. The degree of order (liquid-like or solid-like) can be estimated from the IRRAS band maxima for the C-H stretching vibrations [29]. The presently investigated monolayer shows wavenumbers in the liquid-like regime, which in principle still allows rotation of the molecules. The C=O stretching vibration, although weak, could also be observed, as shown in figure 2b). This vibration is indicative of the presence of ester groups in the banana-monolayer.

The obtained monolayer was also evaluated using AFM. At first glance the surface topography resembles a bare silicon surface, no defects or incomplete monolayers are present, as shown in figure 3a). This could be due to either a clean unmodified silicon surface or a complete monolayer that nicely follows the contours of the silicon surface. Because the second and consecutive scans of the same area gave pictures

which were more blurred or smoothed, it seems that the AFM-tip has "rearranged" the surface layer (not shown). This is normally not observed on a clean "hard" silicon surface and gives evidence that indeed a monolayer is present on the surface. The possibility was ruled out that the smoothing was due to dulling of the AFM-tip, because when a new fresh area was scanned using the same tip again a sharp picture was obtained which became blurred and smoothed in consecutive scans. Figure 3b) shows the section analysis of 14-**P**-11a on Si(111) which is rather smooth, similar to a densely packed alkyl monolayer [29].

a)   b)
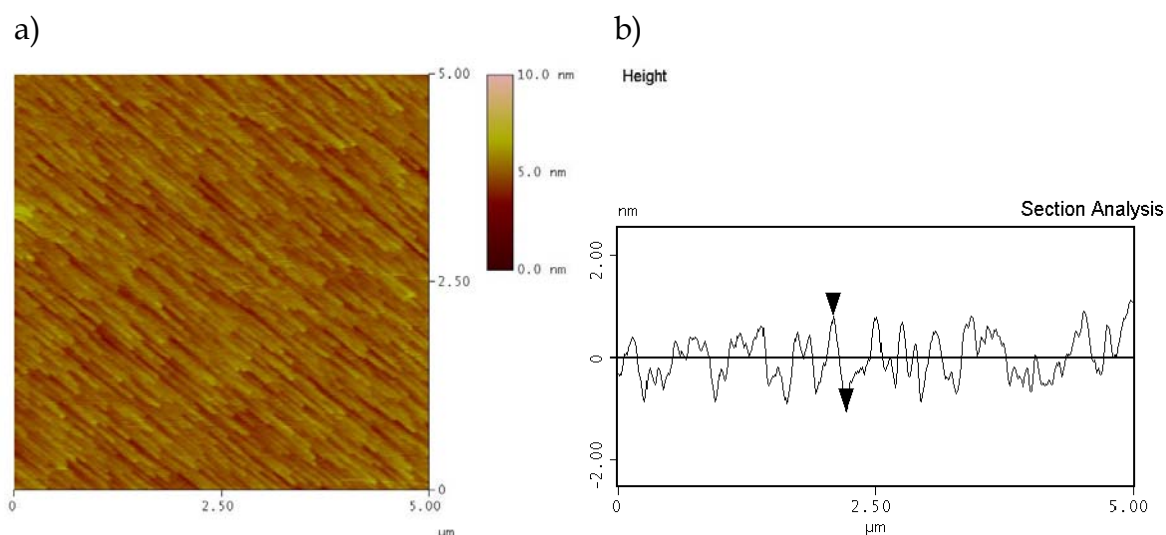
Figure 3. *Contact mode AFM image of a) a 25 μm² area of 14-**P**-F11a on Si(111) and b) corresponding section analysis.*

In order to investigate the thickness of the monolayer, X-ray reflectivity measurements were performed for 14-**P**-F11a on Si(111). The X-ray reflectivity profile is shown in figure 4 and from the fringes and the simulation a monolayer thickness of 34 ± 2 Å can be estimated. This value agrees well with the *d*-spacing of 14-**P**-F11a in bulk (36.5 Å) [20], for which an average tilt angle of ~45° is assumed. This indicates that the "average" tilt angle of the bananas in the monolayer is similar to the tilt angle in the liquid crystalline bulk, although we cannot be sure that the direction of the tilt is cooperative and that domains with the same tilt angle are present. A consequence of the observed "average" tilt angle is that the occupation of the silicon sites at the surface is lower than in the dense alkyl monolayers found for simple alkenes.
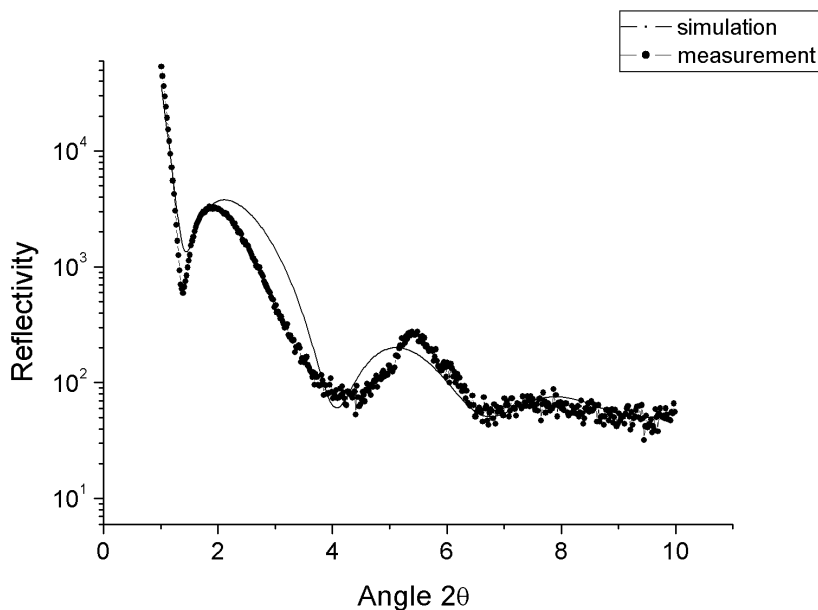
Figure 4. *X-ray reflectivity profile for 14-**P**-11a on Si(111).*

*14-**P**-F11a and 14F-**P**-11a monolayers*

A very useful tool for the investigation of covalently attached monolayers on silicon is X-ray photoelectron spectroscopy (XPS) [32,41,45]. The depth distribution of elements in a monolayer can be studied using angle resolved X-ray photoelectron spectroscopy (AR-XPS) [30,41]. This technique measures the intensity of the photoelectron emission as a function of emission angle. To get more information about the orientation of the bananas in the monolayer, we prepared two fluorine containing molecules, one with a fluorine substituent located at the upper part of the aromatic core (14F-**P**-11a), far from the alkene group, and its structural isomer with a fluorine substituent in the lower part of the aromatic core (14-**P**-F11a), near the alkene group. In the preparation of these monolayers, the bananas were diluted with linear alkene (75% banana; 25% 1-decene) in order to obtain a higher substitution of the silicon sites. Several studies [29,41,46] have shown that there is a relation between the distribution of two different molecules on the surface and their ratio in the solution. The dilution of the bananas with 1-decene will also reduce the formation of Si-O sites on the silicon surface after exposure of the obtained monolayers to air.

The XPS survey spectrum of a mixed monolayer of 14F-**P**-11a and 1-decene is given in figure 5. The survey scan shows peaks due to silicon, carbon and oxygen. The oxygen peak is characteristic for this preparation of monolayers on Si(111) [29]. Additionally, a small peak due the fluorine atom can be observed around ~700 eV. The expanded C_{1s} and F_{1s} regions are also shown in figure 6. The F_{1s} signal, as shown in figure 6a), is the composite peak of Si-F and C-F. For this type of monolayer preparation always small amounts of fluorine are detected, due to the etching

procedure. The C_{1s} region (figure 6b) shows a broad peak with two shoulders. Deconvolution of the peak is indicative for the presence of at least three types of carbon (A, B and C) in different oxidation states, probably C=O (peak C), C-O (peak B) and the "rest-carbons" (peak A).
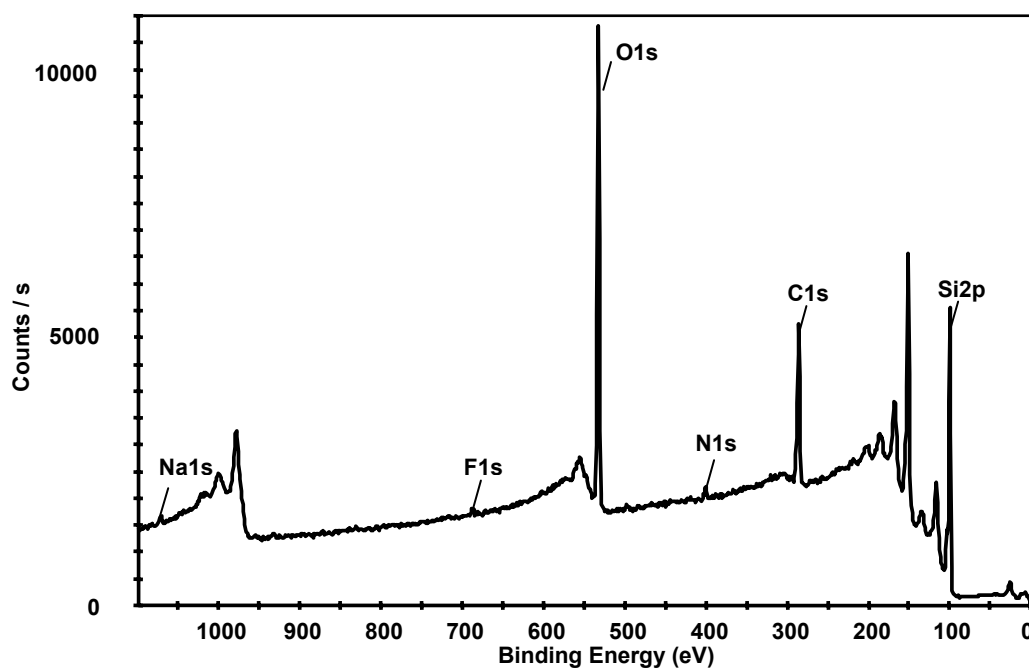

*Figure 5. XPS spectrum of a mixed monolayer of 14F-**P**-11a and 1-decene on Si(111).*
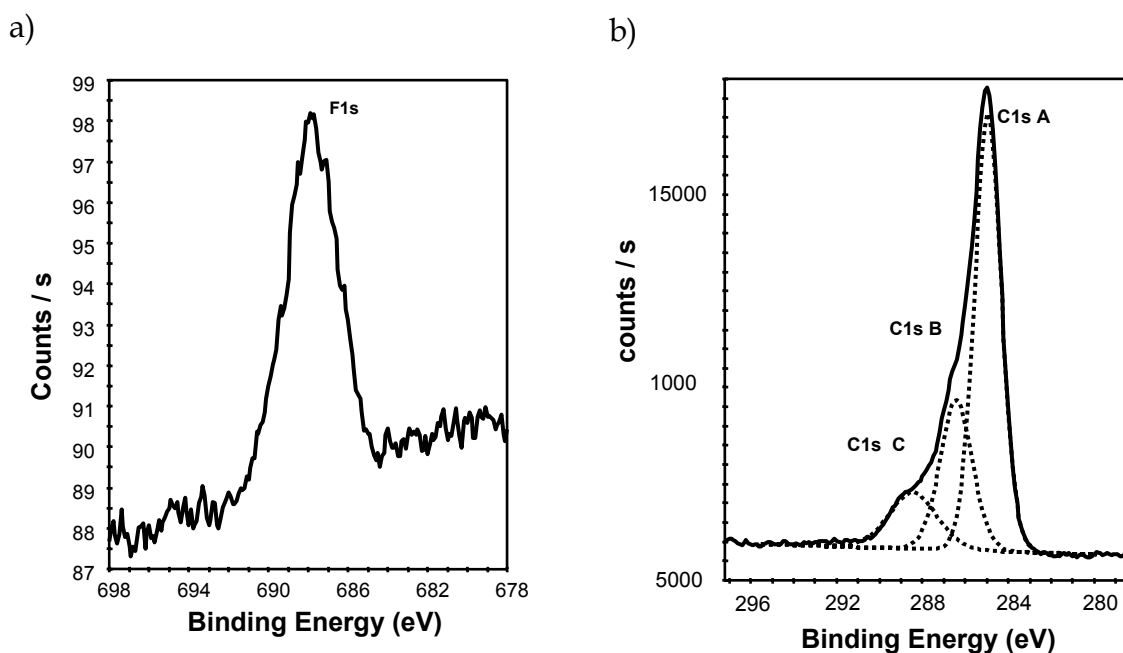
a)   b)

*Figure 6. X-ray photoelectron spectra of mixed monolayer of 14F-**P**-11a and 1-decene on Si(111); a) F_{1s} region, b) C_{1s} region (solid line: measured; dotted lines: deconvoluted signals).*

Figure 7 depicts relative depth profiles obtained with AR-XPS, of the mixed monolayers of 14F-**P**-11a and 14-**P**-F11a, respectively. In both cases bulk Si is located at the bottom (Si_{2p}). Next the peak of Si atoms bound to O ($Si_{2p}O$), and the corresponding O atoms (O_{1s}) can be observed for both monolayers. These signals are due to partial oxidation of the surface, and cannot be avoided in the monolayer preparation. Then the monolayer of 14F-**P**-11a shows the carbon atom signals. On top, nearest to the surface, the F_{1s} signal can be observed. For the other monolayer, 14-**P**-F11a, the signals for C_{1s} and F_{1s} are reversed; *i.e.* in this monolayer the F_{1s} signal is relatively closer to the silicon surface than the average carbon atoms.
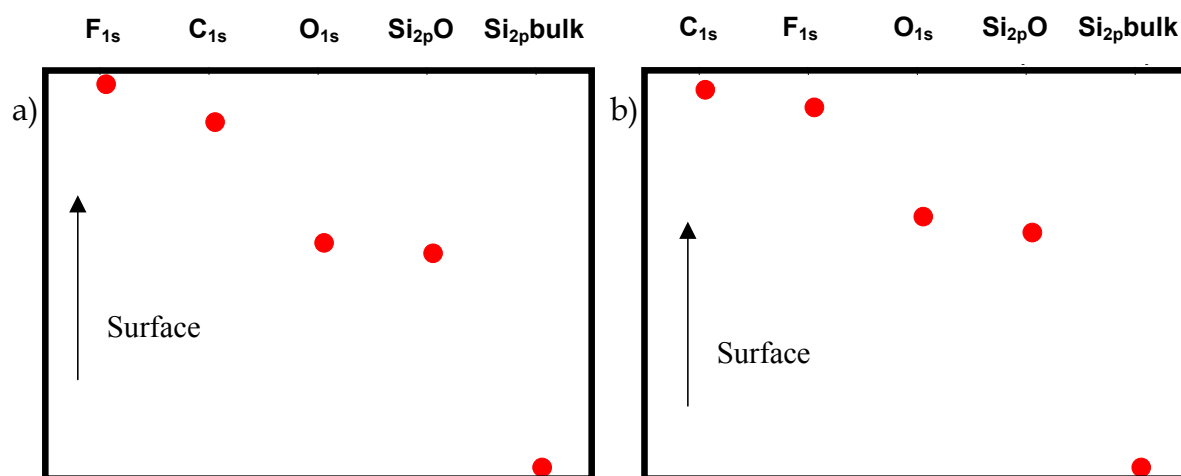
Figure 7. *Relative depth profile of the elements of a monolayer of a) 14F-**P**-11a and b) 14-**P**-F11a on H-terminated Si(111) surface.*

The AR-XPS results show that detailed information about the depth distribution of the elements in the monolayer can be obtained. Even for a very small difference in monolayer composition, *i.e.* the relative position of one F-atom, this technique is able to show this difference. These measurements also show that the orientation of the bananas on the surface is as expected. An orientation in which the aromatic cores of the bananas lie parallel to the Si-surface can be excluded, since a significant difference in the position of the F-atom could be observed, even though some fluorine bound to the surface cannot be excluded.

Preliminary ellipsometric measurements show that the monolayers composed of the fluorinated bananas have a layer thickness that is comparable to the monolayers of the non-fluorinated bananas.

The results of this study show that SAMs of banana-shaped mesogens can be made on silicon surfaces. The properties of these monolayers show similarities with the molecules in bulk and could, theoretically, also show switching behavior in the presence of external electric fields. This should require a rotation of the molecules

around the tilt cone, or around the molecular long axis, reversing the polar direction [47]. Hence these SAMs hypothetically can be used as switchable alignment layers.

8.4   Conclusions

We have demonstrated for the first time that it is possible to make SAMs of banana-shaped molecules. From the static water contact angle is concluded that the quality of the banana monolayer on Si(111) is relatively good, although the values are lower than for a densely packed alkyl monolayer. Further evidence for the presence of a monolayer comes from AFM and IRRAS measurements. Moreover, X-ray reflectivity measurements showed that the thickness of the monolayer was ~34 Å, which is slightly lower than the *d*-spacing in bulk. The size of the bananas could suppress a more complete coverage of the surface. The AR-XPS measurements have shown that the fluorine substituents are located at positions in the monolayer that could be expected from the molecular structure of the constituent bananas.

8.5   References and notes

1.   Niori T., Sekine F., Watanabe J., Furukawa T. and Takezoe H. *J. Mater. Chem.* **1996**, *6*, 1231-1233.
2.   Link D. R., Natale G., Shao R., Maclennan J. E., Clark N. A., Körblova E. and Walba D. M. *Science* **1997**, *278*, 1924-1927.
3.   Tschierske C. and Dantlgraber G. *Pramana* **2003**, *61*, 455-481.
4.   Pelzl G., Diele S. and Weissflog W. *Adv. Mater.* **1999**, *11*, 707-724.
5.   Shen D., Pegenau A., Diele S., Wirth I. and Tschierske C. *J. Am. Chem. Soc.* **2000**, *122*, 1593-1601.
6.   Amaranatha Reddy R. and Sadashiva B. K. *Liq. Cryst.* **2003**, *30*, 1031-1050.
7.   Weissflog W., Nadasi H., Dunemann U., Pelzl G., Diele S., Eremin A. and Kresse H. *J. Mater. Chem.* **2001**, *11*, 2748-2758.
8.   Amaranatha Reddy R. and Tschierske C. *J. Mater. Chem.* **2005**, *15*, DOI: 10.1039/b504400f.
9.   Amaranatha Reddy R. and Sadashiva B. K. *J. Mater. Chem.* **2004**, *14*, 1936-1947.
10.   Amaranatha Reddy R., Sadashiva B. K. and Raghunathan V. A. *Chem. Mater.* **2004**, *16*, 4050-4062.
11.   Bedel J. P., Rouillon J. C., Marcerou J. P., Laguerre M., Nguyen H. T. and Achard M. F. *Liq. Cryst.* **2000**, *27*, 1411-1421.
12.   Zou L., Wang J., Beleva V. J., Kooijman E. E., Primak S. V., Risse J., Weissflog W., Jákli A. and Mann E. K. *Langmuir* **2004**, *20*, 2772-2780.
13.   Kinoshita Y., Park B., Takezoe H., Niori T. and Watanabe J. *Langmuir* **1998**, *14*, 6256-6260.
14.   Ashwell G. J. and Amiri M. A. *J. Mater. Chem.* **2002**, *12*, 2181-2183.

15. Baldwin J. W., Amaresh R. R., Peterson I. R., Shumate W. J., Cava M. P., Amiri M. A., Hamilton R., Ashwell G. J. and Metzger R. M. *J. Phys. Chem. B* **2002**, *106*, 12158-12164.

16. Tang Y., Wang Y., Wang G., Wang H., Wang L. and Yan D. *J. Phys. Chem. B* **2004**, *108*, 12921-12926.

17. Tang Y., Wang Y., Wang X., Xun S., Mei C., Wang L. and Yan D. *J. Phys. Chem. B* **2005**, *109*, 8813-8819.

18. Gong J.-R. and Wan L.-J. *J. Phys. Chem. B.* **2005**, *109*, DOI: 10.1021/jp052581q.

19. Olsen D. A., Cady A., Weissflog W., Nguyen H. T. and Huang C. C. *Phys. Rev. E* **2001**, *64*, 051713.

20. Achten R., Koudijs A., Giesbers M., Marcelis A. T. M. and Sudhölter E. J. R. *Liq. Cryst.* **2005**, *32*, 277-285.

21. Achten R., Smits E. A. W., Amaranatha Reddy R., Giesbers M., Marcelis A. T. M. and Sudhölter E. J. R. *Liq. Cryst.* **2005**, *accepted*.

22. Wayner D. D. M. and Wolkow R. A. *J. Chem. Soc., Perkin Trans. 2* **2002**, 23-24.

23. Buriak J. M. *Chem. Rev.* **2002**, *102*, 1271-1308.

24. Sieval A. B., Linke R., Zuilhof H. and Sudhölter E. J. R. *Adv. Mater.* **2000**, *12*, 1457-1460.

25. Jakli A., Chien L.-C., Kruerke D., Sawade H. and Heppke G. *Liq. Cryst.* **2002**, *29*, 377-381.

26. Jakli A., Kruerke D. and Nair G. G. *Phys. Rev. E* **2003**, *67*, 051702.

27. Park C. S., Furtak T. E., Clark N. A., Liberko C. A. and Walba D. M. *Phys. Rev. E* **2003**, *67*, 051707.

28. Komitov L., Helgee B., Felix J. and Matharu A. *Appl. Phys. Lett.* **2005**, *86*, 023502.

29. Sun Q.-Y., de Smet L. C. P. M., van Lagen B., Giesbers M., Thüne P. C., van Engelenburg J., de Wolf F. A., Zuilhof H. and Sudhölter E. J. R. *J. Am. Chem. Soc.* **2005**, *127*, 2514-2523.

30. de Smet L. C. P. M., Stork G. A., Hurenkamp G. H. F., Sun Q.-Y., Topal H., Vronen P. J. E., Sieval A. B., Wright A., Visser G. M., Zuilhof H. and Sudhölter E. J. R. *J. Am. Chem. Soc.* **2003**, *125*, 13916-13917.

31. Feng W. and Miller B. *Langmuir* **1999**, *15*, 3152-3156.

32. Lin Z., Strother T., Cai W., Cao X., Smith L. M. and Hamers R. J. *Langmuir* **2002**, *18*, 788-796.

33. Dancil K.-P. S., Greiner D. P. and Sailor M. J. *J. Am. Chem. Soc.* **1999**, *121*, 7925-7930.

34. Linford M. R., Fenter P. E., Eisenberger P. M. and Chidsey C. E. D. *J. Am. Chem. Soc.* **1995**, *117*, 3145-3155.

35. Pei Y. and Ma J. *J. Am. Chem. Soc.* **2005**, *127*, 6802-6813.

36. Okano T., Inari H., Ishizaki T., Saito N., Sakamoto W. and Takai O. *Chem. Lett.* **2005**, *34*, 600-601.

37. Sieval A. B., Vleeming V., Zuilhof H. and Sudhölter E. J. R. *Langmuir* **1999**, *15*, 8288.

38. Cicero R. L., Linford M. R. and Chidsey C. E. D. *Langmuir* **2000**, *16*, 5688-5695.

39. Webb L. J. and Lewis N. S. *J. Phys. Chem. B* **2003**, *107*, 5404-5412.

40. Buriak J. M. and Allen M. J. *J. Am. Chem. Soc.* **1998**, *120*, 1339-1340.

41. Sun Q.-Y., de Smet L. C. P. M., van Lagen B., Wright A., Zuilhof H. and Sudhölter E. J. R. *Angew. Chem. Int. Ed.* **2004**, *43*, 1352-1355.

42. Achten R., Cuypers R., Giesbers M., Koudijs A., Marcelis A. T. M. and Sudhölter E. J. R. *Liq. Cryst.* **2004**, *31*, 1167-1174.

43. Lee G. S., Lee Y.-J., Choi S. Y., Park Y. S. and Yoon K. B. *J. Am. Chem. Soc.* **2000**, *122*, 12151-12157.

44. After refluxing 14-P-11a in mesitylene for 2h, small impurities were observed on TLC.

45. Linford M. R. and Chidsey C. E. D. *Langmuir* **2002**, *18*, 6217.

46.   Liu Y.-J., Navasero N. M. and Yu H.-Z. *Langmuir* **2004**, *20*, 4039-4050.
47.   Amaranatha Reddy R., Schröder M. W., Bodyagin M., Kresse H., Diele S., Pelzl G. and Weissflog W. *Angew. Chem. Int. Ed.* **2005**, *44*, 774-778.

Summary

This thesis describes the liquid crystalline properties of molecules with a bent shape. The objective of the research is to allow further insight in structure-property relationships for this class of liquid crystals. Specifically, we are interested in chemically stable compounds with switchable mesophases in order that they can potentially be used in display devices, as a possible alternative for chiral smectic-C compounds. One important objective is to obtain materials with the desired mesophases at temperatures as close to room temperature as possible. Another objective is to obtain materials that can be attached to polymer backbones or hydrogen-terminated silicon surfaces.

In *chapter 1* an overview of liquid crystals is given with a focus on bent-shaped (or banana-shaped) compounds. Bent-core mesogens often contain a 1,3-disubstituted phenyl or a 3,4′-disubstituted biphenyl group, which causes the bend in the molecules. These achiral bent molecules can form chiral phases, due to a combination of tilted molecules in layers, and a polar component perpendicular to the director of the bent molecules. There are four possibilities for the molecules to arrange themselves in the so-called SmCP phase; the polarization direction can be parallel or antiparallel in adjacent layers, giving rise to ferroelectricity (P_F) and antiferroelectricity (P_A), respectively. Secondly, the molecules can tilt in *syn* (C_S) or *anti* (C_A) fashion in successive layers. This results in two macroscopic chiral organizations (SmC$_S$P$_F$ and SmC$_A$P$_A$) and two racemic organizations (SmC$_A$P$_F$ and SmC$_S$P$_A$). In principle the antiferroelectric ground state is energetically preferred due to the escape from macroscopic polar order, and the possibility of out-of-plane interlayer fluctuations.

In order to investigate whether banana-phases could also be obtained in dimeric molecules with an odd number of flexible units in the spacer, three series of compounds were described in *chapter 2*. All three series show a pronounced odd-even effect in the isotropization temperatures with the parity of the spacer. Upon increasing the terminal tail length, the nematic phase was suppressed as was predicted by previous literature. Furthermore, the compounds with an odd number of flexible units between the mesogens did not show features of banana-phases, as was reported for some similar series. A reversal of the ester connecting groups between the aromatic rings resulted in a change from a monolayer smectic organization to (partly) intercalated smectic organizations.

In *chapter 3*, the liquid crystalline properties of four series of salicylaldimine-based dimers is studied. The bend in the molecules is obtained by connecting the mesogenic units via 1,3-phenylene, 1,5-pentylene, 2,2-dimethyl-1,5-pentylene or 3,3-

dimethyl-1,5-pentylene groups. As observed in several other series a 1,3-disubstituted phenyl group promotes formation of B-phases. Upon increasing the terminal chain length the phase sequence B_6-B_1-B_2 (SmC_{int}-Col_r-SmCP) is observed. If the central phenyl group was replaced by a more flexible odd spacer, the switchable SmCP phase completely disappeared. Comparison of unsubstituted pentyl spacers with dimethyl substituted pentyl spacers, showed that the latter promoted intercalated smectic phases. Furthermore, these methyl substituents suppressed the melting temperatures.

In *chapters 4, 5* and *6*, five-ring banana-shaped molecules with esters as linking groups between the rings, and a central 1,3-substituted phenyl group, were studied. This parent-structure was modified in different manners and the influence of these modifications on the liquid crystalline properties was investigated.

Bananas with two terminal alkoxy tails of different length were compared to their symmetric analogues in *chapter 4*. The non-symmetric compounds showed lower melting points while the influence on the isotropization temperatures was small. The switchable SmCP phase was retained. From comparing symmetrical and non-symmetrical bananas with an equal number of carbon atoms in their terminal chains, it was concluded that non-symmetry only slightly destabilizes the SmCP phase whereas the melting points are decreased considerably, thereby increasing the liquid crystalline range. Replacement of the central phenyl group with a 3,4'-disubstited biphenyl group, showed that for this series the melting points can not be lowered by introducing two terminal alkoxy tails of different length. The mesophase range for the biphenyl compounds is significantly larger than for the phenyl analogues, mainly due to higher isotropization temperatures.

In *chapter 5*, the liquid crystalline properties of compounds with one terminal vinyl group were studied. The unsaturated compounds showed the same mesophase and switching behavior as their saturated analogues described in *chapter 4*. The SmCP phase was slightly destabilized however.

The influence of a fluorine substituent at the *ortho* position with respect to the alkoxy group in *one* of the outer aromatic groups, on the liquid crystalline properties of banana-shaped mesogens, is described in *chapter 6*. In contrast to the difluorine substituted bananas, which show ferroelectric switching behavior, the compounds with one fluorine substituent exhibited antiferroelectric switching. The SmCP phase was slightly stabilized if compared to the non-substituted analogues, since the isotropization temperatures increased upon introduction of one (and also a second) fluorine substituent.

For all bananas described in *chapters 4, 5*, and *6*, the liquid crystalline properties were only slightly changed when compared to the non-modified parent-structure. The

switchable SmCP mesophase was in most cases retained, and the melting points could be lowered to about ~80°C by asymmetric tail lengths combined with a terminal vinyl group.

Polymerization of banana-shaped compounds could in principle give a system showing (switchable) mesophases at even lower temperatures. Therefore, the mono-unsaturated bananas described in *chapter 5* have been used to prepare siloxane polymers. The liquid crystalline properties of these polymers, one series with a relatively short and a second series with longer trimethylsilyl terminated polysiloxane backbones, are described in *chapter 7*. Most of the "short" polymers exhibited the SmCP$_A$ phase, with the same switching properties as their olefinic precursors. Crystallization could not be observed, but upon cooling from the SmCP phase a transition to another unidentified mesophase was detected. The longer siloxanes also exhibited two mesophases. However, due to the high viscosity these compounds could not be characterized by polarization optical microscopy and switching experiments, but a lamellar ordering is likely for these materials.

In *chapter 8* a vinyl-terminated banana from *chapter 5* and two fluorine substituted bananas from *chapter 6*, were covalently attached to silicon surfaces via an extremely mild method. The two bananas with the fluorine substituent are isomers and only differ in the position of the substituent: close, or at a more distant position from the double bond. The presence and quality of these banana-shaped self-assembled monolayers was investigated, and indeed showed the presence of a monolayer with a thickness comparable to the *d*-spacing of the corresponding banana molecules in bulk. Moreover, the monolayers of the fluorine substituted bananas were investigated with angle-resolved X-ray photoelectron spectroscopy. These measurements showed that the fluorine substituents could be detected on positions in the monolayer with respect to the silicon bulk that were expected, based on the molecular structure of the molecules.

Samenvatting

In dit proefschrift worden de vloeibaar kristallijne eigenschappen van banaanvormige moleculen besproken. Naast de relatie tussen chemische structuren en vloeibaar kristallijne eigenschappen, zijn we vooral geïnteresseerd in stabiele verbindingen die schakelgedrag vertonen in hun vloeibaar kristallijne fase. Zo zouden deze verbindingen, in theorie, als alternatief voor chiraal smectisch-C verbindingen gebruikt kunnen worden in displays. Een tweede belangrijk doel is om de vloeibaar kristallijne eigenschappen bij zo laag mogelijke temperatuur, liefst kamertemperatuur, te verkrijgen. Eén mogelijkheid om dit voor elkaar te krijgen is de banaanvormige verbindingen te voorzien van een groep die polymerisatie mogelijk maakt, zoals bijvoorbeeld een dubbele band.

In *hoofdstuk 1* wordt een overzicht gegeven over vloeibare kristallen, toegespitst op banaanvormige verbindingen. Deze verbindingen, ook wel gebogen mesogenen genoemd, bevatten meestal een centrale 1,3-digesubstitueerde fenyl of een 3,4'-digesubstitueerde bifenylgroep. Deze groepen zorgen ervoor dat het mesogeen zijn gebogen vorm krijgt. Ondanks het feit dat banaanvormige moleculen niet chiraal zijn, kunnen deze verbindingen toch macroscopisch chirale fasen vormen. Dit is mogelijk doordat ze in de vloeibaar kristallijne fase een lagensysteem vormen waarin de moleculen schuin staan t.o.v. de lagen, gecombineerd met een polaire component loodrecht op de gemiddelde richting van de gebogen moleculen. Er zijn vier mogelijkheden waarop moleculen zich in dergelijke zogenaamde SmCP fasen kunnen ordenen; de richting van de polarisatie kan gelijk zijn in opeenvolgende lagen (P_F: ferro-elektrisch), of kan afwisselen in opeenvolgende lagen (P_A: antiferro-elektrisch). Daarnaast kunnen de moleculen in opeenvolgende lagen schuin staan in dezelfde richting (C_S: synclinisch), of kan de richting waarin de moleculen schuin staan afwisselen in opeenvolgende lagen (C_A: anticlinisch). Twee van de varianten waarin de SmCP fase kan voorkomen, zijn macroscopisch chiraal (SmC_SP_F en SmC_AP_A), en twee zijn racemisch (SmC_AP_F en SmC_SP_A). In principe is de antiferro-elektrische grondtoestand het meest voorkomend en energetisch stabiel doordat enerzijds op deze manier wordt voorkomen dat het systeem macroscopisch polair geordend is, en anderzijds zal de synclinische interactie tussen de alkylstaarten van de moleculen uit verschillende lagen een voorkeur voor de antiferro-elektrische ordening opleveren.

In *hoofdstuk 2* zijn de eigenschappen onderzocht van drie series tweeling vloeibare kristallen. In deze verbindingen zijn twee mesogene groepen met elkaar verbonden door een flexibel oligomethyleentussenstuk. De isotropisatietemperatuur vertoont een sterk even-oneven effect als functie van het aantal flexibele eenheden tussen de

mesogene groepen. Het langer maken van de eindstandige alkylstaarten van deze verbindingen heeft tot gevolg dat de nematische fase wordt onderdrukt. Verder is opvallend dat de verbindingen met een oneven aantal flexibele groepen in het tussenstuk geen eigenschappen vertonen die doen denken aan banaanfasen. Tenslotte is gebleken dat een omkering van de estergroep tussen de twee aromaten in beide mesogene groepen, zorgt voor een overgang van smectische monolagen naar (gedeeltelijk) geïntercaleerde smectische lagen.

In *hoofdstuk 3* worden de eigenschappen van vier series tweeling vloeibare kristallen beschreven, met salicylaldimines als mesogene groepen. Het centrale deel van deze tweelingen bestaat voor de vier series uit respectievelijk: 1,3-fenyleen, 1,5-pentyleen, 2,2-dimethyl-1,5-pentyleen en 3,3-dimethyl-1,5-pentyleen. Het is gebleken dat een centrale fenylgroep de vorming van banaanfasen bevordert. Bij het verlengen van de staartlengte treedt een B_6-B_1-B_2 (SmC_{int}-Col_r-$SmCP_A$) fasenverloop op. Deze volgorde is bekend uit de literatuur en is ook in verschillende andere series waargenomen. Als de centrale fenyleengroep wordt vervangen door een pentyleengroep verdwijnt de schakelbare B_2 ($SmCP_A$) fase. Als een van de CH_2-groepen van de pentyleengroep wordt vervangen door een $C(CH_3)_2$-groep, worden de smeltpunten verlaagd en geïntercaleerde smectische fasen bevorderd.

In de *hoofdstukken 4, 5* en *6* worden vijfring banaanvormige verbindingen, met esters als verbindingsgroepen tussen de aromaten, onderzocht. Alle verbindingen hebben een centrale 1,3-digesubstitueerde fenylgroep die de gebogen vorm van de moleculen veroorzaakt. In deze basisstructuur worden kleine veranderingen aangebracht, en de invloed van deze veranderingen op de eigenschappen wordt beschreven.

Bananen waarvan de twee staarten een verschillende lengte hebben worden beschreven in *hoofdstuk 4*. Deze verbindingen hebben lagere smeltpunten dan de overeenkomstige verbindingen met staarten van gelijke lengte. De schakelbare SmCP fase blijft echter aanwezig. Omdat de isotropisatietemperatuur nauwelijks verlaagd wordt door ongelijke staarten hebben deze niet-symmetrische verbindingen een groter vloeibaar kristallijn gebied. Vervanging van de centrale fenylgroep door een 3,4'-digesubstitueerde bifenylgroep levert een vergroting van het vloeibaar kristallijne gebied op. Dit wordt vooral veroorzaakt door een verhoging van de isotropisatietemperaturen.

Introductie van een dubbele band aan het uiteinde van één van de staarten van de basisstructuur levert een kleine destabilisatie van de SmCP fase op en is beschreven in *hoofdstuk 5*. Deze verbindingen zijn door de aanwezigheid van de dubbele band geschikt om te koppelen aan polymeren. De invloed van fluorsubstituenten is beschreven in *hoofdstuk 6*. Het blijkt dat als de fluorsubstituenten worden

geïntroduceerd op bepaalde posities in de banaanvormige verbindingen, de grondtoestand verandert van antiferro-elektrisch naar ferro-elektrisch. Hiervoor moeten echter wel beide armen van de banaan worden gesubstitueerd. De laagdikte van SmCP fase blijkt toe te nemen door de fluorsubstituenten.

De synthese en eigenschappen van siloxaan oligomeren en polymeren met banaanvormige zijketens worden beschreven in *hoofdstuk 7.* Deze verbindingen zijn gemaakt door de verbindingen uit *hoofdstuk 5* te koppelen aan waterstofgetermineerd siloxaan oligomeer of polymeer. De verkregen oligomeren, met een relatief korte hoofdketen, vertonen de SmCP$_A$ fase. Het schakelgedrag van deze verbindingen is vergelijkbaar met dat van de monomeren, namelijk antiferro-elektisch. De polymeren met een langere hoofdketen konden door hun hoge viscositeit niet op schakeleigenschappen worden onderzocht, maar hebben waarschijnlijk ook een SmCP fase. Zowel voor de oligomeren als voor de polymeren kon geen kristallisatie worden waargenomen bij afkoelen naar kamertemperatuur.

In *hoofdstuk 8* is beschreven hoe een drietal banaanvormige moleculen, met een dubbele band aan het einde van één van de staarten, covalent worden gebonden aan een siliciumoppervlak. Twee van deze verbindingen hebben een fluorsubstituent; één dicht bij de dubbele band en één verder verwijderd van deze dubbele band. Verschillende metingen wijzen uit dat er inderdaad een monolaag op het Si(111) oppervlak aanwezig is. De kwaliteit van deze laag is redelijk goed en heeft een dikte van ~34 Å. Hoek afhankelijke X-ray photoelectron spectroscopy (AR-XPS) metingen wijzen uit dat ook de monolagen van de verbindingen met de fluorsubstituenten relatief goed geordend zijn. De signalen afkomstig van de fluorsubstituenten, zijn in het diepteprofiel te vinden op posities waar ze op grond van hun structuur ook verwacht worden.

146

Dankwoord

Na iets meer dan vier jaar kan ik eindelijk zeggen dat mijn proefschrift af is. In tegenstelling tot wat ik vooraf dacht is het eigenlijk zonder al te grote problemen verlopen, de AIO-dip is geheel uitgebleven. Uiteraard zou dit proefschrift nooit tot stand kunnen zijn gekomen zonder de hulp, adviezen en vriendschap van een groot aantal mensen.

Ten eerste mijn promotor, Ernst Sudhölter. Je tomeloze enthousiasme zorgde altijd weer voor extra motivatie. Ook vond ik onze gezamenlijke reizen naar Duitsland, Zwitserland en de Verenigde Staten erg geslaagd. Mijn copromotor, Ton Marcelis, wil ik vooral bedanken voor het zeer snel, tot in detail nakijken van mijn manuscripten. Daarnaast had je op elk moment van de dag tijd om dingen met mij te bespreken en kan je met recht mijn dagelijks begeleider worden genoemd. Prof. Dick Broer, mijn tweede promotor, wil ik bedanken voor het zorgvuldig bekijken van de verschillende hoofdstukken van dit proefschrift.

Degene die, qua praktische werk, ongetwijfeld de grootste hulp heeft geboden bij het tot stand komen van dit proefschrift is natuurlijk Arie. Ongeveer tweeënhalf jaar hebben we samen op het project van de bananen gewerkt. De laatste verbinding die jij gemaakt hebt is AK183, dat wil zeggen dat je bijna 200 nieuwe verbindingen hebt gesynthetiseerd. Vanzelfsprekend ben ik je hier zeer dankbaar voor. Zbigniew, when I just started as a PhD student you were the only X-ray specialist in our lab, thanks for all your help and good luck with your career in Poland. Marcel, jij hebt het grootste gedeelte van de XRD metingen voor je rekening genomen. Zeker in de laatste weken moesten er nog een aantal metingen snel worden gedaan, bedankt hiervoor. Wat als een grapje begon heeft uiteindelijk geleid tot hoofdstuk 8, bananen op silicium. Louis bedankt voor de oppervlakte modificatie, en Han voor de AR-XPS metingen.

Verder zijn er nog een aantal mensen die in praktische zin hebben bijgedragen aan mijn proefschrift; Ronald voor de chemicaliën, Elbert voor de elementanalyse, Maarten voor de exacte massa metingen (en natuurlijk verhalen 1 t/m 47c), Bep en Barend voor de NMR metingen. Naast alle (ex)collega's van ORC wil ik Michael, Ganesan, Ioan, Louis en Cindy nog in het bijzonder bedanken voor de gezellige tijd. Ook wil ik Ruud en Evelien bedanken die een grote bijdrage hebben geleverd aan hoofdstukken 4 en 6, wat mij betreft heeft de samenwerking altijd op een hele leuke manier plaatsgevonden.

Naast Prof. Broer wil ik ook Ton Verhulst, Leon Stofmeel en Henk de Koning van Philips bedanken voor het mogelijk maken van de current response metingen. Daarnaast zijn er ook verschillende experimenten met banaanvormige verbindingen

Curriculum Vitae

Remko Achten werd geboren op 6 december 1973 in Roermond. Na het behalen van het HAVO diploma in 1991, en het VWO diploma in 1993, aan de Rijksscholengemeenschap Roermond, studeerde hij een jaar Scheikundige Technologie aan de Technische Universiteit Eindhoven. In 1994 begon hij aan de studie Moleculaire Wetenschappen aan Wageningen Universiteit. Hij heeft afstudeervakken gedaan bij het laboratorium voor Organische Chemie en Biochemie, waarna hij in 2000 afstudeerde. Na gewerkt te hebben als onderwijsassistent, werkte hij een half jaar als toegevoegd onderzoeker bij het laboratorium voor Organische Chemie aan Wageningen Universiteit. Vanaf september 2001 volgde een vierjarige aanstelling als Onderzoeker in Opleiding (OIO) bij dit laboratorium. De verkregen onderzoeksresultaten staan beschreven in dit proefschrift.

List of publications

Synthesis and thermotropic properties of novel side-chain dimer liquid crystalline polymers.
Scheerder J., Marcelis A. T. M., Achten R. and Sudhölter E. J. R.
Macromol. Chem. Phys. **2000**, 201, 1303-1310.

Liquid crystalline properties of salicylaldimine-based dimers. Influence of terminal alkyl chain length and central part.
Achten R., Koudijs A., Karzcmarzyk Z., Marcelis A. T. M. and Sudhölter E. J. R.
Liq. Cryst. **2004**, 31, 215-227.

Symmetrical dimer liquid crystals with tilted smectic phases.
Achten R., Koudijs A., Marcelis A. T. M. and Sudhölter E. J. R.
Mol. Cryst. Liq. Cryst. **2004**, 411, 177-184.

Asymmetric banana-shaped liquid crystals with two different terminal alkoxy tails.
Achten R., Cuypers R., Giesbers M., Koudijs A., Marcelis A. T. M. and Sudhölter E. J. R.
Liq. Cryst. **2004**, 31, 1167-1174.

Non-symmetric bent-core mesogens with one terminal vinyl group.
Achten R., Koudijs A., Giesbers M., Marcelis A. T. M. and Sudhölter E. J. R.
Liq. Cryst. **2005**, 32, 277-285.

The effect of shearing on the phase retardation of banana liquid crystals.
Goldbach-Aschemann S., Rasing T., Achten R., Marcelis A. T. M. and Sudhölter E. J. R.
Mol. Cryst. Liq. Cryst. **2005**, 437, 1539-1545.

Monofluorinated unsymmetrical bent-core mesogens.
Achten R., Smits E. A. W., Amaranatha Reddy R., Giesbers M., Marcelis A. T. M. and Sudhölter E. J. R.
Liq. Cryst. **2005**, 32, *in press*.

Banana-shaped side chain liquid crystalline siloxanes.
Achten R., Koudijs A., Giesbers M., Amaranatha Reddy R., Verhulst T., Tschierske C., Marcelis A. T. M. and Sudhölter E. J. R.
Submitted.

Covalent attachment of bent-core molecules to silicon surfaces.

Achten R., de Smet L. C. P. M., Giesbers M., Koudijs A., Smits E. A. W., Zuilhof H., Marcelis A. T. M. and Sudhölter E. J. R.

In preparation.

Dimeric banana-shaped liquid crystals.

Achten R., Koudijs A., Giesbers M., Marcelis A. T. M. and Sudhölter E. J. R.

In preparation.

Biphenyl-containing bent-core mesogens.

Achten R., Koudijs A., Giesbers M., Stofmeel L., de Koning H., Marcelis A. T. M. and Sudhölter E. J. R.

In preparation.

Tilted organosiloxane liquid crystals.

Achten R., Koudijs A., Giesbers M., Marcelis A. T. M. and Sudhölter E. J. R.

In preparation.

The picture on the front cover is an optical photomicrograph of the B$_1$ (Col$_r$) texture observed for compound 12-**BP**-8 (chapter 4, taken by Ruud Cuypers).

The pictures on the back cover are optical photomicrographs of the liquid crystalline textures of compounds **III-5**, **I-12** and **II-8**, respectively (chapter 3).